An Iterative Numerical Method for Nonlinear Vibrations

By J. E. BROCK,[1] ST. LOUIS, MO.

A simple iterative procedure employing numerical integrations is presented for the analysis of free and forced vibrations of undamped systems having nonlinear elasticity. If the elasticity is symmetrical, it is always possible to make an excellent initial approximation, but the method may also be used in cases of unsymmetrical elasticity. Other applications, such as to systems having parameters which vary with time, are discussed.

Introduction

THIS paper presents a rapid and accurate method of determining the characteristics of the oscillations of an undamped system having a single degree of freedom and symmetrical though nonlinear elasticity. The method is essentially an iteration procedure similar in certain respects to methods currently in use. Of these other methods, that of Rauscher (1, 2, 3)[2] seems to have met with very great favor (4, 5, 6). For applications to undamped symmetrical systems, the method to be described seems to afford two advantages as compared to Rauscher's method: (*a*) It is possible to make a better initial approximation which generally assures more rapid convergence; and (*b*) the form of the approximate integrations is simplified and systematized. The basic point of view of the two methods seems to be roughly the same although, besides the differences just mentioned, there is another difference in that Rauscher uses the displacement x as the independent variable in some of his calculations, while the present method always uses time t as the independent variable.

The method to be described may also be applied to cases of unsymmetrical elasticity although its rapidity and simplicity is compromised in the process to the extent that it is doubtful whether it offers many advantages in such applications. The method does not appear suitable for study of damped oscillations.

In this method, the basic procedure and the method of numerical integration employed with it appear to be very fortunately tailored to each other. The actual calculations are extremely simple and with the use of a customary desk-type adding machine only a fraction of them need be recorded. If very high accuracy is required, it may be obtained by use of a simple extrapolation procedure which requires, in effect, that the calculations be performed twice. Accuracy sufficient for most engineering purposes may be obtained without extrapolation, frequently without the necessity of iteration. Another virtue of this method is that it is almost completely "automatic;" no time is required deciding what to do next.

Proof of convergence and the history of the method are omitted The use of an iterative procedure combined with a method of numerical integration was suggested by the method of Stodola for studying the vibrations of turbine shafts (a linear problem). The present application occurred independently to the author; that is not to say that it is original with the author although it is believed to be. There is considerable literature in mathematical publications on iterative methods; an opportunity to study this material may possibly reveal that essentially the same idea had been disclosed earlier. Whether or not this is the case, the present application seems to be unknown to the engineering profession which is ample justification for treating it here. Similarly, while the author has not proved the convergence of the method, that is not to say the mathematical literature does not contain certain proofs applicable to this method. The author hopes to make up these omissions in a later publication.

Principle of the Method

We consider the differential equation

$$\ddot{x} + f(x) = F(t)$$

(dots denoting differentiation with respect to t), or more generally

$$\ddot{x} + g(x, t) = 0$$

subject to the initial conditions $x(0) = A$, $\dot{x}(0) = 0$. It is presumed that there exists a positive number τ (identifiable in many cases with the quarter period of a vibration) such that $x(\tau) = 0$, and it is desired to find the value of τ and to find x as a function of t for $0 \leq t \leq \tau$.

These results are obtained by iterated application of a basic procedure (which will be called a "stage" of the process) followed by a simple calculation. Each stage itself involves what is essentially two integrations. In practice, it is usually necessary (or at least most convenient) to use some method of approximate integration; actually, it is the fact that the simple method of approximate integration to be described later is so well adapted for use in each of the stages which makes this method of more than academic interest. Therefore the integrals exhibited in the following paragraphs are to be usually understood as having been obtained by some approximate method.

To start the process, a "shape" is assumed for the unknown function. This shape must satisfy $x(0) = A$, $\dot{x}(0) = 0$, and $x(\tau) = 0$; but, of course, τ is as yet unknown. The function $x = A \cos(\pi t/2\tau)$ is usually a good first choice, but as will be seen later, the assumption is usually made in a numerical tabular form, so that the assumption of a cosine shape may be modified by experience—or simply for the convenience of dealing at the beginning with numbers consisting of only one or two digits.[3]

If the assumed function had precisely the correct shape, we could recover the function by integrating twice, as follows

---

[1] Department of Applied Mechanics, Washington University. Jun. ASME.

[2] Numbers in parentheses refer to Bibliography at end of paper.

Presented at the Conference of the Applied Mechanics Division, Purdue University, Lafayette, Ind., June 22-24, 1950, of The American Society of Mechanical Engineers.

Discussion of this paper should be addressed to the Secretary, ASME, 29 West 39th Street, New York, N. Y., and will be accepted until April 10, 1951, for publication at a later date. Discussion received after the closing date will be returned.

Note: Statements and opinions advanced in papers are to be understood as individual expressions of their authors and not those of the Society. Manuscript received by the Applied Mechanics Division, September 27, 1949. Paper No. 50—APM-1.

[3] The present method enjoys its chief advantage in that an excellent first approximation may always be made. It has the correct value and slope for $t = 0$, and, what is most striking, it automatically vanishes at the time, $t = \tau$, that it should vanish!

$$\ddot{x} = \frac{d(\dot{x})}{dt} = -g[x(t),t]$$

Multiplying by dt and integrating from 0 to t, we obtain

$$\int_0^t \ddot{x}\,dt = -\int_0^t g[x(t),t]\,dt$$

However, $\ddot{x}\,dt = d(\dot{x})$ and $\dot{x} = 0$ when $t = 0$. Also, it is advisable to emphasize that the variable of integration is actually a dummy by introducing new dummy variables. Thus

$$\dot{x} = -\int_0^t g[x(\xi),\xi]\,d\xi$$

Note also that $\dot{x}\,dt = dx$ and that $x = A$ when $t = 0$ and $x = 0$ when $t = \tau$. Thus

$$x = \int_\tau^t \left\{ -\int_0^\eta g[x(\xi),\xi]\,d\xi \right\} d\eta$$

$$= \int_t^\tau d\eta \int_0^\eta g[x(\xi),\xi]\,d\xi$$

Thus x now appears as a function of both t and τ, the former being the proper independent variable and the latter being a constant which is not yet determined. In particular

$$A = x(0) = \int_0^\tau d\eta \int_0^\eta g[x(\xi),\xi]\,d\xi = \text{a function of } \tau \ldots . [1]$$

which is an equation that can be solved for τ.

However, in general, the first assumed function (which will be denoted by x_1) will not have the correct shape and the function x_2 defined by

$$x_2 = A\,\frac{\displaystyle\int_t^\tau d\eta \int_0^\eta g[x_1(\xi),\xi]\,d\xi}{\displaystyle\int_0^\tau d\eta \int_0^\eta g[x_1(\xi),\xi]\,d\xi}$$

will likewise be in error. However, it is easily verified that $x_2(0) = A$, $\dot{x}_2(0) = 0$, and $x_2(\tau) = 0$. Thus the function x_2 provides a suitable starting point for repeating the process. Continuing in this way by defining[4]

$$x_{n+1} = A\,\frac{\displaystyle\int_t^\tau d\eta \int_0^\eta g[x_n(\xi),\xi]\,d\xi}{\displaystyle\int_0^\tau d\eta \int_0^\eta g[x_n(\xi),\xi]\,d\xi}$$

it will be found that the sequence of functions $x_1, x_2, x_3, \ldots$ converges to a limit function, which thus satisfies the original differential equation and initial conditions. Denoting the limit function by x, the value of τ may be found from Equation [1].

The first example, which follows, is trivial; however, its simplicity permits exact integrations so as to illustrate what has been introduced so far.

[4] By integrating by parts, the definition of the iterated function may be written as

$$x_{n+1} = A\,\frac{(\tau - t)\int_t^\tau g[x_n(\xi),\xi]\,d\xi + \int_t^\tau (\tau - \xi)\,g[x_n(\xi),\xi]\,d\xi}{\int_0^\tau (\tau - \xi)g[x_n(\xi),\xi]d\xi}$$

which involves only single integrals rather than iterated integrals. However, in the numerical procedure later to be employed, it is easier to integrate twice.

Example 1:

$$\ddot{x} + x = 0;\ x(0) = 1,\ \dot{x}(0) = 0$$

As an initial function, make the ridiculous assumption $x_1 \equiv 1$ Then

$$x_2 = 1 - \frac{t^2}{\tau^2}$$

$$x_3 = 1 - \frac{6t^2}{5\tau^2} + \frac{t^4}{5\tau^4}$$

$$x_4 = 1 - \frac{75t^2}{61\tau^2} + \frac{15t^4}{61\tau^4} - \frac{t^6}{61\tau^6}$$

This process could be carried further, but let us stop at this point and obtain an (approximate) evaluation of τ using Equation [1].

$$1 = \left(\frac{1}{2} - \frac{25}{244} + \frac{3}{366} - \frac{1}{3416}\right)\tau^2 = \frac{84485}{208376}\,\tau^2$$

$$\tau^2 = 2.466426;\ \tau = 1.5705$$

The exact value is, of course, $\tau = \pi/2 = 1.5708$.

Using the calculated value for τ in the expression for x_4, we have

$$x_4 = 1 - t^2/2.00 + t^4/24.8 - t^6/917$$

while the correct solution is of course

$$x = \cos t = 1 - t^2/2 + t^4/24 - t^6/720 + t^8/40320 - \ldots .$$

In the preceding solution we failed to take advantage of the fact that we are able to choose a first approximation which vanishes when it should. The function $x_3 = 1 - t^2/\tau^2$ has this property, and making this more intelligent first choice would have saved one stage in the process.

Method of Integration

While the necessary integrations may be performed exactly if $g(x, t)$ is sufficiently simple and if x_1 is assumed in an analytical form, they can also be performed by approximate numerical methods, the simplest and most convenient of which will now be described.

The time interval from $t = 0$ to $t = \tau$ is divided into n parts (where n is an integer chosen at convenience) each of duration $\lambda = \tau/n$. The values of $t = k\lambda$ will be called epochs and will be denoted by e_k ($k = 0, 1, 2, \ldots, n$). Values of x_1 are assumed for each epoch and from these the corresponding values of $\ddot{x}(e_k) = -g[x_1(e_k),e_k]$ are computed. For the sake of definiteness in the explanations we will consider the following example (Figs. 1 and 2; see Appendix):

Example 2:

$$\ddot{x} + x^2\dot{x} = 0;\ x(0) = 4,\ \dot{x}(0) = 0$$

The function x_1 is assumed in a tabular form in the first line of Table 1, in which n has been chosen equal to 8. The corresponding values of $\ddot{x}$ are shown in the second line; for example, at epoch e_4, we have

$$\ddot{x} = -(2.8)^2(4\lambda) = -87.8\lambda$$

The factor λ which is common to all terms in the second line is exhibited at the far right.

In the third line, the values of $\dot{x}$ are calculated at the half-epochs. Recalling that an integral may be regarded as area under a curve (see Fig. 3a) and approximating the curve by a straight line during the first time interval λ, it is easily seen that $\dot{x}(e_{1/2}) \approx$

TABLE 1 SOLUTION OF EXAMPLE 2

	Epoch	0	1	2	3	4	5	6	7	8	Factor
Stage 1	x (line 1)	4.0	3.9	3.7	3.3	2.8	2.2	1.5	0.8	0.0	
	$\ddot{x}$ (line 2)	0.0	-59.3	-101.3	-107.8	-87.8	-53.2	-20.2	-3.6	0.0	λ
	$\dot{x}$ (line 3)		-7.4	-66.7	-168.0	-275.8	-363.6	-416.8	-437.0	-440.6	λ^2
	x (line 4)	2175.9	2168.5	2101.8	1933.8	1658.0	1294.4	877.6	440.6	0.0	λ^3
Stage 2	x	4.00	3.99	3.87	3.66	3.05	2.38	1.61	0.81	0.00	
	$\ddot{x}$	0.0	-63.5	-115.9	-135.4	-113.5	-67.4	-25.0	-3.7	0.0	λ
	$\dot{x}$		-7.9	-71.4	-187.3	-322.7	-436.2	-503.6	-528.6	-532.3	λ^2
	x	2680.0	2582.1	2510.7	2323.4	2000.7	1564.5	1060.9	532.3	0.0	λ^3
Stage 3	x	4.00	3.99	3.88	3.69	3.09	2.42	1.64	0.82	0.00	
	$\ddot{x}$	0.00	-63.52	-116.62	-138.80	-118.01	-70.86	-26.47	-3.88	0.00	λ
	$\dot{x}$		-7.94	-71.46	-188.28	-327.08	-445.09	-515.95	-542.42	-546.28	λ^2
	x	2644.5	2636.6	2565.1	2376.8	2049.7	1604.6	1088.7	546.3	0.0	λ^3
Stage 4	x	4.000	3.988	3.880	3.695	3.100	2.427	1.647	0.826	0.000	

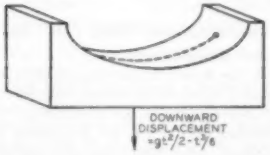

FIG. 1 SYSTEM ILLUSTRATING EXAMPLE 2

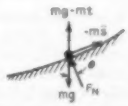

FIG. 2 REAL AND INERTIA FORCES ACTING ON PARTICLE

$\frac{\lambda}{8}[3\dot{x}(e_0) + \dot{x}(e_1)]$, (see Fig. 3*b*).[4] In this case, this gives $\dot{x}(e_{1/2}) = -7.4\lambda^2$. [Recall that $\dot{x}(0) = \dot{x}(e_0) = 0$.] To get $\dot{x}(e_{11/4})$, the shaded area between $e_{1/2}$ and $e_{11/4}$ should be added to $\dot{x}(e_{1/2})$ (see Fig. 3*a*). We presume that the areas of the curvilinear triangles of Fig. 3(*c*) cancel approximately, so that the area in question is approximately that of the dotted rectangle of base λ and height $h = \dot{x}(e_1) = -59.3\lambda$. Thus, $\dot{x}(e_{11/4}) = -7.4\lambda^2 + (\lambda)(-59.3\lambda) = -66.7\lambda^2$. This process is continued so as to get the values exhibited in the third line of Table 1, the common factor, λ^2, being exhibited at the far right. Note that after the first value, $\dot{x}(e_{1/2})$, is obtained, the rest of the values may be obtained simply by adding algebraically the number one line above and half an epoch to the right.

Line 4 of Table 1 is obtained in a similar fashion, but working from the right (where the value of $x(e_8) = x(\tau) = 0$ is known) to the left. Note that simple algebraic addition is the only process used, and note also that the algebraic signs of the entries are positive, e.g., the value $-416.8\lambda^2$ is the value to be added to $x(e_5)$ to get the result $x(e_4) = 877.6\lambda^2$, so that $x(e_4) = 1294.4\lambda^2$. Again the common factor, this time λ^2, is exhibited at the right. The values in line 4 differ from the values in line 1 both because they contain the unknown factor $\lambda^2 = (\tau/8)^2$ and because the values of x chosen initially were not correct.

Therefore the process is repeated using an "assumed" function having the shape given in line 4 of stage 1. The new values of x are obtained by multiplying the values from line 4 of stage 1 by the factor 4/2175.9. Three complete stages of the process are shown in Table 1, and it is seen that the values with which a fourth stage would be started are very close to those with which the third stage was started. While more stages could be carried through so as to obtain greater accuracy, we will now stop and calculate τ. We presume, in effect, that the function with which the third stage was started is correct. Then the values in the fourth line of the third stage should be equal to those in the first line of the third stage, and we have eight equations

$$4.00 = 2644.5\lambda^2$$
$$3.99 = 2636.6\lambda^2$$
$$3.88 = 2565.1\lambda^2$$
and so forth.

Solving these gives

$$\lambda = 0.1148;\ \tau = 0.918$$
$$\lambda = 0.1148;\ \tau = 0.918$$
$$\lambda = 0.1148;\ \tau = 0.918$$
and so forth.

In general, if the convergence has not proceeded to this extent, the values of τ obtained from the several equations will differ slightly, but an average will give good accuracy. It is simplest to obtain the average in the following manner which will be illustrated from the results of the second stage. Adding together all the values in the first line of stage 2 gives $\Sigma = 23.27$; adding together all the values in the fourth line gives $\Sigma' = 15164.6\lambda^2$.

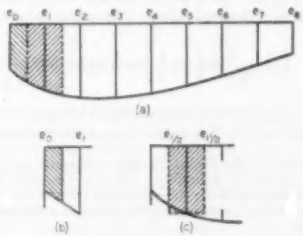

FIG. 3

[4] The present example is a special case in which $\ddot{x}(e_0) = 0$. In later examples the more general situation appears. The factor 8 in the denominator of the formula, is fixed; it bears no relation to the value of n which happens, in this case, to be 8 also.

Equating these gives $\lambda^2 = 0.0015345$, $\lambda = 0.1154$ which is a good approximation to the value obtained from the results of the third stage. Even the first stage with its relatively poor starting values gives a fair approximation, $\lambda = 0.1206$, using this averaging process. The values of x given at the start of stage 4 are sufficiently accurate for most engineering purposes.

Accuracy and Rapidity of Convergence

In the case just worked out an analytical solution is not known. The accuracy of the solution given might be checked by solving the problem by some other method, say, by the method of Störmer.[4] We will illustrate the accuracy and rapidity of convergence by considering an example for which analytical results are readily obtainable.

Example 3. Simple pendulum of length L. The differential equation is

$$\ddot{\theta} + \frac{g}{L}\sin\theta = 0$$

and we will confine attention to the free vibrations with, first of all, a 90-deg amplitude. Using $n = 10$ and starting off with a cosine shape, $\theta(s_k) = (\pi/2)\cos(k\pi/2n)$, the calculations are shown in Table 2. Here, using but four stages, the process has converged to four decimal places. The exact value of τ is

$$\tau = \sqrt{\frac{L}{g}}\,K\left(\sin\frac{\pi}{4}\right) = 1.85407468\sqrt{\frac{L}{g}}$$

where $K(u)$ denotes the complete elliptic integral of the first kind with modulus u (7). The value obtained by the process is

$$\tau = 1.8523\sqrt{\frac{L}{g}}$$

which is in error by 0.1 per cent.

With very little additional labor, however, considerably greater accuracy may be obtained. The error due to the type of approximate integration employed is essentially of the order of n^{-4} where n is the number of intervals (8). Thus, if we repeat the process using another value of n, a simple extrapolation gives a highly refined result. It is easiest to use $n = 5$, starting with alternate (converged) values from Table 2. With very little labor the process may be made to converge to four decimal places and yield $\tau = 1.84692\sqrt{L/g}$ which is in error by 0.4 per cent (which is not a bad error for so little labor). However, by presuming that

$$\tau_n = \tau + c/n^4$$

where τ is the exact result, τ_n is the result obtained using n intervals, and c is a constant, we obtain the equation

$$1.8469\sqrt{L/g} = \tau + c/25$$

$$1.8523\sqrt{L/g} = \tau + c/100$$

and from these we obtain the extrapolated result, $\tau = 1.8541\sqrt{L/g}$ which is correct to four decimal places.

If, instead of using $n = 5$ for the second calculation, we use $n = 20$, starting with the (converged) values from Table 2, with intermediate values estimated by Bessel's formula for interpolation to halves (9), the labor is somewhat greater but the final result is surprisingly accurate. We obtain, after reasonable convergence is achieved, the value $\tau = 1.85361982\sqrt{L/g}$, which is in error by 0.025 per cent. Then, extrapolating with the results for $n = 10$ and $n = 20$, we obtain finally $\tau = 1.85407480\sqrt{L/g}$, which is

[4] This method is developed in most references on the numerical solution of differential equations. Cf., for example, reference (11) which gives a compact derivation (but beware of a few typographical errors). A new engineering textbook (10) also contains a description of the method.

TABLE 2 FREE OSCILLATIONS OF SIMPLE PENDULUM—CALCULATIONS FOR 90 DEG AMPLITUDE

Epoch	0	1	2	3	4	5	6	7	8	9	10	Factor
θ	1.571	1.552	1.494	1.400	1.271	1.111	0.923	0.713	0.485	0.246	0.000	
$\ddot{\theta}$	-1.000	-1.000	-.997	-.985	-.955	-.896	-.797	-.654	-.466	-.244	0.000	ε/L
$\dot{\theta}$		-.500	-1.500	-2.497	-3.482	-4.437	-5.333	-6.130	-6.794	-7.250	-7.494	$\lambda\varepsilon/L$
θ	45.41	44.91	43.41	40.91	37.43	32.99	27.66	21.53	14.74	7.49	0.00	$\lambda^2\varepsilon/L$
θ	1.571	1.554	1.502	1.415	1.295	1.141	0.957	0.745	0.510	0.259	0.000	
$\ddot{\theta}$	-1.000	-1.000	-.998	-.988	-.962	-.909	-.817	-.678	-.488	-.256	0.000	ε/L
$\dot{\theta}$		-.500	-1.500	-2.498	-3.486	-4.448	-5.357	-6.174	-6.852	-7.340	-7.596	$\lambda\varepsilon/L$
θ	45.751	45.251	43.751	41.253	37.767	33.319	27.962	21.788	14.936	7.596	0.000	$\lambda^2\varepsilon/L$
θ	1.5708	1.5536	1.5021	1.4164	1.2967	1.1440	0.9600	0.7481	0.5128	0.2610	0.0	
$\ddot{\theta}$	-1.0000	-.9999	-.9978	-.9881	-.9627	-.9103	-.8192	-.6802	-.4906	-.2580	0.0	ε/L
$\dot{\theta}$		-.5000	-1.4999	-2.4975	-3.4856	-4.4483	-5.3586	-6.1779	-6.8580	-7.3486	-7.6066	$\lambda\varepsilon/L$
θ	45.7809	45.2809	43.7810	41.2835	37.7979	33.3496	27.9610	21.8132	14.9552	7.6066	0.0	$\lambda^2\varepsilon/L$
θ	1.5708	1.5536	1.5022	1.4165	1.2969	1.1443	0.9604	0.7484	0.5131	0.2610	0.0	
$\ddot{\theta}$	-1.0000	-.9999	-.9976	-.9881	-.9627	-.9104	-.8194	-.6805	-.4909	-.2580	0.0	ε/L
$\dot{\theta}$		-.5000	-1.4999	-2.4975	-3.4856	-4.4483	-5.3587	-6.1781	-6.8586	-7.3495	-7.6075	$\lambda\varepsilon/L$
θ	45.7837	45.2837	43.7838	41.2863	37.8007	33.3524	27.9937	21.8156	14.9570	7.6075	0.0	$\lambda^2\varepsilon/L$
θ	1.57080	1.55346	1.50218	1.41649	1.29691	1.14429	0.96044	0.74847	0.51316	0.26101	0.0	

$$\Sigma = 10.9678;\quad \Sigma' = 3.196644\,\tau^2\varepsilon/L;\qquad \tau^2 = 3.4308481\,L/\varepsilon\ ;\quad \tau = 1.852254869\sqrt{L/\varepsilon}$$

in error by 12 units in the eighth decimal place, the percentage error being 0.0000065. In this calculation, the result for $n = 10$ was taken to eight decimal places ($\tau = 1.85225487\sqrt{L/g}$) even though the third decimal place is already in error.

Usually, however, while the engineer may be interested in knowing that such extreme accuracy can be obtained, he is more interested in obtaining reasonably accurate results quickly. That the method leaves little to be desired in this respect is indicated by the results shown in Table 3. In the calculations leading to the results reported in this table only five intervals were used ($n = 5$), and all arithmetic was performed by 10-in. slide rule and mental addition and subtraction, starting with an initial assumption of a cosine shape. Each stage of the calculations required approximately 6 minutes.

TABLE 3 QUARTER-PERIOD OF OSCILLATION OF SIMPLE PENDULUM

Amplitude, deg	(Exact)	One-stage approximation	Two-stage approximation
0	1.5708	...	...
30	1.5981	1.59	...
60	1.6858	1.68	...
90	1.8541	1.84	1.85
120	2.1565	2.12	2.16
150	2.7681	2.60	2.75
180	∞	...	...

NOTE: Values in table to be multiplied by the value of $\sqrt{L/g}$.

FORCED VIBRATION OF A NONLINEAR SYSTEM

The free vibrations of a mass on a nonlinear spring with no damping can be handled by classical methods; two ordinary integrations are performed and the result may be exhibited explicitly in the form of an integral giving time as a function of displacement. If the function defined by the integral has been studied and given a name, and particularly if the inverse function has been studied and named, we generally are more pleased with the solution. This is true in the case studied in Example 3; there we have obtained approximations by the method under discussion and compared them to (better) approximations obtained by more orthodox methods. However, whether the functions defined by the solutions are new or not, the only difficulty present in a classical approach is that involved in performing the quadratures.

This is not the case with the forced oscillations of a mass on a nonlinear spring. Here the problems are essentially far from trivial and essentially far from solution. Since little is known about the theoretical behavior of such systems, the sort of result obtained by most methods which have been employed in their analysis must be regarded as at least partly conjectural. However, here laying aside such questions, we will demonstrate the suitability of the present numerical procedure in obtaining, quickly and conveniently, results similar to those which have been reported.[7]

Example 4. A mass of 15.44 lb vibrates on a spring having the characteristic shown in Fig. 4, and is acted upon by the "sawtooth" periodic force shown in Fig. 5. (Obviously, such a system is unlikely to be encountered in practice. However, it serves as a good example since the free vibrations can easily be investigated by classical means, since simple classical solutions are available for comparison of those forced oscillations having an amplitude no greater than 2 in., and since it illustrates that even a discontinuity in the spring function does not cause trouble with the method.)

[7] While there is some reason to believe that in nonlinear systems there are many frequencies at which forced oscillations, possibly of very distorted shape, may take place with given amplitude, the present method gives only those solutions which are usually presumed to exist.

The point of view adopted is a fairly customary one in which the amplitude of vibration is selected and the frequency is then found at which vibrations of such amplitude can be sustained. Tables 4, 5, and 6 show the final (second) stages of the calculations for an amplitude of 10 in. Table 4 shows the calculations for the free vibrations, Table 5 for the "in-phase" forced vibrations, and Table 6 for the "out-of-phase" forced vibrations.

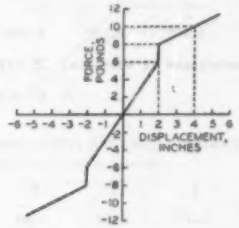

FIG. 4 SPRING CHARACTERISTIC FOR EXAMPLE 4

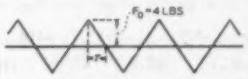

FIG. 5 EXCITING FORCE FOR EXAMPLE 4

The calculations require only a few explanations. The weight is 15.44 lb so that the mass $m = 0.04$ lb-sec^2 per in. To determine $\ddot{x}$, the equation $\ddot{x} = F/m$ is used, the contribution of the spring and of the external force being computed separately and added algebraically. Also, since $n = 10$ in these calculations, the factor of 0.1 has been incorporated in the numbers in the table so that τ and τ^2 appear at the right rather than λ ($= \tau/10$) and λ^2 ($= \tau^2/100$). A cosine shape was used as the starting approximation for the free vibrations and the final result for the free vibrations was used as the starting approximation for the forced vibrations. The progress toward convergence was accelerated slightly by "guessing ahead" or "crystal-ball extrapolation," so that reasonable accuracy was obtained with only two stages for each calculation.

An indication of the accuracy of the method is given in Table 7 which compares frequencies corresponding to several different amplitudes of free vibration as computed by both classical methods and the present numerical procedure. The "response curve" is shown in Fig. 6. Only one curve is shown for forced oscillations corresponding to the exciting force of 4 lb amplitude shown in Fig. 5. In converting quarter-period τ to circular frequency ω, the obvious relation $\omega = \pi/2\tau$ has been used. Points on the curves of Fig. 6, which are denoted by small circles, represent results obtained by the numerical procedure; solid lines represent plots of data obtained by classical methods, and dotted lines have been faired between points given by the numerical procedure in the case of forced oscillations for which there is no (reasonably simple) classical solution. For reasons already alluded to, no

TABLE 7 FREQUENCY OF FREE OSCILLATIONS OF SYSTEM OF EXAMPLE 4

Amplitude, in.	Circular frequency ω — Classical method	Circular frequency ω — Numerical method
1.5	8.6608	8.67
2.0	8.6603	8.67
3.0	8.9320	8.95
4.0	8.3041	8.29
10.0	6.6076	6.61

TABLE 4 FREE OSCILLATIONS OF 10 IN. AMPLITUDE FOR SYSTEM OF EXAMPLE 4

(Second stage of calculations. First stage started with cosine shape)

Epoch	0	1	2	3	4	5	6	7	8	9	10	Factor
x	10.000	9.887	9.550	8.993	8.224	7.284	6.098	4.770	3.291	1.681	0	
$\ddot{x}$	-400.0	-397.2	-388.8	-374.8	-355.6	-331.4	-302.4	-269.2	-232.3	-126.1	0	
$\dot{x}$		-19.96	-59.68	-98.86	-136.04	-171.60	-204.74	-234.98	-261.90	-285.13	-297.74	τ
x	177.033	175.037	169.069	159.213	145.609	128.449	107.975	84.477	58.287	29.774	0	τ^2
x	10.000	9.887	9.550	8.993	8.225	7.256	6.099	4.772	3.292	1.682	0	

Convergence is adequate. $\Sigma = 69.748$; $\Sigma' = 1234.923\ \tau^2$;

$\therefore\ \tau^2 = 0.0564796$; $\tau = 0.23765$; $\omega = 6.6097$

TABLE 5 IN-PHASE FORCED OSCILLATIONS OF 10 IN. AMPLITUDE FOR SYSTEM OF EXAMPLE 4

(Second stage of calculations. First stage started with final result for free oscillations)

Epoch	0	1	2	3	4	5	6	7	8	9	10	Factor
x	10.00	9.89	9.58	9.04	8.30	7.34	6.20	4.87	3.37	1.72	0	
$(F/m)_1$	-400	-397	-390	-378	-358	-334	-306	-272	-234	-129	0	
$(F/m)_2$	100	90	80	70	60	50	40	30	20	10	0	
$\ddot{x}$	-300	-307	-310	-308	-298	-284	-265	-242	-214	-119		
$\dot{x}$		-15.1	-45.8	-76.9	-107.4	-137.2	-165.6	-192.1	-216.3	-237.7	-249.6	τ
x	144.36	142.85	138.27	130.59	119.85	106.13	89.57	70.36	48.73	24.96	0	τ^2
x	10.000	9.895	9.578	9.046	8.302	7.352	6.206	4.874	3.376	1.729	0	

Convergence is adequate. $\Sigma = 70.31$; $\Sigma' = 1015.67\ \tau^2$;

$\tau^2 = 0.069225$; $\tau = 0.2631$; $\omega = 5.970$

Note: $(F/m)_1$ denotes acceleration due to spring force; $(F/m)_2$ denotes acceleration due to external force.

TABLE 6 OUT-OF-PHASE FORCED OSCILLATIONS OF 10 IN. AMPLITUDE FOR SYSTEM OF EXAMPLE 4

(Second stage of calculations. First stage started with final result for free oscillations)

Epoch	0	1	2	3	4	5	6	7	8	9	10	Factor
x	10.00	9.88	9.53	8.96	8.18	7.19	6.03	4.71	3.24	1.65	0	
$(F/m)_1$	-400	-397	-388	-374	-354	-330	-301	-268	-231	-124	0	
$(F/m)_2$	-100	-90	-80	-70	-60	-50	-40	-30	-20	-10	0	
$\ddot{x}$	-500	-487	-468	-444	-414	-380	-341	-298	-251	-134	0	
$\dot{x}$		-24.8	-73.5	-120.3	-164.7	-206.1	-244.1	-278.2	-308.0	-333.1	-346.5	τ
x	209.93	207.45	200.10	188.07	171.60	150.99	126.58	98.76	67.96	34.65	0	τ^2
x	10.00	9.88	9.53	8.96	8.17	7.19	6.03	4.70	3.24	1.65	0	

Convergence is adequate. $\Sigma = 69.37$; $\Sigma' = 1456.09\ \tau^2$;

$\tau^2 = 0.047641$; $\tau = 0.2183$; $\omega = 7.20$

Note: $(F/m)_1$ denotes acceleration due to spring force; $(F/m)_2$ denotes acceleration due to external force.

attempt has been made to extend the curves into the low-frequency range.

Nonsymmetrical Elasticity

In most actual elastic systems, there is a fiduciary value of displacement with respect to which the elasticity is symmetrical. However, because of the presence of steady loads, such as the weight of the body, vibrations will not take place with this fiduciary position as center but will rather occur about the equilibrium position. Therefore, as Rauscher points out (1), usually in actual systems the elasticity is nonsymmetrical with respect to the equilibrium position. No essential difficulty is involved in computing the free vibrations by the present or by a classical method; each "half" cycle may be analyzed separately, and the two parts adjoined to give the full cycle. If the "amplitude" on one side is assumed, that on the other side may easily be determined by obvious energy considerations.

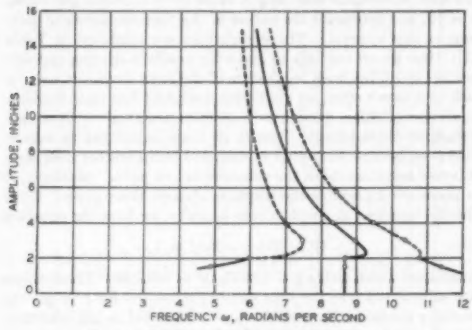

Fig. 6 Response Curves for Example 4

(The circles represent results obtained by the present numerical process. The solid lines represent known solutions and the dotted lines have been faired between the appropriate circles.)

An essential difficulty is, however, involved in the case of forced vibrations of a nonsymmetrical system. The present method may be used to compute such vibrations, but the convergence is not so rapid, the ability to make an excellent starting approximation being sacrificed. This application, next to be described, has not yet been investigated sufficiently to permit a comparison with Rauscher's method, although it seems likely that the present method may suffer in such comparison. A problem treated by Rauscher (1) will be used here to illustrate the procedure.

Example 5. A unit mass is on a spring having the characteristic shown in Fig. 7, and is acted upon by an external force $F = 0.1 \cos \omega t$. The displacement on the "soft" side is 1.5 (units). The free motion for the soft side is determined as if the spring were as shown in Fig. 8. The characteristics of this free motion are shown in Table 8 and the time required for this quarter cycle is $\tau = 2.170$ (units). On the hard side, because of the linearity the quarter-cycle is a pure cosine curve with amplitude 1.32 and quarter-period 1.571.

The free motion is taken as the first approximation to the forced motion. (This logical choice, which was also used in the preceding example, appears to have been first suggested by Rauscher.) In these calculations, the symbol λ will denote one tenth of the time required for the mass to move from $x = 1.5$ to $x = 0$. Thus the mass reaches its extreme negative position at $t = (10 + 1.571/.2170)\lambda = 17.42\,\lambda$. The first assumed displacement-time relation is thus as shown in the first line of the first stage of Table 9. The spring force is then easily calculated. Since $17.24\,\lambda\omega = \pi$, i.e., the external force has reversed itself when $t = 17.24\lambda$, the value of the external force is easily determined at each epoch. The first stage of the calculation is then carried out as indicated. Note in the last line of the first and succeding stages that $x = 0$ when $t = 10\lambda$. Note also that it is the "out-of-phase" motion being considered.

TABLE 8 TIME-DISPLACEMENT RELATION FOR FREE VIBRATIONS ON SOFT SIDE OF SYSTEM OF EXAMPLE 5

Epoch	0	1	2	3	4	5
x	1.500	1.488	1.452	1.390	1.300	1.176
Epoch	6	7	8	9	10	
x	1.104	0.806	0.557	0.286	0.000	

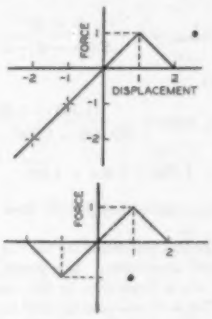

Fig. 7 (*above*) Spring Characteristic for Example 5

Fig. 8 (*below*) Spring Characteristic for Free Motion on Soft Side—Example 5

The second stage is started in the usual fashion and the spring force is determined. To compute the external force, a new approximation for $\lambda\omega$ is necessary. This is obtained by a "parabolic" interpolation as follows:

Let

b = maximum numerical value of x near right end (here at epoch 17)
a = numerical value of x one epoch to left
c = numerical value of x one epoch to right

(here the expression "numerical value" is used to mean "modulus" or "absolute value"); then, the extreme value obtains when

$$t = r\lambda + \frac{\lambda(c - a)}{2(2b - a - c)}$$

where r is the number of the epoch corresponding to b. Thus in this case

$$t = 17\lambda + \frac{\lambda(1.272 - 1.243)}{2(2.574 - 1.272 - 1.243)} = 17.246\lambda$$

The external force is then computed and the stage completed. Four stages are shown in Table 9. (Convergence was delayed by a misguided attempt to "guess ahead" at the beginning of stage 3.)

The values of x at the start of a fifth stage are sufficiently close to those at the start of the fourth stage to permit calculating final results from the fourth stage. We find that $17.364\lambda\omega = \pi$, and to determine λ, we use the same averaging process as before, obtaining for the sum of the numerical or absolute values of x in the first line of stage 4, the value $\Sigma = 18.434$. Similarly, for the last line of stage 4, $\Sigma' = 440.135\lambda^2$. Thus $\lambda = 0.20465$.

(In obtaining these sums, do not add algebraically, for if this is done, the values largely cancel out, emphasizing rather than minimizing the error.) Thus we obtain $\omega = 0.8841$. To get the maximum deflection on the hard (negative) side, a parabolic interpolation is used for which the formula is

$$|x|_{max} = b + \frac{(c-a)^2}{8\,(2b-a-c)}$$

In this case we have

$$|x|_{max} = 1.298 + \frac{(1.290-1.248)^2}{8(2.596-1.290-1.248)}$$

$$= 1.298 + 0.004 = 1.302$$

These values seem to agree closely with those given graphically by Rauscher (1).

Calculations were also performed for the "in-phase" vibrations of 1.5 unit (soft-side) amplitude. As a check, the classical solution was carried out, a possibility in the case of a "piecewise linear" spring. This is an elaborately unpleasant task requiring several times the effort of the numerical approximation because of the necessity of solving simultaneous transcendental equations. The present numerical method gives $\omega = 0.7946$ while the classical method gives $\omega = 0.7935$, the last figure being in doubt. A check by the classical solution was not obtained for the out-of-phase vibrations.

In nonsymmetrical cases, the time for motion on the positive side will be either greater (as in Example 5), or less than the time for motion on the negative side. It seems better to use the longer time as the basic time to be divided into exactly n intervals of duration λ, as was done in Example 5 where the longer time was 10λ and the shorter time was about 7.3λ.

Nonhomogeneous Functions of t, Other Initial Conditions

In all the examples so far, the function $g(x, t)$ has been a homogeneous function of t. In Example 2 it was homogeneous in t of degree one, while in the other examples it was of degree zero (actually not a function of t at all). The same general method with only a slight modification serves, however, to analyze cases in which $g(x, t)$ is not homogeneous in t. This will be illustrated in the following:

Example 6:

$$\ddot{x} + x^2\dot{x}^2 + x^3 = 0; \quad x(0) = 4, \dot{x}(0) = 0$$

Using $n = 8$, the calculations are indicated in Table 10. The first assumed function has a (rough) cosine shape. The values of $\ddot{x}$, $\dot{x}$, and x which are calculated are not homogeneous in t and must be exhibited in two parts as indicated in Table 10. For example, at epoch e_5, $t = 5\lambda$, and $\ddot{x} = -(2.1)^2(5\lambda)^3 - (2.1)^2 = -231.5\lambda^3 - 4.4$. The successive integrations are performed keeping the two nonhomogeneous parts separate. Then from the approximate equation $\Sigma = \Sigma'$, which in this case takes the form $22.2 = 1932\lambda^2 + 34745\lambda^4$, it is easy to solve for $\lambda^2 = 0.0098$, the negative root, $\lambda^2 = -0.0654$, being rejected as without physical significance. With $\lambda^2 = 0.0098$, the obvious substitutions are made in the next to last line of stage 1 to obtain the values exhibited in the last line of stage 1. These results are still in error and the first line of stage 2 is obtained by multiplying the entries in the last line of stage 1 by the factor 4/4.0376. The second stage is completed in the same fashion and indicates satisfactory convergence. In the calculations of the second stage, it was necessary to solve for $\lambda^2 = 0.009694$, and the degree of convergence indicates that this value is satisfactory. From this, then, we obtain $\lambda = 0.09846$, $\tau = 8\lambda = 0.7877$.

The idea of keeping nonhomogeneous parts separate may also be used to extend the method to cases in which the initial velocity is not zero and in which the displacement does not vanish at some later time. This application will be illustrated by the following:

Example 7:

$$\ddot{x} - x^3 = 0, x(0) = 1, \dot{x}(0) = 3$$

We shall investigate how long it takes for x to attain the value, $x = 10$, and determine the nature of the time-displacement relation in this interval. The calculations are exhibited in Table 11. Here we are not able to make the excellent starting approximation which has been the feature of the other examples, and for lack of a better start, we start with a straight line time-displacement curve, which, using $n = 9$, permits us to start with integer values of displacement. Values of $\ddot{x}$ are calculated as before. However, because the initial velocity is 3 (units) rather than zero, it is necessary to exhibit the velocities in two parts. Similarly, it is necessary to exhibit the displacements in three parts. Since the displacement at epoch e_9 is to be unity, we have the equation

$$10 - 27\lambda - 824\lambda^3 = 1$$

solution of which yields $\lambda = 0.0894$; $\lambda^3 = 0.00799$. These values are substituted into the appropriate expressions for x to get the starting values for the second stage. These values are exhibited, but the convergence is slow, so all of the second stage is not shown in Table 11. The sixth stage is shown completely, however. The fact that the initial displacement must be unity yields an equation for λ which gives $\lambda = 0.127196$, $\lambda^3 = 0.0161788$. These values when substituted into the values for x in the sixth stage give starting values for a seventh stage as shown. Since these are almost unchanged, the process is terminated. Finally, the value for λ may be somewhat refined. Using the averaging process described before on the results of stage six, the following equation is obtained

$$100 - 135\lambda - 2624.237\lambda^3 = 40.369$$

This yields $\lambda = 0.127199$, differing by three units in the last figure from the result obtained earlier. From this, $\tau = 1.14479$, where τ is the time required for the displacement to attain the value 10. While this value may be checked by evaluating the solution in the form of an elliptical integral, this has not been done because of the labor of the evaluation.

In Example 7, the function, $g(x, t)$ was homogeneous in t. If it had not been, the procedure would have been obvious, but it would have involved separating the entries in the table into even more parts.

Remarks

It is to be emphasized that the calculations are not nearly as formidable as would be indicated by a cursory glance at any of the tabulations accompanying this paper. As a matter of fact, it is not necessary actually to construct the tables. Except for occasional multiplications and divisions, the bulk of the computation is simply algebraic addition. Use of an adding machine which prints a tape and has a subtotal button eliminates most of the pencil work. The first value of a row of the calculations is put into the machine and the subtotal button is punched; then the next value is added algebraically and a subtotal taken, and so on. The tape then becomes a record of the row of the calculation, the subtotals being the values used in the next "integration" or process of successive algebraic addition.

As is indicated by the application of the procedure in Example 2, it may be used in cases where the parameters of the system are functions of time. It is believed that for calculations giving

TABLE 9 CALCULATION OF OUT-OF-PHASE OSCILLATIONS FOR EXAMPLE 5

Epoch	0	1	2	3	4	5	6	7	8	9	10	11	12	13	14	15	16	17	18	Factor
x	1.50	1.49	1.45	1.39	1.30	1.18	1.01	0.81	0.56	0.29	0.00	−0.29	−0.56	−0.80	−1.00	−1.17	−1.27	−1.31	−1.30	
SF	−.50	−.51	−.55	−.61	−.70	−.82	−.99	−.81	−.56	−.29	0.00	.29	.56	.80	1.00	1.17	1.27	1.31	1.30	
EF	−.10	−.10	−.09	−.08	−.07	−.06	−.04	−.03	−.01	.01	.02	.04	.06	.07	.08	.09	.10	.10	.10	
I	−.60	−.61	−.64	−.67	−.77	−.88	−1.03	−.84	−.57	−.28	.02	.32	.62	.87	1.08	1.26	1.37	1.41	1.40	
ẋ	−.30	−.91	−1.55	−2.22	−2.99	−3.87	−4.90	−5.74	−6.31	−6.59	−6.57	−6.25	−5.63	−4.76	−3.68	−2.42	−1.06	0.36		λ
x	35.38	35.08	34.17	32.62	30.40	27.41	23.54	18.64	12.90	6.89	0.00	−6.57	−12.82	−18.46	−23.21	−26.89	−29.31	−30.36	−30.00	λ^2
x	1.500	1.487	1.449	1.383	1.289	1.162	0.998	0.798	0.567	0.279	0.000	−0.278	−0.543	−0.782	−0.984	−1.140	−1.243	−1.287	−1.272	
SF	−.500	−.513	−.551	−.617	−.711	−.836	−.999	−.798	−.567	−.279	0.000	.278	.543	.782	.984	1.140	1.243	1.287	1.272	
EF	−.100	−.098	−.094	−.085	−.073	−.061	−.046	−.029	−.011	.006	.025	.042	.058	.072	.085	.092	.097	.100	.099	
I	−.600	−.611	−.645	−.702	−.795	−.899	−1.044	−.819	−.586	−.273	.025	.320	.601	.854	1.067	1.232	1.340	1.387	1.371	
ẋ	−.301	−.911	−1.557	−2.259	−3.045	−3.944	−4.988	−5.807	−6.365	−6.638	−6.613	−6.293	−5.692	−4.838	−3.771	−2.539	−1.199	0.188		λ
x	35.816	35.515	34.603	33.046	30.787	27.762	23.798	18.810	12.003	6.838	0.000	−6.613	−12.906	−18.598	−23.436	−27.207	−29.746	−30.945	−30.757	λ^2
x	1.500	1.487	1.449	1.384	1.289	1.162	0.997	0.787	0.544	0.278	0.000	−0.277	−0.540	−0.778	−0.981	−1.139	−1.245	−1.292	−1.280	
SF	−.500	−.513	−.551	−.616	−.711	−.838	−.997	−.787	−.544	−.278	0.000	.277	.540	.778	.981	1.139	1.245	1.292	1.280	
EF	−.100	−.098	−.094	−.086	−.075	−.062	−.047	−.030	−.012	.006	.024	.041	.056	.070	.082	.091	.097	.099	.099	
I	−.600	−.611	−.645	−.702	−.786	−.900	−1.044	−.817	−.556	−.272	.024	.318	.596	.848	1.063	1.230	1.342	1.391	1.379	
ẋ	−.301	−.912	−1.557	−2.259	−3.045	−3.945	−4.989	−5.808	−6.362	−6.634	−6.610	−6.292	−5.696	−4.848	−3.785	−2.556	−1.215	0.176		λ
x	35.810	35.509	34.597	33.040	30.781	27.756	23.791	18.802	12.996	6.834	0.000	−6.610	−12.902	−18.588	−23.446	−27.231	−29.786	−30.999	−30.821	λ^2
x	1.500	1.487	1.449	1.384	1.289	1.162	0.997	0.788	0.544	0.278	0.000	−0.277	−0.540	−0.779	−0.982	−1.141	−1.246	−1.296	−1.291	
SF	−.500	−.513	−.551	−.616	−.711	−.838	−.997	−.788	−.544	−.278	0.000	.277	.540	.779	.982	1.141	1.246	1.296	1.291	
EF	−.100	−.098	−.094	−.086	−.075	−.062	−.047	−.030	−.012	.006	.023	.041	.056	.070	.082	.091	.097	.100	.099	
I	−.600	−.611	−.645	−.702	−.786	−.900	−1.044	−.816	−.586	−.272	.023	.319	.596	.849	1.064	1.232	1.345	1.395	1.390	
ẋ	−.301	−.912	−1.557	−2.259	−3.045	−3.945	−4.989	−5.807	−6.363	−6.635	−6.612	−6.294	−5.698	−4.849	−3.785	−2.553	−1.208	0.180		λ
x	35.813	35.512	34.600	33.043	30.784	27.759	23.794	18.805	12.998	6.835	0.000	−6.612	−12.906	−18.604	−23.463	−27.238	−29.791	−30.999	−30.809	λ^2
x	1.500	1.487	1.449	1.384	1.289	1.162	0.997	0.788	0.544	0.278	0.000	−0.277	−0.541	−0.779	−0.982	−1.141	−1.246	−1.296	−1.290	

SF denotes spring force; EF denotes external (exciting) force.

TABLE 10 SOLUTION OF EXAMPLE 6

Epoch	0	1	2	3	4	5	6	7	8	Factor
x	4.0	3.9	3.7	3.3	2.8	2.1	1.5	0.8	0	
ẋ	−16.0	−15.3	−13.7	−10.9	−7.8	−4.4	−2.2	−0.6	0	$\bar{\lambda}^4$
	0.0	−59.3	−202.6	−323.4	−351.2	−231.5	−121.5	−25.1	0	
ẋ	−7.9	−23.2	−36.9	−47.8	−55.6	−60.0	−62.2	−62.8		λ_3
	−7.4	−66.7	−209.3	−592.7	−913.9	−1175.4	−1296.9	−1322.0		λ^3
x	356.4	348.5	325.3	288.4	240.6	185.0	125.0	62.8	0	λ^4
	5674	5667	5600	5331	4736	3794	2619	1322	0	λ^5
x	4.0376	3.9892	3.7260	3.3379	2.8126	2.1776	1.4769	0.7428	0	
x	4.000	3.922	3.691	3.307	2.786	2.157	1.463	0.736	0	
ẋ	−16.000	−15.382	−13.623	−10.936	−7.762	−4.653	−2.140	−0.542	0	$\bar{\lambda}^4$
	0.000	−60.33	−201.14	−325.60	−345.99	−250.59	−112.75	−19.54	0	
ẋ	−7.92	−23.30	−36.93	−47.86	−55.63	−60.28	−62.42	−62.96		λ_3
	−7.5	−67.9	−269.0	−594.5	−940.5	−1191.4	−1304.1	−1323.7		λ^3
x	367.30	349.38	326.08	289.15	241.29	185.66	125.36	62.96	0	λ^4
	5698.6	5691.1	5625.2	5354.2	4795.7	3819.2	2627.6	1323.7	0	λ^5
x	3.9992	3.9217	3.6894	3.3061	2.7897	2.1587	1.4623	0.7347	0	

TABLE 11 SOLUTION OF EXAMPLE 7

Epoch	0	1	2	3	4	5	6	7	8	9	Factor
x	1	2	3	4	5	6	7	8	9	10	
$\bar{x}$	1	4	9	16	25	36	49	64	81	100	
$\dot{x}$	$\frac{3}{0.9}$	$\frac{3}{4.9}$	$\frac{3}{13.9}$	$\frac{3}{29.9}$	$\frac{3}{54.9}$	$\frac{3}{90.0}$	$\frac{3}{139.9}$	$\frac{3}{203.9}$	$\frac{3}{284.9}$		$\bar{\lambda}$
x	10	10	10	10	10	10	10	10	10	10	$\bar{\lambda}$
	-27	-24	-21	-18	-15	-12	-9	-6	-3	0	λ
	-824	-823	-818	-804	-774	-720	-629	-489	-285	0	λ^2
x	1.00	1.28	1.58	1.96	2.47	3.17	4.17	5.56	7.45	10.00	

The line above represents the starting values for stage 2, the rest of which is omitted. Stages 3, 4, and 5 are likewise omitted. Stage 6 follows. Note that the first line for $\dot{x}$ and the first two lines for x are the same in all stages and do not have to have to be written explicitely in stages after the first.

x	1.000	1.391	1.814	2.290	2.851	3.544	4.439	5.654	7.386	10.000
$\bar{x}$	1.0000	1.9348	3.2906	5.2441	8.1282	12.5699	19.7047	31.9677	54.5530	100.0000
$\dot{x}$	0.6168	2.5516	5.8422	11.0863	19.2145	31.7744	51.4791	83.4468	137.9998	
x	344.0115	343.3957	340.8431	335.0009	323.9146	304.7001	272.9257	221.4466	137.9998	0
x	1.0000	1.3916	1.8146	2.2905	2.8515	3.5440	4.4396	5.6541	7.3857	10.0000

engineering accuracy, this method is superior to the method of Störmer. For example, the reader is invited to compare the labor involved in using this method to that involved in using Störmer's method in a problem given by Timoshenko and Young to illustrate the use of Störmer's method (10). Even in cases where it is necessary to have the assurance of extreme accuracy that is given by the use of Störmer's or other step-by-step method using many higher differences, the present method seems an excellent way of obtaining good starting values from which the necessary differences may be obtained. Available "check" formulas may then be used to improve the starting values before the step-by-step process is continued.[8]

The method has been tried with a damping (first derivative) term in the differential equation, but because of the unknown phase involved between the displacement and the forcing function and because of the fact that the velocities are required for integer rather than half-integer values of the epochs necessitating the use of interpolation or of another method of numerical integration, the calculations are voluminous and very slowly convergent if not actually divergent. While it is planned to give further study to the matter, at present no success can be reported with attempts to include damping.

A remark is called for concerning the errors (operator's mistakes) which are bound to occur in any numerical process. Only those errors which are made in the final stage or in subsequent calculations are serious; since each stage is, in effect, a fresh start, errors made in earlier stages "wash out" although they may impede convergence, especially if they are large. Only experience can advise whether it is more advantageous to go ahead disregarding an error or to go back and correct the error. In the final stage, however, errors can be serious; ordinarily, one can anticipate which will prove to be the final stage and can accordingly exercise more than average care.

Finally, while the advantages of good "guessing ahead" are obvious, this is difficult to do, and, frequently, attempts to guess ahead impede rather than accelerate convergence. The author has found by experience that unless the crystal ball is very clear, it is better to let the process run itself more or less automatically and to awake with a pleasant start to find that it has converged sufficiently.

[8] Cf. reference (11), and reference (9), p. 227.

BIBLIOGRAPHY

1 "Steady Oscillations of Systems With Nonlinear and Unsymmetrical Elasticity," by M. Rauscher, JOURNAL OF APPLIED MECHANICS, Trans. ASME, vol. 60, 1938, p. A-169. Discussion, JOURNAL OF APPLIED MECHANICS, Trans. ASME, vol. 61, 1939, p. A-91.

2 "Steady Forced Oscillations of Permanent Nonlinear Systems," by M. Rauscher, Proceedings of the Fifth International Congress for Applied Mechanics, Sept. 12–16, 1938, pp. 681–684.

3 Thesis, by M. Rauscher, Massachusetts Institute of Technology, 1936 (available on microfilm).

4 "An Experimental Investigation of Forced Vibrations in a Mechanical System Having a Nonlinear Restoring Force," by C. A. Ludeke, *Journal of Applied Physics*, vol. 17, 1946, pp. 603–609.

5 "Mechanical Vibrations," by J. P. Den Hartog, third edition, McGraw-Hill Book Company, Inc., New York, N. Y., 1947, p. 434.

6 "Nonlinear Vibrations" (notes), by J. J. Stoker and A. S. Peters, New York University, New York, N. Y., 1942, p. 47.

7 "Smithsonian Mathematical Formulae and Tables of Elliptic Functions," by E. P. Adams and R. L. Hippisley, Smithsonian Institution, Washington, D. C., 1939, p. 277.

8 "Aufgaben und Lehrsätze aus der Analysis," by G. Pólya and G. Szegö, Dover Publications, vol. 1, 1945, p. 37; problems 11 and 12 of chapt. 2.

9 "Numerical Mathematical Analysis," by J. B. Scarborough, Johns Hopkins University, Baltimore, Md 1930, p. 64.

10 "Advanced Dynamics," by S. Timoshenko and D. H. Young, McGraw-Hill Book Company, Inc., New York, N. Y., 1948, p. 69.

11 "Numerical Integration of Differential Equations," by A. A. Bennett, W. E. Milne, and H. Bateman, National Research Council Bulletin no. 92, Washington, D. C., 1933, pp. 81–83.

Appendix

NOTE ON EXAMPLE 2

Example 2 may be regarded simply as a mathematical exercise designed to illustrate the application of the numerical method to a fairly general case which exhibits features to be found in a variety of physical systems; on the other hand, it may be given a physical realization as follows:

Consider a material particle free to slide without friction on the

cylindrically concave upper surface of a block which is displaced downward (from some fiduciary level) according to the law

$$\text{Downward displacement} = gt^2/2 - t^3/6$$

(where g represents the acceleration of gravity) so that its downward acceleration is $g - t$ (see Fig. 1.) The concave upper surface of the block has the shape given by the equation $y = bs^4$, in which y is the height above the lowest point, s is the arc length of the curve measured from the lowest point, and b is a constant which will be selected later.

Fig. 2 shows actual and inertia forces acting on the particle at a general position. The differential equation of motion is obviously $m\ddot{s} + mt \sin\theta = 0$, from which the common factor m may be canceled. However, for the curved path, $\sin\theta = dy/ds = 4bs^3$, so that we have $\ddot{s} + 4bts^3 = 0$. By introducing a new dependent variable $x = 2s\sqrt{b}$, this becomes $\ddot{x} + x^3t = 0$, which is the equation of Example 2. Since $x(0) = 4$, in the example, we have $s(0) = 2/\sqrt{b}$. But, when $t = 0$, $dy/ds = 4bs^3(0) = 32/\sqrt{b}$, and this must not be greater than unity. Therefore we must choose, b so as to satisfy the condition, $b \geq 1024$, for, unless this is so, the initial condition may not be satisfied.

The curve of the upper surface of the block, which is given simply in terms of ordinate and arc length by the equation $y = bs^4$, is more difficult to express in Cartesian form, but it may be done in terms of incomplete beta functions, or in the form

$$x = \sqrt[4]{\frac{y}{b}} \sum_{k=0}^{\infty} \binom{1/4}{k} \frac{(-16y\sqrt{by})^k}{6k+1}.$$

Note, here, that x denotes the abscissa of a point on the curve while earlier in this appendix, x denoted a dependent variable proportional to arc length. The curve is horizontal at the origin and ends, with a vertical tangent, when $s = (4b)^{-1/3}$. Note that $s(0) = 2/\sqrt{b} \leq (4b)^{-1/3}$, since $b \geq 1024$.

Similarly, Examples 6 and 7 which appear later, may be thought of as simply mathematical exercises to illustrate the use of the procedure, or physical realizations may be designed in a fashion similar to the preceding.

Thermal Effects in Calendering Viscous Fluids[1]

By M. FINSTON,[2] CAMBRIDGE, MASS.

Calendering (rolling) of plastics at high speeds produces blistering and peeling which are attributed to a combination of uneven temperature distribution, and effect of temperature on the physical properties of the material. In this paper the problem is examined by studying the calendering of a viscous liquid in some detail. It is shown that a thermal boundary-layer effect exists of such magnitude as to account for formation of blisters. An example is given using typical calendering dimensions and physical properties of a plastic, which yields a thermal boundary-layer thickness of the order of depth of the blisters as observed. These data furnish further qualitative confirmation to the physical argument.

Introduction

CALENDERING of plastics is a process in which a mass of material is rolled between cylinders to form a smooth sheet of uniform thickness, Fig. 1. Gaskell (1, 2)[3] has pointed

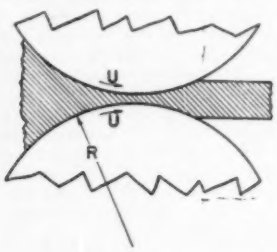

Fig. 1

out that some features of the process can be explained only by considering the somewhat complicated rheological properties of the material being worked and has discussed some of these in detail. However, recent experimental studies[4] have uncovered an important phenomenon whose main features may be explained by considering the calendering of a viscous fluid with viscosity dependent upon temperature.

When calendering is carried out at sufficiently high speeds, the sheet produced has blisterlike formations which seem to originate a short distance beneath the surface. At still higher speeds, these blisters spread in area, and a thin layer may peel away and cling to the roll, Fig. 2. These effects may be explained by considering

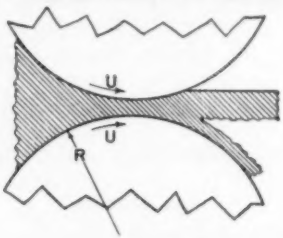

Fig. 2

the temperature distribution set up by shear forces and by the effect of temperature on the physical properties of the material. As the plastic passes between the rolls it undergoes shear forces which are high near the rolls and low at the center of the sheet. Since the materials used have low heat conductivity, the temperature distribution resulting from local heat dissipation is not smoothed out, and the temperature is also highest at the rolls. Furthermore, low conductivity prevents wall cooling from penetrating more than a short distance into the medium so that its effect is to reduce the maximum temperature slightly and also move its position into the interior of the plastic. If the maximum is large enough, the cohesion of the plastic may be reduced below the adhesion between wall and plastic. Then there will be a tendency for the material to stick to the rolls and the observed blisters to form. The maximum temperature will increase with speed so that finally the drop in cohesion is sufficient to permit peeling.

In this paper the problem is examined by studying the calendering of a viscous liquid in more detail. It is shown that there is a thermal boundary-layer effect of sufficient magnitude to account for the formation of blisters. Also, an example using typical calendering dimensions and physical properties of a plastic, is carried out which yields a thermal boundary-layer thickness of the order of depth of the blisters as observed, giving further qualitative confirmation to the physical argument.

Since the length of the curved channel formed by the rolls is very small compared with the axial length of the cylinders, the flow is taken as two-dimensional. Also, both roll speeds are assumed equal, and the roll surfaces are at equal uniform temperatures. The inlet to the channel is taken as the point of maximum

[1] The results in this paper were obtained at Brown University, on a project sponsored by the Armstrong Cork Company, and are substantially those contained in a thesis submitted as partial fulfillment of the requirements for the degree of Doctor of Philosophy in Applied Mathematics, June, 1949. The author wishes to thank Professors William Prager and George F. Carrier who suggested the problem and offered continuous and detailed advice. Dr. G. W. Scott, Jr., and Mr. J. T. Bergen made many helpful suggestions and provided much interesting experimental information.

[2] Naval Supersonic Laboratory, Department of Aeronautical Engineering, Massachusetts Institute of Technology; formerly at Brown University, Providence, R. I.

[3] Numbers in parentheses refer to the Bibliography at the end of the paper.

Contributed by the Applied Mechanics Division and presented at the Semi-Annual Meeting, St. Louis, Mo., June 19–23, 1950, of The American Society of Mechanical Engineers.

Discussion of this paper should be addressed to the Secretary, ASME, 29 West 39th Street, New York, N. Y., and will be accepted until April 10, 1951, for publication at a later date. Discussion received after the closing date will be returned

Note: Statements and opinions advanced in papers are to be understood as individual expressions of their authors and not those of the Society. Manuscript received by the Applied Mechanics Division, November 3, 1949. Paper No. 50—SA-13.

[4] Communicated by J. T. Bergen and G. W. Scott, Jr.

pressure along the channel center line as observed in experiments, and the velocity, for convenience, is assumed uniform there.[5]

In brief, the mathematical procedure is as follows: The equations implying the conservation of mass, momentum, and energy are written in full for the two-dimensional flow of an incompressible fluid of variable viscosity. The fact that the passage width is small compared to the passage length permits the equations to be simplified in a systematic manner (section on Viscosity-Temperature Relationship). An approximate relation between the viscosity and temperature is introduced into these equations. In the forms so obtained, it is convenient to carry out a perturbation about the constant-viscosity solution. This yields sets of linear partial differential equations for the velocity, pressure, and temperature distributions. These are solved, subject to the conditions that the temperature is uniform at the inlet section and is maintained at a constant value along the rolls. The velocity of the fluid at the roll surface, of course, is that of the rolls, i.e., no slip.

Each of the first-order equations found by the perturbation scheme may be solved by explicit integration while further approximations are obtained numerically.

Equations of Motion

The equations of conservation of mass, momentum, and energy are well known (3). For a two-dimensional flow of an incompressible variable-viscosity fluid, when body forces are absent, they may be put in the form

$$u_{i,i} = 0 \qquad [1]$$

$$\rho u_{j,i}\, u_i = -p_{,j} + [\mu e_{ij}]_{,i} \qquad [2]$$

and

$$kT_{,ii} - \rho c u_i T_{,i} + \Phi = 0 \qquad [3]$$

respectively. Here ρ, k, c, μ denote the density, thermal conductivity, specific heat, and viscosity, respectively; u_i is a velocity component; p, the pressure; e_{ij} the rate of strain given by $u_{i,j} + u_{j,i}$; T, the temperature distribution; and Φ, the dissipation given by $\frac{1}{2}\mu[e_{11}^2 + e_{22}^2 + 2e_{12}^2]$. The subscripts i and j refer to the rectilinear orthogonal co-ordinates and, as usual, a subscript after a comma indicates differentiation with respect to the corresponding co-ordinate. The summation convention is used, i.e., if a subscript appears twice in the same monomial, it should be given the successive values 1 and 2, and the corresponding terms should be summed.

It is convenient to introduce bipolar co-ordinates α, β where (4)

$$\alpha = \log\left(\frac{r_1}{r_2}\right), \quad \beta = \theta_1 - \theta_2 \qquad [4]$$

and the meaning of r_1, r_2, θ_1, θ_2 may be seen from Fig. 3. Evidently

$$x = \frac{a \sin\beta}{\cosh\alpha - \cos\beta}, \quad y = \frac{a \sinh\alpha}{\cosh\alpha - \cos\beta} \qquad [5]$$

and, with a suitable choice of a, the roll contours are given by the circles $\alpha = \alpha_0$, $\alpha = -\alpha_0$. Note that α, β are dimensionless quantities used here as orthogonal curvilinear co-ordinates.

If ds represents an element of arc length in the plane of rolling,

$$(ds)^2 = h_1^2(d\alpha)^2 + h_2^2(d\beta)^2 = (dx)^2 + (dy)^2 \qquad [6]$$

Thus from Equation [5]

$$h_1 = h_2 = \frac{a}{\cosh\alpha - \cos\beta} = h \qquad [7]$$

Now let u, v be the components of velocity along the curvilinear orthogonal co-ordinates β, α, respectively. Equations [1] to [3] then take the forms (3)

$$\frac{\partial}{\partial\beta}(hu) + \frac{\partial}{\partial\alpha}(hv) = 0 \qquad [8]$$

$$\rho\left[hu\frac{\partial}{\partial\beta}\left(\frac{u}{h}\right) + hv\frac{\partial}{\partial\alpha}\left(\frac{v}{h}\right)\right] = -\frac{\partial p}{\partial\beta} + \frac{\partial}{\partial\alpha}\left[\mu\left\{\frac{\partial}{\partial\alpha}\left(\frac{u}{h}\right) + \frac{\partial}{\partial\beta}\left(\frac{v}{h}\right)\right\}\right] + \frac{\partial}{\partial\beta}\left[\mu\left\{\frac{2}{h}\left(\frac{\partial u}{\partial\beta}\right) + \frac{2v}{h^2}\frac{\partial h}{\partial\alpha}\right\}\right] \qquad [9]$$

$$\rho\left[hu\frac{\partial}{\partial\beta}\left(\frac{v}{h}\right) + hv\frac{\partial}{\partial\alpha}\left(\frac{u}{h}\right)\right] = -\frac{\partial p}{\partial\alpha} + \frac{\partial}{\partial\alpha}\left[\mu\left\{\frac{2}{h}\frac{\partial v}{\partial\alpha} + \frac{2u}{h^2}\frac{\partial h}{\partial\beta}\right\}\right] + \frac{\partial}{\partial\beta}\left[\mu\left\{\frac{\partial}{\partial\alpha}\left(\frac{u}{h}\right) + \frac{\partial}{\partial\beta}\left(\frac{v}{h}\right)\right\}\right]$$

$$\frac{k}{h^2}\left\{\frac{\partial^2 T}{\partial\beta^2} + \frac{\partial^2 T}{\partial\alpha^2}\right\} - \frac{\rho c}{h}\left\{u\frac{\partial T}{\partial\beta} + v\frac{\partial T}{\partial\alpha}\right\} + \mu\left[2\left\{\frac{1}{h}\frac{\partial v}{\partial\alpha} + \frac{u}{h^2}\frac{\partial h}{\partial\beta}\right\}^2 + 2\left\{\frac{1}{h}\frac{\partial u}{\partial\beta} + \frac{v}{h^2}\frac{\partial h}{\partial\alpha}\right\}^2 + \left\{\frac{\partial}{\partial\alpha}\left(\frac{u}{h}\right) + \frac{\partial}{\partial\beta}\left(\frac{v}{h}\right)\right\}^2\right] = 0 \qquad [10]$$

Approximate Equations of Motion

For the purpose of the present investigation, the foregoing equations may be simplified considerably. The distance between the rolls is very small compared to the distance between the inlet section and some suitable section downstream. Since the passage is narrow, i.e., since α is small, β essentially determines the position along the stream and varies little on any given cross section. Let β' be the change in β from the inlet section to, say, the line of centers of the roll and let[6]

$$\epsilon = \frac{\alpha_0}{\beta'} \qquad [11]$$

Define ξ, η by

$$\xi = \frac{\beta}{\beta'}, \quad \eta = \frac{\alpha}{\alpha_0} \qquad [12]$$

Then from Equation [8]

$$\frac{1}{\beta'}\frac{\partial}{\partial\xi}(hu) + \frac{1}{\alpha_0}\frac{\partial}{\partial\eta}(hv) = 0$$

or

$$\epsilon\frac{\partial}{\partial\xi}(hu) + \frac{\partial}{\partial\eta}(hv) = 0 \qquad [13]$$

[5] Thermal effects upstream, of the inlet as defined, in actual calendering should not change the qualitative nature, an assumption supported by the agreement with experiment already mentioned.

[6] A typical case is given by $\alpha_0 \cong 0.05$, and $\beta' \cong 1.2$, so that $\epsilon \cong 0.04$

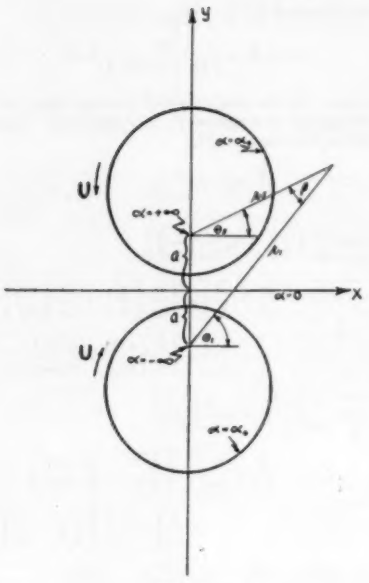

FIG. 3

where ϵ is the small quantity defined by Equation [11]. Now if u is expanded in terms of ϵ, i.e.

$$u = V\,[u_0(\xi, \eta) + \epsilon u_1(\xi, \eta) + \epsilon^2 u_2(\xi, \eta) + \dots\,]$$

it is seen that

$$v = V[\epsilon v_1(\xi, \eta) + \epsilon^2 v_2(\xi, \eta) + \dots\,] \quad [14]$$

The simplification of the equations of motion is then obtained by substituting Equation [14] into Equations [9] and [10] and equating coefficients of powers of ϵ. Retaining only terms of lowest order in the usual fashion, one has

$$\frac{\partial p}{\partial \beta} = \frac{\partial}{\partial \alpha}\left[\mu \frac{\partial}{\partial \alpha}\left(\frac{u}{h}\right)\right] \quad [15]$$

in place of Equation [9], since the equation involving $\partial p/\partial \alpha$ starts with terms of second order in ϵ. Equation [10] becomes

$$\frac{k}{h^2} T_{\alpha\alpha} - \frac{\rho c}{h}(uT_\beta + v\,T_\alpha) + \mu\left[\frac{\partial}{\partial \alpha}\left(\frac{u}{h}\right)\right]^2 = 0 \quad [16]$$

Assuming the variation of h with α to be negligible, one has in x, y-co-ordinates

$$\frac{\partial p}{\partial x} = \frac{\partial}{\partial y}\left(\mu \frac{\partial u}{\partial y}\right) \quad [17]$$

and

$$k \frac{\partial^2 T}{\partial y^2} - \rho c\left(u \frac{\partial T}{\partial x} + v \frac{\partial T}{\partial y}\right) + \mu\left(\frac{\partial u}{\partial y}\right)^2 = 0 \quad [18]$$

From this form it is easy to see that the approximations obtained are equivalent to those usually made in slow-flow problems (5).

Another convenient form of Equation [8] is obtained as follows: Integrating with respect to α, one has

$$hv\Big]_0^\infty + \int_0^\infty \frac{\partial}{\partial \beta}(hu)\,d\alpha = 0$$

At α_2, $v = 0$ and, in the symmetric case discussed here, $v = 0$ at $\alpha = 0$. Therefore

$$\int_0^\infty \frac{\partial}{\partial \beta}(hu)\,d\alpha = 0, \text{ or } \int_0^\infty hu\,d\alpha = Q \quad [19]$$

Later, an expression will be given for Q.

Viscosity-Temperature Relationship

The μ-T relationship for liquids is usually found to be approximately exponential in character. In the current application, only moderate temperature differences are anticipated, so that a simplified expression seems justified. Furthermore, the objective is a qualitative description of the behavior of the flow rather than a precise quantitative treatment. A convenient form is given by replacing the μ-T curve by the tangent line at some point in the working range, i.e., by setting

$$\mu = \mu_0\left[1 - \delta\left(\frac{T - T^*}{T^*}\right)\right] \quad [20]$$

Note that

$$\frac{d\mu}{dT} = -\frac{\mu_0}{T^*}\delta, \text{ or } \delta = -\frac{T^*}{\mu_0}\left(\frac{d\mu}{dT^*}\right)_{\mu=\mu_0}$$

For convenience, T^* may be taken as the uniform temperature at inlet, in which case μ_0 is the inlet viscosity.

Now let

$$\frac{T - T^*}{T^*} = \theta \quad [21]$$

and rewrite Equations [15] and [16] as

$$\frac{\partial p}{\partial \beta} = \frac{\partial}{\partial \alpha}\left[\mu_0(1 - \delta\theta)\frac{\partial}{\partial \alpha}\left(\frac{u}{h}\right)\right] \quad [22]$$

and

$$\frac{kT^*}{h^2}\theta_{\alpha\alpha} - \frac{\rho c T^*}{h}(u\theta_\beta + v\theta_\alpha) + \mu_0(1 - \delta\theta)\left\{\frac{\partial}{\partial \alpha}\left(\frac{u}{h}\right)\right\}^2 = 0 \quad [23]$$

Recalling the symmetry condition mentioned earlier and the fact that $\partial p/\partial \beta$ is independent of α (since $\partial p/\partial \alpha$ was neglected)

$$\left[\frac{\partial}{\partial \alpha}\left(\frac{u}{h}\right)\right]_{\alpha=0} = 0$$

and

$$\alpha \frac{\partial p}{\partial \beta} = \mu_0(1 - \delta\theta)\frac{\partial}{\partial \alpha}\left(\frac{u}{h}\right) \quad [24]$$

For flows in which viscosity variations are moderate, δ provides a convenient parameter to be used in a perturbation scheme. Let

$$\frac{\partial p}{\partial \beta} = f_0(\beta) + \delta f_1(\beta) + \delta^2 f_2(\beta) + \dots \quad [25]$$

$$\theta = \theta_0(\alpha, \beta) + \delta\theta_1(\alpha, \beta) + \dots \quad [26]$$

$$u = u_0(\alpha, \beta) + \delta u_1(\alpha, \beta) + \dots \quad [27]$$

$$v = v_0(\alpha, \beta) + \delta v_1(\alpha, \beta) + \dots \quad [28]$$

Equation [23] then becomes[7]

$$\frac{kT^*}{h^2}\left[\theta_0'' + \delta\theta_1'' + \delta^2\theta_2 + \dots\right] - \frac{\rho c T^*}{h}\left[(u_0 + \delta u_1 + \dots)\left(\frac{\partial\theta_0}{\partial\beta} + \delta\frac{\partial\theta_1}{\partial\beta} + \dots\right) + (v_0 + \delta v_1 + \dots)(\theta_0' + \delta\theta_1' + \dots)\right] + \mu_0\left[1 - \delta(\theta_0 + \delta\theta_1 + \dots)\right]\left[\frac{\partial}{\partial\alpha}\left(\frac{u_0 + \delta u_1 + \dots}{h}\right)\right]^2 = 0 \quad \dots [29]$$

and Equation [24] becomes

$$\alpha(f_0 + \delta f_1 + \dots) = \mu_0(1 - \delta\theta_0 - \delta^2\theta_1 - \dots)\frac{\partial}{\partial\alpha}\left(\frac{u_0 + \delta u_1 + \dots}{h}\right) \quad \dots [30]$$

The continuity equation takes the form

$$\int_0^{\alpha_0} hu_0 d\alpha = Q, \quad \int_0^{\alpha_0} hu_1 d\alpha = \int_0^{\alpha_0} hu_2 d\alpha = \dots = 0 \quad \dots [30]$$

and the boundary conditions are

$$\left.\begin{aligned} \theta &= 0 \text{ at } \beta = \beta_0 \\ \theta &= \theta^{**}, \quad \alpha = \pm\alpha_0 \end{aligned}\right\} \quad \dots [31]$$

$$\left.\begin{aligned} u_0 &= V, \quad \beta = \beta_0 \\ u_0 &= V, \quad \alpha = \pm\alpha_0 \end{aligned}\right\} \quad \dots [32]$$

V is the peripheral speed of the rolls. From Equation [32] and the first Equation [30], it follows that

$$\int_0^{\alpha_0} hu_0 d\alpha = Q = Vh^*\alpha_0$$

Then

$$h^* = \frac{1}{\alpha_0}\int_0^{\alpha_0} h d\alpha \text{ at } \beta = \beta_0$$

i.e., the inlet section

$$\int_0^{\alpha_0} h d\alpha = \int_0^{\alpha_0} \frac{a d\alpha}{\cosh\alpha - \cos\beta_0}$$

Then letting $\cos\gamma = -\cos\beta_0$

$$h^* = \frac{1}{\alpha_0}\left\{2a\csc\gamma\tan\left[\tanh\frac{\alpha}{2}\tan\frac{\gamma}{2}\right]\right\}_{\alpha=0}^{\alpha=\alpha_0}$$

Also $\theta_1 = \theta_2 = \theta_3 = \dots = 0$ at inlet and on the walls, and the same conditions hold for $v_0, v_1, v_2, \dots$; $u_1, u_2, \dots$

Returning to Equations [29] and [30], and equating coefficients of powers of δ, one obtains the following sets of equations

$$\left.\begin{aligned} &\frac{kT^*}{h^2}\theta_0'' - \frac{\rho c T^*}{h}\left(u_0\frac{\partial\theta_0}{\partial\beta} + v_0\theta_0'\right) + \mu_0\left\{\frac{\partial}{\partial\alpha}\left(\frac{u}{h}\right)\right\}^2 = 0 \\ &\frac{kT^*}{h^2}\theta_1'' - \frac{\rho c T^*}{h}\left(u_0\frac{\partial\theta_1}{\partial\beta} + u_1\frac{\partial\theta_0}{\partial\beta} + v_0\theta_1' + v_1\theta_0'\right) + \mu_0\left[\left\{\frac{\partial}{\partial\alpha}\left(\frac{2u_0u_1}{h}\right)\right\}^2 - \theta_0\left\{\frac{\partial}{\partial\alpha}\left(\frac{u_0}{h}\right)\right\}^2\right] = 0 \end{aligned}\right\} \quad \dots [33]$$

[7] The prime denotes differentiation with respect to α.

and

$$\left.\begin{aligned} \alpha f_0 &= \mu_0\frac{\partial}{\partial\alpha}\left(\frac{u}{h}\right) \\ \alpha f_1 &= \mu_0\left[\frac{\partial}{\partial\alpha}\left(\frac{u_1}{h}\right) - \theta_0\frac{\partial}{\partial\alpha}\left(\frac{u_0}{h}\right)\right] \end{aligned}\right\} \quad \dots [34]$$

Equations [34], [33], and [30] are used to obtain the terms in u, T, $\partial p/\partial\beta$, while the terms in v are found from

$$\left.\begin{aligned} &\frac{\partial}{\partial\alpha}(hv_i) + \frac{\partial}{\partial\beta}(hu_i) = 0, \quad i = 0, 1, 2, \dots \\ &\text{or} \\ &hv_i = -\frac{\partial}{\partial\beta}\int_0^{\alpha} hu_i d\alpha \end{aligned}\right\} \quad \dots [35]$$

Also, the first Equations [33] and [34] are those associated with a constant-viscosity flow. That is, the perturbation scheme here employed starts with the constant-viscosity solution.

Solution of Perturbation Equations

From the form of the equations it is apparent that u_0 may be found by integration in terms of f_0 and the latter may be determined from Equations [30] while v_0 may be found from Equations [35]. Substituting in the first of Equations [33] yields a nonhomogeneous second-order partial differential equation for θ_0. When this is solved, the second of Equations [34] will give u_1 via integration and, in principle, the foregoing schemes may then be repeated.

The solution for u_0 and θ_0 may be written explicitly, but it is convenient to use a numerical procedure for further calculations. It is apparent, even in the first-order term θ_0, that a thermal boundary layer is present, however, and this is the principal result which serves to explain the phenomena encountered.

From Equation [34] it follows that

$$\frac{u_0}{h} = \frac{f_0}{\mu_0}\frac{\alpha^2}{2} + c(\beta)$$

At $\alpha = \alpha_0$, $u_0 = V$, so that

$$\frac{V}{h} = \frac{f_0}{\mu_0}\frac{\alpha_0^2}{2} + c(\beta)$$

and

$$\frac{u_0}{h} = \frac{V}{h} + \frac{f_0}{2\mu_0}(\alpha^2 - \alpha_0^2) \quad \dots [36]$$

Substituting this into Equation [30], we obtain

$$\int_0^{\alpha_0}\left[Vh + \frac{f_0h^2}{2\mu_0}(\alpha^2 - \alpha_0^2)\right]d\alpha = Vh^*\alpha_0$$

Now

$$h = \frac{a}{\cosh\alpha - \cos\beta} = \frac{a}{(1 - \cos\beta) + (\cosh\alpha - 1)}$$

or

$$h = \frac{a}{1 - \cos\beta}\left\{\frac{1}{1 + \dfrac{\cosh\alpha - 1}{1 - \cos\beta}}\right\}$$

Expanding the bracketed expression, we find

$$\frac{1}{1+\dfrac{\cosh\alpha-1}{1-\cos\beta}} = 1-\left(\frac{\cosh\alpha-1}{1-\cos\beta}\right)+\left(\frac{\cosh\alpha-1}{1-\cos\beta}\right)^2-\cdots$$

Thus for sufficiently small α, we have, approximately

$$h \cong \frac{a}{1-\cos\beta}$$

thus

$$Vh\alpha_0 - \frac{f_0 h^2}{\mu_0}\frac{\alpha_0^2}{3} = Vh^*\alpha_0$$

and

$$-\frac{f_0}{\mu_0} = \frac{3V(h^*-h)}{\alpha_0^2 h^2}$$

Finally

$$u_0 = V\left[1-\frac{3}{2}\frac{(h^*-h)}{h}\frac{(\alpha^2-\alpha_0^2)}{\alpha_0^2}\right] \quad [37]$$

It will be recalled that earlier the independence of h on α was used to obtain Equations [17] and [18].

Now

$$hv_0 = -V\frac{\partial}{\partial\beta}h\int_0^\alpha\left[1-\frac{3}{2}\frac{(h^*-h)}{h}\frac{(\alpha^2-\alpha_0^2)}{\alpha_0^2}\right]d\alpha$$

$$= -V\frac{\partial}{\partial\beta}h\left[\alpha-\frac{3}{2}\frac{(h^*-h)}{h}\frac{(\alpha^3/3-\alpha\alpha_0^2)}{\alpha_0^2}\right]$$

or

$$v_0 = \frac{V}{2}\frac{\alpha(\alpha_0^2-\alpha^2)}{\alpha_0^2}\frac{h_\beta}{h} \quad [38]$$

With these results the first Equation [33] becomes

$$\frac{kT^*}{h^2}\theta_0'' - \frac{\rho cT^*}{h}V\left\{\left[1-\frac{3}{2}\frac{(h^*-h)}{h}\frac{(\alpha^2-\alpha_0^2)}{\alpha_0^2}\right]\frac{\partial\theta_0}{\partial\beta} + \frac{\alpha(\alpha_0^2-\alpha^2)}{2\alpha_0^2}\frac{h_\beta}{h}\theta_0'\right\} + \mu_0\left\{\frac{2V(h^*-h)}{\alpha_0^2 h}\right\}^2 = 0 \quad [39]$$

Equation [39] is, of course, difficult to solve exactly. In a fluid with low conductivity, however, except in the immediate neighborhood of the walls, the energy balance is maintained essentially between the convection along the stream and the dissipation. A solution based on this assumption will not fulfill the boundary conditions but will have some distribution, say, θ_0^*, $\alpha = \alpha_0$. It is possible, however, to find a solution to the homogeneous equation, derived from Equation [39], which will take the values

$$\theta^* - \frac{T^{**}-T^*}{T^*}$$

on α_0. Adding the "particular" and "complementary" solutions gives a satisfactory solution for θ_0.

In view of the approximate form of the particular solution, Equation [39] may be simplified further by replacing u by its average value $\bar{u}$

$$\bar{u}h\alpha_0 = \int_0^{\alpha_0} hu_0 d\alpha = h^*V\alpha_0$$

or

$$\bar{u} = V\frac{h^*}{h} \quad [40]$$

Then

$$\frac{kT^*}{h^2}\theta_0'' - \frac{\rho cT^*}{h^2}h^*V\frac{\partial\theta_0}{\partial\beta} - \frac{\rho cT^*}{h}v_0\theta_0' + \mu_0\frac{9V^2(h^*-h)^2\alpha^2}{h^2\alpha_0^4} = 0 \quad [41]$$

On the basis of the preceding argument

$$-\frac{\rho cT^*}{h^2}h^*V\frac{\partial\theta_0}{\partial\beta} = -9V^2\mu_0\frac{(h^*-h)^2}{h^2}\frac{\alpha^2}{\alpha_0^4}$$

or

$$\frac{\partial\theta_0}{\partial\beta} = \frac{9\mu_0 V}{\rho cT^*}\frac{(h^*-h)^2}{h^*}\frac{\alpha^2}{\alpha_0^4}$$

yields a particular solution.

Then

$$\theta_0 = \frac{9\mu_0 V}{\rho cT^*}\frac{\alpha^2}{\alpha_0^4}\int_{\beta_0}^{\beta}\frac{(h^*-h)^2}{h^*}d\beta$$

or

$$\theta_0 = \frac{9\mu_0 V}{\rho cT^*}\frac{\alpha^2}{\alpha_0^4}\left[h^*(\beta-\beta_0) - 2\int_{\beta_0}^{\beta}hd\beta + \frac{1}{h^*}\int^{\beta}h^2 d\beta\right] \quad [42]$$

When $\alpha = \alpha_0$, $\theta_0 = \theta_0^*(\beta)$, and the value may be found easily.

The homogeneous part of Equation [41] is

$$k\theta_0'' - \rho ch^*V\frac{\partial\theta_0}{\partial\beta} - \rho chv_0\theta_0' = 0 \quad [43]$$

Let $\eta = K(\alpha_0 - \alpha)$, $\xi = \beta/\beta'$, where β' is the change in β between the inlet section and some section downstream

$$K^2k\frac{\partial^2\theta_0}{\partial\eta^2} - \rho c\left[\frac{h^*V}{\beta'}\frac{\partial\theta_0}{\partial\xi} - hKv_0\frac{\partial\theta_0}{\partial\eta}\right] = 0$$

Let

$$K^2 = \frac{\rho ch^*V}{k\beta'}, \quad K = \sqrt{\frac{\rho ch^*V}{k\beta'}}$$

The transformation puts Equation [43] into a form, Equation [44], which is apparently equally difficult to solve. From this form, however, after interpreting v_0 suitably, it is easier to see that a further transformation, Equations [46] and [47], leads to a simple equation, i.e., Equation [48]. Then

$$\frac{\partial^2\theta_0}{\partial\eta^2} - \frac{\partial\theta_0}{\partial\xi} + \frac{h}{h^*}\frac{\beta'K}{V}v_0\frac{\partial\theta_0}{\partial\eta} = 0 \quad [44]$$

Notice that $\eta = 0$ when $\alpha = \alpha_0$ and, as will be seen later, for the fluids considered K is large. Then let $1/K = \sigma$, where σ is a small number and

$$\alpha_0 - \alpha = \sigma\eta, \quad d\alpha = -\sigma d\eta$$

Now

$$u_0 = V\left[1-\frac{3}{2}\frac{(h^*-h)}{h}\left(\frac{\alpha^2-\alpha_0^2}{\alpha_0^2}\right)\right]$$

and

$$v_0 = \frac{1}{h}\int_0^\alpha (hu_0)_\xi\, d\alpha = -\frac{\sigma}{h\beta'}\int_{\alpha/\sigma}^{\frac{\alpha+\sigma\eta}{\sigma}}(hu_0)_\xi\, d\eta$$

Near the wall, however

$$u_0 = V\left[1 + \frac{3}{2}\frac{(h^* - h)}{h}(\sigma\eta)\frac{(2\alpha_0 + \sigma\eta)}{\alpha_0^2}\right] \cong V$$

so that

$$v_0 \cong -\frac{h_\xi}{h}\frac{V}{\beta'}\sigma\eta$$

and $(h_\xi)/(\beta' h)$ is essentially a function of ξ alone.

With $\sigma = 1/K$, Equation [44] becomes

$$\frac{\partial^2\theta}{\partial\eta^2} - \frac{h_\xi}{h^*}\eta\frac{\partial\theta_0}{\partial\eta} - \frac{\partial\theta_0}{\partial\xi} = 0 \quad \ldots\ldots [45]$$

Let us now introduce new co-ordinates p, q

$$\frac{\partial\theta_0}{\partial\eta} = \frac{\partial\theta_0}{\partial p}p_\eta + \frac{\partial\theta_0}{\partial q}q_\eta$$

$$\frac{\partial^2\theta_0}{\partial\eta^2} = \frac{\partial^2\theta_0}{\partial p^2}(p_\eta)^2 + \ldots.$$

The coefficient of $\partial\theta_0/\partial p$ is

$$p_{\eta\eta} - \frac{h_\xi}{h^*}\eta p_\eta - p_\xi$$

If $p = \eta g\ (\xi)$, this coefficient vanishes whenever $g'/g = h_\xi/h^*$. Then $\log g = h/h^*$ and $g = e^{h/h^*}$, or

$$p = \eta e^{h/h^*} \quad \ldots\ldots [46]$$

Furthermore, if q is assumed independent of η

$$\frac{\partial^2\theta_0}{\partial p^2}(p_\eta)^2 - \frac{\partial\theta_0}{\partial q}q_\xi = 0$$

Setting

$$q_\xi = e^{h/h^*}$$

we have

$$q = \int_{\xi_0}^{\xi} e^{2h/h^*}\,d\xi \quad \ldots\ldots [47]$$

Thus a co-ordinate transformation is found which reduces Equation [45] to

$$\frac{\partial^2\theta_0}{\partial p^2} - \frac{\partial\theta_0}{\partial q} = 0 \quad \ldots\ldots [48]$$

It will be noted that $p = 0$ when $\eta = 0$, i.e., when $\alpha = \alpha_0$ so that Equation [46] is to be solved with

$$\theta_0 = \theta_0^* - \frac{T^{**} - T^*}{T'^*}$$

when $p = 0$. Also in Equation [47], choosing ξ_0 to be the value corresponding to the inlet value of β, $q = 0$ at inlet, and $\theta_0 = 0$ when $q = 0$.

Let $F(\xi)$ denote

$$\theta_0^* - \frac{T^{**} - T^*}{T^*}$$

and $f(S) = L[F(\xi)]$ where $L[\ ]$ denotes the Laplace operator (6). With

$$\bar\theta_0 = L[\theta_0],$$

$$\frac{\partial^2\bar\theta_0}{\partial p^2} - s\bar\theta_0 = 0$$

With

$$\bar\theta_0(s, 0) = f(s), \quad \bar\theta_0 = f(s)e^{-\sqrt{s}\,p}$$

and

$$\theta_0 = L^{-1}[f(s)e^{-\sqrt{s}\,p}]$$

or

$$\theta_0(p, q) = \int_0^q F'(q - z)\,erfc\left(\frac{p}{2\sqrt{z}}\right)dz \quad \ldots\ldots [49]$$

Since the integrand will, in general, be complicated, numerical integration is indicated. Combining Equation [49] with Equation [42], an approximate solution is obtained for θ_0 with which, in principle, u_1 may be found from the second of Equations [34] by integration, and f_1, θ_1 found as in the foregoing. Actually, of course, further terms must be found numerically. In the next section a typical problem is considered and θ_0 is calculated.

Application to a Typical Calendering Problem

The theory just developed has been used to determine the temperature distribution in linoleum color mix while being rolled. The material properties are as follows:[8]

Specific heat, 0.36 – 0.38 Btu/(lb) (deg F)

Thermal conductivity, 1.48 ± 0.18 Btu, in./(sq ft) (hr) (deg F)

Specific gravity, 1.35 – 1.40

Rolls of 14-in. radii are considered, and the nip separation is assumed to be 0.10 in. The roll peripheral speed is 10 fps.

The term α_0, determined from Equation [4], is found to be 0.084, so that, as the theory requires, α is always small; β_0, β_1, the entrance and exit sections corresponding to $\xi = \pm 6$, respectively, are $(37/30)\pi$, and $(23/30)\pi$ (see footnote[9]), in the order named; a is 1.185 in.

After calculating u_0, Equation [37], θ_0 is found. The boundary conditions imposed are that $\theta_0 = 0$ when $\beta = \beta_0$, and $\theta_0 = 0$ when $\alpha = \pm\alpha_0$. Fig. 4 shows the results of the calculation in the form of the temperature distribution at the nip and exit sections.

At each section, T' differs from θ_0 only by a constant multiplier given by

$$\frac{9\mu\ Vl_1}{\rho c}$$

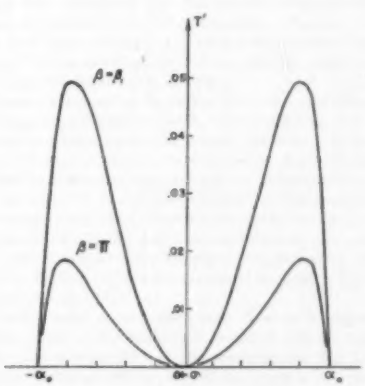

Fig. 4

[8] The values are contained in a letter from Mr. J. T. Bergen, January 27, 1947.

[9] These values are shown to be appropriate in a summary report to the Armstrong Cork Company by Dr. R. E. Gaskell.

where

$$t_1 = \frac{a \sinh \alpha_2 (\cosh \alpha_2 - \cos \beta_1)}{(\cosh \alpha_2 - \cos \beta)^2}$$

It is seen that the maximum temperature, the point at which blistering is to be expected, is found about one fifth of the distance from the surface to the center of the sheet. This is of the same order of magnitude as the blisters observed in Mr. Bergen's experiments previously noted and offers an explanation of the phenomenon.

In addition to its applicability, as demonstrated, the theory has intrinsic interest. Recently, Carrier and Lewis (7) classified the problems of the flow of a viscous fluid through a narrow channel where the temperature distribution must be considered. They found that three general classes may be distinguished, one of which, characterized by the presence of a thermal boundary layer, includes the problem discussed here. Further, they discuss methods of solution but otherwise there is little published work of the type given here.

BIBLIOGRAPHY

1 "The Calendering of Non-Newtonian Liquids," by R. E. Gaskell (to be published).

2 "The Occurrence of Slip During Calendering," by R. E. Gaskell (to be published).

3 "Modern Development in Fluid Dynamics," edited by Sydney Goldstein, Oxford University Press, London, England, 1938.

4 "Plane Stress and Plane Strain in Bipolar Coordinates," by G. B. Jeffreys, Philosophical Transactions Royal Society of London series A, vol. 221, 1920, pp. 265–293.

5 "Hydrodynamics," by H. Lamb, Dover Publications, New York, N. Y., 1945.

6 "Modern Operational Mathematics in Engineering," by R. V. Churchill, McGraw-Hill Book Company, Inc., New York, N. Y., 1944.

7 "On Heat Transfer Problems in Viscous Flow," by G. F. Carrier and J. A. Lewis, Quarterly Applied Mathematics 7, 1950, pp. 450–457.

Stress Concentrations Around Spheroidal Inclusions and Cavities

By R. H. EDWARDS,[1] CHICAGO, ILL.

Previous investigations have been concerned with the stress concentration around a spheroidal cavity under certain restricted loading assumptions.[2] In this paper exact closed solutions are obtained for the following: (*a*) The distribution of stress around a spheroidal inclusion in an elastic body which is in an arbitrary uniform state of stress infinitely far from the inclusion, and, in particular, for the distribution of stress around a spheroidal cavity under the same loading conditions. (*b*) The thermal stress distribution arising from distinct uniform temperature changes applied to the spheroidal inclusion and the surrounding medium. Technically important features of the solutions obtained are discussed.

Nomenclature

The following nomenclature is used in the paper:

(x, y, z) = Cartesian co-ordinates

(u, v, w); $(\sigma_x, \ldots, \tau_{xy} \ldots)$ = Cartesian components of displacement and stress, respectively

ϵ = dilatation

$\varphi, \vartheta, \lambda$ = harmonic stress functions (displacement potentials)

(α, β, γ) = orthogonal curvilinear co-ordinates in general, and spheroidal co-ordinates in particular

(h_1, h_2, h_3); $[\cos(\alpha, x), \ldots]$ = local scale coefficients, and local direction cosines, respectively

$(u_\alpha, u_\beta, u_\gamma)$; $(\sigma_\alpha, \ldots, \tau_{\alpha\beta} \ldots)$ = curvilinear components of displacement and stress, respectively, for outer region

$(u_\alpha', u_\beta', u_\gamma')$; $(\sigma_\alpha', \ldots \tau_{\alpha\beta}', \ldots)$ = curvilinear components of displacement and stress, respectively, for inner region

$q = \cosh\alpha$, $\bar{q} = \sinh\alpha$; $p = \cos\beta$, $\bar{p} = \sin\beta$; $h = h_1 = h_2 = 1/\sqrt{q^2 - p^2}$ = auxiliary position parameters for spheroidal co-ordinate system

$Q = 1 + \frac{\bar{q}}{2}\log\frac{q-1}{q+1}$ = auxiliary harmonic function

$q_0, \bar{q}_0, h_0, Q_0$ = values of $q, \bar{q}, h, Q$ at $\alpha = \alpha_0$

$a = \cosh\alpha_0 = q_0$; $b = \sinh\alpha_0 = \bar{q}_0$ = polar and equatorial semiaxes, respectively, of spheroidal cavity

$s = b/a$ = shape ratio

G, ν; G', ν' = shear modulus and Poisson's ratio for outer and inner regions, respectively

$\Delta \equiv \frac{\partial^2}{\partial x^2} + \frac{\partial^2}{\partial y^2} + \frac{\partial^2}{\partial z^2}$ = Laplacian operator

$H \equiv \left(\frac{G'}{G} - 1\right)$ = measure of relative rigidity of the inclusion and surrounding medium

T, T'; T_0, T_0'; T_1, T_1' = temperatures

ϵ, ϵ' = linear-thermal-expansion coefficients for the outer and inner regions, respectively

M = factor of proportionality used in thermal stress problem

D = determinant of coefficients of the linear equations arising from continuity conditions

Statement of the Problem

Three-Function Approach in Spheroidal Co-Ordinates

Consider an infinite body which possesses an inclusion in the shape of a prolate[3] spheroid. It is assumed that the spheroidal core and the surrounding body are each composed of homogeneous isotropic material, but that the elastic properties of the two materials may be distinct. At the contact surface between the two media, complete bond is presupposed. An exact solution for the distribution of stress will be determined under the condition that the surrounding body is in an arbitrary uniform state of stress infinitely far from the inclusion.

Solutions corresponding to certain particular or limiting cases of the foregoing problem are known. These solutions offer valuable partial confirmation of the results obtained. In this connection, reference is made to the solution for the problem of the spheroidal cavity under uniaxial tension perpendicular to the axis of the cavity by M. A. Sadowsky and E. Sternberg (1), J. N. Goodier's determination of the stress distribution around a spherical inclusion (3), H. Neuber's investigation of the spheroidal cavity under uniaxial tension parallel to the axis of the spheroid (2), and L. H. Donnell's two-dimensional analysis of the elliptic cylindrical inclusion (4).

Let the Cartesian co-ordinate system $Oxyz$ be introduced with O at the center of the spheroidal inclusion and Oz coincident with the axis of symmetry of the configuration, Fig. 1. Since the state of stress at infinity is uniform, Oxy may be oriented so that $\tau_{xy} = 0$ at infinity. The stress distribution throughout the body may then be obtained as a linear combination of the

---

[1] Formerly Instructor of Mathematics, Illinois Institute of Technology. Now Research Physicist, Hughes Aircraft Co., Culver City, Calif.

[2] References (1) and (2). Numbers in parentheses refer to the Bibliography at the end of the paper.

Presented at the Annual Conference of the Applied Mechanic Division, Purdue University, Lafayette, Ind., June 22–24, 1950, of The American Society of Mechanical Engineers.

Discussion of this paper should be addressed to the Secretary, ASME, 29 West 39th Street, New York, N. Y., and will be accepted until April 10, 1951, for publication at a later date. Discussion received after the closing date will be returned.

Note: Statements and opinions advanced in papers are to be understood as individual expressions of their authors and not those of the Society. Manuscript received by the Applied Mechanics Division, October 21, 1949. Paper No. 50—APM-20.

[3] If the inclusion has an oblate spheroidal shape, the results of this analysis may be applied directly after a trivial transformation of variables.

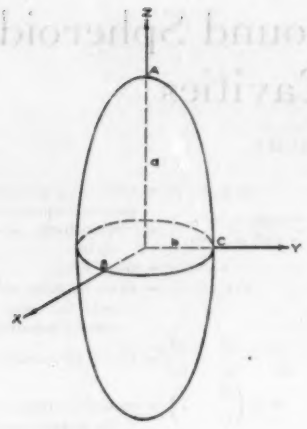

FIG. 1

solutions to the following five loading conditions at infinity:

Case 1: (plane hydrostatic state of stress)

$$\sigma_x, \sigma_y \to 1;\ \sigma_z, \tau_{xy}, \tau_{yz}, \tau_{zx} \to 0$$

Case 2: (plane state of pure shearing stress)

$$\sigma_x, -\sigma_y \to 1;\ \sigma_z, \tau_{xy}, \tau_{yz}, \tau_{zx} \to 0$$

Case 3: (state of uniaxial tension)

$$\sigma_z \to 1;\ \sigma_x, \sigma_y, \tau_{xy}, \tau_{yz}, \tau_{zx} \to 0$$

Case 4: (plane state of pure shearing stress)

$$\tau_{zx} \to 1;\ \sigma_x, \sigma_y, \sigma_z, \tau_{xy}, \tau_{yz} \to 0$$

Case 5: (plane state of pure shearing stress)

$$\tau_{yz} \to 1,\ \sigma_x, \sigma_y, \sigma_z, \tau_{xy}, \tau_{zx} \to 0$$

It will be noted that Cases 4 and 5 are intrinsically the same.

In the analysis of each loading case, two solutions to the basic equations of elasticity are sought. The first, which will define the stress and displacement fields over the inclusion, will be called $R_j'(j = 1, 2, 3, 4, 5)$, where j denotes the number of the loading case under consideration. The second, which will define these fields over the surrounding body, will be designated by R_j.

The classical three-function approach in the theory of elasticity will be used[4] in the particular formulation employed by Sadowsky and Sternberg (1) whose notation will be adhered to. According to this formulation, the general solution of the displacement-equilibrium equations in the absence of body forces is taken as

$$\left.\begin{aligned} [u, v, w] &= \frac{1}{2G}\ \text{grad}\ \varphi \\ [u, v, w] &= \frac{1}{G}\ \text{curl}\ [0, 0, \vartheta] \\ [u, v, w] &= \frac{z}{2G}\ \text{grad}\ \lambda - \left[0, 0, \frac{3-4\nu}{2G}\lambda\right] \end{aligned}\right\} \quad \ldots\ldots [1]$$

where $\Delta\varphi = \Delta\vartheta = \Delta\lambda = 0$. It is readily shown that any solution of the displacement-equilibrium equations may be represented as a linear combination of these solutions provided the harmonic functions φ, ϑ, and λ are chosen properly. These solutions will be referred to as basic solutions 1, 2, and 3, respectively.

Sadowsky and Sternberg (1) have determined the stress and displacement fields corresponding to Equations [1] and referred to prolate spheroidal co-ordinates. For the sake of completeness, these results are summarized here.

The prolate spheroidal co-ordinate system is defined by the equations of transformation

$$\left.\begin{aligned} x &= \sinh\alpha \cdot \sin\beta \cdot \cos\gamma \\ y &= \sinh\alpha \cdot \sin\beta \cdot \sin\gamma \\ z &= \cosh\alpha \cdot \cos\beta \end{aligned}\right\} \quad \ldots\ldots [2]$$

The surfaces $\alpha = \text{const}$, $\beta = \text{const}$, and $\gamma = \text{const}$ form a triply orthogonal family of prolate spheroids, hyperboloids of two sheets, and meridional half-planes.

For convenience, the following auxiliary variables are introduced

$$\left.\begin{aligned} q &= \cosh\alpha,\ \bar{q} = \sinh\alpha = \sqrt{q^2-1} \\ p &= \cos\beta,\ \bar{p} = \sin\beta = \sqrt{1-p^2} \end{aligned}\right\} \quad \ldots\ldots [3]$$

where

$$\left.\begin{aligned} 1 \le q < \infty,\ 0 \le \bar{q} < \infty \\ -1 \le p \le 1,\ 0 \le \bar{p} \le 1 \end{aligned}\right\} \quad \ldots\ldots [4]$$

If the differential of arc length is written in the form

$$(ds)^2 = \left(\frac{d\alpha}{h_1}\right)^2 + \left(\frac{d\beta}{h_2}\right)^2 + \left(\frac{d\gamma}{h_3}\right)^2 \quad \ldots\ldots [5]$$

the local scale coefficients become

$$\frac{1}{h_1^2} = \frac{1}{h_2^2} = \frac{1}{h^2} = q^2 - p^2;\ \frac{1}{h_3} = \bar{q}\bar{p} \quad \ldots\ldots [6]$$

In this co-ordinate system, the three basic solutions yield the following representations of the displacement fields

$$u_\alpha = \frac{h}{2G}\,\bar{q}\varphi_{\bar{q}};\ u_\beta = \frac{-h}{2G}\,\bar{p}\,\varphi_{\bar{p}};\ u_\gamma = \frac{1}{2G}\frac{\varphi_\gamma}{\bar{p}\bar{q}} \quad \ldots\ldots [7]$$

$$\left.\begin{aligned} u_\alpha &= \frac{h}{G}\,\frac{q}{\bar{q}}\,\vartheta_\gamma;\ u_\beta = \frac{h}{G}\,\frac{p}{\bar{p}}\,\vartheta_\gamma \\ u_\gamma &= \frac{h^2}{G}\,(p\vartheta_p - q\vartheta_q)\bar{p}\bar{q} \end{aligned}\right\} \quad \ldots\ldots [8]$$

$$\left.\begin{aligned} u_\alpha &= \frac{h}{2G}\,[q\lambda_q - (3-4\nu)\lambda]\bar{p}\bar{q} \\ u_\beta &= \frac{h}{2G}\,[-\bar{p}\lambda_p + (3-4\nu)\lambda]\bar{p}q \\ u_\gamma &= \frac{1}{2G}\,\frac{\bar{p}\bar{q}}{\bar{p}\bar{q}}\,\lambda\gamma \end{aligned}\right\} \quad \ldots\ldots [9]$$

The corresponding stress fields become

First basic solution

$$\left.\begin{aligned} \sigma_\alpha &= h^3\bar{q}^3\varphi_{\bar{q}\bar{q}} + h^4\bar{p}^2(q\varphi_q - p\varphi_p) \\ \sigma_\beta &= h^3\bar{p}^3\varphi_{\bar{p}\bar{p}} + h^4\bar{q}^2(q\varphi_q - p\varphi_p) \\ \sigma_\gamma &= \frac{\varphi_{\gamma\gamma}}{\bar{p}^2\bar{q}^2} + h^2(q\varphi_q - p\varphi_p) \\ \tau_{\alpha\beta} &= [-h^3\varphi_{\bar{p}\bar{q}} + h^4(q\varphi_p - p\varphi_q)]\bar{p}\bar{q} \\ \tau_{\alpha\gamma} &= h\,\frac{\bar{q}^2\varphi_{\bar{q}\gamma} - q\varphi_\gamma}{\bar{p}\,\bar{q}^2} \\ \tau_{\beta\gamma} &= h\,\frac{-\bar{p}^2\varphi_{\bar{p}\gamma} - p\varphi_\gamma}{\bar{p}^2\bar{q}} \end{aligned}\right\} \quad \ldots\ldots [10]$$

[4] The three-function approach was apparently originated by Boussinesq (6), and subsequently investigated by Papcovich (7) and Neuber (2).

Second basic solution

$$\left.\begin{aligned}
\sigma_\alpha &= 2h^3q\left[\vartheta_{\alpha\gamma}-\frac{q}{\bar{q}^2}\,\vartheta_\gamma\right]\\
\sigma_\beta &= -2h^3p\left[\vartheta_{p\gamma}+\frac{p}{\bar{p}^2}\,\vartheta_\gamma\right]\\
\sigma_\gamma &= \frac{2\vartheta_\gamma}{p^2\bar{q}^2}+2h^3[p\vartheta_{p\gamma}-q\vartheta_{q\gamma}]\\
\tau_{\alpha\beta} &= \frac{h^2}{p\bar{q}}\,[p\bar{q}^2\vartheta_{q\gamma}-\bar{p}^2q\vartheta_{p\gamma}-2pq\vartheta_\gamma]\\
\tau_{\alpha\gamma} &= \frac{hq\vartheta_{\gamma\gamma}}{p\bar{q}^2}+h^3p\bar{q}^2[p\vartheta_{pq}-q\vartheta_{qq}]\\
&\qquad +h^3p\bar{q}^2[(q^2+p^2)\vartheta_q-2pq\vartheta_p]\\
\tau_{\beta\gamma} &= \frac{hp\vartheta_{\gamma\gamma}}{\bar{p}^2\bar{q}}-h^3\bar{p}^2q[p\vartheta_{pp}-q\vartheta_{pq}]\\
&\qquad -h^3\bar{p}^2q\,[(q^2+p^2)\vartheta_p-2pq\vartheta_q]
\end{aligned}\right\}\ldots[11]$$

Third basic solution

$$\left.\begin{aligned}
\sigma_\alpha &= h^2(q\lambda_{qq}-2\lambda_q)p\bar{q}^2-2\nu h^2(q\bar{p}^2\lambda_p-p\bar{q}^2\lambda_q)\\
&\qquad +h^4(q\lambda_q-p\lambda_p)pq\bar{p}^2\\
\sigma_\beta &= h^2(p\lambda_{pp}-2\lambda_p)q\bar{p}^2+2\nu h^2(q\bar{p}^2\lambda_p-p\bar{q}^2\lambda_q)\\
&\qquad +h^4(q\lambda_q-p\lambda_p)pq\bar{q}^2\\
\sigma_\gamma &= \frac{pq\lambda_{\gamma\gamma}}{\bar{p}^2\bar{q}^2}+(1-2\nu)h^2pq(q\lambda_q-p\lambda_p)\\
&\qquad -2\nu h^2(q\lambda_p-p\lambda_q)\\
\tau_{\alpha\beta} &= h^2[(1-2\nu)(p\lambda_p+q\lambda_q)-pq\lambda_{pq}]p\bar{q}\\
&\qquad +h^4pp_qq\bar{q}(q\lambda_p-p\lambda_q)\\
\tau_{\alpha\gamma} &= \frac{hp}{\bar{p}}\left[q\lambda_{,\gamma}-\left(2-2\nu+\frac{1}{\bar{q}^2}\right)\lambda_\gamma\right]\\
\tau_{\beta\gamma} &= \frac{hq}{\bar{q}}\left[-p\lambda_{p\gamma}+\left(2-2\nu-\frac{1}{\bar{p}^2}\right)\lambda_\gamma\right]
\end{aligned}\right\}\ldots[12]$$

The harmonic functions which will be used subsequently are the Lamé products associated with the spheroidal co-ordinate system. These are

$$\varphi(q,\,p,\,\gamma)=[F_n^{(m)}(q)\text{ or }S_n^{(m)}(q)]\cdot[F_n^{(m)}(p)\text{ or }S_n^{(m)}(p)]\cdot[\cos m\gamma\text{ or }\sin m\gamma]\ldots[13]$$

$$(n,\,m=0,\,1,\,2,\,3,\ldots)$$

or for ϕ independent of γ

$$\phi(q,\,p)=[F_n(q)\text{ or }S_n(q)]\cdot[F_n(p)\text{ or }S_n(p)]\ldots[14]$$

where $F_n(q)$, $S_n(q)$, $F_n^{(m)}(q)$, $S_n^{(m)}(q)$ are the ordinary and associated Legendre functions of the first and second kind.

These functions may be defined as follows

$$F_n(q)=\frac{1}{2^n n!}\frac{d^n}{dq^n}(q^2-1)^n\ldots[15]$$

$$S_n(q)=\frac{1}{2}F_n(q)\cdot\log\left(\frac{q-1}{q+1}\right)-T_n(q)\ldots[16]$$

where $T_n(q)$ is the polynomial part of the expansion

$$-F_n(q)\cdot\sum_{k=1,3,5,\ldots}^{n}\frac{1}{kq^k}\ldots[17]$$

and

$$F_n^{(m)}(q)=\frac{1}{\bar{q}^m}\int_1^q\cdots\int_1^q F_n(q)\,dq\ldots dq\ldots[18]$$

the integration being m-fold.

Also

$$S_n^{(m)}(q)=\bar{q}^m\frac{d^mS_n(q)}{dq^m}\ldots[19]$$

The analogous definitions for the Legendre functions of p are obtained by replacing q, $\bar{q}$, $\log(q-1)/(q+1)$ with p, $\bar{p}$, $\log(1-p)/(1+p)$, respectively.

Let the boundary of the inclusion be defined by the equation $\alpha=\alpha_0$ or $q=q_0$. The continuity conditions then take the form at $q=q_0$

$$\left.\begin{aligned}
[u_\alpha,\,u_\beta,\,u_\gamma] &\equiv [u_\alpha',\,u_\beta',\,u_\gamma']\\
[\sigma_\alpha,\,\tau_{\alpha\beta},\,\tau_{\alpha\gamma}] &\equiv [\sigma_\alpha',\,\tau_{\alpha\beta}',\,\tau_{\alpha\gamma}']
\end{aligned}\right\}\ldots[20]$$

The primed stress and displacement components are those corresponding to the solution $R_i'(j=1,2,3,4,5)$.

In order to fulfill the boundary conditions at infinity, R_j will be represented in all cases as a sum of the form

$$R_j=R_{oj}+\sum_i a_{ij}R_{ij}\ldots[21]$$

where R_{oj} is the uniform field solution which would be obtained in the absence of an inclusion. The R_{ij} are solutions obtained from Equations [1] for which the corresponding stress fields vanish at infinity. The a_{ij} are coefficients of superposition.

Similarly, R_j' will be represented in the form

$$R_j'=\sum_i b_{ij}R_{ij}'\ldots[22]$$

where the b_{ij} are constants and the R_{ij}' are solutions to the basic equations of elasticity.

Solution for Case 1

The boundary conditions for this case are

$$\left.\begin{aligned}
\text{as } q\to\infty\quad &\sigma_\alpha,\ \sigma_\beta\to 1\\
&\sigma_\alpha,\ \tau_{\alpha\beta},\ \tau_{\alpha\gamma},\ \tau_{\beta\gamma}\to 0
\end{aligned}\right\}\ldots[23]$$

or equivalently

$$\left.\begin{aligned}
\text{as } q\to\infty\quad &\sigma_\alpha\to q^2-h^2q^2\bar{q}^2\\
&\sigma_\beta\to-\bar{q}^2+h^2q^2\bar{q}^2\\
&\sigma_\gamma\to 1\\
&\tau_{\alpha\beta}\to h^2p\bar{p}q\bar{q}\\
&\tau_{\alpha\gamma},\ \tau_{\beta\gamma}\to 0
\end{aligned}\right\}\ldots[24]$$

Suitable harmonic functions to generate basic solutions for this loading case are found to be:

For the solution R_1

$$R_{11}\colon\ \varphi=S_0(q)F_0(p)=\frac{Q-1}{q}\ldots[25]$$

$$R_{21}\colon\ \lambda=S_1(q)F_1(p)=Qp\ldots[26]$$

$$R_{31}\colon\ \varphi=S_2(q)F_2(p)=\frac{1}{4}(3p^2-1)\frac{1+(3q^2-1)Q}{q}\ldots[27]$$

where

$$Q\equiv 1+\frac{q}{2}\log\frac{q-1}{q+1}$$

For the solution R_1'

$$R_{11}'\colon \lambda = F_1(q)F_1(p) = q\cdot p \qquad [28]$$

$$R_{21}'\colon \varphi = F_2(q)F_2(p) = \frac{1}{4}(3q^2-1)(3p^2-1) \qquad [29]$$

The stress and displacement fields corresponding to the solutions under consideration are as follows:

Solution R_{21}

$$\left.\begin{aligned}
u_\alpha &= \frac{hq\bar{q}}{2G(1+\nu)}\,[(1-\nu)-(1+\nu)p^2]\\
u_\beta &= \frac{hp\bar{p}}{2G(1+\nu)}\,[(1+\nu)q^2-(1-\nu)]\\
u_\gamma &= 0\\
\sigma_\alpha &= q^2 - h^2q^2\bar{q}^2\\
\sigma_\beta &= -\bar{q}^2 + h^2q^2\bar{q}^2\\
\sigma_\gamma &= 1\\
\tau_{\alpha\beta} &= h^2p\bar{p}q\bar{q}\\
\tau_{\alpha\gamma} &= \tau_{\beta\gamma} = 0
\end{aligned}\right\} \qquad [30]$$

Basic solution R_{11}

$$\left.\begin{aligned}
u_\alpha &= \frac{h}{2G\bar{q}},\ u_\beta = u_\gamma = 0\\
\sigma_\alpha &= -\frac{h^2q}{\bar{q}^3} - h^4q\\
\sigma_\beta &= h^4q\\
\sigma_\gamma &= h^2\frac{q}{\bar{q}^2}\\
\tau_{\alpha\beta} &= -\frac{h^4p\bar{p}}{\bar{q}}\\
\tau_{\alpha\gamma} &= \tau_{\beta\gamma} = 0
\end{aligned}\right\} \qquad [31]$$

Basic solution R_{22}

$$\left.\begin{aligned}
u_\alpha &= \frac{h}{2G}\left[(4\nu-2)Q + \frac{1}{\bar{q}^2}\right]p^2\bar{q}\\
u_\beta &= \frac{h}{2G}\,[(2-4\nu)p\bar{p}q\bar{q}Q]\\
u_\gamma &= 0\\
\sigma_\alpha &= \frac{3-2\nu}{q} + \frac{1}{q\bar{q}^2} + \frac{(2-4\nu)q^2-2+2\nu}{q}\,Q\\
&\quad + h^2[(-2+2\nu)q - \frac{q}{\bar{q}^2} + (4\nu-2)q\bar{q}^2Q] - h^4q^3\\
\sigma_\beta &= \frac{2\nu}{q} + \frac{(-2+4\nu)q^2-2\nu}{q}\,Q + h^2[(-1-2\nu)q\\
&\quad + (2-4\nu)q\bar{q}^2Q + h^4q\\
\sigma_\gamma &= \frac{(-1+2\nu)q^2-2\nu}{q\bar{q}^2} - \frac{2\nu Q}{q}\\
&\quad + h^2\left[(1-2\nu)q + \frac{q}{\bar{q}^2}\right]\\
\tau_{\alpha\beta} &= h^2p\bar{p}\left[\frac{1-2\nu}{\bar{q}} + (2-4\nu)\bar{q}Q\right]\\
&\quad - h^4p\bar{p}\left(\bar{q} + \frac{1}{\bar{q}}\right)\\
\tau_{\alpha\beta} &= \tau_{\beta\gamma} = 0
\end{aligned}\right\} \qquad [32]$$

Basic solution R_{12}

$$\left.\begin{aligned}
u_\alpha &= \frac{h}{2G}\,\bar{q}\cdot\frac{3p^2-1}{2}\left(3Q + \frac{1}{\bar{q}^2}\right)\\
u_\beta &= -\frac{h}{2G}\,p\bar{p}\cdot\frac{3}{2}\left[\frac{1+(3q^2-1)Q}{q}\right]\\
u_\gamma &= 0\\
\sigma_\alpha &= \frac{3}{2}\left(\frac{-q^2+2}{q\bar{q}^2}\right) + \frac{3}{2}\left(\frac{-3q^2+2}{q}\right)Q\\
&\quad + \frac{3}{2}h^2\left[\frac{3q^2-5q}{3\bar{q}^2} + 3q\bar{q}^2Q\right] - h^4q\\
\sigma_\beta &= \frac{3}{2q} + \frac{9q^2-3}{2q}\,Q - \frac{3}{2}h^2(q + 3q\bar{q}^2Q) + h^4q\\
\sigma_\gamma &= -\frac{3}{2}\cdot\frac{1}{q\bar{q}^2} - \frac{3}{2}\frac{Q}{q} + \frac{h^2q}{\bar{q}^2}\\
\tau_{\alpha\beta} &= -h^2\cdot\frac{3}{2}\,p\bar{p}\left(\frac{1}{\bar{q}} + 3\bar{q}Q\right) - \frac{h^4p\bar{p}}{\bar{q}}\\
\tau_{\alpha\gamma} &= \tau_{\beta\gamma} = 0
\end{aligned}\right\} \qquad [33]$$

Basic solution R_{11}'

$$\left.\begin{aligned}
u_\alpha' &= \frac{h}{2G'}\,(4\nu'-2)p^2q\bar{q}\\
u_\beta' &= \frac{h}{2G'}\,(2-4\nu')q^2p\bar{p}\\
u_\gamma' &= 0\\
\sigma_\alpha' &= 2\bar{q}^2 + 2\nu'(1-2q^2) + h^2q^2\bar{q}^2(4\nu'-2)\\
\sigma_\beta' &= -2q^2 + 2\nu'(2q^2-1) + h^2q^2\bar{q}^2(2-4\nu')\\
\sigma_\gamma' &= -2\nu'\\
\tau_{\alpha\beta}' &= h^2(2-4\nu')p\bar{p}q\bar{q}\\
\tau_{\alpha\gamma}' &= \tau_{\beta\gamma}' = 0
\end{aligned}\right\} \qquad [34]$$

Basic solution R_{21}'

$$\left.\begin{aligned}
u_\alpha' &= \frac{h}{2G'}\,q\bar{q}\cdot\frac{3}{2}(3p^2-1)\\
u_\beta' &= -\frac{h}{2G'}\,p\bar{p}\cdot\frac{3}{2}(3q^2-1)\\
u_\gamma' &= 0\\
\sigma_\alpha' &= -\frac{3}{2}(3\bar{q}^2+1) + \frac{9}{2}h^2q^2\bar{q}^2\\
\sigma_\beta' &= \frac{3}{2}(3q^2-1) - \frac{9}{2}h^2q^2\bar{q}^2\\
\sigma_\gamma' &= -\frac{3}{2}\\
\tau_{\alpha\beta}' &= -\frac{9}{2}\,p\bar{p}q\bar{q}h^2\\
\tau_{\alpha\gamma}' &= \tau_{\beta\gamma}' = 0
\end{aligned}\right\} \qquad [35]$$

R_1 and R_1' may be represented as in Equations [21] and [22] with the foregoing values for R_{21} and R_{21}' provided the constants a_{11}, a_{21}, a_{31}, b_{11}, and b_{21} are chosen so that the continuity conditions are fulfilled. Equations [20] will be satisfied if these constants satisfy eight simultaneous linear equations. The equations are compatible and their solutions are

$$a_{21} = \frac{Hq_0}{D}\left\{H\left[Q_0(1+\nu')\frac{4\nu-2}{1+\nu}+\frac{1}{\bar{q}_0^2}\frac{2\nu(1+\nu')}{1+\nu}\right]+3Q_0\frac{2'\nu-2\nu'}{1+\nu}+\frac{1}{\bar{q}_0^2}\frac{2-4\nu'+4\nu-2\nu\nu'}{1+\nu}\right\} \quad \text{..[36]}^{1}$$

$$a_{31} = \frac{2}{3}\frac{q_0}{D}\left\{H^2\left[\frac{(4\nu-2)(1-\nu)(1+\nu')}{1+\nu}Q_0-\frac{2\nu(1+\nu')}{(1+\nu)\bar{q}_0^2}-(1+\nu')\right]+H\left[\frac{(2\nu'-2\nu)(3\nu-3)}{1+\nu}Q_0+\frac{-8\nu+4\nu'-2\nu\nu'+2\nu^2+4\nu^2\nu'}{(1+\nu)\bar{q}_0^2}-(3-3\nu')\right]-\frac{1}{\bar{q}_0^2}\left[\frac{(2\nu-2)(2\nu'-2\nu)}{1+\nu}\right]\right\} \quad \text{..[37]}$$

$$a_{11} = -a_{21}q_0^2 - a_{31} \quad \text{..[38]}$$

where

$$H \equiv \left(\frac{G'}{G}-1\right) \quad \text{..[39]}$$

and

$$D \equiv H^2(1+\nu')\left[(4\nu-2)Q_0^2+\frac{Q_0}{\bar{q}_0^2}(4\nu-4-3\bar{q}_0^2)-\frac{1}{\bar{q}_0^2}\right]+H\left\{(6\nu-6\nu')Q_0^2+\frac{Q_0}{\bar{q}_0^2}[(4\nu'-8)(1-\nu)-9(1-\nu')\bar{q}_0^2]+\frac{2-2\nu}{\bar{q}_0^4}-\frac{3-3\nu'}{\bar{q}_0^2}\right\}+\frac{1}{\bar{q}_0^4}(2-2\nu')(2-2\nu) \quad \text{..[40]}$$

A simple calculation shows that R_{11}' and R_{31}' correspond to uniform stress fields; hence the inclusion is in a uniform state of stress under this loading condition.

Solution for Case 2

The boundary conditions here are

$$\text{as } q \to \infty \qquad \sigma_x, -\sigma_y \to 1 \qquad \sigma_z, \tau_{xy}, \tau_{yz}, \tau_{zx} \to 0 \quad \text{.....[41]}$$

Appropriate harmonic functions generating basic solutions are found to be

$$R_{12}: \quad \varphi = S_0^{(2)}(q)\,[-F_0^{(2)}(p)+\tfrac{1}{2}S_0^{(2)}(p)]\cos 2\gamma, \quad \vartheta = S_0^{(2)}(q)\,[-F_0^{(2)}(p)+\tfrac{1}{2}S_0^{(2)}(p)]\sin 2\gamma, \quad \lambda = S_1^{(2)}(q)[3F_1^{(2)}(p)+\tfrac{1}{2}S_1^{(2)}(p)]\cos 2\gamma \quad \text{..[42]}$$

$$R_{32}: \quad \varphi = 8S_2^{(2)}(q)\,F_2^{(2)}(p)\cos 2\gamma \quad \text{.....[43]}$$

$$R_{32}: \quad \vartheta = 8S_2^{(2)}(q)\,F_2^{(2)}(p)\sin 2\gamma \quad \text{.....[44]}$$

[1] The subscript 0 is used to denote functions evaluated at $q = q_0$.

These functions take the form

$$R_{12}: \quad \varphi = \frac{q}{\bar{q}^2}\frac{1+p^2}{p^2}\cos 2\gamma, \quad \vartheta = \frac{q}{\bar{q}^2}\frac{1+p^2}{p^2}\sin 2\gamma, \quad \lambda = \frac{1}{\bar{q}^2}\frac{3p-p^3}{p^3}\cos 2\gamma \quad \text{.....[45]}$$

$$R_{32}: \quad \varphi = \frac{\bar{q}^3-2+3\bar{q}^4Q}{q\bar{q}^2}p^2\cos 2\gamma \quad \text{.....[46]}$$

$$R_{32}: \quad \vartheta = \frac{\bar{q}^3-2+3\bar{q}^4Q}{q\bar{q}^2}p^2\sin 2\gamma \quad \text{.....[47]}$$

Each of the harmonic functions given by Equations [45] is singular at $p = 0$. The z-axis is then a line of singularities for these functions, and they do not individually generate solutions which are regular over the region $q > q_0$. However, a linear combination of these three solutions which is regular over this region may be constructed. This solution is called R_{12}.

R_{12}' is taken to be the uniform field solution R_{32} with G and ν replaced by G' and ν'.

The displacement and stress fields are:

Solution R_{32}

$$u_\alpha = \frac{h\bar{q}\bar{q}p^2}{2G}\cos 2\gamma; \quad u_\beta = \frac{h\bar{q}^2p\bar{p}}{2G}\cos 2\gamma; \quad u_\gamma = -\frac{p\bar{q}}{2G}\sin 2\gamma$$

$$\sigma_\alpha = (q^2-h^2q^2\bar{q}^2)\cos 2\gamma, \quad \sigma_\beta = (-\bar{q}^2+h^2q^2\bar{q}^2)\cos 2\gamma, \quad \sigma_\gamma = -\cos 2\gamma, \quad \tau_{\alpha\beta} = h^2p\bar{p}q\bar{q}\cos 2\gamma, \quad \tau_{\alpha\gamma} = -hpq\sin 2\gamma, \quad \tau_{\beta\gamma} = -hp\bar{q}\sin 2\gamma \quad \text{..[48]}$$

Basic solution R_{12}

$$u_\alpha = \frac{h}{2G}\frac{p^2}{q^3}[(5-4\nu)q^2-(3-4\nu)]\cos 2\gamma, \quad u_\beta = \frac{h}{2G}\frac{q}{\bar{q}^3}(2-4\nu)p\bar{p}\cos 2\gamma, \quad u_\gamma = \frac{h^2}{G}\frac{q\bar{p}}{\bar{q}^3}[p^2+(-1+2\nu)\bar{q}^2]\sin 2\gamma$$

$$\sigma_\alpha = \left\{\frac{(-7+2\nu)q}{\bar{q}^2}-\frac{6q}{\bar{q}^4}+h^2\left[(4-2\nu)q+\frac{(6-4\nu)q}{\bar{q}^2}\right]+h^4[3q\bar{q}^2+4\nu q]\right\}\cos 2\gamma$$

$$\sigma_\beta = \left\{-\frac{(2+2\nu)q}{\bar{q}^2}+h^2\left[(5+2\nu)q+\frac{2q}{\bar{q}^2}\right]+h^4(-3q\bar{q}^2-4\nu q)\right\}\cos 2\gamma$$

$$\sigma_\gamma = \left\{\frac{(3-6\nu)q}{\bar{q}^2}+\frac{6q}{\bar{q}^4}+h^2\left[(-3+6\nu)q+\frac{(-8+4\nu)q}{\bar{q}^2}\right]\right\}\cos 2\gamma \quad \text{..[49]}$$

$$
\left.
\begin{aligned}
\tau_{\alpha\beta} &= p\bar{p}\left\{h^2\left(\frac{-1+2\nu}{\bar{q}}+\frac{-2+4\nu}{\bar{q}^3}\right)\right. \\
&\qquad \left. + h^4\left(3\bar{q}+\frac{4\nu}{\bar{q}}\right)\right\}\cos 2\gamma \\
\tau_{\alpha\gamma} &= \bar{p}\left\{h\left(\frac{-8+4\nu}{\bar{q}^2}-\frac{6}{\bar{q}^4}\right)\right. \\
&\qquad \left. + h^3(2-2\nu)\left(1+\frac{2}{\bar{q}^2}\right)+h^4(4-4\nu)q^2\right\}\sin 2\gamma \\
\tau_{\beta\gamma} &= p\left\{h\frac{(-2+4\nu)q}{\bar{q}^3}+h^3\frac{(4-4\nu)q}{\bar{q}}\right. \\
&\qquad \left. + h^4(-4+4\nu)q\bar{q}\right\}\sin 2\gamma
\end{aligned}
\right\} \ldots [49]\ (cont.)
$$

Basic solution R_{22}

$$
\left.
\begin{aligned}
u_\alpha &= \frac{h}{2G}\left(\frac{2\bar{q}^3+2}{\bar{q}^3}+6\bar{q}Q\right)\bar{p}^2\cos 2\gamma \\
u_\beta &= \frac{h}{2G}\left(\frac{\bar{q}^3-2+3\bar{q}^4Q}{q\bar{q}^3}\right)\cdot 2p\bar{p}\cos 2\gamma \\
u_\gamma &= -\frac{2}{2G}\left(\frac{\bar{q}^3-2+3\bar{q}^4Q}{q\bar{q}^3}\right)\bar{p}\sin 2\gamma \\
\sigma_\alpha &= \left\{\frac{2q}{\bar{q}^2}-\frac{12q}{\bar{q}^4}+6qQ\right. \\
&\qquad \left. + h^2\left(-2q+\frac{4q}{\bar{q}^3}-6q\bar{q}^2Q\right)+8h^4q^3\right\}\cos 2\gamma \\
\sigma_\beta &= \left\{-\frac{2}{q}+\frac{4}{q\bar{q}^2}-\frac{6\bar{q}^2Q}{q}\right. \\
&\qquad \left. + h^2\left(2q+\frac{4q}{\bar{q}^3}+6q\bar{q}^2Q\right)-8h^4q^3\right\}\cos 2\gamma \\
\sigma_\gamma &= \left\{\frac{6}{q\bar{q}^2}+\frac{12}{q\bar{q}^4}-\frac{6Q}{q}-h^2\frac{8q}{\bar{q}^2}\right\}\cos 2\gamma \\
\tau_{\alpha\beta} &= p\bar{p}\left\{h^2\left(\frac{2}{\bar{q}}+\frac{4}{\bar{q}^3}+6\bar{q}Q\right)+h^4\frac{8}{\bar{q}}\right\}\cos 2\gamma \\
\tau_{\alpha\gamma} &= p\bar{h}\left(-\frac{2}{\bar{q}^3}-\frac{12}{\bar{q}^4}-6Q\right)\sin\ \gamma \\
\tau_{\beta\gamma} &= p\bar{h}\left(-\frac{2}{q\bar{q}}+\frac{4}{q\bar{q}^2}-\frac{6\bar{q}Q}{q}\right)\sin 2\gamma
\end{aligned}
\right\} \ldots [50]
$$

Basic solution R_{32}

$$
\left.
\begin{aligned}
u_\alpha &= \frac{2h}{G}\left(\frac{\bar{q}^3-2+3\bar{q}^4Q}{\bar{q}^3}\right)\bar{p}^2\cos 2\gamma \\
u_\beta &= \frac{2h}{G}\left(\frac{\bar{q}^3-2+3\bar{q}^4Q}{q\bar{q}^3}\right)p\bar{p}\cos 2\gamma \\
u_\gamma &= \frac{1}{G}\left[\frac{8h^3p^2\bar{p}}{q\bar{q}}-\frac{(2q^3+2+6\bar{q}^4Q)\bar{p}}{q\bar{q}^3}\right]\sin 2\gamma \\
\sigma_\alpha &= \left[\frac{4q}{\bar{q}^2}+\frac{24q}{\bar{q}^4}+12qQ\right. \\
&\qquad \left. + h^2\left(-4q-\frac{24q}{\bar{q}^2}-12q\bar{q}^2Q\right)\right]\cos 2\gamma \\
\sigma_\beta &= \left[-\frac{4}{q}+\frac{8}{q\bar{q}^2}-\frac{12\bar{q}^2Q}{q}\right. \\
&\qquad \left. + h^2\left(4q-\frac{8q}{\bar{q}^2}+12q\bar{q}^2Q\right)\right]\cos 2\gamma
\end{aligned}
\right\} \ldots [51]
$$

$$
\left.
\begin{aligned}
\sigma_\gamma &= \left[-\frac{36}{q\bar{q}^2}-\frac{24}{q\bar{q}^4}-\frac{12Q}{q}+h^2\frac{32\bar{q}}{\bar{q}^3}\right]\cos 2\gamma \\
\tau_{\alpha\beta} &= p\bar{p}h^2\left(\frac{4}{\bar{q}}+\frac{8}{\bar{q}^3}+12\bar{q}Q\right)\cos 2\gamma \\
\tau_{\alpha\gamma} &= \bar{p}\left[h\left(\frac{20}{\bar{q}^2}+\frac{24}{\bar{q}^4}-12Q\right)\right. \\
&\qquad \left. + h^3\left(-8-\frac{16}{\bar{q}^2}\right)-16h^4q^2\right]\sin 2\gamma \\
\tau_{\beta\gamma} &= p\left[h\left(-\frac{4}{q\bar{q}}+\frac{8}{q\bar{q}^3}-\frac{12\bar{q}Q}{q}\right)\right. \\
&\qquad \left. - h^3\frac{16q}{\bar{q}}+h^4 16q\bar{q}\right]\sin 2\gamma
\end{aligned}
\right\} \ldots [51]\ (cont.)
$$

R_1 and R_1' may be represented as in Equations [21] and [22] with the foregoing solutions provided a_{11}, a_{21}, a_{31}, and b_{12} are chosen so that the continuity conditions defined in Equations [20] are fulfilled.

Although eleven simultaneous linear equations arise from the continuity conditions, the rank of the augmented matrix is but four.

The solutions for the coefficients are found to be

$$
\left.
\begin{aligned}
a_{12} &= 8/k \\
a_{22} &= (-3\bar{q}_0{}^2-4\nu\ )/k \\
a_{32} &= 2(1-\nu)/k \\
b_{12} &= \frac{48(1-\nu)}{q_0\bar{q}_0{}^2\left(\dfrac{G}{G'}-1\right)k}
\end{aligned}
\right\} \ldots\ldots [52]
$$

where

$$
k \equiv \frac{1}{q_0\bar{q}_0{}^2}\left[\frac{48(1-\nu)}{\left(\dfrac{G}{G'}-1\right)}+12+6\bar{q}_0{}^2+(18\bar{q}_0{}^2-24+48\nu)\bar{q}_0{}^2Q_0\right] \ldots [53]
$$

Again, the inclusion is found to be in a uniform state of stress.

Solution for Loading Case 3

The boundary conditions are

$$
\text{as } q \to \infty \qquad \sigma_z \to 1;\ \sigma_x, \sigma_y, \tau_{xy}, \tau_{yz}, \tau_{zx} \to 0 \ldots\ldots [54]
$$

R_{13}, R_{23}, and R_{33} are taken as equal to R_{11}, R_{21}, and R_{31}, the stress and displacement components of which are defined by Equations [31], [32], and [33], respectively. R_{13}' and R_{23}' are obtained from R_{21} and R_{23} by replacing G and ν by G' and ν'. The components of stress and displacement corresponding to R_{01} and R_{02} are given in Equations [30] and [55].

Solution R_{03}.

$$
\left.
\begin{aligned}
u_\alpha &= \frac{hq\bar{q}}{2G(1+\nu)}\left[(1+\nu)\bar{p}^2-\nu\right] \\
u_\beta &= \frac{hp\bar{p}}{2G(1+\nu)}\left[\nu-(1+\nu)q^2\right] \\
u_\gamma &= 0 \\
\sigma_\alpha &= -\bar{q}^2+h^2q^2\bar{q}^2 \\
\sigma_\beta &= q^2-h^2q^2\bar{q}^2
\end{aligned}
\right\} \ldots\ldots [55]
$$

$$\left.\begin{aligned} \sigma_\gamma &= 0 \\ \tau_{\alpha\beta} &= -h^3 q\bar{q} p\bar{p} \\ \tau_{\alpha\gamma} &= \tau_{\beta\gamma} = 0 \end{aligned}\right\} \quad \text{(cont.)} \qquad [55]$$

The coefficients are determined through the continuity conditions defined by Equations [20] and are found to have the values

$$a_{23} = \left.\begin{aligned} &\frac{H q_0}{D}\left\{H(1+\nu')\left[\frac{2\nu-1}{1+\nu}Q_0 - \frac{1}{(1+\nu)\bar{q}_0^3}\right]\right. \\ &\left. + \frac{3(\nu-\nu')Q_0}{1+\nu} + \frac{1}{(1+\nu)\bar{q}_0^3}\left[(2\nu'-2)(1+\nu)+\nu-\nu'\right]\right\} \end{aligned}\right\} \qquad [56]$$

$$a_{33} = \left.\begin{aligned} &-\frac{2}{3}\frac{q_0}{D}\left\{H^3\frac{1+\nu'}{1+\nu}\left[(4\nu-2)\nu Q_0 - (1+\nu)\frac{1}{\bar{q}_0^3}\right]\right. \\ &+ H\left[\frac{\nu-\nu'}{1+\nu}6\nu Q_0 - (3-3\nu') + \frac{1}{(1+\nu)\bar{q}_0^3}\right. \\ &\left.\left.(-2+\nu-\nu'+4\nu\nu'-2\nu^2)\right] + \frac{(2-2\nu)(\nu-\nu')}{(1+\nu)\bar{q}_0^3}\right\} \end{aligned}\right\} \qquad [57]$$

$$a_{13} = -a_{23}Q_0^3 - a_{33} \qquad [58]$$

Solution for Loading Case 4

The boundary conditions are

$$\text{as } q \to \infty \; \tau_{xz} \to 1; \; \sigma_x, \sigma_y, \sigma_z, \tau_{xy}, \tau_{yz} \to 0 \qquad [59]$$

The following harmonic functions will be used

$$R_{14}: \quad \left.\begin{aligned} \varphi &= S_0^{(1)}(q)[F_0^{(1)}(p) + S_0^{(1)}(p)]\cos\gamma \\ \vartheta &= S_0^{(1)}(q)\,[F_0^{(1)}(p) + S_0^{(1)}(p)]\sin\gamma \end{aligned}\right\} \qquad [60]$$

$$R_{24}: \; \varphi = 2S_2^{(1)}(q)F_2^{(1)}(p)\cos\gamma \qquad [61]$$

$$R_{24}: \; \vartheta = 2S_2^{(1)}(q)F_2^{(1)}(p)\sin\gamma \qquad [62]$$

$$R_{44}: \; \lambda = 2S_1^{(1)}(q)F_1^{(1)}(p)\cos\gamma \qquad [63]$$

These functions have the form

$$R_{14}: \quad \left.\begin{aligned} \varphi &= \frac{1}{\bar{q}}\frac{p}{\bar{p}}\cos\gamma \\ \vartheta &= \frac{1}{\bar{q}}\frac{p}{\bar{p}}\sin\gamma \end{aligned}\right\} \qquad [64]$$

$$R_{24}: \; \varphi = \bar{q}\left(3Q + \frac{1}{\bar{q}^3}\right)p\bar{p}\cos\gamma \qquad [65]$$

$$R_{24}: \; \vartheta = \bar{q}\left(3Q + \frac{1}{\bar{q}^3}\right)p\bar{p}\sin\gamma \qquad [66]$$

$$R_{44}: \; \lambda = \frac{\bar{q}}{q}\left(Q + \frac{1}{\bar{q}^3}\right)p\cos\gamma \qquad [67]$$

Again, the harmonic functions given in Equations [64] are each singular along the z-axis. However, a linear combination of these two solutions may be constructed in such a way that the resulting stress field is regular in the region $q > q_0$. This combination is called R_{14}.

R_{14}' is set equal to R_{01} except, of course, that G and ν are replaced by G' and ν'. R_{24}' corresponds to a rigid-body rotation about the y-axis.

The pertinent stress and displacement fields are

Solution R_{01}

$$\left.\begin{aligned} u_\alpha &= \frac{h}{2G}(2q^2-1)\,p\bar{p}\cos\gamma \\ u_\beta &= \frac{h}{2G}q\bar{q}\,(2p^2-1)\cos\gamma \\ u_\gamma &= -\frac{1}{2G}q\bar{p}\sin\gamma \\ \sigma_\alpha &= 2h^3 q\bar{q}p\bar{p}\cos\gamma \\ \sigma_\beta &= -2h^3 q\bar{q}p\bar{p}\cos\gamma \\ \sigma_\gamma &= 0 \\ \tau_{\alpha\beta} &= \{-(2q^2-1)+2h^3q^2\bar{q}^2\}\cos\gamma \\ \tau_{\alpha\gamma} &= -h\bar{q}p\sin\gamma \\ \tau_{\beta\gamma} &= h q\bar{p}\sin\gamma \end{aligned}\right\} \qquad [68]$$

Basic solution R_{14}

$$\left.\begin{aligned} &u_\alpha = 0,\; u_\beta = -\frac{h}{G}\left(\frac{1}{\bar{q}}\right)\cos\gamma,\; u_\gamma = \frac{h^3 p}{G} \\ &\sigma_\alpha = -2h^4\frac{p\bar{p}}{\bar{q}}\cos\gamma \\ &\sigma_\beta = 2h^4\frac{p\bar{p}}{\bar{q}}\cos\gamma \\ &\sigma_\gamma = 0 \\ &\tau_{\alpha\beta} = \left(\frac{h^3 q}{\bar{q}^3} + 2h^4 q\right)\cos\gamma \\ &\tau_{\alpha\gamma} = \left(-\frac{h^3 p q}{\bar{q}} - 2h^5 p q\bar{q}\right)\sin\gamma \\ &\tau_{\beta\gamma} = \left[\frac{h^3 p}{\bar{q}^3}(2q^2-1) - 2h^5 q^2 p\right]\sin\gamma \end{aligned}\right\} \qquad [69]$$

Basic solution R_{24}

$$\left.\begin{aligned} u_\alpha &= \frac{h}{2G}\left[\frac{6q^3-3}{q}Q + \frac{2q^3-3}{q\bar{q}^3}\right]p\bar{p}\cos\gamma \\ u_\beta &= -\frac{h}{2G}\left[\bar{q}\left(3Q + \frac{1}{\bar{q}^3}\right)(1-2p^2)\right]\cos\gamma \\ u_\gamma &= -\frac{1}{2G}\left(3Q + \frac{1}{\bar{q}^3}\right)p\sin\gamma \\ \sigma_\alpha &= \left[h^3\left(6q\bar{q}Q + \frac{2q^3}{\bar{q}^3}\right)p\bar{p} + h^4\left(\frac{2}{\bar{q}}\right)p\bar{p}\right]\cos\gamma \\ \sigma_\beta &= \left[-h^3\left(6q\bar{q}Q + \frac{2}{\bar{q}}\right)p\bar{p} - h^4\left(\frac{2}{\bar{q}}\right)p\bar{p}\right]\cos\gamma \\ \sigma_\gamma &= -2h^2\frac{p\bar{p}}{\bar{q}^3}\cos\gamma \\ \tau_{\alpha\beta} &= \left\{-\left[\frac{6q^3-3}{q}Q + \frac{2q^3-3}{q\bar{q}^3}\right]\right. \\ &\qquad \left. + h^2 2q\bar{q}^2\left(3Q + \frac{1}{\bar{q}^3}\right) - 2qh^4\right\}\cos\gamma \\ \tau_{\alpha\gamma} &= -hp\left(\frac{3\bar{q}}{q}Q + \frac{q^2-3}{q\bar{q}^3}\right)\sin\gamma \\ \tau_{\beta\gamma} &= h\bar{p}\left(3Q + \frac{1}{\bar{q}^3}\right)\sin\gamma \end{aligned}\right\} \qquad [70]$$

Basic solution R_{34}

$$
\begin{aligned}
u_\alpha &= \frac{h}{G}\, q \left(3Q + \frac{1}{\bar{q}^2}\right) p\bar{p} \cos\gamma \\
u_\beta &= \frac{h}{G}\, \bar{q} \left(3Q + \frac{1}{\bar{q}^2}\right) p^2 \cos\gamma \\
u_\gamma &= \frac{1}{G} \left\{\left(-3Q + \frac{1}{\bar{q}^2}\right) - 2h^2 \right\} p \sin\gamma \\
\sigma_\alpha &= 2h^2 \left(3\bar{q}Q + \frac{q^2-3}{\bar{q}^3}\right) p\bar{p} \cos\gamma \\
\sigma_\beta &= -2h^2\bar{q} \left(3Q + \frac{1}{\bar{q}^2}\right) p\bar{p} \cos\gamma \\
\sigma_\gamma &= \frac{4h^2 p\bar{p}}{\bar{q}^2} \cos\gamma \\
\tau_{\alpha\beta} &= \left\{-\left(\frac{6q^2-3}{q}Q + \frac{2q^2-3}{q\bar{q}^2}\right) \right. \\
&\qquad \left. + h^2 q\bar{q} \left(6\bar{q}Q + \frac{2q^2-4}{\bar{q}^3}\right)\right\} \cos\gamma \\
\tau_{\alpha\gamma} &= \left\{h \left(-\frac{3\bar{q}}{q} Q - \frac{7q^2-3}{q\bar{q}^3}\right) \right. \\
&\qquad \left. + 2h^2 \frac{q}{\bar{q}} + 4\, h^4 q\bar{q}\right\} p \sin\gamma \\
\tau_{\beta\gamma} &= \left\{h \left(3Q + \frac{1}{\bar{q}^2}\right) + h^2 \left(\frac{-4q^2+2}{\bar{q}^2}\right) \right. \\
&\qquad \left. + 4\, h^4 q^2 \right\} p \sin\gamma
\end{aligned}
\qquad \ldots [71]
$$

Basic solution R_{44}

$$
\begin{aligned}
u_\alpha &= \frac{hp\bar{p}}{2G} \left[q \left(Q - \frac{1}{\bar{q}^2}\right) \right. \\
&\qquad \left. - (3-4\nu) \frac{\bar{q}^2}{q} \left(Q + \frac{1}{\bar{q}^2}\right)\right] \cos\gamma \\
u_\beta &= \frac{h}{2G} \left[\bar{q} \left(Q + \frac{1}{\bar{q}^2}\right) p^2 \right. \\
&\qquad \left. + (3-4\nu)\bar{q} \left(Q + \frac{1}{\bar{q}^2}\right) p^2 \right] \cos\gamma \\
u_\gamma &= -\frac{1}{2G} \left(Q + \frac{1}{\bar{q}^2}\right) p \sin\gamma \\
\sigma_\alpha &= \left\{h^2 \left[-2\bar{q}Q + \frac{1}{\bar{q}^3}\,(4q^2-2)\right] + 4\nu h^2 \bar{q} Q \right. \\
&\qquad \left. + h^4 \left(\frac{2q^2}{\bar{q}}\right)\right\} p\bar{p} \cos\gamma \\
\sigma_\beta &= \left\{2h^2\bar{q} \left(Q + \frac{1}{\bar{q}^2}\right) - 4\nu h^2 \bar{q} Q \right. \\
&\qquad \left. - h^4 \left(\frac{2q^2}{\bar{q}}\right)\right\} p\bar{p} \cos\gamma \\
\sigma_\gamma &= h^2 p\bar{p} \left(-\frac{2q^2}{\bar{q}^3} + \frac{4\nu}{\bar{q}}\right) \cos\gamma \\
\tau_{\alpha\beta} &= \left\{(1-2\nu) \left(\frac{2q^2-1}{q} Q - \frac{1}{q\bar{q}^2}\right) \right. \\
&\qquad \left. + h^2[(1-2\nu)(-2q\bar{q}^2 Q) + 2q] - 2h^4 q^3\right\} \cos\gamma
\end{aligned}
\qquad \ldots [72]
$$

$$
\begin{aligned}
\tau_{\alpha\gamma} &= -h \left[\frac{\bar{q}}{q} Q(2\nu-1) - \left(\frac{2q^2}{\bar{q}^2} + 1 - 2\nu\right) \right. \\
&\qquad \left. \cdot \frac{1}{q\bar{q}}\right] p \sin\gamma \\
\tau_{\beta\gamma} &= -h \left(Q + \frac{1}{\bar{q}^2}\right) (1-2\nu) \bar{p} \sin\gamma
\end{aligned}
\qquad \ldots [72] \textit{(cont.)}
$$

Solution R_{24}'

$$
\begin{aligned}
u_\alpha &= \frac{h}{2G'}\, p\bar{p} \cos\gamma \\
u_\beta &= \frac{h}{2G'}\, q\bar{q} \cos\gamma \\
u_\gamma &= -\frac{qp}{2G'} \sin\gamma \\
\sigma_\alpha &= \sigma_\beta = \sigma_\gamma = \tau_{\alpha\beta} = \tau_{\alpha\gamma} = \tau_{\beta\gamma} = 0
\end{aligned}
\qquad \ldots [73]
$$

Again, solutions of the type of Equations [21] and [22] are sought. It is found that the continuity conditions will be fulfilled provided the coefficients have the following values

$$
\begin{aligned}
a_{14} &= \frac{2}{3}(1-\nu)\, a_{44} \\
a_{24} &= \left[\frac{2}{3}(1-\nu) - q_0^2\right] a_{44} \\
a_{34} &= \frac{1}{3}(1-\nu)\, a_{44} \\
b_{14} &= \frac{G'}{G} \frac{2-2\nu}{H\bar{q}_0^2 q_0}\, a_{44} \\
b_{24} &= \frac{G'}{G} \cdot \frac{1}{q_0} (3-2\nu) \left(Q_0 + \frac{1}{\bar{q}_0^2}\right) a_{44} \\
a_{44} &= -q_0 \Big/ \left\{Q_0(2-\nu-3q_0^2) \right. \\
&\qquad \left. + \frac{1}{\bar{q}_0^2}\left[\nu - q_0^2 - \frac{1}{H}(2-2\nu)\right]\right\}
\end{aligned}
\qquad \ldots [74]
$$

Discussion of Results

Numerical evaluations based on the foregoing analysis were made for the technically most significant loading case of uniaxial tension at infinity which is characterized by the boundary conditions

$$\text{as} \quad q \to \infty \quad \sigma_x \to 1; \quad \sigma_y, \sigma_z, \tau_{xy}, \tau_{xz}, \tau_{yz} \to 0 \ldots\ldots [75]$$

It is evident that the arithmetic mean of the solutions to Cases 1 and 2 is the solution corresponding to the conditions of Equation [75]. Regardless of the loading, the state of stress at any point of the medium depends on the shape parameter q_0, the elastic constants ν, ν', and $H = (G'/G - 1)$, as well as on the position of the point. In all computations it was assumed that $\nu = \nu' = 0.3$.

The stress component σ_x was evaluated at the three points A, B, and C on the boundary of the inclusion, Fig. 1. Since the interior region is in a homogeneous state of stress whenever the limiting stress field at infinity is uniform, σ_x' is independent of position in the region $q < q_0$. Furthermore, because of the continuity conditions, σ_x is equal to σ_x at B.

In Figs. 2, 3, and 4, σ_x at A, B, and C is plotted as a function of the shape ratio s for various values of the material parameter H. Here s is the ratio b/a, where a and b are the lengths of the semi-

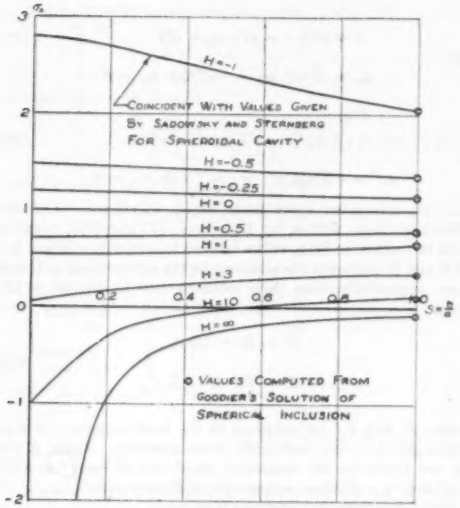

FIG. 2 UNIAXIAL TENSION $\sigma_z = 1$ AT INFINITY
(σ_z at polar point A' as a function of shape ratio for various values of $H = [(G'/G) - 1]$, $\nu = \nu' = 0.3$.)

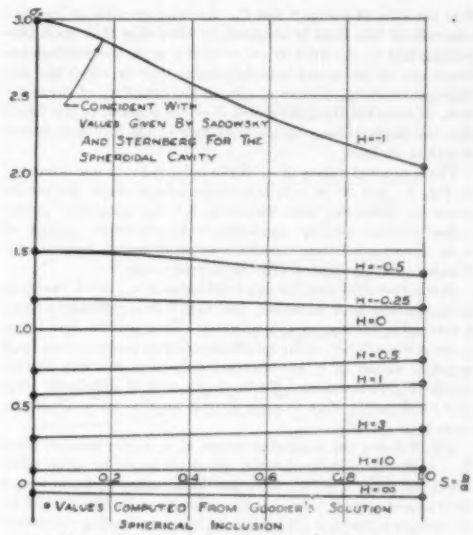

FIG. 4 UNIAXIAL TENSION $\sigma_z = 1$ AT INFINITY
(σ_z at equator point C as a function of shape ratio for various values of $H = [(G'/G) - 1]$, $\nu = \nu' = 0.3$.)

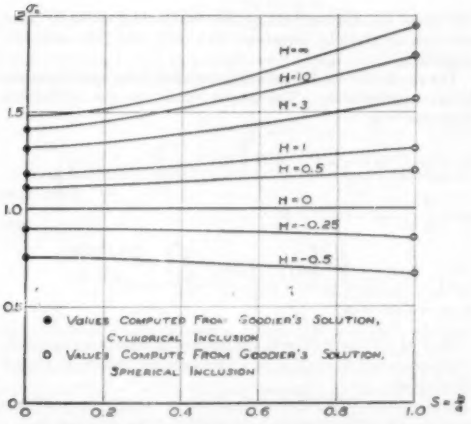

FIG. 3 UNIAXIAL TENSION $\sigma_z = 1$ AT INFINITY
σ_z at equator point B as a function of shape ratio for various values of $H = [(G'/G) - 1]$, $\nu = \nu' = 0.3$.)

major and semiminor axes, respectively, of a meridian of the inclusion. It is to be noted that specification of s is equivalent to fixing q_0, since $s = \bar{q}_0/q_0$.

Certain particular values of H are of special interest. If $H = -1$, the problem reduces to that of the spheroidal cavity; if $H = 0$, the stress distribution throughout is that of the uniform field at infinity, since the elastic properties of the core are then identical with those of the surrounding medium; the limit $H > \infty$ corresponds to an ideally rigid inclusion.

In turn certain limiting values of s deserve special attention. If $s = 1$, the inclusion is spherical in shape. The known solution to the problem of the spherical inclusion (3) then affords a check for the limiting case $s \to 1$.

The limit $s \to 0$ can be interpreted geometrically in two ways. If $b \to 0$ with a fixed, the spheroid degenerates into a straight-line segment. However, if b is fixed and $a \to \infty$, the shape of the inclusion approaches that of an infinite circular cylinder of radius b, whose geometric axis coincides with the z-axis.

In the region $q > 1$, the state of stress tends to that of the uniform field at infinity as $s \to 0$. However, the corresponding limit of σ_z at (p, q, γ) is not uniform with respect to q. For fixed values of p and γ, the limit of σ_z

$$\text{as} \begin{cases} s \to 0 \\ q \to q_0 \end{cases}$$

does not exist. If the limit is taken in the order $s \to 0, q \to q_0$, the limiting value of σ_z is that of the uniform field. However, proceeding to the limit in the order $q \to q_0, s \to 0$, a different limiting value of σ_z is obtained. This behavior is typical of problems involving stress concentrations around cavities or inclusions.

In determining values of σ_z at A, B, and C, the limit $q \to q_0$ was taken at the outset, hence the limit of σ_z as $s \to 0$, which is indicated in Figs. 2, 3, and 4, is not the uniform field value of unity. At the equatorial points B and C, the limit of σ_z as $s \to 0$ is in fact equal to the value of σ_z at corresponding points computed from the solution to the problem of the infinite cylindrical-shaped inclusion under analogous loading conditions,[6] provided H is finite.

However, the limit of σ_z

$$\text{as} \begin{cases} s \to 0 \\ H \to \infty \end{cases}$$

[6] Reference (3), p. 43.

does not exist at points B and C. An interpretation of the nonexistence of this limit is obtained by observing that upon proceeding first to the limit $H \to \infty$ with $s \neq 0$, the problem becomes one of the mixed boundary-value type in which the displacements are specified to vanish on the boundary of the inclusion. If, however, the order $s \to 0$, $H \to \infty$ is adhered to, it is found that the displacements on the boundary of the inclusion do not vanish in the limit.

The computed values of σ_x at the polar point A are presented in Fig. 2. For $H = -1$, the computations check the results given by Sadowsky and Sternberg for the spheroidal cavity under similar loading conditions.[7] Furthermore, values of σ_x at A computed from Goodier's solution[8] for the spherical inclusions are in agreement with the present results.

It is noteworthy that for any fixed value of s, σ_x at A decreases monotonically as H increases; and that if H is sufficiently large, a reversal in the sign of σ_x is effected. This reversal already appears in the solution of the spherical-inclusion problem,[8] but large negative values of σ_x are obtained only with the very slender needle-shaped inclusion. Furthermore, with H sufficiently large and s sufficiently close to zero, σ_x at A may be made arbitrarily large in magnitude.

Fig. 3 shows the computed values of σ_x at the equator point B. Again, the solution for the spherical-shaped inclusion offers check points at $s = 1$. Also, for finite values of H, as $s \to 0$ the value of σ_x at B reduces to the value given by the solution for the infinite cylindrical inclusion with the same loading conditions.

Quite apparently, σ_x at B must be zero for $H = -1$. With s fixed, as the rigidity of the inclusion increases, the magnitude of σ_x increases and the maximum value of σ_x is attained if the inclusion is ideally rigid. The maximum σ_x at point B is obtained for the ideally rigid spherical inclusion.

The computed values of σ_x at C, Fig. 4, coincide with the corresponding results for the spheroidal cavity and the spherical inclusion. Again, as $s \to 0$, σ_x approaches values obtained from the plane-strain solution for the cylindrical inclusion. The most critical values of σ_x at C arise in the case $H = -1$ with small values of s.

Associated Thermal Stress Problem

Consider the previously defined system, composed of an infinite body containing a prolate spheroidal-shaped inclusion. Let the system be in an unstrained state at a uniform temperature T_0, with no loading at infinity. The distribution of stress will be determined under the assumption that the body and inclusion are at uniform temperatures T_1 and T_1', respectively.

A particular case of this problem was investigated by N. O. Myklestad (5), who determined the stress concentration due to a difference in temperature between the inclusion and the body surrounding, under the assumption that the elastic properties associated with the two regions are identical.

The method of solution to be followed in the present problem is essentially the same as that used in the preceding analysis.

Let

$$T = (T_1 - T_0),\ T' = (T_1' - T_0) \qquad [76]$$

and let ϵ, ϵ' designate the coefficients of linear thermal expansion for the materials occupying the exterior and interior regions, respectively.

The displacement and stress distribution, due to a uniform temperature change of each of the two media, in the absence of the other, is readily obtainable. These displacements are

$$\left.\begin{aligned} &q > q_0 \\ &u = \epsilon T x,\ v = \epsilon T y,\ w = \epsilon T z \\ \text{or} \\ &u_\alpha = \epsilon T h q \bar{q},\ u_\beta = -\epsilon T h p \bar{p},\ u_\gamma = 0 \end{aligned}\right\} \qquad [77]$$

$$\left.\begin{aligned} &q < q_0 \\ &u' = \epsilon' T' x,\ V' = \epsilon' T' y,\ w' = \epsilon' T' z \\ \text{or} \\ &u_\alpha' = \epsilon' T' h q \bar{q},\ u'_\beta = -\epsilon' T' h p \bar{p},\ u_\gamma' = 0 \end{aligned}\right\} \qquad [78]$$

and the associated stress fields vanish identically. The displacement fields defined by Equations [77] and [78], together with the null stress field, will be referred to as solutions R_0 and R_0'. If R and R' represent the solutions for the surrounding body and core, respectively, then these solutions may be written in the form

$$\left.\begin{aligned} R &= R_0 + \sum_i a_i R_i \\ R' &= R_0' + \sum_i b_i R_i \end{aligned}\right\} \qquad [79]$$

where R_i and R_i' are solutions to the basic equations of elasticity and a_i, b_i are coefficients of superposition. Again, R and R' are linked by the continuity conditions of Equations [20], and as $q \to \infty$ all stress components of R must vanish.

The following basic solutions will be used

$$R_1 = R_{11},\ R_2 = R_{21},\ R_3 = R_{31}$$
$$R_1' = R_{21},\ R_2' = R_{22}$$

The stress and displacement components corresponding to these solutions are given by Equations [31], [32], [33], [30], and [55], respectively.

The continuity conditions will be satisfied if the coefficients are chosen appropriately. The proper values for the coefficients are found to be

$$\left.\begin{aligned} a_2 &= -\frac{q_0}{D}(\epsilon T - \epsilon' T') \cdot E' H \left(3Q_0 + \frac{1}{\bar{q}_0^2}\right) \\ a_3 &= \frac{2}{3}\frac{q_0}{D}(\epsilon T - \epsilon' T') \cdot E' \\ &\quad \left\{ H\left[(4\nu - 2) Q_0 + \frac{1}{\bar{q}_0^2}\right] + \frac{2 - 2\nu}{\bar{q}_0^2} \right\} \\ a_1 &= -a_2 q_0^2 - a_3 \end{aligned}\right\} \qquad [80]$$

If $\epsilon T = \epsilon' T'$, or if $G' = 0$, the stress components are annulled. Furthermore, if $G = G'$, $\nu = \nu'$, the solution reduces to that of Myklestad.

Comparision With Myklestad's Solution. According to Myklestad (5), the displacements in the exterior region are given by

$$(u, v, w) = \text{grad } V(x, y, z) \qquad [81]$$

where

$$\left.\begin{aligned} V = \frac{\pi \rho a^2 c}{c^2 - a^2}\Bigg[&\left(2\sqrt{c^2 - a^2} + \frac{x^2 + y^2 - 2z^2}{\sqrt{c^2 - a^2}}\right) \\ \sinh^{-1}\sqrt{\frac{c^2 - a^2}{a^2 + k}} &- \frac{\sqrt{c^2 + k}}{a^2 + k}(x^2 + y^2) + \frac{2z^2}{\sqrt{c^2 + k}}\Bigg] \end{aligned}\right\} \qquad [82]$$

and

$$\rho = \frac{1 + \nu}{1 - \nu}\frac{\epsilon T - \epsilon' T'}{4\pi},\ T = 0 \qquad [83]$$

[7] Reference (1), p. 4.
[8] Reference (3), p. 42.

the surface of the inclusion being defined by

$$\frac{x^2 + y^2}{a^2} + \frac{z^2}{c^2} = 1 \quad \ldots\ldots\ldots\ldots\ldots [84]$$

whereas k is defined through

$$\frac{x^2 + y^2}{a^2 + k} + \frac{z^2}{c^2 + k} = 1 \quad \ldots\ldots\ldots\ldots\ldots [85]$$

With a modification of scale, one may write

$$\left.\begin{array}{ll} a^2 + k = \bar{q}^2, & c^2 + k = q^2 \\ a = \bar{q}_0, & c = q_0 \end{array}\right\} \quad \ldots\ldots\ldots [86]$$

so that

$$V = \pi\rho\bar{q}_0^3 q_0 \left[(2 + \bar{q}^2 p^2 - 2q^2 p^2) \sinh^{-1} \frac{1}{\bar{q}} - q(1 - 3p^2) \right] \quad [87]$$

or equivalently

$$V = \frac{1}{4} \frac{1 + \nu}{1 - \nu} \bar{q}_0^3 q_0 (\epsilon T - \epsilon' T') \left[p^2 \frac{1 + (3q^2 - 1)Q}{q} + \frac{1 - (1 + q^2)Q}{q} \right] \quad \ldots\ldots [88]$$

The displacement field defined by Equations [88] and [81] will be compared to the displacement field previously obtained for the special case wherein $G' = G$, $\nu' = \nu$.

For this special case, it follows from Equations [80] that

$$a_2 = 0, \quad a_3 = -a_1 = 2G \frac{q_0 \bar{q}_0^2 (1 + \nu)}{3(1 - \nu)} (\epsilon T - \epsilon' T') \quad \ldots [81]$$

Since solutions R_1 and R_3 are both of the class called basic solution 1, the displacement field is of the form

$$(u, v, w) = \frac{1}{2G} \operatorname{grad} \varphi \quad \ldots\ldots\ldots\ldots\ldots [82]$$

Utilizing Equations [81], [25], and [27] the form of φ is found to be given by

$$\varphi = 2G \frac{q_0 \bar{q}_0^2 (1 + \nu)}{3(1 - \nu)} (\epsilon T - \epsilon' T') \left[\frac{1}{4} (3p^2 - 1) \frac{1 + (3q^2 - 1)Q}{q} + \frac{1 - Q}{q} \right] \quad \ldots [83]$$

By elementary manipulations, one finds that $\varphi = 2GV$, and the displacement fields of the exterior region are thus identical.

Discussion of Results. The dimensionless normal stress component $\sigma_\alpha / E(\epsilon T - \epsilon' T')$ has been computed at the pole and at an equatorial point of the inclusion. The results are presented in Figs. 5 and 6. The method of presentation is similar to that of Figs. 2, 3, and 4.

In the thermal-stress problem under consideration, the state of stress at any point of the medium depends upon the parameters s, H, ν, ν', and $M \equiv E(\epsilon T - \epsilon' T')$, as well as on position. All stress components contain M as a linear factor. In numerical computations it was assumed that $\nu = \nu' = 0.3$.

As $s \to 0$, the state of stress at any point in the region $q > 1$ reduces to the null state. This limit is, however, not uniform in q. The limit of σ_α as $q \to q_0$, $s \to 0$ is not zero unless $H = -1$. Since in computing σ_α at two points on the boundary of the inclusion the limit $q \to q_0$ was taken at the start, the limit of σ_α / M as $s \to 0$ which is indicated in Figs. 5 and 6 is not zero for $H \neq -1$.

In Fig. 5, σ_α / M at the equatorial point B is plotted as a func-

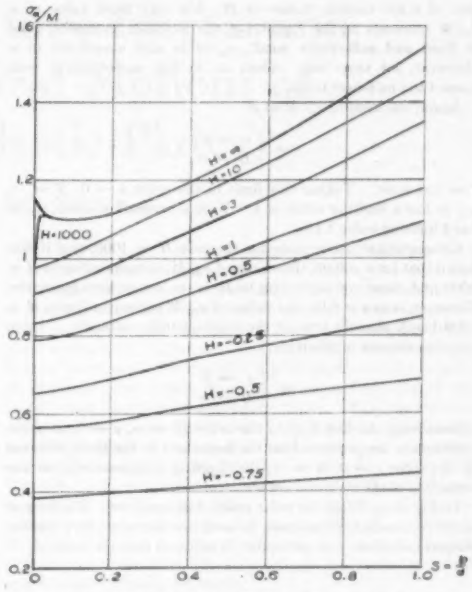

FIG. 5 NORMAL STRESS σ_α / M AT EQUATOR POINT B AS A FUNCTION OF SHAPE RATIO FOR VARIOUS VALUES OF $H = [(G'/G) - 1]$ ($\nu = \nu' = 0.3$. $M = E[\epsilon T - \epsilon' T']$.)

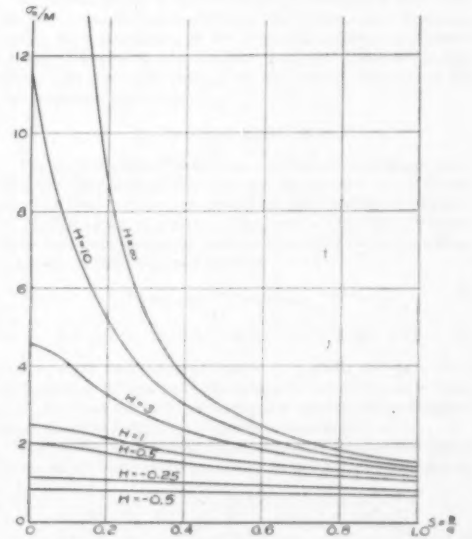

FIG. 6 NORMAL STRESS σ_α / M AT THE POLAR POINT A AS A FUNCTION OF SHAPE RATIO FOR VARIOUS VALUES OF $H = [(G'/G) - 1]$ ($\nu = \nu' = 0.3$ $M = E[\epsilon T - \epsilon' T']$.)

tion of s for various values of H. For any fixed value of s, σ_a/M increases as the rigidity of the inclusion increases. For H fixed and sufficiently small, σ_a/M is also monotonic in s. However, for very large values of H, this monotonicity with respect to s no longer holds.

Again, the limit of σ_a/M at B

$$\text{as} \begin{cases} s \to 0 \\ H \to \infty \end{cases}$$

does not exist. Taking this limit in the order $s \to 0$, $H \to \infty$, σ_a/M has a limiting value of 1. With a reversal of order, σ_a/M has a limiting value 1.15.

Computations were made for the case $H = 1000$, and it was found that for $s > 0.05$, the values of σ_a/M, corresponding to $H = 1000$ and those corresponding to $H = \infty$, are indistinguishable. However, near $s = 0.01$, the values of σ_a/M corresponding to $H = 1000$ break sharply toward the limiting value of unity. Again the nonexistence of this limit

$$\text{as} \begin{cases} s \to 0 \\ H \to \infty \end{cases}$$

follows from the fact that in the order $H \to \infty$, $s \to 0$, zero displacements are preserved on the boundary in the limit, whereas in the order $s \to 0$, $H \to \infty$, the limiting displacements on the boundary of the inclusion are not zero.

In Fig. 6, σ_a/M at the polar point A is presented. The largest stress concentrations are seen to occur for the very sharp needle-shaped inclusion. In particular, it is found that the limit

$$\text{as} \begin{cases} s \to 0 \\ H \to \infty \end{cases}$$

of σ_a/M at A is infinity.

Acknowledgment

The author wishes to express his gratidude to Prof. E. Sternberg of the Illinois Institute of Technology for his valuable suggestions and generous help in the preparation of this paper.

BIBLIOGRAPHY

1 "Stress Concentration Around an Ellipsoidal Cavity in an Infinite Body Under Arbitrary Plane Stress Perpendicular to the Axis of the Cavity," by M. A. Sadowsky and E. Sternberg, JOURNAL OF APPLIED MECHANICS, Trans. ASME, vol. 69, 1947, p. A-191.

2 "Kerbspannungslehre," by H. Neuber and J. W. Edwards, Ann Arbor, Mich., 1944.

3 "Concentration of Stress Around Spherical and Cylindrical Inclusions and Flaws," by J. N. Goodier, JOURNAL OF APPLIED MECHANICS, Trans. ASME, vol. 55, 1933, p. A-39.

4 "Stress Concentrations Due to Elliptical Discontinuities in Plates Under Edge Forces," by L. H. Donnell, Theodore von Kármán Anniversary Volume, 1941, pp. 293–309.

5 "Two Problems of Thermal Stress in the Infinite Solid," by N. O. Myklestad, JOURNAL OF APPLIED MECHANICS, Trans. ASME, vol. 64, 1942, p. A-136.

6 "Application des Poténtiels, by J. Boussinesq, Gauthier-Villars, 1885.

7 "Solution Générale des Équations Différentielles Fondamentales dé Elasticité, Exprimée par Trois Fonctions Harmoniques," by P. F. Papcovich, Academie des Sciences Comptes Rendus, vol. 195, 1932, pp. 513–515.

Influence of Rotatory Inertia and Shear on Flexural Motions of Isotropic, Elastic Plates

By R. D. MINDLIN,[1] NEW YORK, N. Y.

A two-dimensional theory of flexural motions of isotropic, elastic plates is deduced from the three-dimensional equations of elasticity. The theory includes the effects of rotatory inertia and shear in the same manner as Timoshenko's one-dimensional theory of bars. Velocities of straight-crested waves are computed and found to agree with those obtained from the three-dimensional theory. A uniqueness theorem reveals that three edge conditions are required.

Introduction

According to the classical two-dimensional theory of flexural motions of elastic plates, leading to Lagrange's equation

$$D\nabla^4 w + \rho h \frac{\partial^2 w}{\partial t^2} = q(x, y, t) \quad \ldots\ldots [1]$$

the wave velocity of straight-crested waves is inversely proportional to the wave length. The exact solution, by Rayleigh (1),[2] Lamb (2), and Timoshenko (3), of the general equations of the linear theory of elasticity, for the case of straight-crested flexural waves, confirms this result only for waves which are long in comparison with the thickness of the plate. As the wave length diminishes, the velocity in the three-dimensional theory has as its upper limit the velocity of Rayleigh surface waves. Hence the classical plate theory cannot be expected to give good results for sharp transients or for the frequencies of modes of vibration of high order. A similar situation exists in regard to the classical one-dimensional theory of flexural motions of elastic bars, leading to the Bernoulli-Euler equation.

In the case of bars, correction terms have been supplied by Rayleigh and Timoshenko. Rayleigh (4) introduced the effect of rotatory inertia but, although the upper limit of the velocity is thereby made finite, its magnitude is too large. It was not until Timoshenko (5, 6) included the effect of transverse shear deformation that a one-dimensional theory of flexural motions of bars was obtained which gives satisfactory results for short waves and high modes of vibration.

In the case of plates, equations of motion analogous to Timoshenko's bar equations have been given by Uflyand (7) and a corresponding theory of plate equilibrium has been given by Hencky (8). One purpose of the present paper is to show how a more comprehensive two-dimensional theory of flexural motions of plates, analogous to Timoshenko's one-dimensional theory for bars, may be deduced directly from the three-dimensional equations of elasticity. Uflyand's equations of motion are reached, but are later modified in the light of a comparison of the velocity of straight-crested waves with the corresponding velocity obtained from the three-dimensional theory. The modification consists of the selection of the value of a constant, appearing in the relation between average transverse shear stress and strain, variously chosen as 2/3 and 8/9 by Timoshenko, and 2/3 by Uflyand. A formula for this constant, involving Poisson's ratio, is suggested (see Equation [47]). By its use, the limiting velocity for very short waves is made identical with the velocity of Rayleigh surface waves, and velocities intermediate between very long and very short waves are brought into close agreement with the three-dimensional theory.

In addition to the derivation of equations of motion, there are derived theorems dealing with kinetic and potential energies, uniqueness, initial and boundary conditions, and single-valuedness of displacements corresponding to similar theorems in the three-dimensional theory.

At various stages of the development, attention is directed to the very close similarities between the theory under discussion and E. Reissner's theory (9, 10) of flexural equilibrium of plates. Of special interest is the conclusion that, as in Reissner's theory, three boundary conditions are to be satisfied rather than the two of classical plate theory.

Plate-Stress Components

The plate is referred to an x, y, z-system of rectangular co-ordinates. The faces of the plate are the planes $z = \pm h/2$ and its cylindrical surfaces are defined by plane curves or polygons C_f parallel to the x, y-plane. The faces of the plate are taken to be free from tangential traction but under normal pressures q_1 and q_2. Thus in the usual notation

$$\tau_{xz}]_{z=\pm h/2} = \tau_{yz}]_{z=\pm h/2} = 0 \quad \ldots\ldots [2]$$

$$\sigma_z]_{z=h/2} = -q_1(x, y, t), \sigma_z]_{z=-h/2} = -q_2(x, y, t) \quad \ldots [3]$$

For convenience the notation $q = q_2 - q_1$ will be used. Normal pressures are retained on both faces in order that one of them may, if desired, be made proportional to the transverse displacement to simulate the effect of an elastic foundation.

The bending and twisting moments and the transverse shearing forces, all per unit of length, are defined in the customary manner

$$\left.\begin{aligned} (M_x, M_y, M_{xy}) &= \int_{-h/2}^{h/2} (\sigma_x, \sigma_y, \tau_{xy})\, z\, dz \\ (Q_x, Q_y) &= \int_{-h/2}^{h/2} (\tau_{xz}, \tau_{yz})\, dz \end{aligned}\right\} \quad \ldots [4]$$

---

[1] Professor of Civil Engineering, Columbia University; and Consultant, Bell Telephone Laboratories, Murray Hill, N. J. Mem. ASME.

[2] Numbers in parentheses refer to the Bibliography at the end of the paper.

Presented at the Annual Conference of the Applied Mechanics Division, Purdue University, Lafayette, Ind., June 22–24, 1950, of The American Society of Mechanical Engineers.

Discussion of this paper should be addressed to the Secretary, ASME, 29 West 39th Street, New York, N. Y., and will be accepted until April 10, 1951, for publication at a later date. Discussion received after the closing date will be returned.

Note: Statements and opinions advanced in papers are to be understood as individual expressions of their authors and not those of the Society. Manuscript received by the Applied Mechanics Division, January 23, 1950. Paper No. 50—APM-22.

For brevity these will be designated as the "plate-stress components."

Stress-Strain Relations

In three-dimensional elasticity theory there are six components of stress which are expressed in terms of six components of strain through Hooke's law. The stress-strain relations and the expressions for the six components of strain in terms of three components of displacement are then used to reduce to three the number of unknowns in the three equations of motion. In the present theory there are only five plate-stress components and these will be expressed in terms of the same number of "plate-strain components." The latter will then be expressed in terms of three "plate-displacement components."

Consider the general Hooke's law in the form wherein each of the six components of strain is expressed in terms of the six components of stress. Of the six equations, one is ignored, namely, the one containing the unit-elongation (ϵ_z) normal to the faces of the plate. The remaining five equations are then solved for σ_x, σ_y, τ_{yz}, τ_{zx}, and τ_{xy} in terms of ϵ_x, ϵ_y, γ_{yz}, γ_{zx}, γ_{xy} and σ_z. Alternatively, one may start with the expressions for the components of stress in terms of the components of strain, solve the one containing σ_z for ϵ_z and use this to eliminate ϵ_z from the remaining five equations. Integrations are now performed on these equations so as to convert the stress components into plate-stress components in accordance with Equations [4]. The results are then altered in two respects: (*a*) The integrals containing σ_z are dropped; (*b*) the coefficients of the integrals containing γ_{zx} and γ_{yz} are replaced by constants whose magnitudes are to be determined later. This procedure is applicable to anisotropic materials. In the case of an isotropic material, we find

$$\left.\begin{aligned} M_x &= D(\Gamma_x + \mu\Gamma_y), \quad M_y = D(\Gamma_y + \mu\Gamma_x), \\ M_{xy} &= (1-\mu)\,D\Gamma_{xy}/2 \\ Q_x &= G'h\Gamma_{xz}, \quad Q_y = G'h\Gamma_{yz} \end{aligned}\right\} \quad \ldots [5]$$

where the plate modulus D is expressed in terms of Poisson's ratio μ and Young's modulus E, or the modulus of rigidity G, by

$$D = \frac{Eh^3}{12(1-\mu^2)} = \frac{Gh^3}{6(1-\mu)} \quad \ldots [6]$$

and

$$G' = \kappa^2 G \quad \ldots [7]$$

so that G' is the constant which replaces the coefficient, G, of the integrals containing γ_{xz} and γ_{yz} in the integrated stress-strain relations and κ is the constant, referred to in the introduction, for which a formula involving Poisson's ratio will be given presently. The Γ's in Equations [5] are the plate-strain components defined by

$$\left.\begin{aligned} (\Gamma_x, \Gamma_y, \Gamma_{xy}) &= 12h^{-3}\int_{-h/2}^{h/2} (\epsilon_x, \epsilon_y, \gamma_{xy})\,z\,dz \\ (\Gamma_{xz}, \Gamma_{yz}) &= h^{-1}\int_{-h/2}^{h/2} (\gamma_{xz}, \gamma_{yz})\,dz \end{aligned}\right\} \quad \ldots [8]$$

Equations [5] would have been obtained if it had been assumed that $\sigma_z = 0$ at the start. However, the procedure adopted reveals that only a linearly weighted, average effect of σ_z is neglected, rather than σ_z itself.

Plate-Displacement Components

To proceed toward the establishment of plate-strain-displacement relations, the strain-displacement relations of the three-dimensional theory are integrated in accordance with the right-hand sides of Equations [8]. Thus

$$\left.\begin{aligned} \int_{-h/2}^{h/2} (\epsilon_x, \epsilon_y, \gamma_{xy})\,z\,dz &= \int_{-h/2}^{h/2} \left(\frac{\partial u}{\partial x}, \frac{\partial v}{\partial y}, \frac{\partial v}{\partial x} + \frac{\partial u}{\partial y}\right) z\,dz \\ \int_{-h/2}^{h/2} (\gamma_{xz}, \gamma_{yz})\,dz &= \int_{-h/2}^{h/2} \left(\frac{\partial u}{\partial z} + \frac{\partial w}{\partial x}, \frac{\partial v}{\partial z} + \frac{\partial w}{\partial y}\right) dz \end{aligned}\right\} \quad \ldots [9]$$

It is now assumed that u and v are proportional to z and w is independent of z

$$u = z\psi_x(x, y, t),\ v = z\psi_y(x, y, t),\ w = \bar{w}(x, y, t) \ldots [10]$$

The functions ψ_x and ψ_y correspond to the negative of the function ψ introduced by Timoshenko (6) in his bar theory and to the negatives of the functions ψ/h and χ/h used by Hencky (8).

Questions raised by Goodier (11), in connection with the appearance of Equations [10] in the first version (9) of Reissner's theory of plates, were answered in Reissner's second version (10) by replacing Equations [10] with averages while retaining his assumptions regarding the z-dependence of the components of stress. It appears that the reverse procedure leads to the consideration of shear deformation in the manner adopted by Timoshenko.

From Equations [8], [9], and [10], we have the relations between the plate-strain components and the plate-displacement components $\psi_x, \psi_y, \bar{w}$

$$\left.\begin{aligned} \Gamma_x &= \frac{\partial \psi_x}{\partial x},\ \Gamma_y = \frac{\partial \psi_y}{\partial y},\ \Gamma_{xy} = \frac{\partial \psi_y}{\partial x} + \frac{\partial \psi_x}{\partial y} \\ \Gamma_{xz} &= \psi_x + \frac{\partial \bar{w}}{\partial x},\ \Gamma_{yz} = \psi_y + \frac{\partial \bar{w}}{\partial y} \end{aligned}\right\} \quad \ldots [11]$$

The analogous relations for classical plate theory are obtained by setting $\Gamma_{xz} = \Gamma_{yz} = 0$.

Substituting Equations [11] into Equations [5], the following relations are obtained between the plate-stress and plate-displacement components

$$\left.\begin{aligned} M_x &= D\left(\frac{\partial \psi_x}{\partial x} + \mu\frac{\partial \psi_y}{\partial y}\right),\ M_y = D\left(\frac{\partial \psi_y}{\partial y} + \mu\frac{\partial \psi_x}{\partial x}\right) \\ M_{xy} &= \frac{1-\mu}{2} D\left(\frac{\partial \psi_y}{\partial x} + \frac{\partial \psi_x}{\partial y}\right) \\ Q_x &= \kappa^2 Gh\left(\frac{\partial \bar{w}}{\partial x} + \psi_x\right),\ Q_y = \kappa^2 Gh\left(\frac{\partial \bar{w}}{\partial y} + \psi_y\right) \end{aligned}\right\} \quad \ldots [12]$$

Equations [12] are similar to the corresponding formulas in E. Reissner's theory.[2] His "equivalent changes of slope," β_x and β_y, are here replaced by ψ_x and ψ_y; his "weighted average displacement" is here replaced by $\bar{w}$. The transverse load q does not appear in the present expressions for M_x and M_y due to the omission of the integrals containing σ_z in the integrated stress-strain relations. The constant $\kappa^2 Gh$ plays a role similar to Reissner's C_2, which has the value $(5/6)Gh$ for isotropic materials and a quadratic variation of transverse shear stress through the thickness of the plate. Hence κ^2 in Reissner's equilibrium theory has the value 5/6. In the present theory the z-dependence of the components of stress is not specified and κ is, as yet, not determined.

Equations of Motion

The stress-equations of motion of three-dimensional elasticity theory

[2] See reference (10), Equations [8], [23], and [28].

$$\left.\begin{aligned}\frac{\partial\sigma_x}{\partial x}+\frac{\partial\tau_{yx}}{\partial y}+\frac{\partial\tau_{zx}}{\partial z}&=\rho\frac{\partial^2 u}{\partial t^2}\\ \frac{\partial\tau_{yx}}{\partial x}+\frac{\partial\sigma_y}{\partial y}+\frac{\partial\tau_{yz}}{\partial z}&=\rho\frac{\partial^2 v}{\partial t^2}\\ \frac{\partial\tau_{zx}}{\partial x}+\frac{\partial\tau_{yz}}{\partial y}+\frac{\partial\sigma_z}{\partial z}&=\rho\frac{\partial^2 w}{\partial t^2}\end{aligned}\right\}\quad\ldots\ldots\ldots[13]$$

are converted to plate-stress equations of motion in the following manner.[4] The first two of Equations [13] are multiplied by z and integrated over the plate thickness. These become, after making use of Equations [2], [4], and [10]

$$\left.\begin{aligned}\frac{\partial M_x}{\partial x}+\frac{\partial M_{yx}}{\partial y}-Q_x&=\frac{\rho h^3}{12}\frac{\partial^2\psi_x}{\partial t^2}\\ \frac{\partial M_{yx}}{\partial x}+\frac{\partial M_y}{\partial y}-Q_y&=\frac{\rho h^3}{12}\frac{\partial^2\psi_y}{\partial t^2}\end{aligned}\right\}\quad\ldots\ldots\ldots[14]$$

(The right-hand sides of Equations [14] represent the influence of rotatory inertia.) The third of Equations [13] is integrated over the plate thickness and, after using Equations [3], [4], and [10], becomes

$$\frac{\partial Q_x}{\partial x}+\frac{\partial Q_y}{\partial y}+q=\rho h\frac{\partial^2\bar{w}}{\partial t^2}\quad\ldots\ldots\ldots[15]$$

The three plate-stress equations of motion, Equations [14] and [15], may be expressed in terms of the plate-displacements ψ_x, ψ_y, $\bar{w}$ by using Equations [12], with the result

$$\left.\begin{aligned}\frac{D}{2}\left[(1-\mu)\nabla^2\psi_x+(1+\mu)\frac{\partial\Phi}{\partial x}\right]&\\ -\kappa^2 Gh\left(\psi_x+\frac{\partial\bar{w}}{\partial x}\right)&=\frac{\rho h^3}{12}\frac{\partial^2\psi_x}{\partial t^2}\\ \frac{D}{2}\left[(1-\mu)\nabla^2\psi_y+(1+\mu)\frac{\partial\Phi}{\partial y}\right]&\\ -\kappa^2 Gh\left(\psi_y+\frac{\partial\bar{w}}{\partial y}\right)&=\frac{\rho h^3}{12}\frac{\partial^2\psi_y}{\partial t^2}\\ \kappa^2 Gh(\nabla^2\bar{w}+\Phi)+q&=\rho h\frac{\partial^2\bar{w}}{\partial t^2}\end{aligned}\right\}\quad\ldots[16]$$

where

$$\Phi=\frac{\partial\psi_x}{\partial x}+\frac{\partial\psi_y}{\partial y}$$

and ∇^2 is Laplace's two-dimensional operator.

Equations [16] are the same as Uflyand's equations of motion (7) except for the value of κ.

Energy Functions

The strain-energy-function W in the three-dimensional theory is given by

$$\left.\begin{aligned}2W&=\sigma_x\epsilon_x+\sigma_y\epsilon_y+\sigma_z\epsilon_z+\tau_{xy}\gamma_{xy}+\tau_{yz}\gamma_{yz}+\tau_{zx}\gamma_{zx}\\ &=\sigma_x\frac{\partial u}{\partial x}+\sigma_y\frac{\partial v}{\partial y}+\sigma_z\frac{\partial w}{\partial z}+\tau_{xy}\left(\frac{\partial v}{\partial x}+\frac{\partial u}{\partial y}\right)\\ &\quad+\tau_{yz}\left(\frac{\partial w}{\partial y}+\frac{\partial v}{\partial z}\right)+\tau_{zx}\left(\frac{\partial u}{\partial z}+\frac{\partial w}{\partial x}\right)\end{aligned}\right\}\quad\ldots[17]$$

[4] This method was employed by Boussinesq (12) to derive plate equations without using the calculus of variations. A. E. Green (13) has shown, recently, how the equations of E. Reissner's plate theory (10) may be obtained in a similar manner.

The analogous plate-strain-energy-function $\overline{W}$ is obtained by substituting Equations [10] into Equations [17] and integrating over the plate thickness, with the result

$$\left.\begin{aligned}2\overline{W}&=M_x\frac{\partial\psi_x}{\partial x}+M_y\frac{\partial\psi_y}{\partial y}+M_{yx}\left(\frac{\partial\psi_y}{\partial x}+\frac{\partial\psi_x}{\partial y}\right)\\ &\quad+Q_x\left(\frac{\partial\bar{w}}{\partial x}+\psi_x\right)+Q_y\left(\frac{\partial\bar{w}}{\partial y}+\psi_y\right)\\ &=M_x\Gamma_x+M_y\Gamma_y+M_{yx}\Gamma_{yx}+Q_x\Gamma_{xz}+Q_y\Gamma_{yz}\end{aligned}\right\}\quad\ldots[18]$$

and this becomes, through Equations [5]

$$\begin{aligned}4\overline{W}&=D(1+\mu)(\Gamma_x+\Gamma_y)^2+2\kappa^2Gh(\Gamma_{yx}^2+\Gamma_{xz}^2)\\ &\quad+D(1-\mu)[(\Gamma_x-\Gamma_y)^2+\Gamma_{yx}^2]\quad\ldots[19]\end{aligned}$$

If $E/(1+\mu)$ and $E/(1-\mu)$ are required to be positive, $\overline{W}$ is positive. Then, if $\overline{W}=0$, all the plate-strain components vanish and, through Equations [5], so do the plate-stress components.

From Equations [19] and [5], we find

$$\left.\begin{aligned}\frac{\partial\overline{W}}{\partial\Gamma_x}&=M_x,\quad\frac{\partial\overline{W}}{\partial\Gamma_y}=M_y,\quad\frac{\partial\overline{W}}{\partial\Gamma_{yx}}=M_{yx}\\ \frac{\partial\overline{W}}{\partial\Gamma_{xz}}&=Q_x,\quad\frac{\partial\overline{W}}{\partial\Gamma_{yz}}=Q_y\end{aligned}\right\}\quad\ldots[20]$$

The kinetic energy per unit of volume, according to the general linear theory, is

$$\frac{\rho}{2}\left[\left(\frac{\partial u}{\partial t}\right)^2+\left(\frac{\partial v}{\partial t}\right)^2+\left(\frac{\partial w}{\partial t}\right)^2\right]\quad\ldots[21]$$

By using Equations [10] and integrating over the thickness, this becomes, for the plate

$$\frac{\rho h^3}{24}\left[\left(\frac{\partial\psi_x}{\partial t}\right)^2+\left(\frac{\partial\psi_y}{\partial t}\right)^2\right]+\frac{\rho h}{2}\left(\frac{\partial\bar{w}}{\partial t}\right)^2\quad\ldots[22]$$

Total Energy and External Work

The kinetic energy in the plate at time t is given by

$$\overline{T}=\int\int\left\{\frac{\rho h^3}{24}\left[\left(\frac{\partial\psi_x}{\partial t}\right)^2+\left(\frac{\partial\psi_y}{\partial t}\right)^2\right]+\frac{\rho h}{2}\left(\frac{\partial\bar{w}}{\partial t}\right)^2\right\}dx\,dy\quad\ldots[23]$$

and the potential energy is

$$\overline{V}=\int\int\overline{W}\,dx\,dy\quad\ldots[24]$$

where the integrations are extended over the surface of the plate.

The total energy at time t is the sum of $\overline{T}$ and $\overline{V}$, which may be written as

$$\begin{aligned}\overline{T}+\overline{V}&=\int_{t_0}^{t}dt\int\int\frac{\partial}{\partial t}\left\{\frac{\rho h^3}{24}\left[\left(\frac{\partial\psi_x}{\partial t}\right)^2+\left(\frac{\partial\psi_y}{\partial t}\right)^2\right]\right.\\ &\quad\left.+\frac{\rho h}{2}\left(\frac{\partial\bar{w}}{\partial t}\right)^2\right\}dx\,dy\\ &\quad+\int_{t_0}^{t}dt\int\int\frac{\partial\overline{W}}{\partial t}\,dx\,dy+\overline{T}_0+\overline{V}_0\quad\ldots[25]\end{aligned}$$

where $\overline{T}_0$ and $\overline{V}_0$ are the values of $\overline{T}$ and $\overline{V}$ at an initial time t_0.

Performing the operations $\partial/\partial t$ as indicated in Equation [25], the first integrand becomes

$$\frac{\rho h^3}{12}\left[\frac{\partial\psi_x}{\partial t}\frac{\partial^2\psi_x}{\partial t^2}+\frac{\partial\psi_y}{\partial t}\frac{\partial^2\psi_y}{\partial t^2}\right]+\rho h\frac{\partial\bar{w}}{\partial t}\frac{\partial^2\bar{w}}{\partial t^2}\quad\ldots[26]$$

and the second integrand is

$$\frac{\partial \overline{W}}{\partial t} = \frac{\partial \overline{W}}{\partial \Gamma_x}\frac{\partial \Gamma_x}{\partial t} + \frac{\partial \overline{W}}{\partial \Gamma_y}\frac{\partial \Gamma_y}{\partial t} + \frac{\partial \overline{W}}{\partial \Gamma_{yz}}\frac{\partial \Gamma_{yz}}{\partial t} + \frac{\partial \overline{W}}{\partial \Gamma_{zx}}\frac{\partial \Gamma_{zx}}{\partial t} + \frac{\partial \overline{W}}{\partial \Gamma_{xy}}\frac{\partial \Gamma_{xy}}{\partial t} = \left(M_x\frac{\partial}{\partial x} + M_{yz}\frac{\partial}{\partial y} + Q_z\right)\frac{\partial \psi_z}{\partial t} + \left(M_{yz}\frac{\partial}{\partial x} + M_y\frac{\partial}{\partial y} + Q_y\right)\frac{\partial \psi_y}{\partial t} + \left(Q_x\frac{\partial}{\partial x} + Q_y\frac{\partial}{\partial y}\right)\overline{w}_t \quad \ldots\ldots [27]$$

by Equations [11] and [20].

In the surface integral of $\partial \overline{W}/\partial t$, Equation [25], the terms containing space derivatives may be integrated by parts to obtain

$$\int\int \frac{\partial \overline{W}}{\partial t}\,dx\,dy = \oint\left[\frac{\partial \psi_x}{\partial t}(M_x l + M_{xy} m) + \frac{\partial \psi_y}{\partial t}(M_{xy} l + M_y m) + \frac{\partial \overline{w}}{\partial t}(Q_x l + Q_y m)\right] ds - \int\int\left[\frac{\partial \psi_x}{\partial t}\left(\frac{\partial M_x}{\partial x} + \frac{\partial M_{yx}}{\partial y} - Q_x\right) + \frac{\partial \psi_y}{\partial t}\left(\frac{\partial M_{yx}}{\partial x} + \frac{\partial M_y}{\partial y} - Q_y\right) + \frac{\partial \overline{w}}{\partial t}\left(\frac{\partial Q_x}{\partial x} + \frac{\partial Q_y}{\partial y}\right)\right] dx\,dy \quad \ldots\ldots [28]$$

in which l and m are the direction cosines of the normal to the boundary and the line integral is taken around all (external and internal) boundaries. In the integration by parts it is assumed that ψ_x, ψ_y, and $\overline{w}$ are single-valued, otherwise additional line integrals would be required.

In terms of components referred to co-ordinates ν and s measured normal to and along the boundary, respectively, the line integral in Equation [28] may be written as

$$\oint\left(\frac{\partial \psi_\nu}{\partial t}M_\nu + \frac{\partial \psi_s}{\partial t}M_{\nu s} + \frac{\partial \overline{w}}{\partial t}Q_\nu\right) ds$$

Combining these results, we have

$$\overline{T} + \overline{V} = \int_{t_0}^{t} dt \oint\left(\frac{\partial \psi_\nu}{\partial t}M_\nu + \frac{\partial \psi_s}{\partial t}M_{\nu s} + \frac{\partial \overline{w}}{\partial t}Q_\nu\right) ds + \int_{t_0}^{t} dt \int\int\left[\frac{\partial \psi_x}{\partial t}\left(\frac{\rho h^3}{12}\frac{\partial^2 \psi_x}{\partial t^2} - \frac{\partial M_x}{\partial x} - \frac{\partial M_{yx}}{\partial y} + Q_x\right) + \frac{\partial \psi_y}{\partial t}\left(\frac{\rho h^3}{12}\frac{\partial^2 \psi_y}{\partial t^2} - \frac{\partial M_{yx}}{\partial x} - \frac{\partial M_y}{\partial y} + Q_y\right) + \frac{\partial \overline{w}}{\partial t}\left(\rho h\frac{\partial^2 \overline{w}}{\partial t^2} - \frac{\partial Q_x}{\partial x} - \frac{\partial Q_y}{\partial y}\right)\right] dx\,dy + \overline{T}_0 + \overline{V}_0$$

If Equations [14] and [15] (the plate equations of motion) are satisfied, this reduces to

$$\overline{T} + \overline{V} = \int_{t_0}^{t} dt \oint\left(\frac{\partial \psi_\nu}{\partial t}M_\nu + \frac{\partial \psi_s}{\partial t}M_{\nu s} + \frac{\partial \overline{w}}{\partial t}Q_\nu\right) ds + \int_{t_0}^{t} dt \int\int q\frac{\partial \overline{w}}{\partial t}\,dx\,dy + \overline{T}_0 + \overline{V}_0 \quad \ldots\ldots [29]$$

Equation [29] is simply the form, in the present theory, of the statement that the total energy in the plate at time t is equal to the sum of the energy at time t_0 and the work done by the external forces along the edge and over the surface of the plate during the interval $t - t_0$.

Initial and Boundary Conditions

Appropriate initial and boundary conditions for a system of differential equations are those which are sufficient to assure a unique solution. In the preceding two sections the groundwork has been laid for the application of a plate analog of F. Neumann's uniqueness theorem (14).

Consider two sets of plate displacements and surface loads. If the components of each set satisfy the equations of motion, so will their differences. Then the energies and the plate-stress components calculated from the differences will satisfy an equation of the same form as Equation [29]. If the right-hand side of Equation [29] vanishes, $\overline{T}$ and $\overline{V}$ vanish separately, since they are both positive. If $\overline{T}$ vanishes, the kinetic energy per unit of volume vanishes, since it is positive, and hence the plate velocities vanish. If $\overline{V}$ vanishes, $\overline{W}$ vanishes, since it is positive, and if $\overline{W}$ vanishes, so do the plate-strain and plate-stress components, as long as $E/(1+\mu)$ and $E/(1-\mu)$ are required to be positive. Hence, if the right-hand side of Equation [29] (calculated from the differences) vanishes, the two systems must be identical, except possibly for a rigid-body displacement (independent of time, since the velocities vanish) and the latter can be eliminated by requiring the initial displacements to be the same.

Returning, now, to a single set of solutions, appropriate initial and boundary conditions to be specified for the present theory are as follows:

1 On the edges of plate: any combination which contains one member of each of the three pairs of terms in the line integral of Equation [29].

2 Throughout the plate: (a) either q or $\overline{w}$, and (b) the initial values of ψ_x, ψ_y, $\overline{w}$ and their time derivatives.

The relation (see Equations [12])

$$\psi_s = \frac{Q_s}{\kappa^2 Gh} - \frac{\partial \overline{w}}{\partial s}$$

is replaced, in the classical theory of plates, by

$$\psi_s \stackrel{?}{=} -\frac{\partial \overline{w}}{\partial s}$$

since the transverse shear deformation $Q_s/\kappa^2 Gh$ vanishes. The term $M_{\nu s}\,\partial \psi_s/\partial t$ in Equation [29] would then be replaced by $-M_{\nu s}\,\partial^2 \overline{w}/\partial s\,\partial t$. But

$$-\oint M_{\nu s}\frac{\partial}{\partial s}\left(\frac{\partial w}{\partial t}\right) ds = \oint \frac{\partial \overline{w}}{\partial t}\frac{\partial M_{\nu s}}{\partial s}\,ds$$

Hence the second and third terms in the integrand of the line integral of Equation [29] would combine into the single term

$$\frac{\partial \overline{w}}{\partial t}\left(\frac{\partial M_{\nu s}}{\partial s} + Q_\nu\right)$$

leaving only the two edge conditions of Kirchoff. In the present theory, however, three edge conditions are required, as in E. Reissner's theory.

Compatibility Equations

In the integration by parts leading to Equation [29] it was assumed that ψ_x, ψ_y, and w are single-valued. If this restriction were relaxed, additional line integrals would appear in Equation [29], and hence there would be additional requirements for uniqueness. If the restriction to single-valued displacements is retained, it is necessary to specify that

$$\oint d\psi_x = 0, \quad \oint d\psi_y = 0, \quad \oint d\overline{w} = 0 \quad \ldots\ldots [30]$$

where the line integrals are taken around any closed path in the plate.

Usually, single-valuedness may be ascertained by inspection. However, if the differential equations are expressed entirely in terms of plate-stress components, as they may be in equilibrium problems, additional conditions are introduced by Equations [30]. These may be found as follows

$$\oint d\psi_x = \oint \frac{\partial \psi_x}{\partial x}\,dx + \frac{\partial \psi_x}{\partial y}\,dy$$

$$= \oint \left(\Gamma_x\,dx + \frac{1}{2}\,\Gamma_{yx}\,dy\right) - \oint \Omega_z dy$$

where

$$\Omega_z = \frac{1}{2}\left(\frac{\partial \psi_y}{\partial x} - \frac{\partial \psi_x}{\partial y}\right)$$

Now

$$-\oint \Omega_z dy = \oint (y - y_0)d\Omega_z$$

where y_0 is the y-co-ordinate of the starting point of integration. Also

$$d\Omega_z = \frac{\partial \Omega_z}{\partial x}\,dx + \frac{\partial \Omega_z}{\partial y}\,dy$$

and

$$2\,\frac{\partial \Omega_z}{\partial x} = \frac{\partial \Gamma_{yx}}{\partial x} - 2\,\frac{\partial \Gamma_x}{\partial y}, \quad 2\,\frac{\partial \Omega_z}{\partial y} = 2\,\frac{\partial \Gamma_y}{\partial x} - \frac{\partial \Gamma_{yx}}{\partial y}$$

Combining these results, we have

$$\oint d\psi_x = \oint (\xi_x dx + \eta_x dy) \quad \ldots\ldots\ldots\ldots [31]$$

where

$$\xi_x = \Gamma_x + (y - y_0)\,\frac{1}{2}\left(\frac{\partial \Gamma_{yx}}{\partial x} - \frac{\partial \Gamma_y}{\partial y}\right)$$

$$\eta_x = \frac{1}{2}\,\Gamma_{yx} + (y - y_0)\left(\frac{\partial \Gamma_y}{\partial x} - \frac{1}{2}\,\frac{\partial \Gamma_{xy}}{\partial y}\right)$$

Similarly

$$\oint d\psi_y = \oint (\xi_y\,dx + \eta_y\,dy) \quad \ldots\ldots\ldots\ldots [32]$$

where

$$\xi_y = \frac{1}{2}\,\Gamma_{yx} - (x - x_0)\left(\frac{1}{2}\,\frac{\partial \Gamma_{yx}}{\partial x} - \frac{\partial \Gamma_x}{\partial y}\right)$$

$$\eta_y = \Gamma_y - (x - x_0)\left(\frac{\partial \Gamma_y}{\partial x} - \frac{1}{2}\,\frac{\partial \Gamma_{xy}}{\partial y}\right)$$

For the condition on $\bar{w}$, we have

$$\oint d\bar{w} = \left(\frac{\partial \bar{w}}{\partial x}\,dx + \frac{\partial \bar{w}}{\partial y}\,dy\right)$$

$$= \frac{1}{2}\oint (\Gamma_{xz}\,dx + \Gamma_{yz}\,dy) - \oint (\Omega_y\,dx - \Omega_x\,dy)$$

where

$$\Omega_x = \frac{1}{2}\left(\frac{\partial \bar{w}}{\partial y} - \psi_x\right), \quad \Omega_y = \frac{1}{2}\left(\psi_x - \frac{\partial \bar{w}}{\partial x}\right)$$

(Note that Ω_x, Ω_y, Ω_z are the plate-rotation components.)

Now

$$-\oint (\Omega_y\,dx - \Omega_x dy) = \oint [(x - x_0)d\Omega_y - (y - y_0)d\Omega_x]$$

where (x_0, y_0) is the starting point of integration. Also

$$d\Omega_x = \frac{\partial \Omega_x}{\partial x}\,dx + \frac{\partial \Omega_x}{\partial y}\,dy, \quad d\Omega_y = \frac{\partial \Omega_y}{\partial x}\,dx + \frac{\partial \Omega_y}{\partial y}\,dy$$

and

$$2\,\frac{\partial \Omega_y}{\partial x} = \frac{\partial \Gamma_{yz}}{\partial y} - \Gamma_{yx}, \; 2\,\frac{\partial \Omega_x}{\partial y} = \frac{\partial \Gamma_{yz}}{\partial y} - 2\Gamma_x$$

$$2\,\frac{\partial \Omega_y}{\partial y} = \Gamma_{yz} - \frac{\partial \Gamma_{yz}}{\partial x}, \; 2\,\frac{\partial \Omega_x}{\partial x} = 2\Gamma_y - \frac{\partial \Gamma_{xz}}{\partial x}$$

Combining these results, we have

$$\oint d\bar{w} = \oint (\xi_z\,dx + \eta_z\,dy) \quad \ldots\ldots\ldots\ldots [33]$$

where

$$\xi_z = \frac{1}{2}\,\Gamma_{xz} + (x - x_0)\left(\Gamma_x - \frac{1}{2}\,\frac{\partial \Gamma_{xz}}{\partial x}\right) + \frac{1}{2}\,(y - y_0)\left(\Gamma_{yz} - \frac{\partial \Gamma_{xz}}{\partial y}\right)$$

$$\eta_z = \frac{1}{2}\,\Gamma_{yz} + \frac{1}{2}\,(x - x_0)\left(\Gamma_{yz} - \frac{\partial \Gamma_{yz}}{\partial x}\right) + (y - y_0)\left(\Gamma_y - \frac{1}{2}\,\frac{\partial \Gamma_{yz}}{\partial y}\right)$$

Equations [31], [32], and [33] constitute the plate analog of Cesàro's theorem[4] for closed paths. Applying Green's theorem to these equations, we find, for reducible paths

$$\left.\begin{aligned}
\oint d\psi_x &= \iint (y - y_0)\left(\frac{\partial^2 \Gamma_y}{\partial x^2} + \frac{\partial^2 \Gamma_x}{\partial y^2} - \frac{\partial^2 \Gamma_{yx}}{\partial x\,\partial y}\right) dx\,dy \\
\oint d\psi_y &= -\iint (x - x_0)\left(\frac{\partial^2 \Gamma_y}{\partial x^2} + \frac{\partial^2 \Gamma_x}{\partial y^2} - \frac{\partial^2 \Gamma_{yx}}{\partial x\,\partial y}\right) dx\,dy \\
\oint d\bar{w} &= \frac{1}{2}\iint (y - y_0)\left(2\,\frac{\partial \Gamma_x}{\partial x} - \frac{\partial \Gamma_{yx}}{\partial y} - \frac{\partial^2 \Gamma_{yx}}{\partial x\,\partial y} + \frac{\partial^2 \Gamma_{xx}}{\partial y^2}\right) dx\,dy \\
&\quad - \frac{1}{2}\iint (x - x_0)\left(2\,\frac{\partial \Gamma_x}{\partial y} - \frac{\partial \Gamma_{yx}}{\partial x} - \frac{\partial^2 \Gamma_{xx}}{\partial x\,\partial y} + \frac{\partial^2 \Gamma_{yx}}{\partial x^2}\right) dx
\end{aligned}\right\} \quad \ldots [34]$$

Hence, three necessary conditions on the plate strains for single-valuedness of ψ_x, ψ_y, $\bar{w}$ are

[4] See reference (14), p. 223.

$$\left.\begin{aligned}
&\frac{\partial^2\Gamma_x}{\partial x^2}+\frac{\partial^2\Gamma_x}{\partial y^2}=\frac{\partial^2\Gamma_{yz}}{\partial x\,\partial y}\\
&2\frac{\partial\Gamma_x}{\partial y}=\frac{\partial}{\partial x}\left(-\frac{\partial\Gamma_{yz}}{\partial x}+\frac{\partial\Gamma_{zx}}{\partial y}+\Gamma_{xy}\right)\\
&2\frac{\partial\Gamma_y}{\partial x}=\frac{\partial}{\partial y}\left(-\frac{\partial\Gamma_{zx}}{\partial y}+\Gamma_{yz}+\frac{\partial\Gamma_{xy}}{\partial x}\right)
\end{aligned}\right\}\quad\ldots\ldots[35]$$

and these are also sufficient conditions for a simply connected plate. In an $(n+1)$ connected plate, each application of Green's theorem introduces n integrals around the n internal boundaries. Hence there are $3n$ additional conditions

$$\oint_{C_i} d\psi_x = 0,\quad \oint_{C_i} d\psi_y = 0,\quad \oint_{C_i} d\bar{w} = 0,\ i = 1, 2 \ldots n$$

where the paths C_i are the internal boundaries.

Equations [35] are the analogs, in the present theory, of the six compatibility equations in 3-dimensional linear elasticity theory. That they are necessary conditions for single-valuedness of ψ_x, ψ_y, and $\bar{w}$ may be determined directly by eliminating these quantities from Equations [11]. The plate-compatibility equations may be expressed in terms of the plate-stress components by using Equations [5].

Equations Governing $\bar{w}$

A single differential equation for $\bar{w}$ may be obtained by eliminating ψ_x and ψ_y from Equations [16] in the following manner: Differentiate the first and second of Equations [16] with respect to x and y, respectively, and add to obtain

$$\left(D\nabla^2 - G'h - \frac{\rho h^3}{12}\frac{\partial^2}{\partial t^2}\right)\Phi = G'h\nabla^2\bar{w}\ldots\ldots[36]$$

Then eliminate Φ between Equation [36] and the third of Equations [16] with the result

$$\left(\nabla^2 - \frac{\rho}{G'}\frac{\partial^2}{\partial t^2}\right)\left(D\nabla^2 - \frac{\rho h^3}{12}\frac{\partial^2}{\partial t^2}\right)\bar{w} + \rho h\frac{\partial^2\bar{w}}{\partial t^2} = \left(1 - \frac{D\nabla^2}{G'h} + \frac{\rho h^2}{12G'}\frac{\partial^2}{\partial t^2}\right)q\ldots\ldots[37]$$

Equation [37] is the two-dimensional analog of Timoshenko's beam equation (6).

If the rotatory inertia terms are omitted from Equation [37], it reduces to

$$D\left(\nabla^2 - \frac{\rho}{G'}\frac{\partial^2}{\partial t^2}\right)\nabla^2\bar{w} + \rho h\frac{\partial^2\bar{w}}{\partial t^2} = \left(1 - \frac{D\nabla^2}{G'h}\right)q\ldots[38]$$

If the transverse shear deformation is neglected, but the rotatory inertia terms are retained, Equation [37] reduces to

$$\left(D\nabla^2 - \frac{\rho h^2}{12}\frac{\partial^2}{\partial t^2}\right)\nabla^2\bar{w} + \rho h\frac{\partial^2\bar{w}}{\partial t^2} = q\ldots\ldots[39]$$

Finally, if both the transverse shear deformation and rotatory inertia terms are omitted, Equation [37] reduces to Equation [1] in which $\nabla^4 = \nabla^2\nabla^2$.

Straight-Crested Waves

The exact solution of the three-dimensional equations of elasticity is known for the case of straight-crested flexural waves in an infinite plate (1, 2, 3). This solution will be used to test the present theory and to complete the equations of motion and the stress-strain-displacement relations by choosing the value of κ.

Three-Dimensional Theory. In the three-dimensional theory, the wave velocity c of wave length λ is given in the form of the transcendental equation (1, 2, 3)

$$\frac{4c_s^2\sqrt{(c_s^2-\alpha c^2)(c_s^2-c^2)}}{(2c_s^2-c^2)^2} = \frac{\tanh\frac{\pi h}{\lambda c_s}\sqrt{c_s^2-\alpha c^2}}{\tanh\frac{\pi h}{\lambda c_s}\sqrt{c_s^2-c^2}},\ 0<\frac{c}{c_s}<1$$

$\ldots\ldots[40]$

where

$$c_s = \sqrt{G/\rho}$$

i.e., the velocity of shear waves and

$$\alpha = \frac{1-2\mu}{2(1-\mu)}$$

Lamb's values (2) for c/c_s versus h/λ (with $\mu = 1/2$) are plotted

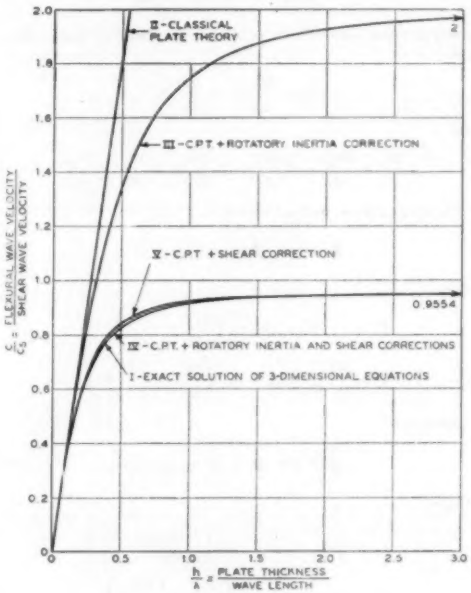

FIG. 1

as curve I in Fig. 1. For long waves ($\lambda \gg h$) Equation [40] reduces to

$$\frac{c^2}{c_s^2} = \frac{2\pi^2}{3(1-\mu)}\left(\frac{h}{\lambda}\right)^2\ldots\ldots[41]$$

while the limit for short waves ($\lambda \to 0$) is

$$4c_s^2\sqrt{(c_s^2-\alpha c^2)(c_s^2-c^2)} = (2c_s^2-c^2)^2,\ 0<\frac{c}{c_s}<1\ldots[42]$$

i.e., the equation for the velocity of Rayleigh surface waves For $\mu = 1/2$, Equation [42] gives $c = 0.9554\,c_s$.

Classical Plate Theory. If the solution for a straight-crested wave

$$\bar{w} = \cos\frac{2\pi}{\lambda}(x - ct) \quad [43]$$

is substituted into Equation [1], with $q = 0$, we find

$$c^2 = \frac{D}{\rho h}\left(\frac{2\pi}{\lambda}\right)^2 = \frac{2\pi^2 c_s^2}{3(1-\mu)}\left(\frac{h}{\lambda}\right)^2 \quad [44]$$

which is identical with Equation [41]. Thus, as observed by Rayleigh (1), classical plate theory gives good results for long waves. Equation [44] is plotted (for $\mu = 1/2$) as curve II in Fig. 1. It may be seen that when the wave length becomes less than 5 or 10 times the plate thickness the classical plate theory departs markedly from the three-dimensional theory.

Rotatory Inertia Correction. We consider, next, Equation [39] (with $q = 0$), which contains only the rotatory inertia correction. Insertion of $\bar{w}$ from Equation [43] results in

$$\frac{c^2}{c_s^2} = \frac{2\pi^2}{3(1-\mu)}\left(\frac{h}{\lambda}\right)^2\left[1 + \frac{\pi^2}{3}\left(\frac{h}{\lambda}\right)^2\right]^{-1} \quad [45]$$

Equation [45], with $\mu = 1/2$, is plotted in Fig. 1 as curve III. For $\lambda \gg h$, Equation [45] reduces to [41] as it should; but the limit of c^2/c_s^2 as $\lambda \to 0$ is $2/(1-\mu)$, a value that is much too large in comparison with the solution of Equation [42].

Rotatory Inertia and Shear Corrections. In this case the complete left-hand side of Equation [37] is used, with the result

$$\frac{\pi^2}{3}\left(\frac{h}{\lambda}\right)^2\left(1 - \frac{c^2}{\kappa^2 c_s^2}\right)\left(\frac{c_p^2}{c^2} - 1\right) = 1 \quad [46]$$

where

$$c_p = \sqrt{\frac{E}{\rho(1-\mu^2)}}$$

Accordingly, there are two roots for c^2. Confining attention to the smaller root, Equation [46] reduces to Equation [41] for long waves, as it should. The limit of Equation [46] as $\lambda \to 0$ is

$$c^2 = \kappa^2 c_s^2$$

According to the three-dimensional theory, this should be the velocity of Rayleigh surface waves. Hence, by Equation [42] the appropriate value of κ^2 is the root of

$$4\sqrt{(1-\alpha\kappa^2)(1-\kappa^2)} = (2-\kappa^2)^2, \quad 0 < \kappa < 1 \quad [47]$$

For anisotropic plates the analogous constants would be obtained from the algebraic equations whose roots give the velocities of surface waves appropriate to the medium. The dependence of κ^2 on Poisson's ratio is illustrated by noting that it ranges almost linearly from 0.76 for $\mu = 0$ to 0.91 for $\mu = 1/2$.

The smaller root of Equation [46], with $\mu = 1/2$ and $\kappa = 0.9554$, is plotted as curve IV in Fig. 1. The correspondence with the exact solution of the three-dimensional equations is so close that no difference between the two can be detected in computations carried to three figures. Curves IV and I are therefore the same in Fig. 1.

Shear Correction Only. It is interesting to notice that the transverse shear deformation accounts almostly entirely for the discrepancy between classical plate theory and the three-dimensional theory over the whole wave-length spectrum. Equation [38], which contains the shear-correction term only, yields

$$\frac{c^2}{c_s^2} = \frac{2\pi^2}{3(1-\mu)}\left(\frac{h}{\lambda}\right)^2\left[1 + \frac{2\pi^2}{3\kappa^2(1-\mu)}\left(\frac{h}{\lambda}\right)^2\right]^{-1} \quad [48]$$

This is plotted, for $\mu = 1/2$, as curve V in Fig. 1.

Thickness-Shear Motion

The circular frequency of the first antisymmetric mode of thickness-shear vibration, according to the exact theory, is[6]

$$p = \pi c_s/h \quad [49]$$

The corresponding solution in the present theory is obtained by setting

$$\psi_y = \bar{w} = 0, \quad \psi_x = e^{ipt}$$

in Equations [16], with the result

$$p = \kappa c_s\sqrt{12}/h \quad [50]$$

To make Equations [49] and [50] identical requires

$$\kappa^2 = \pi^2/12 \quad [51]$$

a value very close to Reissner's 5/6.

Substituting $\kappa^2 = \pi^2/12$ into Equation [47] we find

$$\mu = 0.176$$

Thus, in a material with a Poisson's ratio of 0.176, there is no conflict between Equations [51] and [47]. For other values of μ, one must choose or compromise between Equations [51] and [47] in accordance with the relative importance of the two modes of motion.

Reduction to Wave Equations

In the absence of surface loading, the equations of motion may be transformed to an exceptionally simple form with the loss of only trivial solutions.

If two of the plate-displacement components are expressed in terms of the potentials which give rise to the areal dilatation and rotation

$$\psi_x = \partial\varphi/\partial x + \partial H/\partial y, \quad \psi_y = \partial\varphi/\partial y - \partial H/\partial x \quad [52]$$

and a factor e^{ipt} (hereafter omitted) is assumed, Equations [16] become

$$\left.\begin{aligned}
&\frac{\partial}{\partial x}\left[\nabla^2\varphi + (Rb_0^4 - S^{-1})\varphi - S^{-1}\bar{w}\right] \\
&\qquad + \frac{1-\mu}{2}\frac{\partial}{\partial y}(\nabla^2 + \omega^2)H = 0 \\
&\frac{\partial}{\partial y}\left[\nabla^2\varphi + (Rb_0^4 - S^{-1})\varphi - S^{-1}\bar{w}\right] \\
&\qquad - \frac{1-\mu}{2}\frac{\partial}{\partial x}(\nabla^2 + \omega^2)H = 0 \\
&\nabla^2(\varphi + \bar{w}) + Sb_0^4\bar{w} = 0
\end{aligned}\right\} \quad [53]$$

where

$$R = h^2/12, \quad S = D/\kappa^2 Gh, \quad b_0^4 = \rho p^2 h/D,$$
$$\omega^2 = 2(Rb_0^4 - S^{-1})/(1-\mu) \quad [54]$$

The constants R and S represent the effects of rotary inertia and transverse shear deformation, respectively.

H may be separated from φ and $\bar{w}$ by differentiation, addition, and subtraction of the first two of Equations [53]. These equations become

$$\left.\begin{aligned}
&\nabla^2(\nabla^2 + \omega^2)H = 0 \\
&\nabla^2[\nabla^2\varphi + (Rb_0^4 - S^{-1})\varphi - S^{-1}\bar{w}] = 0
\end{aligned}\right\} \quad [55]$$

[6] Reference (2), p. 122.

It now remains to separate φ and $\bar{\psi}$ between the second of Equations [55] and the third of Equations [53]. It will be observed that these equations are satisfied by

$$\varphi = (\sigma - 1)\bar{w} \quad [56]$$

where σ is a constant, provided

$$\sigma^{-1}S\delta_0^4 = R\delta_0^4 - S^{-1} - [S(\sigma - 1)]^{-1} = \delta^2 \text{ (say)} \quad [57]$$

and

$$\nabla^2\bar{w} + \delta^2\bar{w} = 0 \quad [58]$$

Solution of Equations [57] yields

$$\delta_1^2, \delta_2^2 = \frac{1}{2}\delta_0^4\left[R + S \mp \sqrt{(R - S)^2 + 4\delta_0^{-4}}\right] \quad [59]$$

$$\sigma_1, \sigma_2 = (\delta_2^2, \delta_1^2)(R\delta_0^4 - S^{-1})^{-1} \quad [60]$$

Hence, two deflection functions ($\bar{w}_1$ and $\bar{w}_2$) are obtained by setting σ, in Equation [56], equal to σ_1 or σ_2 and these functions are governed by separate wave equations obtained by setting δ equal to δ_1 or δ_2 in Equation [58]. Equation [56] is now shown to be nonrestrictive by noting that Equation [37] may be written as

$$(\nabla^2 + \delta_1^2)(\nabla^2 + \delta_2^2)\bar{w} = 0 \quad [61]$$

when $q = 0$. Finally, in view of Equations [56] and [58], the bracketed terms in Equations [53] vanish, so that the equation governing H reduces to

$$(\nabla^2 + \omega^2)H = 0$$

To sum up, we may write

$$\psi_x = (\sigma_1 - 1)\partial\bar{w}_1/\partial x + (\sigma_2 - 1)\partial\bar{w}_2/\partial x + \partial H/\partial y$$
$$\psi_y = (\sigma_1 - 1)\partial\bar{w}_1/\partial y + (\sigma_2 - 1)\partial\bar{w}_2/\partial y - \partial H/\partial x \quad [62]$$
$$w = \bar{w}_1 + \bar{w}_2$$

and

$$(\nabla^2 + \omega^2)H = 0 \qquad (\nabla^2 + \delta_1^2)\bar{w}_1 = 0 \qquad (\nabla^2 + \delta_2^2)\bar{w}_2 = 0 \quad [63]$$

It may be observed that, if $R = S = 0$, H and σ vanish and $\delta^2 = -\delta_0^2$, i.e., the present equations all reduce to those of classical plate theory when the effects of rotatory inertia and shear are removed.

BIBLIOGRAPHY

1 "On the Free Vibrations of an Infinite Plate of Homogeneous Isotropic Elastic Matter," by Lord Rayleigh, Proceedings of the London Mathematical Society, London, England, vol. 10, 1889, pp. 225–234.

2 "On Waves in an Elastic Plate," by H. Lamb, Proceedings of the Royal Society of London, England, series A, vol. 93, 1917, pp. 114–128.

3 "On the Transverse Vibrations of Bars of Uniform Cross Section," by S. Timoshenko, *Philosophical Magazine*, series 6, vol. 43, 1922, pp. 125–131.

4 "Theory of Sound," by Lord Rayleigh, second edition, The Macmillan Company, New York, N. Y., vol. 1, p. 258.

5 "On the Correction for Shear of the Differential Equation for Transverse Vibrations of Prismatic Bars," by S. Timoshenko, Philosophical Magazine, series 6, vol. 41, 1921, pp. 744–746.

6 "Vibration Problems in Engineering," by S. Timoshenko, second edition, D. Van Nostrand Company, Inc., New York, N. Y., 1937, p. 337.

7 "The Propagation of Waves in the Transverse Vibrations of Bars and Plates," by Ya. S. Uflyand, Akad. Nauk SSSR. Prikl. Mat. Meh., vol. 12, 1948, pp. 287–300 (Russian).

8 "Über die Berücksichtigung der Schubverzerrung in ebenen Platten," by H. Hencky, Ingenieur Archiv., vol. 16, 1947, pp. 72–76.

9 "The Effect of Transverse Shear Deformation on the Bending of Elastic Plates," by E. Reissner, JOURNAL OF APPLIED MECHANICS, Trans. ASME, vol. 67, 1945, p. A-69.

10 "On Bending of Elastic Plates," by E. Reissner, *Quarterly of Applied Mathematics*, vol. 5, 1947, pp. 55–68.

11 Discussion of Ref. (9), by J. N. Goodier, JOURNAL OF APPLIED MECHANICS, Trans. ASME, vol. 68, 1946, p. A-251.

12 "Étude nouvelle sur l'équilibre et le mouvement des corps solides élastiques dont certaines dimensions sont très-petites par rapport à d'autres," by J. Boussinesq, Journ. de Math., Paris, France, series 2, vol. 16, 1871, pp. 125–274, and series 3, vol. 5, 1879, pp. 329–344.

13 "On Reissner's Theory of Bending of Elastic Plates," by A. E. Green, *Quarterly of Applied Mathematics*, vol. 7, 1949, pp. 223–228.

14 "Theory of Elasticity," by A. E. H. Love, fourth edition, The Macmillan Company, New York, N. Y., p. 176.

Fluid Flow Through Porous Metals[1]

By LEON GREEN, JR.,[2] and POL DUWEZ[3]

A method is outlined for correlating experimental data obtained in studies of the flow of gases and liquids through porous metals. The correlation is based upon the suggestion of Forcheimer that the pressure gradient attending the flow of a liquid through a porous medium can be expressed as a function of flow rate by a simple quadratic equation. An equation of this type defines two length parameters necessary for characterization of a porous structure and permits a general definition of the Reynolds number for a structure of arbitrary complexity.

Introduction

THE flow of homogeneous fluids through porous media is a problem of great importance in several branches of engineering. Most of the contributions in the field have been initiated by problems dealing with the flow of fluids through consolidated or loosely packed particles commonly encountered in soil mechanics or in chemical engineering processes. In mechanical engineering the subject probably will become of greater importance with the use of porous metals for such applications as sweat-cooled parts (1 and 2)[4] or boundary-layer control devices (3). Although the flow of fluids through porous metals is not essentially different from that through any other porous medium, special problems arise from the fact that the porous metal is a sintered mass with a very complicated network of open channels, and, as a consequence, it is difficult to describe the flow in terms of an average particle size, as for a bed of granular material.

In the use of porous metals as machine parts, it is imperative to assure a certain rate of fluid flow under given conditions of pressure drop. Such design requires knowledge of the permeability of the metal of which the part is to be made. The complexity of the metal structure, of course, precludes any analytical approach to the problem of predicting the permeability. In the course of earlier experimental studies of the flow of gas through different porous-metal specimens conducted at the Jet Propulsion Laboratory, it was found that for a given metal, prepared under a fixed set of conditions of compaction and sintering, the permeability coefficient (defined on the basis of Darcy's law) is a unique function of the fractional void volume, or porosity, of the metal. A more general correlation of the measured permeability values obtained from different metals, however, could not be realized.

The permeability problem in the case of porous metals is complicated by the fact that the method of manufacture produces some porosity which does not affect permeability; that is, not all of the pores or channels are necessarily continuous throughout the metal specimen; some may be dead ends. As the porosity of the metal is increased, the proportion of continuous or connected pores also increases; thus the permeability is doubly sensitive to porosity changes, sometimes varying as rapidly as the tenth power of the porosity.

Another complication is introduced by the fact that Darcy's law, which defines the permeability coefficient, is valid only for low velocity flow. The upper limit of this "creeping" regime, in which inertia forces are negligible, can be expressed by a critical Reynolds number. In the case of porous metals, however, it is not possible by inspection to define the characteristic length entering into the Reynolds number expression.

Resistance Coefficients of a Porous Medium

The complexity of the porous-metal structures requires the use of dimensional analysis in order to approach the fluid-flow problem. In the case of a viscous liquid flowing through a porous medium, dimensional considerations proposed by Muskat (4) show that when changes in elevation are neglected, the pressure gradient in the system may be expressed as

$$-\frac{dp}{dx} = \text{const}\ \frac{\mu^2}{\rho\delta^3}\ F\left(\frac{\delta\rho v}{\mu}\right) \qquad [1]$$

where

p = fluid pressure
x = length variable
μ = viscosity of fluid
ρ = density of fluid
δ = a length characterizing pore openings
F = an unknown function
v = superficial bulk velocity of fluid

For low values of velocity (or Reynolds number) the value of the function F has been found simply to equal its argument, so that

$$-\frac{dp}{dx} = \text{const}\ \frac{\mu v}{\delta^2} \qquad [2]$$

which is the result experimentally verified by Darcy. Flows at sufficiently high values of Reynolds number, however, are characterized by the fact that the function F is proportional to the square of its argument. Thus Equation [1] takes the form

$$-\frac{dp}{dx} = \text{const}\ \frac{\rho v^2}{\delta} \qquad [3]$$

It will be recalled that in the case of flow in pipes, for instance, the transition from laminar to turbulent flow occurs abruptly over a short transition range. In the case of a porous medium, the losses due to the inertia of the fluid become progressively more important with increasing velocity. The gradual transition from the Darcy regime is marked by losses due to both viscous shear in creeping flow and to inertial effects; hence terms proportional

[1] Some of the material presented in this paper has been taken from a thesis submitted by Leon Green, Jr., at the California Institute of Technology in partial fulfillment of the requirements for the degree of Doctor of Philosophy, July, 1949.

[2] Research Engineer, Jet Propulsion Laboratory, California Institute of Technology, Pasadena, Calif.; now with North American Aviation, Inc., Downey, Calif.

[3] Associate Professor of Mechanical Engineering and Chief of the Material Section of the Jet Propulsion Laboratory, California Institute of Technology, Pasadena, Calif.

[4] Numbers in parentheses refer to the Bibliography at the end of the paper.

Contributed by the Applied Mechanics Division and presented at the Semi-Annual Meeting, St. Louis, Mo., June 19–23, 1950, of The American Society of Mechanical Engineers.

Discussion of this paper should be addressed to the Secretary, ASME, 29 West 39th Street, New York, N. Y., and will be accepted until April 10, 1951, for publication at a later date. Discussion received after the closing date will be returned.

Note: Statements and opinions advanced in papers are to be understood as individual expressions of their authors and not those of the Society. Manuscript received by the Applied Mechanics Division, February 9, 1950. Paper No. 50—SA-17.

to both the first and second power of the velocity must be included in the pressure-gradient equation as suggested by Forcheimer (5). By including the length parameter δ in the unknown constants, Equations [2] and [3] may be combined into the form

$$-\frac{dp}{dx} = \alpha\mu v + \beta\rho v^2 \quad [4]$$

The two coefficients α and β defined by Equation [4] are independent of the mechanical properties of the fluid which were considered in the derivation. Having only the dimensions of length, they characterize the structure of the porous material itself, and henceforth will be referred to as viscous and inertial resistance coefficients of the material. It may be noted that the viscous coefficient α, of dimension $[L^{-2}]$, is the inverse of a permeability coefficient defined by Darcy's law. The inertial coefficient β with dimensions $[L^{-1}]$ may be interpreted as a measure of the tortuosity of the flow channels, perhaps as an average curvature of the streamlines determining the accelerations experienced by the fluid. In terms of the conventional concept of kinetic-energy losses, β might represent a resistance equivalent to a certain number of contractions and expansions per unit length of path.

The foregoing considerations need not be restricted to an incompressible fluid. In the case of a gas in one-dimensional steady flow through a porous medium, the mass rate of flow ρv is constant throughout the medium and may serve as an independent variable. In this case, however, effects due to macroscopic changes in the momentum of the fluid cannot be ruled out a priori; thus Equation [4] must first be rewritten as a momentum equation[1]

$$dp + \alpha\mu v dx + \beta\rho v^2 dx + \rho v dv = 0 \quad [5]$$

Introduction of the variable ρv then gives

$$\rho dp + \alpha\mu(\rho v)dx + \beta(\rho v)^2 dx + \rho(\rho v)dv = 0 \quad [6]$$

It is convenient to replace the mass density ρ by the specific weight σ, and the mass flow rate ρv by the weight flow rate G. With these changes, Equation [6] becomes

$$\sigma dp + \alpha\mu G dx + \beta\frac{G^2}{g}dx + \frac{G^2}{g}\sigma d\left(\frac{1}{\sigma}\right) = 0 \quad [7]$$

If isothermal flow of a perfect gas is assumed

$$\sigma = \frac{p}{bT}$$

where $b = R/M$. With this substitution

$$\frac{p}{bT}dp + \alpha\mu G dx + \beta\frac{G^2}{g}dx + \frac{G^2}{g}\frac{p}{bT}d\left(\frac{bT}{p}\right) = 0 \quad [8]$$

Integrating over the complete path of length L

$$\frac{1}{bT}\frac{p_2^2 - p_1^2}{2} + \alpha\mu GL + \beta\frac{G^2}{g}L + \frac{G^2}{g}\ln\frac{p_1}{p_2} = 0 \quad [9]$$

or

$$\frac{p_1^2 - p_2^2}{L} = \alpha(2bT\mu)G + \left(\beta + \frac{1}{L}\ln\frac{p_1}{p_2}\right)\left(2\frac{bT}{g}\right)G^2 \quad [10]$$

At this point it may be noted that all the experimental results so far obtained with porous metals have shown the momentum-change term to be of negligible magnitude, and that the equation for the difference between the squares of the upstream and downstream pressures per unit length of path (usually abbreviated as the pressure-square gradient) may be written simply as

$$\frac{\Delta p^2}{L} = \alpha(2bT\mu)G + \beta\left(2b\frac{T}{g}\right)G^2 \quad [11]$$

which is the equation used as the basis for correlation of the data presented in this paper.

A two-term quadratic equation such as Equation [11] not only is in accord with a reasonable picture of the resistance mechanism, but when written in dimensionless form provides a definition of the Reynolds number of a flow through porous structures too complicated for description. By definition the Reynolds number of a flow system represents the ratio of the inertia forces to the viscous forces. By comparing the corresponding terms of the quadratic Equations [4] or [11], the Reynolds number may be recognized as

$$N_{Re} = \frac{\beta\rho v}{\alpha\mu} = \frac{\beta G}{\alpha\mu g} \quad [12]$$

and it may be seen that the unknown length entering into the expression is the ratio β/α, involving both the inertial and viscous resistance coefficients. The ratio of "dissipative" forces to inertia forces, on the other hand, defines the friction factor as

$$C_f = \frac{-\frac{1}{\beta}\frac{dp}{dx}}{\frac{\rho v^2}{2}} = \frac{\frac{1}{\beta}\frac{\Delta p^2}{L}}{\frac{bTG^2}{g}} \quad [13]$$

$$= 2 \text{ in the inertial regime}$$
$$= 2/N_{Re} \text{ in the Darcy regime}$$

Over the entire range of flows, then, Equations [4] and [11] become

$$C_f = \frac{2}{N_{Re}} + 2 \quad [14]$$

It has been found that this type of representation, which requires two characteristic length parameters, is the only one which can be applied successfully to complex consolidated materials such as porous metals, since it can correlate the behavior of specimens whose pressure-square gradient versus flow-rate curves intersect or cross one another. Such behavior is not uncommon in porous metals, since the inertial resistance coefficient apparently is more sensitive to sintering conditions than is the viscous coefficient. Intersecting curves of this type have also been obtained in tests upon consolidated sands (6).

Experimental Procedure

In order to demonstrate that two resistance coefficients are required for characterization of a porous structure, the results obtained from various porous-metal specimens of widely differing structures were examined. The porous specimens were prepared by a powder-metallurgy technique which has been described in detail (2). The principle of the method consists of adding to the metal powder a powdered substance that decomposes into a gaseous phase at a temperature below the sintering temperature of the metal. The two powders are intimately mixed, pressed in a die in order to form a compact, then sintered at high temperature. When the nonmetallic powder decomposes, empty spaces are left in the interior of the compact. Since the gases generated by the decomposition of the porosity-forming material

[1] The following development, since it is concerned with deviations from the Darcy law at high rates of flow, does not take into consideration the effects which occur in fine capillaries at the lower end of the Darcy regime as a result of molecular slip in gases at low pressures.

must escape, small channels are formed in the compact and the pores are therefore interconnected. Although some of these channels may be closed during the sintering of the metal powder, enough of them remain open to render the metal permeable. Various substances have been used successfully as porosity-producing agents, among them ammonium bicarbonate, phthalic anhydride, and salicylic acid.

The experiments described here were selected from an experimental survey of various types of porous metals. Two series of specimens will be considered. The first series includes four specimens, namely, two of porous iron having a coarse structure, one of low porosity, the other of high; a fine-structure stainless steel of low porosity; and a porous bronze obtained from the Moraine Division of the General Motors Corporation. Photomicrographs of the four specimens under a magnification of 50 diam are presented in Fig. 1. The bronze sample is made of almost spherical particles and was included as an example of a comparatively simple matrix structure. The second series of specimens consisted of samples of porous stainless steel prepared under identical conditions, but with various amounts of phthalic anhydride, namely 5, 7, 9, 11, 13, 15, and 17 per cent by weight. By this method a consistent set of specimens of increasing porosity is obtained, since there is a unique relation between porosity and amount of porosity-producing agent (2). This relation is shown in Fig. 2.

The permeability experiments consisted in measuring the rate of flow of gas passing through a porous specimen 1.4 in. diam and about $^1/_4$ in. thick. Four Fischer-Porter Flowrators were used to

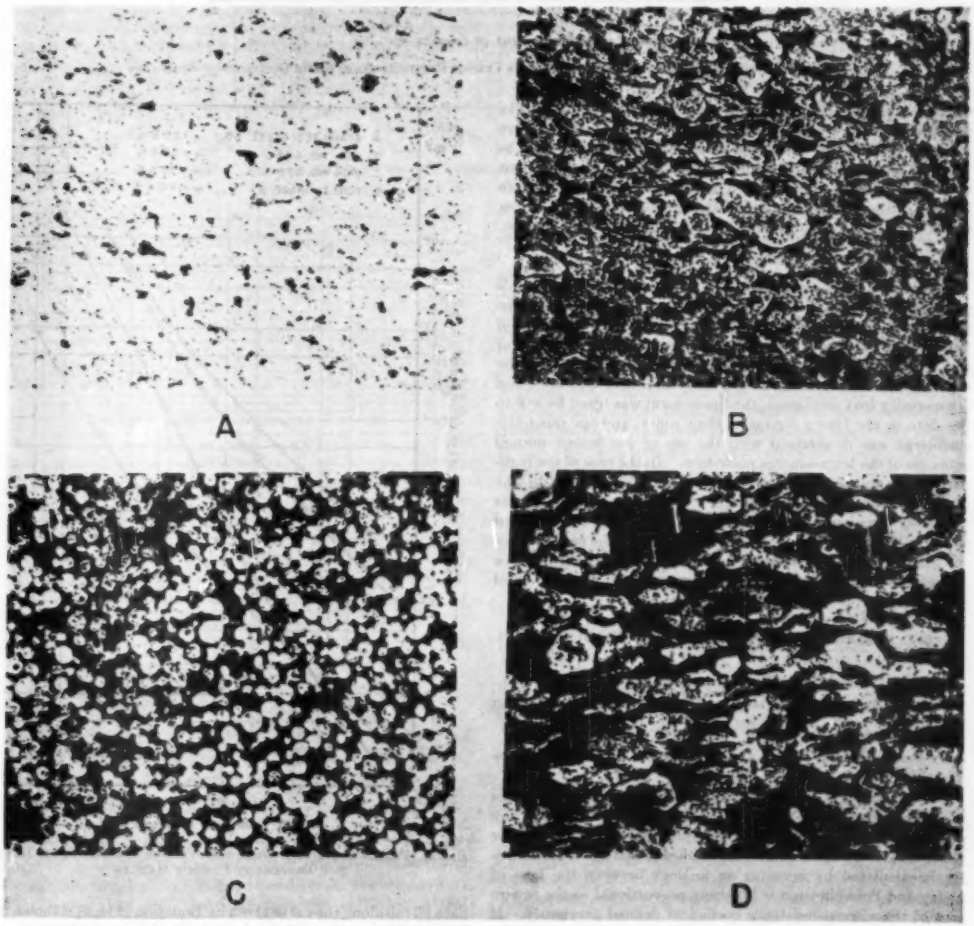

A, Stainless Steel No. 1, Porosity = 25.6 Per Cent
C, Porex Grade 4, Porosity = 46.2 Per Cent
B, Iron No. 641, Porosity = 32.7 Per Cent
D, Iron No. 672, Porosity = 59.5 Per Cent

Fig. 1 Structure of Porous-Metal Specimens

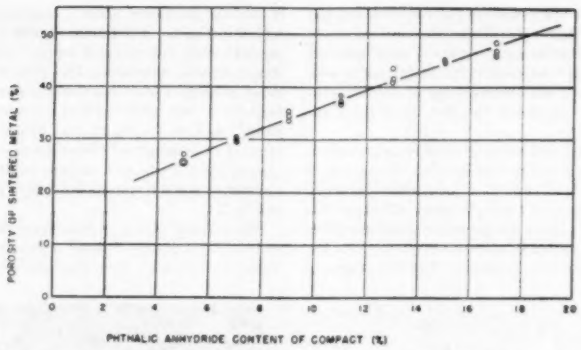

FIG. 2 POROSITY OF STAINLESS-STEEL SPECIMENS VERSUS PHTHALIC-ANHYDRIDE CONTENT OF COMPACTS

cover a range of flow rates from about 0.02 to 100 cfm. The pressure of bottled nitrogen gas was controlled by three Grove regulators. Pressure differences across the specimen as great as 1500 psi were sometimes required in order to attain the highest flow rates. The gas temperature used in the calculations was an average of the upstream and downstream absolute temperatures, which differed from the average by about 2 per cent at the most.

EXPERIMENTAL RESULTS

The experimental results obtained from the four porous metals of the first series described are presented in Fig. 3 in terms of the pressure-square gradient plotted as a function of weight rate of flow per unit area of the specimen. Fig. 3 also shows curves of the type prescribed by Equation [11], which were fitted to the experimental data. In the case of the stainless steel, Porex, and low-porosity iron specimens, the linear term was fitted by eye to the data in the Darcy regime of slope unity, and the quadratic coefficient was determined with the use of the second normal equation of the least-squares procedure. In the case of the high-porosity-iron specimen, however, the data lay largely in the inertial or quasi-turbulent range. Thus this procedure was reversed; the quadratic coefficient was determined visually, and the least-squares equation was used to calculate the coefficient of the linear term. The values of the viscous and inertial resistance coefficients α and β thus determined for each of the porous-metal specimens are presented in Table 1.

TABLE 1 RESISTANCE COEFFICIENTS OF POROUS-METAL SPECIMENS

Specimen identification	Porosity, per cent	Viscous resistance coefficient α (10^{-8} in.$^{-2}$)	Inertial resistance coefficient β (10^{4} in.$^{-1}$)	Ratio β/α (10^{-4} in.)
Stainless steel No. 1	25.6	101.0	147.0	1.45
Iron No. 641	32.7	36.3	160.0	4.40
Iron No. 672	59.5	0.335	40.4	121.0
Porex Grade 4	46.2	0.911	0.481	0.528

The lack of parallelism exhibited by the curves in Fig. 3 makes it apparent that the data cannot be correlated by the use of any single length parameter, such as the equivalent capillary diameter which has been employed in some studies (7 and 8). This diameter is calculated by invoking an analogy between the laws of Darcy and Poiseuille and is inversely proportional to the square root of the viscous-resistance coefficient defined previously. If it is used in the Reynolds number and friction-factor expressions, the curves in Fig. 3 are brought together in the Darcy zone but diverge markedly in the quasi-turbulent regime. When plotted in terms of the dimensionless groups mentioned, however, the

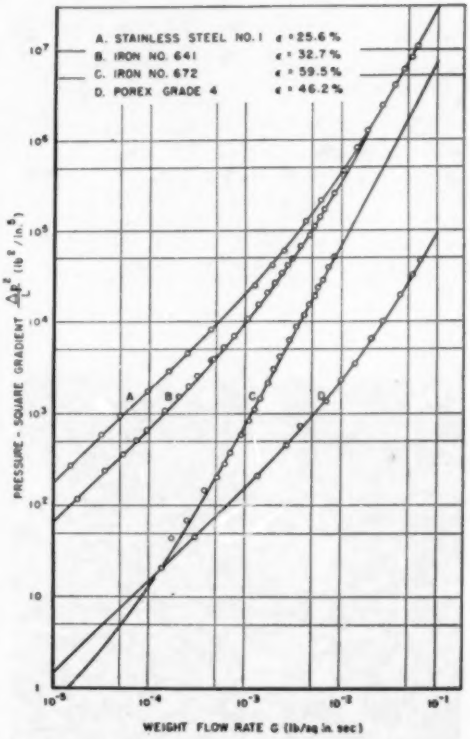
A. STAINLESS STEEL NO. 1 ε = 25.6 %
B. IRON NO. 641 ε = 32.7 %
C. IRON NO. 672 ε = 59.5 %
D. POREX GRADE 4 ε = 46.2 %
PRESSURE - SQUARE GRADIENT
WEIGHT FLOW RATE G (lb/sq in. sec)

FIG. 3 PRESSURE-SQUARE GRADIENT VERSUS WEIGHT-FLOW RATE FOR DIFFERENT POROUS METALS

data all fall along the curve given by Equation [14], as is shown in Fig. 4. Examination of the data obtained from the highly porous iron specimen shows that the scatter of the experimental points apparent in Fig. 3 (presumably attributable to inaccurate determinations of relatively small differences between large pres-

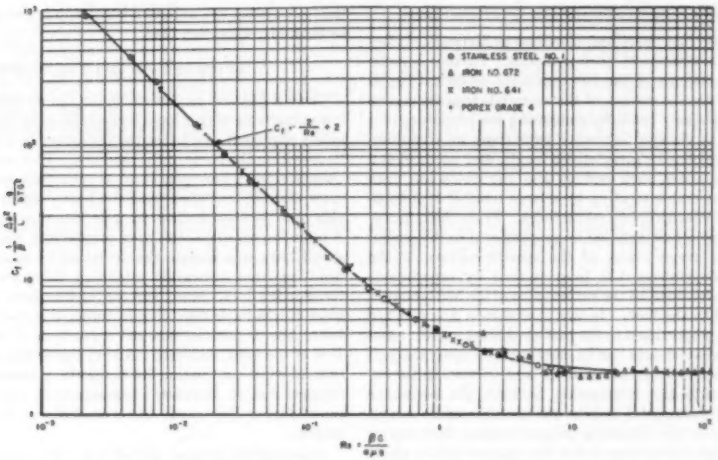

FIG. 4 FRICTION FACTOR VERSUS REYNOLDS NUMBER FOR VARIOUS POROUS METALS

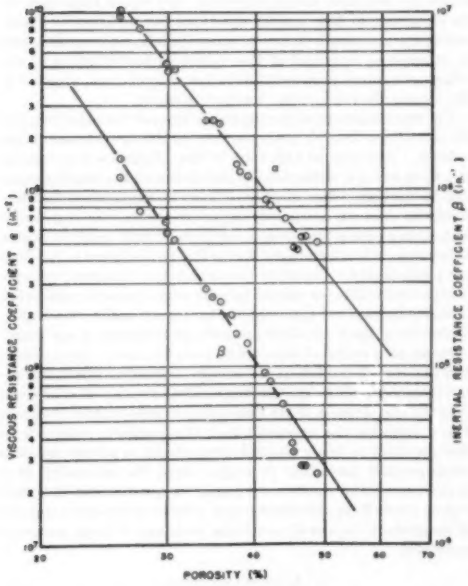

FIG. 5 VISCOUS AND INERTIAL RESISTANCE COEFFICIENTS VERSUS POROSITY

sures) has been magnified in Fig. 4, thus indicating that the dimensionless representation is not insensitive to deviations of the experimental data from the quadratic curve of Equation [11].

It may be noted that although Equation [14] provides a means of correlation and presentation of experimental data in dimensionless groups, the whole advantage of friction-factor versus Reynolds number representation does not necessarily extend to porous materials of complicated structures. In the special cases of flow through closed conduits and unconsolidated beds of geometrically simple particles, the experimental data can be reduced with the use of a single visually measurable length parameter, and the unified basis of representation afforded by the friction-factor versus Reynolds number graph is of real value in simplifying calculations. From the point of view of the present discussion, however, it may be seen that an extension of dimensionless grouping to the more general case of complex bonded structures such as porous metals requires knowledge of two experimentally determined characteristic length parameters, and in this case the unified representation affords only an esthetic advantage over direct calculation of flow rates or pressure drops from the basic quadratic Equation [11].

As mentioned previously, the second series of porous metals consisted of seven sets of porous stainless steel prepared under identical conditions but having porosities between about 25 and 47 per cent. The values obtained for viscous and inertial resistance coefficients α and β are presented as functions of porosity in Fig. 5. It can be seen that over a wide range of porosity the experimental results can be approximated in logarithmic co-ordinates by a straight line, indicating that both the viscous and inertial resistance coefficients vary inversely as the porosity raised to a certain power. The data in Fig. 5 show this power to be 5.3 for the viscous coefficient, and 6.0 for the inertial coefficient. It should be pointed out that the near equality of the two power factors, 5.3 and 6.0, found in this case is not significant. Measurements made on various porous metals have shown that in some cases the exponent of the porosity could be as high as 10 for α and as low as 5 for β. In interpreting such results, it must be noted that complete control of the specific surface of the metal samples cannot be assumed, since the degree to which the closely sized metal particles forming the compacts lose their identity during the sintering process is highly sensitive to the sintering conditions. The specific surface, which was not measured in these early experiments, also varies with the particle size of the non-metallic powder as well as the proportion of this powder in the compact.

Comparison of Porous Metals and Granular Beds

The experiments just described represent preliminary studies of the flow characteristics of porous metals. Further investigation of the dependence of the two resistance coefficients upon the porosity and specific surface of the materials appears desirable. Such studies may profit by comparing the properties of a highly complicated sintered structure with those of a medium possessing a well-defined characteristic length and no dead-end channels. The simplest such system, and one which has been subjected to considerable scrutiny by a large number of investigators, is a bed of smooth spherical particles. From their dimensions it is seen that α and β should be proportional to the second and first powers, respectively, of the specific surface of the medium. This dependence has been verified by experiments with sphere beds, in which all the surface area of the bed is convex and well exposed to the flow. In this special case β/α and $1/\beta$ are both directly proportional to the particle diameter and, consequently, the sphere-bed data can be correlated by using the particle diameter in the Reynolds number and friction-factor expressions. Although the relationship between the resistance coefficients of a porous metal and its true specific surface cannot be expected to obey the foregoing proportionality, flow experiments can establish the fraction of the true specific surface which is effective in resisting fluid motion.

A similar comparison possibly may permit determination of the effective fraction of the total measured porosity of a porous metal, but at the present time the influence of porosity on even a sphere bed is a subject of controversy. The work of a significant number of investigators, however, such as Ergun and Orning (9) as a recent example, indicates that the viscous and inertial resistance coefficients of a sphere bed may be approximated satisfactorily by functions (derived by use of the highly idealized Kozeny model) of the type

$$\alpha = k_1 S_0^2 \frac{(1-\epsilon)^2}{\epsilon^3} \quad [15]$$

$$\beta = k_2 S_0 \frac{1-\epsilon}{\epsilon^3} \quad [16]$$

where

ϵ = porosity of bed
S_0 = specific surface of bed $[L^{-1}]$
k_1, k_2 = dimensionless constants

Following the usual convention, Ergun and Orning define Reynolds number as $\rho v D_p/\mu$, where D_p is the particle diameter. As a consequence they necessarily find that "the friction factor implicitly involves the fractional void volume and is not a function of the Reynolds number alone, as has often been assumed." It is apparent, however, that the ratio of the inertial forces to the viscous forces in the fluid system (as modeled by a "true" Reynolds number) must be profoundly influenced by the spacing of the spherical surfaces bounding the system. For comparison with porous-metal structures, therefore, it appears logical to include porosity in the definition of both the Reynolds number and friction factor in the manner of Equations [12] and [13], which for liquid flow become

$$N_{R_\epsilon} = \frac{k_2 \rho v}{k_1 \mu S_0 (1-\epsilon)} \quad [17]$$

$$C_f = \frac{\dfrac{-\epsilon^3}{k_2 S_0 (1-\epsilon)} \dfrac{dp}{dx}}{\rho \dfrac{v^2}{2}} \quad [18]$$

thus preserving the unique relationship between the two groups as shown by Equation [14].

State of Flow in a Porous Metal

Various physical explanations for the deviation from Darcy's law at high rate of flow have been proposed in the literature. The oldest argument attributes the departure to the onset of turbulence within the pores of the medium. This explanation appears unsatisfactory, however, since experiments with granular beds show that the transition from the Darcy regime begins at a Reynolds number (based upon particle diameter) of the order of 4. A more logical model has been proposed by Bakhmeteff and Feodoroff (10), who explain the deviation by analogy to form drag resulting from separation attending the growth of the inertia forces in the fluid. Many current investigators picture the mechanism of quadratic resistance in terms of so-called kinetic-energy losses due to contractions and expansions of the cross-sectional area of the fluid filaments. An expansion loss results from separation,[6] while contraction losses may be attributed to momentum changes due to entrance adjustments of the velocity profiles, or, at higher flow rates, to separation and vena-contracta formation.

A generalized laminar picture has been suggested by Hubbert (11), who proposes that "the distortion of the flow lines by the inertial forces increases the velocity gradients, which in turn increase the frictional forces over what they would have been for the same rate of flow had the distortion not occurred." Eliminating the turbulence picture as unacceptable, it is expedient not to attempt an appraisal of the individual contributions of the other mechanisms proposed, but rather to lump them together in the necessarily vague term "inertial resistance."

The experiments upon porous metals support the belief that the deviation from Darcy's law is not attributable to the onset of turbulence. Although at high rates of flow, Equation [11] reduces to a form which is dimensionally identical with the familiar equation for turbulent flow in pipes, it must be emphasized that this similarity does not necessarily imply the existence of true turbulent mixing within the pores of the medium but merely indicates a flow regime in which losses due to the inertia forces in the fluid are predominant. Certainly the existence of turbulent velocity fluctuations within the minute interstices of a material such as the porous stainless-steel specimen in Fig. 1 is not easily conceivable. Distortion of the streamlines and perhaps formation of stationary vortexes as a result of separation, however, are to be expected, and under such conditions the energy dissipation would still result from momentum transfer on a molecular scale. It is believed that the effectiveness of the dimensionless presentation shown in Fig. 4 supports the argument that the quadratic resistance to flow provided by fine-grained structures such as porous metals is fundamentally molecular in origin, since the suitability of a smooth quadratic resistance equation is questionable in a flow regime where Reynolds stresses may arise from turbulent transfer of momentum on a scale involving exchange of large groups of molecules.

Acknowledgment

The experiments described in this paper were performed at the Jet Propulsion Laboratory under contract number W-04-200-ORD-455 with the Army Ordnance Department, Washington, D. C. The authors wish to thank this agency for the permission to publish the experimental results.

[6] This statement refers to the cumulative expansion loss incurred over a succession of alternate expansions and contractions, in which case the presence of viscosity prevents the recovery (during contraction) of the momentum lost in the preceding expansion.

BIBLIOGRAPHY

1 "Experimental Study of Cooling by Injection of a Fluid Through a Porous Material," by Pol Duwez and H. L. Wheeler, Jr., *Journal of the Aeronautical Sciences*, vol. 15, 1948, pp. 509–521.

2 "The Powder Metallurgy of Porous Metals and Alloys Having a Controlled Porosity," by Pol Duwez and H. E. Martens, Trans. AIME, vol. 175, 1948, pp. 848–875.

3 "Über Flussigkeitsbewegung mit sehr kleiner Reibung," by L. Prandtl, *Verhandl. d. 3 Internat. Math. Kong.*, Heidelberg, Germany, 1904.

4 "The Flow of Homogeneous Fluids Through Porous Media," by M. Muskat, McGraw-Hill Book Company, Inc., New York, N. Y., 1937.

5 "Wasserbewegung durch Boden," by P. Forcheimer, *Zeitschrift des Vereines deutscher Ingenieure*, vol. 45, 1901, p. 1781.

6 "Flow of Air and Natural Gas Through Porous Media," by T. W. Johnson and D. B. Taliaferro, Jr., Technical Paper No. 592, Bureau of Mines, Department of Interior, Washington, D. C., 1938.

7 "Flow of Air and Gas Through Porous Media," by J. Chalmers, D. B. Taliaferro, Jr., and E. Z. Rawlins, Trans. AIME, Petroleum Division, vol. 98, 1932, p. 375.

8 "Fluid Flow Through Porous Carbon," by M. R. Hatfield, *Industrial and Engineering Chemistry*, vol. 31, 1939, p. 1419.

9 "Fluid Flow Through Randomly Packed Columns and Fluidized Beds," by S. Ergun and A. A. Orning, *Industrial and Engineering Chemistry*, vol. 41, 1949, pp. 1179–1184.

10 "Flow Through Granular Media," by B. A. Bakhmeteff and N. V. Feodoroff, JOURNAL OF APPLIED MECHANICS, Trans. ASME, vol. 59, 1937, p. A-97.

11 "Field Equations of the Flow of Liquids Through Porous Solids," by M. K. Hubbert; paper presented at the Sixth International Congress for Applied Mechanics, Paris, France, Sept. 22–29, 1946.

A Method of Numerical Analysis of Plastic Flow in Plane Strain and Its Application to the Compression of a Ductile Material Between Rough Plates

By R. HILL,[1] E. H. LEE,[2] AND S. J. TUPPER[3]

Problems of plastic flow which arise in practice, with complicated boundary conditions, are seldom amenable to exact analysis, and it becomes necessary to devise some numerical method of solution. This paper describes a rapid numerical procedure for the determination of the stress and velocity distributions in plane plastic flow where the plastic strains are large. The method is applied to the problem of the squeezing of a plastic material between rough plates. This example has been chosen as it illustrates the treatment of most types of boundary condition likely to be encountered and supplies for contrast several incomplete solutions attempted by previous authors. The solution shows the fallacy of the apparent static determinancy of the plane plastic problem, indicating the need to consider the velocity field in obtaining the true distribution of stress. A further advantage of this example is the possibility of checking the numerical procedure, which is found to be extremely accurate.

Introduction

THE problem of analyzing the stress distribution and deformation in metals, which are flowing plastically, occurs in many fields of engineering, particularly in methods of metal forming. In many applications the problem reduces to one of plane strain, or can be considered to be such, as an approximation. The general plane plastic problem as it occurs in practice with complicated boundary conditions rarely can be solved analytically, and therefore it is necessary to devise a satisfactory method of numerical solution.

We consider plastic flow in plane strain, involving strains large in comparison with elastic strains. In analyzing conditions in the regions of large strain, it is permissible to neglect strains of the order of elastic strain and so to consider elastic material to be rigid. This type of solution applies whenever the freedom of movement of metal in plastic flow is not constrained completely by material still elastic. A large class of technically important problems can be dealt with satisfactorily on the basis of this limitation.

In this paper we select as an example to show in detail the numerical procedure, the problem of the compression of a metal between rough parallel plates. Historically this is an important problem in the development of plasticity theory, and a number of attempts have been made to solve it, originally by Prandtl (1)[4] and later, principally by Geiringer and Prager (2). However, as will be shown, none of these solutions is complete. The numerical attack described in this paper enables a complete solution to be obtained, which demonstrates some interesting properties of plastic-flow problems. Moreover, this solution can be obtained analytically in finite terms in a certain region near the ends of the compressed metal, so that it is possible to assess the accuracy of the numerical method. This provides a valuable check on its application to other cases of practical importance where exact analysis is impossible.

Equations Governing Plastic Flow in Plane Strain

The development of the equations governing plane plastic flow when plastic strains are large has been reported previously by the present authors (3) [see in particular Section 3 and the Appendix of (3)], and only a brief résumé of the final equations will be given here, using the nomenclature of that paper.

It is assumed that the material has a well-defined yield point and exhibits negligible work-hardening. For flow in two dimensions the maximum shear stress k is constant throughout the field, equal to $Y/\sqrt{3}$ for Mises' criterion, where Y is the yield stress in tension.[5] As was shown by Hencky (5), it is convenient to use as curvilinear co-ordinates (α, β) the two orthogonal sets of

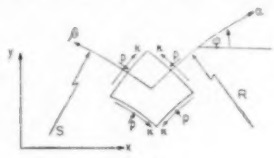

FIG. 1

directions of maximum shear stress, or slip lines, as shown in Fig. 1. The α and β sets are distinguished by the direction of the shear stress k.

---

[1] Head of Solid Mechanics Section, British Iron & Steel Research Association. Doncaster, Sheffield, England.

[2] Associate Professor of Applied Mathematics, Graduate Division of Applied Mathematics, Brown University, Providence, R. I. Mem. ASME.

[3] Experimental Officer, Armaments Research Department, Ministry of Supply, London, England.

Presented at the Annual Conference of the Applied Mechanics Division, Purdue University, Lafayette, Ind., June 22–24, 1950, of THE AMERICAN SOCIETY OF MECHANICAL ENGINEERS.

Discussion of this paper should be addressed to the Secretary, ASME, 29 West 39th Street, New York, N. Y., and will be accepted until April 10, 1951, for publication at a later date. Discussion received after the closing date will be returned.

NOTE: Statements and opinions advanced in papers are to be understood as individual expressions of their authors and not those of the Society. Manuscript received by the Applied Mechanics Division, January 17, 1950. Paper No. 50—APM-17.

[4] Numbers in parentheses refer to the Bibliography at the end of the paper.

[5] Mises' criterion reduces to this form when strains greater than 2 or 3 times the yield-point strain have occurred. For strains of the order of elastic strains, the analysis of plane strain is more complicated. See, for example, the elastic-plastic solution for a thick tube in plane strain (4).

In terms of these co-ordinates the equations of equilibrium determine the equation

$$\frac{\partial^2 \varphi}{\partial \alpha \, \partial \beta} = 0 \quad \ldots\ldots [1]$$

Expressed geometrically, this states that the angle between two slip lines of the same family, where they are cut by a slip line of the other family, is constant along their lengths.

The mean compressive stress p satisfies the relations

$$\left.\begin{aligned} p + 2k\varphi &\text{ is constant along an } \alpha\text{-line} \\ p - 2k\varphi &\text{ is constant along a } \beta\text{-line} \end{aligned}\right\} \quad \ldots\ldots [2]$$

Equation [1], governing the slip-line field, can be expressed in terms of the radii of curvature R, S of the slip lines, giving the alternative relations

$$\left.\begin{aligned} dS + R\,d\varphi &= 0 \text{ along an } \alpha\text{-line} \\ dR - S\,d\varphi &= 0 \text{ along a } \beta\text{-line} \end{aligned}\right\} \quad \ldots\ldots [3]$$

This form is particularly convenient for numerical integration as will be shown in the next section and enables the Cartesian co-ordinates (x, y) of the field points to be determined by integrals such as

$$x = -\int R \cos\varphi \, d\varphi, \quad y = -\int R \sin\varphi \, d\varphi \quad \ldots\ldots [4]$$

where the integrals are taken along an α-slip line.

The relationship between stress and strain-rate tensors in plastic flow determines similar equations for the components of velocity u, v along the slip lines, giving

$$\left.\begin{aligned} du - v\,d\varphi &= 0 \text{ along an } \alpha\text{-line} \\ dv + u\,d\varphi &= 0 \text{ along a } \beta\text{-line} \end{aligned}\right\} \quad \ldots\ldots [5]$$

In a particular problem, the boundary conditions usually determine the value of the radius of curvature of one of the sets of slip lines along part of the boundary, or some relation between the two radii, combined with a condition governing the variation of φ. Starting from these boundaries, application of Equations [3] and [4] enables the values of R, S, x, y over the whole field to be built up. There will also be conditions governing the flow velocities on a part of the boundary, from which the velocity field is built up using Equations [5].

Numerical Procedure

The basis of the method is the replacing of the differential forms of Equations [3] and [5] by linear difference relations across a network of slip lines. The field is thus split into an assembly of unit cells, of which a typical one is shown in Fig. 2. In the particular problem to be considered, as for many others, the boundary conditions are such that it is possible to choose the network so that the increment of slope $\Delta\varphi$ between consecutive points is the same throughout the whole field. This introduces a considerable simplification in the numerical procedure. In cases where this simplification is not possible the method is still applicable by an obvious generalization.

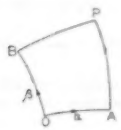

Fig. 2

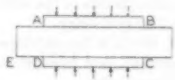

Fig. 3

In Fig. 2 we suppose that values of R and S are known at A and B, and we wish to determine R and S at P. Equations [3] are replaced by

$$\left.\begin{aligned} S_P - S_B &= \tfrac{1}{2} \cdot \Delta\varphi (R_P + R_B) \\ R_P - R_A &= \tfrac{1}{2} \cdot \Delta\varphi (S_P + S_A) \end{aligned}\right\} \quad \ldots\ldots [6]$$

where $\Delta\varphi$ is an essentially positive quantity when the slip lines are curved in the sense shown in Fig. 2. This will always be so for our particular problem. In other problems a change of sign may be required in Equations [6] with a corresponding modification deduced from these equations. We shall take $\Delta\varphi = 5$ deg $= 0.0872665$ radian; solution of Equations [6] then gives

$$\left.\begin{aligned} R_P &= 1.001907\, R_A + 0.043716(S_A + S_B) + 0.001907\, R_B \\ S_P &= 1.001907\, S_B + 0.043716(R_A + R_B) + 0.001907\, S_A \end{aligned}\right\} \quad [7]$$

Repetition of this procedure enables the whole field to be constructed from known boundary conditions.

In a similar way Equations [4] can be expressed in finite-difference form, giving

$$\left.\begin{aligned} x_P &= x_B + \tfrac{1}{2} \cdot \Delta\varphi (R_B \cos\varphi_B + R_P \cos\varphi_P) \\ y_P &= y_B + \tfrac{1}{2} \cdot \Delta\varphi (R_B \sin\varphi_B + R_P \sin\varphi_P) \end{aligned}\right\} \quad \ldots\ldots [8]$$

The velocity components are calculated from finite-difference relations based upon Equations [5]. We have

$$\left.\begin{aligned} u_P - u_B &= -\tfrac{1}{2} \cdot \Delta\varphi (v_P + v_B) \\ v_P - v_A &= -\tfrac{1}{2} \cdot \Delta\varphi (u_P + u_A) \end{aligned}\right\} \quad \ldots\ldots [9]$$

which can be combined to give Equations similar to Equations [7].

The foregoing equations are particularly simple and rapid to use with a calculating machine, the present problem requiring about 1 week with a single computer.

Both Equations [3] and [5] when expressed in the form of partial differential equations reduce to the telegraph equation as shown in the Appendix. Hence the solution of a particular problem can be obtained in the form of an integral using Riemann's method, but the integral can be evaluated analytically only for simple boundary conditions and in certain parts of the field.

As shown in the Appendix, such an analytic solution is available for the particular problem we consider and provides a useful check of the numerical method.

Compression of a Ductile Material Between Rough Plates

We shall demonstrate the application of the numerical method discussed in the previous section by determining the stress and velocity distributions for a ductile material compressed between rough parallel plates with an overhang of arbitrary initial shape. This problem involves in principle all the main types of boundary-value problems which usually occur.

We consider the metal in Fig. 3 to be constrained to deform in plane strain with no motion normal to the plane of the paper, the metal being free to flow out between the plates at each end. As mentioned in an earlier section, we consider the motion when a state of flow has been built up in which the strains are large compared with elastic strains. Material not subjected to such large strain will be considered to be rigid.

The contact between the plates and the metal is considered to be perfectly rough, sufficient slip having occurred to break down the intervening grease film or other adsorbed layers so that full contact is made between plate and metal. Under the compressive stress of several times the yield stress of the ductile metal, the friction will be limited, not by the contact surfaces but by the flow stress of the metal. The state of motion we are considering, for strains large compared with elastic strains, is not influenced

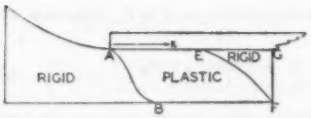

FIG. 4

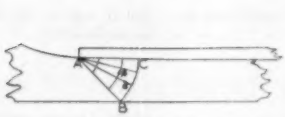

FIG. 5

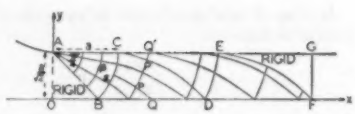

FIG. 6

by the detailed mechanism of the build-up of frictional force, which is considered to reach its full value while the strain is still small.

Determination of Boundary of Plastic Region

It might appear that the stress distribution can be determined without considering velocities, since Equations [1] to [4] do not involve u, v; but this concept of static determinancy due to Hencky (5) is quite illusory. For, although it is true that when the boundary of the plastic region is known the stresses can be straightway found, yet the position and shape of a part at least of this boundary is often dependent on the velocity-boundary conditions.

In the present problem it is clear that the overhanging part cannot be completely plastic, for in the neighborhood of the external corner E in Fig. 3, the normal and shear stresses on perpendicular planes are zero, which is incompatible with plastic flow there. This particular problem was discussed in general terms by Geiringer and Prager (2) who inferred that the boundary conditions specified a solution with the whole block of material in plastic flow. In fact, very restricting conditions would have to be satisfied by the boundary stresses to determine a solution plastic throughout. The question therefore arises of the momentary position of the line of separation between rigid and plastic material.

Fig. 4 shows a quarter of the block at some stage in the compression. AG is the plate, F is the center of the block, BF and FG are axes of symmetry. Velocity conditions at the plastic-rigid boundary determine that, apart from very special conditions which do not apply in the present case, the boundary between plastic and rigid regions must be a slip line. This is to be expected since the slip lines are characteristics of the velocity equations. It is reasonable to assume a trial position of the boundary of the rigid overhang in the form of a curve AB through A. The material to the left of AB is thus assumed to move outward as a rigid body, the material to the right being compressed plastically. The sense of the relative straining determines AB to be an α-slip line. Symmetry determines that AB cuts BF at an angle $\pi/4$.

AB having been chosen, the slip-line configuration in the plastic material between the plates is uniquely determined by Equation [1] and the stress-boundary conditions. These are that the β-lines meet the plate orthogonally (since the friction acts in the direction shown, to oppose the relative motion), and that both sets meet BF in $\pi/4$, since it is an axis of symmetry. The plastic region is thus determined up to the α-line through F, FE in the figure. The conditions of the problem are satisfied if the region of large plastic strain is bounded by the slip line FE, EFG being considered to move as a rigid body attached to the compression plates to the order of accuracy in strain magnitudes considered here. A velocity discontinuity will occur across this slip line. The resulting infinite rate of shear strain across FE is compatible with its being a slip line according to the strain-rate relations.

Having completed the slip-line field (further details of which are given in the next section) the velocity solution is built up from the right in Fig. 4 and is uniquely determined by the conditions on AE, EF, and BF. On AE and EF, the normal velocity is specified by the speed of compression, and the velocity component normal to BF is zero by symmetry. Thus the velocity on AB is uniquely determined by the initial choice of AB. But the velocity normal to AB must be compatible with the fact that material which has crossed AB moves as a single rigid body. This condition fixes the choice of AB. Finally, the equation of equilibrium for the overhang determines the value of p at, say, B, since by Equations [2] its variation along AB is known. By applying Equations [2] to the whole slip-line field, we can find the value of p, and therefore of the stress, at any point.

The suitable choice of AB turns out to be a straight line making $\pi/4$ with the axis, and this holds for every stage in the compression. In fact, this can be easily seen to be straightway, without any lengthy trial-and-error process suggested by the foregoing discussion, for, if AB is a straight line, a region ABC is uniquely determined in which the α-slip lines are radii from A, and the β-lines are concentric circular arcs meeting the plate orthogonally, Fig. 5. This configuration is such that, whatever happens to the right of BC, the velocity normal to AB is uniform and so is compatible with a rigid-body motion. We see from Equations [5] that u is constant on each α-line, and, by integration along a β-line, that v is therefore a function of φ only since v is constant on AC. Thus the friction conditions on AC in our particular problem enable the shape and position of the plastic boundary to be inferred a priori. This would not be so, in general, for other friction conditions.

Determination of Stress Distribution

Having established that AB is a straight line, let us now consider the stress solution at any stage of the compression in more detail. Region ABC, Fig. 6, consists, as we have seen, of radii from A and concentric circular arcs. To extend the slip-line field to the right of BC the numerical procedure is used as described in the section on "numerical procedure," with some modification for the boundaries BF, CE. The net points on BC were chosen to divide it into equal arcs; nine segments of 5 deg each were found satisfactory. The net points on BD were taken as the intersections of the α-lines (through the net points on BC) with BD. Since the value of φ is constant on each of the two boundaries BF, CE the continuation of the net thus defined is such that there is always an interval of 5 deg between consecutive points.

To calculate points of the network on BF we use the condition that $R = S$ by symmetry.

On CE, which is the envelope of the α-lines, we have $S = 0$ (see Appendix), and this permits the solution to be extended along this boundary.

It is to be noted that there is a discontinuity in S across the α-line CD in Fig. 6, S decreasing by amount a proceeding from left to right. Similarly, there is a discontinuity in R across the α-line DE with R decreasing by a. The discontinuity in curvature is, however, not propagated beyond the point E. The slip-line configuration has been determined as far as is indicated in Fig. 6; this corresponds to a stage in the compression when the length-height ratio is 6.72. In Fig. 7 this slip-line field is shown to scale.

When the slip-line configuration has been completed the values

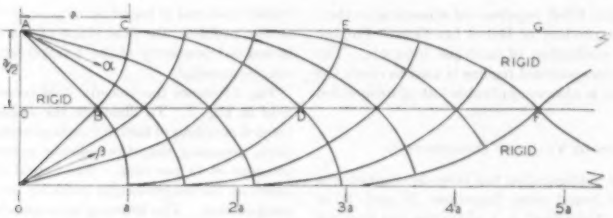

FIG. 7 SHOWING SLIP-LINE FIELD TO SCALE FOR BLOCK OF LENGTH-HEIGHT RATIO 6.72 AT INTERVALS OF 15 DEG IN ϕ

of p at points of the network can be found from Equations [2]. The initial value of p on AB is k from the equilibrium equation in the x-direction for the rigid overhang. It is easily seen that $p = k(1 + \pi/2)$ on AC.

It is necessary to study the history of the compression in order to visualize the development of the rigid region at the center of the block, shown in Fig. 6. As pressure on the plates is built up from zero, the material will at first deform elastically and the normal pressure will tend to produce the Poisson lateral expansion, causing slip along the whole surface AG, symmetry prescribing zero lateral velocity at G. This incipient slip will bring frictional resistance into play which will modify the stress distribution, producing a build-up of the mean hydrostatic pressure from O toward F. With increasing pressure the elastic limit will be exceeded, probably first in the neighborhood of A, and the plastic region will spread into the material. As long as the elastic region has a finite width for all values of y, the approach of the compression plates will be limited to the order of elastic strains which are neglected in this problem. Not until the plastic region has spread to the configuration shown in Fig. 4, with point contact between the rigid regions at F, can displacements occur involving strains large in comparison with elastic strains, the condition covered by the analysis in this paper.

In a full solution where strains of the order of elastic strains are not neglected, the center region would appear as in Fig. 8, for a sudden change to an elastic solution across EFE' would involve a discontinuity in the stress normal to the plane EFE', which on the basis of Mises' criterion would lead to incompatible stress conditions. In the shaded region, plastic and elastic strains are generally of the same order, with the former predominating near FE, FE'. The region of pure elastic strains is then

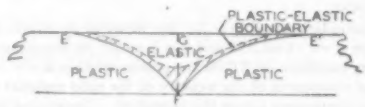

FIG. 8

smaller than is indicated by the rigid regions in our present approximate solution. This is confirmed by experiment. The strain in the shaded region normal to FE, FE' will be comparatively small (so that the condition $v = 0$ on FE is effectively true), while the shear strain parallel to FE, FE' will build up continually and rapidly to approximately the value obtained in our solution.

Similarly, the line AB is an idealization of a diffuse region, in most of which plastic and elastic strains are comparable, the former predominating rapidly as AB is approached. The strains normal to AB are small and so the velocity condition which we have applied on AB is effectively correct.

The stress distribution corresponding to Fig. 7 has been obtained, and the resulting distribution of pressure on the plate is shown by the full line in Fig. 9. The distribution in the elastic region is not known, but the average value of the pressure over EG, shown in Fig. 9, can be determined by integrating the known stresses along EF. The total force required to compress the block can be obtained by integration of the pressure curve.

The possibility of obtaining an analytical solution for R and S was mentioned in the section, Numerical Procedure. A brief outline of the method is given in the Appendix. Values in the region BCD in Fig. 6 can be expressed simply in terms of Bessel

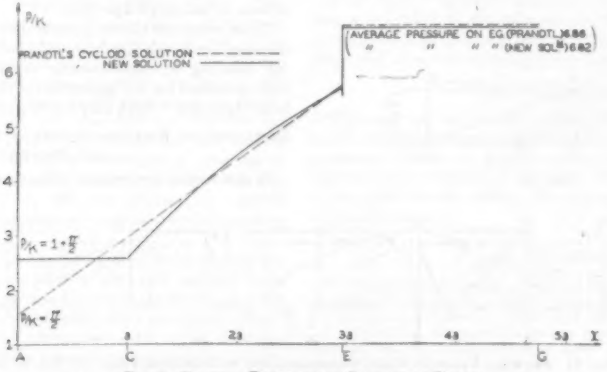

FIG. 9 SHOWING PRESSURE ON SURFACE OF BLOCK

functions, while the region CDE requires the numerical evaluation of the integral of a product of Bessel functions. Further extension involves the evaluation of multiple integrals. The analytical solution in these restricted regions is used to check the numerical method, which is always applicable but of unspecified accuracy.

Determination of Velocity Distribution

Now that the slip-line configuration has been determined, the velocity solution can be found using Equations [5] and [9] in finite-difference form. "Velocities" u, v along the slip lines are referred to unit velocity of the plates, and not to a time scale since we are considering quasi-static motion in which inertia forces play no part.

The boundary conditions for the material in plastic flow in Fig. 6 are $v = -1$ on AE, and $u = v$ on BF by symmetry. The boundary condition on EF for the plastic solution is $v = -\cos\varphi$, since the component of the velocity of the rigid material normal to EF is continuous across the boundary. Integrating the first of Equations [5] along the α-line EF, and using the condition $u = v$ at F, determines $u = -\sqrt{2} - \sin\varphi$ on this boundary. This involves a discontinuity of magnitude $\sqrt{2}$ in the tangential component of velocity across EF, implying a momentary infinite rate of shear strain. Since EF is a slip line this agrees with the flow hypothesis that directions of maximum shear-stress and shear-strain rate must coincide. With no work-hardening the resulting discontinuity in shear strain involves no incompatibility with the equations of equilibrium. Because EF is tangential to the plate at E, this velocity discontinuity is not propagated from E along ED.

From these boundary conditions, application of Equations [9], with suitable modification for boundary points on AE and BF, determines the velocity solution in successive regions DEF, CDE, BCD, ABC. The procedure is similar to that for the slip-line field discussed in more detail in the previous section.

As discussed in the section, Determination of Boundary of Plastic Region, u and v are constant along radii in region ABC. The outward velocity of the overhang (including AOB) is equal to the velocity found at B in the last stage of the numerical process in region BCD. Referring to Fig. 10, the incompressibility of the material is expressed by the differential relationship $y\,dx = -L\,dy$, where $y = y(x)$ is the shape of the extruded material. It is clear that the outward velocity of B is therefore $L/(AO)$ times the plate velocity. By integration, the surface of the extruded material is found to be $y = he^{-x/L}$. Thus for this particular problem, the final shape of the deformed material is obtained independently of the detailed strain distribution throughout the material.

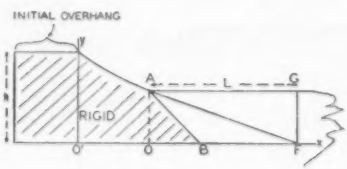

Fig. 10

Fig. 11 shows the velocity field corresponding to the slip-line field in Fig. 7. To illustrate the velocity components, the deformed positions of initially vertical sections are shown by broken lines, assuming that the velocity remains constant for a compression of 14 per cent. The actual displacements differ inasmuch as the length-height ratio for the block varies during the compression. The lettering corresponds with Fig. 7 and a dash denotes the deformed position of a point.

Discussion of Results—Accuracy

Since it would be difficult to specify the accuracy of the numerical procedure discussed in the section, Numerical Procedure, comparison of the particular solution with values obtained using the analytical method of the Appendix provides a useful estimate of accuracy.

Equation [15] gives the radii of curvature of the slip lines, R and S, at D in the form

$$\frac{S}{a} = \frac{R}{a} = I_0\left(\frac{\pi}{2}\right) + I_1\left(\frac{\pi}{2}\right) = 2.708$$

to three decimal places. The numerical method gave 2.773, indicating an error of less than 0.2 per cent after covering a field of 45 unit cells.

The first section of the Appendix shows that the solution in the region CDE can be expressed as a definite integral. In order to check the solution as far as it can be conveniently extended using the analytical method, the value of R/a at E was found by numerical integration to be 3.590. The finite-difference method gives 3.597, again indicating an error of less than 0.2 per cent after covering a field of 90 unit cells.

These values indicate that satisfactory accuracy for practical purposes could have been obtained with fewer net points on the arc BC. This would effect a considerable saving of time.

The analytical method of solution can be applied to the velocity field, but numerical evaluation of the resulting definite integrals is necessary for all regions. However, a more convenient check is supplied by the a priori knowledge of the velocity at B discussed in the previous section. The velocity with which AB is squeezed out for the particular block dimensions is determined by the condition of incompressibility to be 6.722, independently of the complete solution. Numerical integration throughout the whole field, starting from EF, determines the value 6.707, indicating an error of just over 0.2 per cent.

These numerical checks indicate that the numerical procedure discussed previously produces extremely accurate results without resorting to inconveniently small arcs. These examples lend confidence for the application of this method to other problems where such a check may not be possible.

Discussion of Results—Significance of Particular Solution Obtained

In this section we consider what there is to be learned about

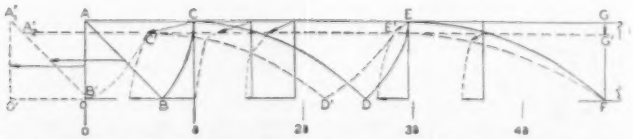

Fig. 11 Showing Velocity Field Corresponding to Slip-Line Field of Fig. 7, Assuming Velocity Remains Constant for Compression of 14 Per Cent or 0.1 in $1/\sqrt{2}$

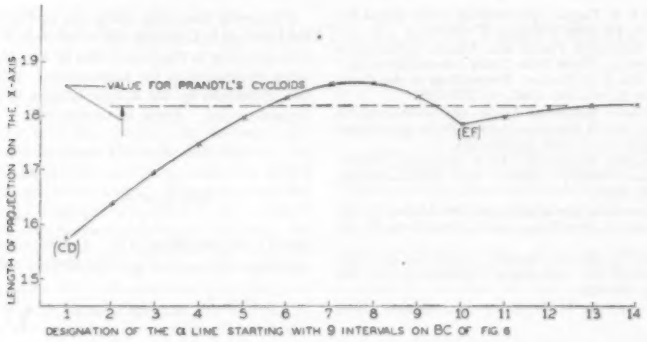

FIG. 12

problems of plane plastic flow from the numerical stress and velocity solution.

The problem of the compression of a rectangular block of ductile material between rough plates has been considered previously by several authors (1, 2, 6, 9), but to our knowledge no complete solution has been obtained so far. All former attempts appear to be implicitly limited to the initial stages of compression when the displacements are small, and it does not seem to have been realized that the type of slip-line configuration in Fig. 7 holds at all stages.

Prandtl (1) gave a qualitative picture similar to Fig. 7 but did not develop the corresponding quantitative stress or velocity solution; nor did he give the required justification for making AB straight. He also obtained an analytical solution on the assumption that the shear stress τ_{xy} is a function of y only. This leads to a linear distribution of τ_{xy} across all vertical sections, an elliptical distribution of σ_x, and a slip-line field consisting of orthogonal families of cycloids which retain the same form throughout the field. With these restrictions it is impossible to satisfy the conditions for rigid-body motion to the left of AB, and so the stress distribution cannot supply the required solution. However, the stresses on OA can be chosen so that the resultant force on the overhang is zero, which may supply a satisfactory solution for regions away from the end by analogy with Saint Venant's principle in elasticity.

Geiringer and Prager (2) have discussed Prandtl's cycloid solution and obtained the corresponding velocity solution. They do not, however, attempt to satisfy the conditions at the ends. Eichinger (6) gave the correct solution in the region ABC (without the necessary justification derived from a consideration of velocities) and fitted this approximately to Prandtl's cycloid solution, but he does not discuss the significance of the discontinuities of stress involved. He also does not consider the possibility of an overhang and assumes that the flow limit is reached in AOB. Sokolovski (9) has carried out a numerical integration of Prandtl's stress field (1) to determine the stress distribution in the region $ABDE$. He does not, however, consider the velocity solution, nor the associated justification for the stress field.

The broken line in Fig. 9 shows the pressure distribution on the plate, according to Prandtl's solution with zero resultant force over the ends. The pressure rises linearly to the beginning of the rigid region at E. Thus the influence of the free boundary OA, which produces the constant pressure over AC, is lost, although this linear expression provides a good approximation to the correct pressure toward the center of the block.

The approach of the correct solution toward Prandtl's solution can be studied more sensitively in another way. The α-curves in Fig. 7 are similar in form to cycloids, so that the lengths of their projections on the x-axis give a measure of their deviation from true cycloid form. Fig. 12 shows this deviation and includes an extension of the plastic solution beyond EF, i.e., for a greater length-height ratio. The constant length of the Prandtl cycloids is shown by a broken line. The first branch of the curve (CD) to (EF) brings the value closer to the limit, but the gradient appears to indicate subsequent larger deviation. However, the hyperbolic nature of the equations, which involves the possibility of the propagation of discontinuities along the characteristics, modifies this expectation, and the second branch involves a repetition of the first with a smaller deviation from the limit. Subsequent branches, which may not, however, exhibit discontinuity in gradient at their junctions, will oscillate about the limiting length of the Prandtl cycloid to which they approach. The approach of these curves to cycloidal form has a direct bearing on the stress distribution, for Equations [2] relate the mean hydrostatic pressure with φ, and it follows that as the slip-line curves approach the cycloidal form, the stress distribution approaches that given by Prandtl.

This solution thus demonstrates an analogy in plastic theory to Saint Venant's principle in elasticity. The approach to a steady solution independent of the distribution of the external forces over the end occurs in a typical hyperbolic manner in contrast with the smooth variation obtained in elasticity. The same influence is evident in the deformations shown in Fig. 11 where discontinuities in gradient occur in the lines showing the displacement of vertical sections where they intersect $C'D'E'$.

ACKNOWLEDGMENT

This work was carried out while the authors were members of the Theoretical Research Branch of the Armament Research Department, Ministry of Supply, United Kingdom, and was first circulated as an official report in 1946. The authors are indebted to the Chief Scientific Officer, Ministry of Supply, for permission to publish this paper.

BIBLIOGRAPHY

1 "Anwendungsbeispiele zu einem Henckyschen Satz über das plastische Gleichgewicht," by L. Prandtl, *Zeitschrift für angewandte Mathematik und Mechanik*, vol. 3, 1923, pp. 401–406.

2 "Mechanik isotroper Koerper im plastischen Zustand," by H. Geiringer and W. Prager, *Ergeb. d. exact. Naturwiss*, vol. 13, 1934, pp. 310–363.

3 "The Theory of Wedge Indentation of Ductile Materials," by

R. Hill, E. H. Lee, and S. J. Tupper, Proceedings of the Royal Society of London, series A, vol. 188, 1947, pp. 273–289.

4 "The Theory of Combined Plastic and Elastic Deformation With Particular Reference to a Thick Tube Under Internal Pressure," by R. Hill, E. H. Lee, and S. J. Tupper, Proceedings of the Royal Society of London, series A, vol. 191, 1947, pp. 278–303.

5 "Über einige statische bestimmte Faelle des Gleichgewichts in plastischen Koerpern," by H. Hencky, *Zeitschrift für angewandte Mathematik und Mechanik*, vol. 3, 1923, pp. 241–251.

6 "Verahleiss metallischer Werkstoffe," by A. Eichinger, Mitteilungen aus dem Kaiser-Wilhelm Institut für Eisenforschung. Band xxiii, Lieferung 13, 1941.

7 "Die Differential- und Integralgleichungen der Mechanik und Physik," by P. Frank and R. von Mises, vol. 1, Rosenberg, N. Y., 1943.

8 "Über die Hencky-Prandtlschen Kurven," by C. Caratheodory and E. Schmidt, *Zeitschrift für angewandte Mathematik und Mechanik*, vol. 3, 1923, pp. 468–475.

9 "Theory of Plasticity," by W. W. Sokolovski, Moscow, 1946, chapter 8.

Appendix

Analytical Method of Solution

Without loss of generality, Equation [1] shows that the values of α, β associated with the slip lines can be chosen so that

$$\varphi = -\alpha + \beta + \text{const} \quad \ldots\ldots [10]$$

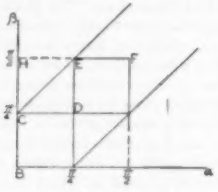

Fig. 13

and the equations of the slip-line field corresponding to Equations [3] become

$$\frac{\partial S}{\partial \alpha} = R; \quad \frac{\partial R}{\partial \beta} = S \quad \ldots\ldots [11]$$

Eliminating S and R, respectively, we have

$$\frac{\partial^2 R}{\partial \alpha\, \partial \beta} = R; \quad \frac{\partial^2 S}{\partial \alpha\, \partial \beta} = S \quad \ldots\ldots [12]$$

Thus both R and S satisfy the telegraph equation. The Equations [5] for the velocity components become

$$\frac{\partial v}{\partial \beta} = -u; \quad \frac{\partial u}{\partial \alpha} = -v \quad \ldots\ldots [13]$$

and

$$\frac{\partial^2 u}{\partial \alpha\, \partial \beta} = u; \quad \frac{\partial^2 v}{\partial \alpha\, \partial \beta} = v \quad \ldots\ldots [14]$$

which are again the same equations. This type of equation can be treated by Riemann's method using the Green's function $J_0[2i\sqrt{(\alpha - \alpha_1)(\beta - \beta_1)}]$ (see reference 7) which was first applied to these equations by Caratheodory and Schmidt (8).

For application to the particular problem treated in this report the constant in Equation [10] is taken as $-\pi/4$ and the α, β field, corresponding to Fig. 6 is shown in Fig. 13, corresponding points being designated by the same letters. The boundary conditions are determined by the known solution in the region $OABC$ and Equations [11]. For S, this determines

$$S(\alpha, 0) = a(1 + \alpha) \qquad 0 < \alpha < \frac{\pi}{4}$$

$$S(0, \beta) = a \qquad 0 < \beta < \frac{\pi}{4}$$

where a is the radius AB. Application of Riemann's method[6] determines $S(\alpha_1, \beta_1)$ in terms of Bessel functions in the form

$$\frac{S(\alpha_1, \beta_1)}{a} = I_0\left(2\sqrt{\alpha_1\beta_1}\right) + \sqrt{\frac{\alpha_1}{\beta_1}}\, I_1\left(2\sqrt{\alpha_1\beta_1}\right) \ldots [15]$$

By symmetry

$$S(\alpha_1, \beta_1) = R(\beta_1, \alpha_1)$$

To extend the solution into the region CDE, we have the boundary condition $S = 0$ on CE. This is conveniently treated by a solution covering the square $HCDE$ and taking $S(0, \pi/4 + \alpha)$ on CH equal to the known value $S(\alpha, \pi/4)$ on CD with a negative sign. Asymmetry then determines $S = 0$ on CE, and the boundary conditions are in the form of given functions along two characteristics. For convenience, C is taken as the new origin of co-ordinates, and the solution reduces to[6]

$$\frac{S(\alpha_1, \beta_1)}{a} = \int_0^{\alpha_1} \left\{ I_0\left(2\sqrt{(\alpha - \alpha_1)(\beta - \beta_1)}\right) \right\} \left\{ I_0\left(2\sqrt{\alpha \cdot \frac{\pi}{4}}\right) + \sqrt{\frac{\pi}{4\alpha}}\, I_1\left(2\sqrt{\alpha \cdot \frac{\pi}{4}}\right) \right\} d\alpha - \int^{\beta_1} \left\{ I_0\left(2\sqrt{(\alpha - \alpha_1)(\beta - \beta_1)}\right) \right\} \left\{ I_0\left(2\sqrt{\beta \cdot \frac{\pi}{4}}\right) + \sqrt{\frac{\pi}{4\beta}}\, I_1\left(2\sqrt{\beta \cdot \frac{\pi}{4}}\right) \right\} d\beta$$

R can be expressed in a similar form using Equations [11]. As these integrals do not appear amenable to evaluation analytically, the values of R and S on DE are not in a suitable form for analytical extension of the solution into the region DEF.

Boundary Condition at Plate Surface CE

Expanding the equation for an α-line in a Maclaurin series about the point of contact as origin we have

$$y = a_2x^2 + a_3x^3 + a_4x^4 + \ldots$$

$$\frac{dy}{dx} = 2a_2x + 3a_3x^2 + 4a_4x^3 + \ldots$$

The radius of curvature of the orthogonal β-line adjacent to the point of contact is therefore

$$S = \lim_{x \to 0} \frac{y}{\frac{dy}{dx}} = \lim_{x \to 0} \frac{a_2x^2 + a_3x^3 + a_4x^4 + \ldots}{2a_2x + 3a_3x^2 + 4a_4x^3 + \ldots}$$

which is zero whatever the order of contact of the α-line with the boundary CE.

[6] Refer to Bibliography (7), p. 815.

Emissivity Calculations for Diatomic Gases[1]

By S. S. PENNER,[2] PASADENA, CALIF.

An approximate method for estimating radiant-heat transfer from gaseous emitters has been developed. An average absorption coefficient is used for an effective width of an entire vibration-rotation band. The procedure for determining an average absorption coefficient in terms of integrated absorption can be justified, approximately, for very large total pressures where the spectral half-width is no longer small compared with the rotational spacing. Because of this limitation, it is to be expected that the procedure proposed here will be particularly useful only in estimating gaseous emissivities for emitters in high-pressure combustion chambers. Nevertheless, it appears that the simplified procedure yields reasonable results even at relatively low total pressures. Thus a comparison of calculated and observed emissivities for CO at atmospheric pressure shows satisfactory agreement, especially at large optical densities. Representative emissivity calculations over a wide temperature range are described. Emissivity calculations on CO, NO, HF, HCl, HBr, and HI can be carried out very rapidly by the use of recently published data on these gases.

Introduction

A SIMPLIFIED method for the approximate determination of emissivities of diatomic and polyatomic gases at thermodynamic equilibrium can be developed by a detailed consideration of the basic relations involved in radiant-heat-transfer calculations. The formulation of the problem will be the more complex, the greater the desired degree of accuracy. In a recently published report,[3] a brief survey of basic theory and a detailed description of a simplified treatment and of theoretical results have been presented.

It is the purpose of this discussion to demonstrate the relation between the simplified theoretical approach and experimental spectroscopic and heat-transfer studies. In particular, it will be shown that the drastic simplifications involved in the previously published analysis[3] are suggested by empirical measurements of infrared absorption spectra of pure gases. Furthermore, the theoretical results obtained previously[3] will be used for carrying out a number of representative emissivity calculations. The approximate method for making emissivity calculations can be justified only for large values of the total pressure where extensive broadening and overlapping of spectral lines occur. Nevertheless, it appears that the simplified procedure yields reasonable results even at relatively low total pressures. Thus a comparison of experimentally determined emissivities for carbon monoxide[4] with theoretical calculations shows fair agreement for large optical densities. For small optical densities the calculated emissivities are found to be too large. This observation is in agreement with theoretical predictions and can be derived, for example, from an analysis of the effect of total pressure on infrared absorption measurements.

Absorption Spectroscopy of Diatomic Molecules

The reason for examining the absorption spectra of molecules whose emissivities are to be calculated is evident from Kirchhoff's law. According to Kirchhoff's law the emissive power at a given wave length is equal to the absorptivity at this same wave length, multiplied by the spectral intensity of radiation emitted by a black body. Hence, if the absorptivity is zero, the emissive power is zero; if the absorptivity is unity, the emissive power reaches a maximum value, namely, the emissive power of a black body. Of course, the emissivity, absorptivity, and emissive power of a black body are dependent on temperature. The temperature dependence of these three quantities can be calculated by a straightforward though laborious procedure. Hence, by the use of theoretical relations, it is possible to extend room-temperature results. In the following paragraphs we shall be concerned with a discussion of absorption spectra, remembering that whatever conclusions are reached are immediately applicable to the calculations of emissive power.

Fig. 1 is a plot of the percentage of light transmitted by a 6-cm-long cell filled with carbon monoxide to a pressure of 1 atm, as a function of wave length. The results shown[5] in Fig. 1 were

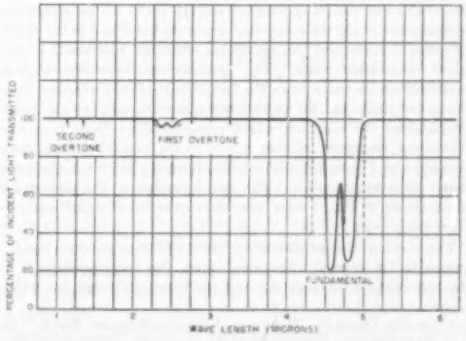

Fig. 1 Transmission Spectrum of 6 Cm of CO at 1 Atmosphere Pressure and at Room Temperature, Observed With Low Spectral Resolution

---

[1] This paper presents the results of one phase of research carried out at the Jet Propulsion Laboratory, California Institute of Technology, under U. S. Army Ordnance Department Contract No. W-04-200-ORD-1482.

[2] Jet Propulsion Laboratory, California Institute of Technology.

[3] "The Emission of Radiation From Diatomic Gases. I. Approximate Calculations," by S. S. Penner, *Journal of Applied Physics*, vol. 21, 1950, p. 685; also "The Emission of Radiation From Nitric Oxide: Approximate Calculations," by L. E. Benitez and S. S. Penner, *Journal of Applied Physics*, vol. 21, 1950, p. 907.

Presented at the Heat Transfer and Mechanics Institute Meeting, Los Angeles, Calif., June 28–30, 1950.

Discussion of this paper should be addressed to the Secretary, ASME, 29 West 39th Street, New York, N. Y., and will be accepted until April 10, 1951, for publication at a later date. Discussion received after the closing date will be returned.

Notes: Statements and opinions advanced in papers are to be understood as individual expressions of their authors and not those of the Society. Manuscript received by the ASME Applied Mechanics Division of the ASME, October 10, 1950.

[4] "Heat Transmission by Radiation From Non-Luminous Gases. Experimental Study of Carbon Monoxide," by W. Ullrich (thesis), Massachusetts Institute of Technology, Cambridge, 1935.

[5] "All of the experimental spectroscopic data presented in this paper were obtained by the author in collaboration with Dwight Weber of the Jet Propulsion Laboratory.

obtained with a low-resolution infrared spectrometer which is incapable of showing very rapid alternations in the transmitted-light intensity, if these alternations occur over very short wave-length ranges. Thus Fig. 1 gives only the broad contours of the absorption bands. Reference to Fig. 1 shows a region of prominent absorption, designated as the fundamental vibration-rotation band, and a region of weaker absorption, designated as the first overtone. If the optical density of the absorber (i.e., the product of the partial pressure of absorber and the cell length or optical path length) were made very large, additional regions of absorption would be observed corresponding to the second, third, and higher overtones. The position of the second overtone of CO is indicated in Fig. 1. It is well known from spectroscopy that the fundamental vibration-rotation band results from a change in energy of the absorbing molecules described by an increase of unity in the vibrational quantum number; the first overtone corresponds to a change of 2 in vibrational quantum number, etc.

It has been found experimentally that the absorption spectra of all diatomic molecules show distinct regions of absorption similar to CO. Furthermore, for all ordinary optical densities encountered in practical work, only the absorption of the fundamental and the first overtone is large enough to be of practical significance. We therefore arrive at the important conclusion that emissivity calculations on diatomic molecules require consideration of only two distinct wave-length regions.

If an instrument of very high resolving power were used to examine the intensity of transmitted light, it would be found that each of the absorption bands shown in Fig. 1 consists in reality of many more or less discrete rotational lines. Representative lines of the fundamental vibration-rotation band are shown in Fig. 2. The wave length λ has been replaced as abscissa in Fig. 2 by the wave number ν where $\nu = 1/\lambda$. The percentage of transmitted light $100\, I_\nu/I_{o\nu}$ has been replaced as ordinate by the spectral absorption coefficient P_ν. Here $I_\nu/I_{o\nu}$ and P_ν are related by the well-known relation

$$I_\nu/I_{o\nu} = exp(-P_\nu pL) \quad \ldots\ldots\ldots\ldots\ldots [1]$$

where I_ν = transmitted intensity at the wave number ν; $I_{o\nu}$ = incident intensity at the wave number ν; p = partial pressure of absorber, which is CO in the present case; and L = optical path length. The data shown in Fig. 2 were calculated, within an undetermined proportionality constant, by the use of a theoretical relation derived by Oppenheimer.[6] A designation such as $j = 3 \rightarrow j = 2$ in Fig. 2, shows that we are dealing with the absorption coefficient resulting from an energy jump of the absorbing molecule involving the rotational quantum number 3 in the lower vibrational state and the rotational quantum number 2 in the upper vibrational state. The fundamental vibration-rotation band derives its name from the fact that it is characterized by a change of unity in the vibrational quantum number (at room temperature the only important transitions are those from the vibrational quantum number $n = 0$ to the vibrational quantum number $n = 1$) coupled with all the changes $j \rightarrow j \pm 1$ in the rotational quantum number. The two branches of the absorption bands shown in Fig. 1 arise from the two series of transitions $j \rightarrow j + 1$ and $j \rightarrow j - 1$.

The width of the rotational lines of a vibration-rotation band is known to be strongly dependent upon the total pressure.[7] It also varies with temperature and the type of foreign gas which

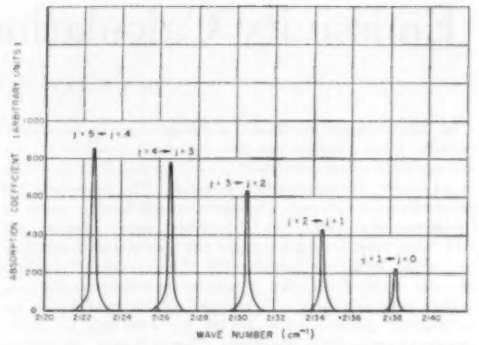

FIG. 2 DEPENDENCE OF ABSORPTION COEFFICIENT ON WAVE NUMBER FOR CO AT 300 K AND ATMOSPHERIC PRESSURE

may be present.[7] The data shown in Fig. 2 utilize experimental measurements of line width by Matheson.[8] If it is assumed that the line width varies with pressure according to the dispersion formula,[7] then it is found that the rotational lines shown in Fig. 2 assume the shape shown in Fig. 3, at room temperature, but at a pressure of 30 atm. Since the contributions from all of the rotational lines to the absorption coefficient are additive, it can be seen from the dotted curve shown in Fig. 3 that at high pressure the absorption coefficient is a continuous function of wave number. It should be noted that the area under the absorption coefficient versus wave-number curve (i.e., the integrated absorption) presumably does not change with pressure. Hence the effect of high pressure is primarily that of decreasing the variations of P_ν with ν.

From Equation [1] it is readily seen that

$$\int_{\Delta\nu} (I_\nu/I_{o\nu})\, d\nu = \int_{\Delta\nu} exp(-\bar{P}_\nu\, p\, L)\, d\nu \ldots\ldots [2]$$

if $\Delta\nu$ represents the wave-number width which is resolved by the spectrometer. For a vibration-rotation band it can readily be shown that the quantity on the left-hand side of Equation [2] will become smaller as the variation of P_ν with ν is decreased, as long as the sum of the integrated absorption for the rotational lines remains constant. It is therefore to be expected that for a given partial pressure of absorbing gas in an absorption cell of fixed length, the percentage of transmitted light will decrease as the total pressure is increased by the addition of a nonabsorbing gas, such as helium, argon, or nitrogen. The percentage of transmitted light will continue to decrease until the total pressure is large enough to make P_ν a continuous function of ν. Beyond this point an enormous increase in pressure is required in order to produce a further decrease in the integrated percentage of transmitted light.

Experimental verification of the conclusions reached as the result of the foregoing considerations is shown in Fig. 4 for CO pressurized with N_2.[8] Reference to Fig. 4 shows a large decrease in transmitted light when the total pressure is raised from 15 to 50 psia and then to 300 psia. However, addition of N_2 to raise the total pressure from 300 to 700 psia produces very little change in the percentage of transmitted light.

The discussion of the effect of pressure on absorption coefficient is thus seen to lead to the conclusion that, at sufficiently large values of the total pressure, the fraction of absorbed light be-

[6] "On the Quantum Theory of Vibration-Rotation Bands," by J. R. Oppenheimer, *Proceedings of the Cambridge Philosophical Society*, vol. 23, 1926, p. 327.

[7] "Pressure Effects on Spectral Lines," by H. Margenau and W. W. Watson, *Reviews of Modern Physics*, vol. 8, 1936, p. 22.

[8] "The Intensity of Infrared Absorption Bands," by L. A. Matheson, *Physical Review*, vol. 40, 1932, p. 813.

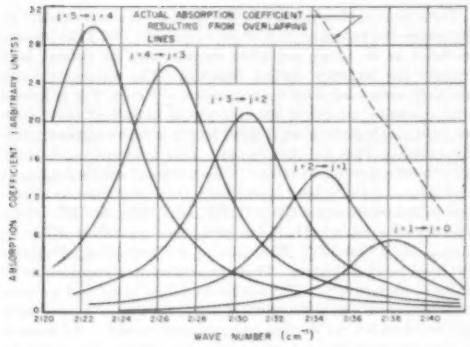

FIG. 3 DEPENDENCE OF ABSORPTION COEFFICIENT ON WAVE NUMBER FOR CO AT 300 K AND 30-ATMOSPHERE PRESSURE

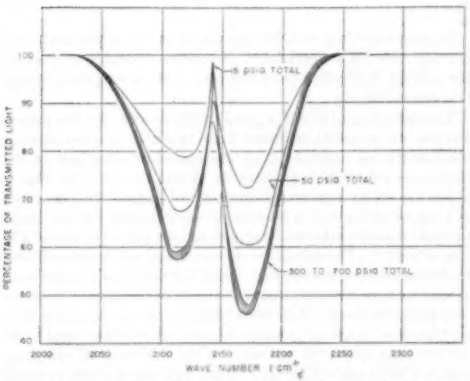

FIG. 4 TRANSMISSION SPECTRUM OF A 6-CM CELL OF CO—PARTIAL PRESSURE OF CO = 60 MM—PRESSURIZED WITH NITROGEN AT ROOM TEMPERATURE

comes practically independent of the total pressure although it continues to increase as the optical density is increased. The pressure at which absorption of light becomes relatively insensitive to total pressure would not be expected to vary greatly with temperature or type of added and optically inactive gas. On the other hand it is evidently dependent on the distance between the centers of adjacent rotational lines (this distance is independent of temperature and pressure for a given molecule), the required pressure increasing with increasing line spacing.

Experimental absorption measurements of the type shown in Fig. 4, as well as theoretical considerations,[8] lead to the conclusion that at sufficiently large total pressures we can replace Equation [2] by the relation

$$\int_{\Delta\nu} (I_\nu/I_{0\nu})\, d\nu = \Delta\nu\, exp(-\bar{P}\, p\, L) \quad \ldots\ldots\ldots [3]$$

where $\bar{P}$ is an appropriately chosen average absorption coefficient for the wave-number interval $\Delta\nu$. Furthermore, as a first approximation, we can choose $\Delta\nu$ so wide that it includes an entire vibration-rotation band. In this case the following relations are obtained for the fundamental and the first overtone, respectively

$$\Delta\nu \int_{n\to n+1} (I_\nu/I_{0\nu})\, d\nu = \Delta\nu_{n\to n+1}\, exp(-\bar{P}_F\, p\, L) \ldots [4]$$

$$\Delta\nu \int_{n\to n+2} (I_\nu/I_{0\nu})\, d\nu = \Delta\nu_{n\to n+2}\, exp(-\bar{P}_O'\, p\, L) \ldots [5]$$

Here $\bar{P}_F$ and $\bar{P}_O$ represent appropriate values for the average absorption coefficients of the fundamental and the first overtone, respectively. The quantities $\Delta\nu_{n\to n+1}$ and $\Delta\nu_{n\to n+2}$ represent the corresponding effective band widths. For example, for the spectrum shown in Fig. 1 it would be appropriate to use rectangular boxes, shown by dotted lines, to represent, in first approximation, the absorption bands. The calculation of values of average absorption coefficients and the calculation of effective band widths are evidently related problems. Their determination from spectroscopic data is discussed in the next section.

As was pointed out earlier in this section, the problems of absorption and emission of radiation are closely related, and the same quantities which determine the fraction of transmitted light in absorption measurements also determine the emissive power, to the same approximation. In particular, it is readily shown[3] that the intensity of radiation I_F' emitted by the fundamental vibration-rotation band is given, in first approximation, by the relation

$$I_F' = [1 - exp(-\bar{P}_F\, p\, L)]\, J(\bar{\nu}_F, T)\, \Delta\nu_{n\to n+1} \ldots [6]$$

whereas the intensity of radiation emitted by the first overtone is

$$I_O' = [1 - exp(-\bar{P}_O\, p\, L)]\, J(\bar{\nu}_O, T)\, \Delta\nu_{n\to n+2} \ldots [7]$$

Here $J(\nu, T)\, d\nu$ is the intensity of radiation emitted by a blackbody radiator at the temperature T and in the wave-number interval between ν and $\nu + d\nu$ per square centimeter of surface per second into a solid angle of 2π steradians, and $\bar{\nu}_F$ and $\bar{\nu}_O$ represent, respectively, average wave numbers for the fundamental and the first overtone. The quantities $J(\bar{\nu}, T)$ can be calculated readily from Planck's equation. The emissivity, as ordinarily defined, is equal to the ratio of the intensity of radiation actually emitted divided by the intensity of radiation emitted by a black body over all wave numbers. Since the latter quantity is

$$\int_0^\infty J(\nu, T)\, d\nu = \sigma\, T^4 \ldots\ldots\ldots\ldots [8]$$

where σ is the Stefan-Boltzmann constant, it follows that the emissivity ϵ is given by the relation

$$\epsilon = (I_F' + I_O')/\sigma\, T^4 \quad \ldots\ldots\ldots\ldots [9]$$

or

$$\epsilon = [1 - exp(-\bar{P}_F\, p\, L)]\, \frac{J(\bar{\nu}_F, T)\, \Delta\nu_{n\to n+1}}{\sigma\, T^4} + [1 - exp(-\bar{P}_O\, p\, L)]\, \frac{J(\bar{\nu}_O, T)\, \Delta\nu_{n\to n+2}}{\sigma\, T^4} \ldots\ldots [10]$$

Equation [10] is the fundamental relation used to make approximate emissivity calculations for diatomic molecules.

DETERMINATION OF EFFECTIVE BAND WIDTHS AND OF AVERAGE ABSORPTION COEFFICIENTS

Emissivity calculations by the use of Equation [9] depend on the successful evaluation, from available spectroscopic data, of average absorption coefficients and effective band widths. Since the average absorption coefficient must vary inversely as the corresponding effective band widths, it is apparent that Equation [10] contains two quantities which will tend to compensate one another. Thus choosing too large an effective band width will

lead automatically to a low value of average absorption coefficient and vice versa. For this reason the choice of an appropriate effective band width, although important, is not really critical for the successful calculation of approximate emissivities. This last statement is, however, not true if the optical densities are so large that the emitter radiates practically as a black body in the regions of its emission bands. In this case a reasonable choice of band width is of the utmost importance if more than semi-quantitative information is desired.

Calculation of Effective Band Widths. For the theoretical calculation of effective band widths we proceed from Oppenheimer's equation which allows us to determine the relative intensities of the rotational lines of a given vibration-rotation band.[8] The principal factor determining the relative intensities of the rotational lines is of the form.

$$j\ exp(-E_{n,j}/kT)$$

where $E_{n,j}$ is the energy of the nth vibrational and jth rotational energy levels, k is the Boltzmann constant, and T represents the absolute temperature. The quantities $E_{n,j}$ can be calculated, with a high degree of precision, from available spectroscopic data.[9] The variation of $j\ exp(-E_{n,j}/kT)$ with j is shown in Fig. 5 for CO at several temperatures. The plots of $j\ exp(-E_{n,j}/kT)$ as a function of n for all values of n which are of importance in practical problems are similar to those shown in Fig. 5. If it is remembered that the magnitude of the factor $j\ exp(-E_{n,j}/kT)$ or $j\ exp(-E_{n,j}/kT)$ determines the intensity of emitted radiant energy, it is apparent that only a small number of j-values needs to be considered for a given molecule. In particular, reference to Fig. 5 shows that for CO at 300 K the value of $28\ exp(-E_{n,28}/kT)$ is only about 10^{-5} as large as the maximum value corresponding to $8\ exp(-E_{n,8}/kT)$. At 3000 K, on the other hand, the first ninety j-values lead to appreciable values of $j\ exp(-E_{n,j}/kT)$. Hence we conclude that for ordinary values of the optical density, about thirty rotational lines of CO lying in each of the two branches characterized by the rotational transitions $j \rightarrow j-1$ and $j \rightarrow j+1$, respectively, will yield measurable intensities at room temperature. At 3000 K, somewhat more than ninety lines will contribute to emission of radiation from each of the two band branches. Similar remarks apply at other temperatures.

[8] "Molekülspektren," by H. Sponer, Julius Springer, Berlin, 1935.

From plots of the type shown in Fig. 5 it is a simple matter to determine the values of j for which $j\ exp(-E_{n,j}/kT)$ has become so small as to assure negligible contributions to radiant heat transfer for ordinary optical densities. The values of j are uniquely associated with wave numbers. Hence, if it is known that a definite number of lines contribute to radiant heat transfer, it is also known in what wave length or wave-number range the emitting lines are distributed. This information, in turn, fixes the effective band widths.[3] Effective band widths $\Delta\nu_{n\rightarrow n+1}$ and $\Delta\nu_{n\rightarrow n+2}$ have been calculated by this procedure, as a function of temperature, for CO, NO, HF, HCl, HBr, and HI. From the effective band widths, in turn, the quantities $J(\bar{\nu}_P,\ T)\ \Delta\nu_{n\rightarrow n+1}/\sigma T^4$ and $J(\bar{\nu}_O, T)\Delta\nu_{n\rightarrow n+2}/\sigma T^4$ appearing in Equation [9] have been evaluated. These quantities are designated as ϵ_P' and ϵ_O', respectively. The numerical values of ϵ_P' and ϵ_O' have been presented, as a function of temperature, in a previously published report, for the diatomic gases mentioned.[3] In terms of the known quantities ϵ_P' and ϵ_O' Equation [9] for the emissivity becomes

$$\epsilon = \epsilon_P'[1 - exp(-\bar{P}_P\ p\ L)] + \epsilon_O'[1 - exp(-\bar{P}_O\ p\ L)] \quad \ldots\ldots\ldots [11]$$

Before proceeding with the discussion of the determination of average absorption coefficients, it appears desirable to examine the concept of effective band width in terms of empirical absorption measurements.

The definition of effective band width adopted for the present analysis will be useful, provided it can be shown that the effective band width, as determined by the procedure described in this section, is relatively insensitive to optical density. In Figs. 6 and 7 are shown experimentally observed data of the percentage of transmitted light as a function of wave number for the fundamental vibration-rotation band and for the first overtone of CO, respectively.[5] The calculated effective band widths are indicated by dotted vertical lines in Figs. 6 and 7, which show experimental results for approximately 1 and 50 atm of CO contained in a 6-cm-long absorption cell. Reference to these data shows that a fifty-fold increase in optical density changes the effective band width by less than about 30 per cent for the fundamental vibration-rotation band and by perhaps 10 per cent for the first overtone. Therefore we are justified in concluding that the concept of effec-

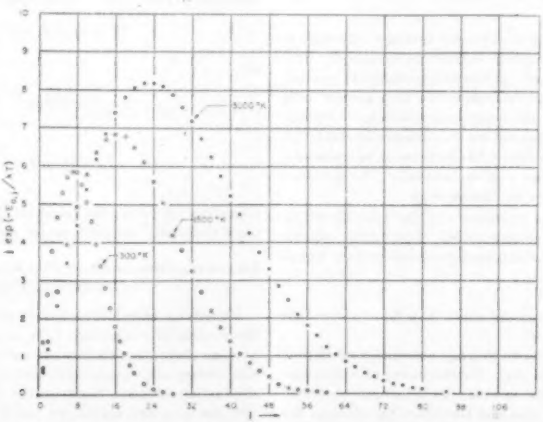

FIG. 5 REPRESENTATIVE PLOTS OF $j\ exp(-E_{n,j}/kT)$ VERSUS j FOR CO

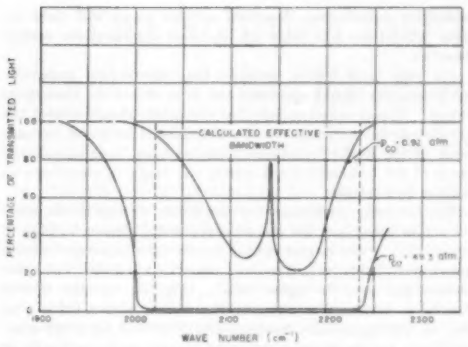

FIG. 6 PERCENTAGE OF TRANSMITTED LIGHT AS A FUNCTION OF WAVE NUMBER FOR FUNDAMENTAL VIBRATION-ROTATION BAND OF CO(Cell length = 6.22 cm.)

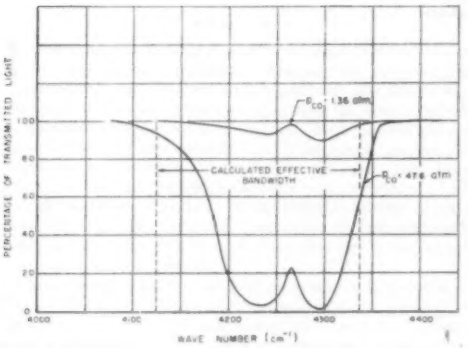

FIG. 7 PERCENTAGE OF TRANSMITTED LIGHT AS A FUNCTION OF WAVE NUMBER FOR FIRST OVERTONE OF CO(Cell length = 6.22 cm.)

tive band width, determined by use of the procedure described in this section, will be of practical value in making emissivity calculations, at least for the optical densities which are likely to arise in rocket combustion engines.

Calculation of Average Absorption Coefficients. The calculation of appropriate average absorption coefficients for the fundamental and the first overtone is a difficult problem which can be carried out with relative ease only if a number of restrictive assumptions are introduced.[3] The absorption coefficients depend on the integrated absorption as well as on the effective band widths. At the present time, reliable numerical values of integrated absorption, which is determined from studies of room-temperature infrared transmission, are known for only a few molecules. A critical review of available data (as well as a list of suggested values of $\bar{P}_F$ and $\bar{P}_O$ for the diatomic gases CO, NO, HF, HCl, HBr, and HI) has been published previously.[3] In line with the approximations involved in effective band-width calculations, a simple procedure for estimating average absorption coefficients has been developed.[3] Tentative plots of $\bar{P}_F$ and $\bar{P}_O$ as a function of temperature for diatomic gases have also been prepared by the author. It is apparent that emissivity calculations by the use of Equation [11] can be carried out in a few minutes for given values of p and of L by referring to the graphs giving ϵ_F', ϵ_O', $\bar{P}_F$, and $\bar{P}_O$ as a

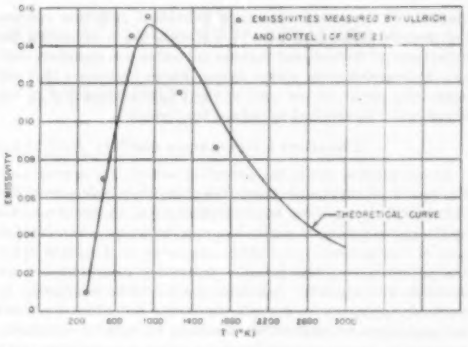

FIG. 8 COMPARISON OF CALCULATED AND OBSERVED EMISSIVITIES FOR CO ($p\,L$ = 6 FT-ATM)

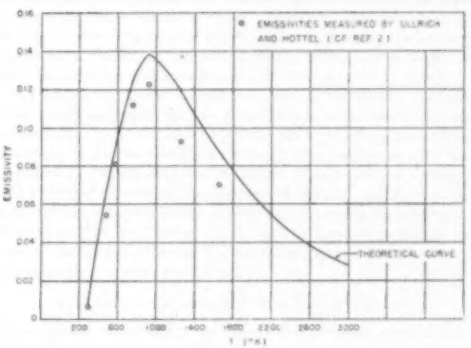

FIG. 9 COMPARISON OF CALCULATED AND OBSERVED EMISSIVITIES FOR CO ($p\,L$ = 2 FT-ATM)

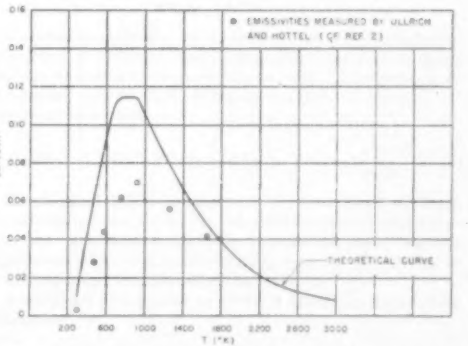

FIG. 10 COMPARISON OF CALCULATED AND OBSERVED EMISSIVITIES FOR CO ($p\,L$ = 0.2 FT-ATM)

function of temperature for each individual molecular species. Calculations of this type have been of some use in estimating the importance of radiant heat transfer in combustion chambers such as a hydrogen-fluorine rocket motor, where it appears that not more than about 25 per cent of the total heat transfer in the chamber can be ascribed to radiant heat transfer.

Emissivity Calculations for CO

As was pointed out in the preceding section, the approximate theoretical calculation of emissivities of diatomic molecules at elevated total pressures can be accomplished in a matter of minutes by the use of published graphs showing the temperature dependence of the unknown parameters appearing in Equation [11].[3] Unfortunately, no high-pressure emissivity measurements are available with which the calculated results can be compared. It therefore appears to be desirable to use the procedure developed for high-pressure combustion chambers in order to determine emissivities at atmospheric pressure where a comparison with available experimental measurements[4] can be made.

It is apparent, Fig. 2, that at atmospheric pressure for CO the rotational lines do not overlap sufficiently for the present method of emissivity calculations to be strictly applicable. Lack of overlapping of rotational lines means that the procedure for making emissivity calculations described in this paper will yield results which are too large at low and intermediate optical densities.

For very large optical densities the experimental emissivity measurements should approach and then exceed the theoretical values. Experimental emissivities ultimately should exceed the calculated emissivities, as the optical density is increased, because some of the weaker rotational emission lines, lying outside the range of the estimated band width, will begin to contribute to radiant heat transfer.

The foregoing predictions are completely verified by the comparison of calculated and observed emissivities shown in Figs. 8, 9, and 10. At the largest optical density for which experimental data are available (viz., 6 ft-atm), calculated and observed emissivities are seen to agree closely, Fig. 8. As the optical density is decreased to 2 ft-atm, Fig. 9, and then to 0.2 ft-atm, Fig. 10, the discrepancy between calculated and observed emissivities is seen to increase, the calculated values being too large. Since these results are in line with theoretical predictions, it appears likely that the approximate procedure for making radiant-heat-transfer calculations described in this paper will yield satisfactory results at elevated pressure for which it was developed.

The Solution of Elastic Plate Problems by Electrical Analogies[1]

By R. H. MacNEAL,[2] PASADENA, CALIF.

A dynamic-analogy method for the solution of elastic plate problems is described in this paper. The electrical circuits developed here can be set up and studied on an electric-analog computer. Problems involving deflections under constant load, transient vibrations, or normal modes can be solved in this way. The method of applying boundary conditions to plates with irregular edges is given, together with a detailed description of the representation of the boundary conditions for a rectangular variable-thickness plate. Solutions that have been obtained on the Cal Tech electric-analog computer are presented for the static deflections and normal modes of a rectangular cantilever plate.

Introduction

IN this paper an analogy method is developed for the solution of elastic plate problems. Because the mathematical formulation of plate problems is complex, only limited success has been achieved in the solution of these problems by classical methods. Expansions in orthogonal functions have yielded the solution of a few problems involving simple geometrical shapes and simple boundary conditions. In most cases, more general methods are required, among the more powerful of which is the finite-difference method. In the electrical-analogy method described here, the problem is formulated in finite-difference terms, and the solution of the difference equations is carried out on an electric-analog computer.

The analogies to be developed are an extension to two dimensions of the beam analogy derived in a previous paper (1).[3] They share with it the advantage that they are completely dynamic analogies in that the values of none of the electrical components depend on frequency. This permits normal mode and transient-vibration problems to be solved. Another feature of the plate analogy is that all of the quantities of physical interest (slopes, moments, and shears) can be measured directly. This aids the development of an intuitive approach to the problem with the result that it becomes unnecessary to set up the mathematical equations before attacking each problem. An even more important result is the fact that it is possible to make statements about the electrical analogy that have equal validity when applied to the elastic plate and vice versa.

The electrical analogies to be developed are based on the equations for a thin plate with the assumption of small deflections. The equations for large deflections are nonlinear and cannot be solved by an analog computer consisting of passive electrical elements only.

No restrictions are made on the elastic properties of the plate as regards homogeneity and isotropy. Analogies for variable-thickness plates and anisotropic plates can be set up so that, for example, the vibrations of thin airplane wings can be investigated under realistic assumptions. In the electric-analogy method, free edges cause no particular difficulty. The representation of irregular edges has been developed by an intuitive method, using the close correlation between the physical properties of the plate and of its electrical analogy.

Among the advantages of the analogy method is the fact that plates with inhomogeneous elastic properties, irregular edges, or any condition of loading or support can in principle be solved as easily as a uniform symmetrical plate. Problems in which a plate is coupled to other mechanical systems can also be solved.

An analog computer capable of solving reasonably difficult plate problems (requiring more than 20 or 30 cells) does not at the present time exist. A few of the simpler problems have been investigated on the Cal Tech electric-analog computer with the intention of determining the feasibility of the analogy method. The principal unsatisfied requirement of the plate analogy is the existence of a large number of essentially perfect transformers. It is estimated that 250 of these, or five times the number at present available in the Cal Tech computer, are a reasonable requirement for complex problems.

Electrical Analogy for Bending of a Beam

The electrical analogy for an elastic plate is more easily introduced by discussing first the dynamic analogy for the bending of a beam. Although this analogy is the subject of an earlier paper (1) it will be rederived here in a slightly different form.

The differential equation for the bending of a beam is

$$\frac{\partial^2}{\partial x^2}\left(EI\frac{\partial^2 w}{\partial x^2}\right) = q \qquad [1]$$

where w is the deflection and q the load density. The nature of q, whether it represents static loading, inertia loading, or spring loading, need not at present concern us. For a uniform beam EI is constant, and the finite difference equivalent of Equation [1] may easily be derived

$$w_{n+2} - 4\,w_{n+1} + 6\,w_n - 4\,w_{n-1} + w_{n-2} = \frac{q\,\Delta x^4}{EI} \qquad [2]$$

An electrical ladder network can be constructed in which Kirchhoff's current law for the nth node is identical with Equation [2]. This network, however, requires the use of negative impedances which is a serious disadvantage for the solution of normal mode and transient-vibration problems.

A less direct analogy will be used. If the slope and shear are defined as

$$\theta = \frac{\partial w}{\partial x} \qquad [3]$$

---

[1] This study was accomplished under a United States Air Forces Contract.

[2] Instructor of Electrical Engineering, California Institute of Technology.

[3] Numbers in parentheses refer to the Bibliography at the end of the paper.

Contributed by the Applied Mechanics Division and presented at the Semi-Annual Meeting, St. Louis, Mo., June 19–23, 1950, of The American Society of Mechanical Engineers.

Discussion of this paper should be addressed to the Secretary, ASME, 29 West 39th Street, New York, N. Y., and will be accepted until April 10, 1951, for publication at a later date. Discussion received after the closing date will be returned.

Note: Statements and opinions advanced in papers are to be understood as individual expressions of their authors and not those of the Society. Manuscript received by the Applied Mechanics Division, October 19, 1949. Paper No. 50—SA-23.

and

$$Q = -\frac{\partial}{\partial x}\left(EI\frac{\partial \theta}{\partial x}\right) \quad [4]$$

then Equation [1] becomes

$$-\frac{\partial Q}{\partial x} = q \quad [5]$$

When EI is not constant, it is simpler to write the finite-difference equations corresponding to Equations [3], [4], and [5] separately, than it is to write the finite-difference equation corresponding to Equation [1]. This method has the advantage that it immediately reveals the correct form of the electrical network for the solution of transient problems. The equivalent finite-difference equations are, respectively

$$\theta_{n+1/2} = \frac{w_{n+1} - w_n}{\Delta x} \quad [6]$$

$$-Q_{n+1/2} = (\theta_{n+3/2} - \theta_{n+1/2}) \cdot \frac{EI_{n+1}}{\Delta x^2} + (\theta_{n-1/2} - \theta_{n+1/2}) \frac{EI_n}{\Delta x^2} \quad [7]$$

$$-\frac{(Q_{n+1/2} - Q_{n-1/2})}{\Delta x} = q_n \quad [8]$$

The subscript $n + 1/2$ refers to the mid-point between x_n and x_{n+1}, the points at which the deflection is defined.

Equations [7] and [8] may be regarded as expressions of Kirchhoff's current laws in an electrical network. The circuit in Fig. 1 satisfies all three of these equations if w and θ are regarded as voltages. Equation [6] expresses the relationship between the primary and secondary voltages of a transformer where the turns ratio is Δx. Equation [7] is Kirchhoff's law for the sum of the

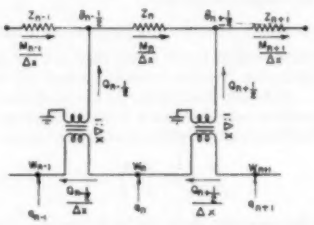

FIG. 1 DYNAMIC ANALOGY FOR BENDING OF A BEAM; $Z_n = \frac{\Delta x^2}{EI_n}$

currents entering the node $\theta_{n+1/2}$. The impedance of the branch connecting $\theta_{n+1/2}$ and $\theta_{n+3/2}$ is $(\Delta x^2)/(EI_{n+1})$. The current flowing in the secondary of the transformer is the turns ratio times the current in the primary, i.e., $Q_{n+1/2}$.

Equation [8] is Kirchhoff's law for the sum of currents entering the node w_n. The bending moment

$$M = -EI\frac{\partial^2 w}{\partial x^2} \quad [9]$$

is the current flowing in the slope circuit, multiplied by Δx as shown. For static-loading problems, the impedances Z_n may be purely resistive, while for transient and normal mode problems they must be inductive.

The transformers in Fig. 1 must be essentially perfect. Any leakage or magnetizing inductance associated with them detracts from the accuracy of the solution.

DYNAMIC ANALOGY FOR CONSTANT-THICKNESS PLATE

The differential equation for the deflection of a constant-thickness plate is

$$\frac{\partial^4 w}{\partial x^4} + 2\frac{\partial^4 w}{\partial x^2 \partial y^2} + \frac{\partial^4 w}{\partial y^4} = \frac{q}{D} \quad [10]$$

where D is the stiffness constant and q is the load density. The finite-difference expression equivalent to Equation [10] can be written down directly, resulting in a relationship coupling the general node point with twelve of its nearest neighbors. This procedure is always employed when a digital method of solution is to be used and has even been extended to the solution of skew-plate problems (2). When applied to the analogy method, however, it leads to the unwelcome necessity of negative circuit elements. The method that we shall use is similar to that employed in the derivation of the dynamic-beam analogy. In fact, by making use of this previous derivation, it is possible to derive the plate analogy without referring to the finite-difference equations at all.

Equation [10] can be written in the following form

$$\frac{\partial}{\partial x}\left[\left(\frac{\partial^2}{\partial x^2} + \frac{\partial^2}{\partial y^2}\right)\frac{\partial w}{\partial x}\right] + \frac{\partial}{\partial y}\left[\left(\frac{\partial^2}{\partial x^2} + \frac{\partial^2}{\partial y^2}\right)\frac{\partial w}{\partial y}\right] = \frac{q}{D} \quad [11]$$

The equation for a uniform beam is

$$\frac{\partial}{\partial x}\left[\left(\frac{\partial^2}{\partial x^2}\right)\frac{\partial w}{\partial x}\right] = \frac{q}{EI} \quad [12]$$

The brackets in Equation [12] indicate the manner in which this equation was broken up into three equations in the derivation of the dynamic-beam analogy. The first term of Equation [11] is the same as the left side of Equation [12] with $(\partial^2/\partial x^2) + (\partial^2/\partial y^2)$ replacing $\partial^2/\partial x^2$. For the beam analogy it was shown that the operator $\partial^2/\partial x^2$ is represented by impedances in the θ circuit connecting neighboring nodes. For the plate, $\partial^2/\partial x^2 + \partial^2/\partial y^2$ is represented by impedances connecting neighboring nodes in *both* the x and y-directions. The network to represent the first term of Equation [11] is shown in Fig. 2. By definition, the slope in the x-direction is

$$\theta_x = \frac{\partial w}{\partial x}$$

The additional impedances Z_{xy} oriented parallel to the y-axis represent the term $\partial^2/\partial y^2$. Consequently a two-dimensional grid of impedances connects nodes in the θ_x circuit.

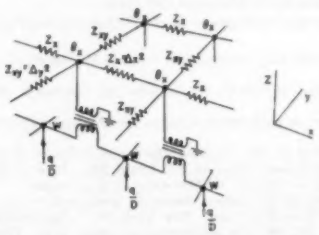

FIG. 2 DYNAMIC ANALOGY FOR FIRST TERM OF EQUATION [11]

The second term of Equation [11] is represented by a second network entirely similar to that in Fig. 2. It has a two-dimen-

sional grid of impedances connecting nodes in the θ_y circuit. The primaries of its transformers which are oriented parallel to the y-axis are joined at the nodes of the w-circuit with the x-transformers so that a two-dimensional grid of transformer primary windings is formed. Thus the complete analogy consists of three separate two-dimensional grids in which the voltages to ground are, respectively

$$w,\ \theta_x = \frac{\partial w}{\partial x} \text{ and } \theta_y = \frac{\partial w}{\partial y}$$

The coupling between these three networks is by means of the magnetic fields of the transformers only. Since no conductive interconnection exists, the circuit diagrams of the three networks can be drawn separately. Plan views of these networks are shown in Fig. 3.

Dynamic Analogy for a Variable-Thickness Plate

The equations given for the bending moments by Timoshenko (3) are

$$M_x = -D\left(\frac{\partial \theta_x}{\partial x} + \nu \frac{\partial \theta_y}{\partial y}\right) \quad [13]$$

$$M_y = -D\left(\frac{\partial \theta_y}{\partial y} + \nu \frac{\partial \theta_x}{\partial x}\right) \quad [14]$$

$$M_{xy} = -D(1-\nu)\frac{\partial \theta_x}{\partial y} = -D(1-\nu)\frac{\partial \theta_y}{\partial x} \quad [15]$$

The shears are given by

$$Q_x = \frac{\partial M_x}{\partial x} + \frac{\partial M_{xy}}{\partial y} \quad [16]$$

$$Q_y = \frac{\partial M_y}{\partial y} + \frac{\partial M_{xy}}{\partial x} \quad [17]$$

The static equilibrium of the plate requires that

$$\frac{\partial Q_x}{\partial x} + \frac{\partial Q_y}{\partial y} + q = 0 \quad [18]$$

Combining Equations [13] through [18], where D need not be constant, the equation of the plate may be written as

$$\frac{\partial}{\partial x}\left\{\frac{\partial}{\partial x}\left[D\left(\frac{\partial \theta_x}{\partial x} + \nu \frac{\partial \theta_y}{\partial y}\right)\right] + \frac{\partial}{\partial y}\left[D(1-\nu)\frac{\partial \theta_x}{\partial y}\right]\right\}$$
$$+ \frac{\partial}{\partial y}\left\{\frac{\partial}{\partial y}\left[D\left(\frac{\partial \theta_y}{\partial y} + \nu \frac{\partial \theta_x}{\partial x}\right)\right] + \frac{\partial}{\partial x}\left[D(1-\nu)\frac{\partial \theta_y}{\partial x}\right]\right\} = q \quad [19]$$

Although it appears imposing, the only terms of Equation [19] that cannot be represented by the network in Fig. 3 are those involving

$$\nu \frac{\partial \theta_y}{\partial y} \text{ and } \nu \frac{\partial \theta_x}{\partial x}$$

The other terms can be represented by the network with

$$Z_x = \frac{\Delta x^2}{D} \qquad Z_{xy} = \frac{\Delta y^2}{D(1-\nu)}$$

$$Z_y = \frac{\Delta y^2}{D} \qquad Z_{yx} = \frac{\Delta x^2}{D(1-\nu)}$$

The terms $\nu(\partial\theta_y/\partial y)$ and $\nu(\partial\theta_x/\partial x)$ represent a mutual coupling between the θ_x and θ_y circuits. By superimposing the networks in Fig. 3 it will be seen that the Z_x and Z_y branches cross each other, and that the centers of these branches are at the same geometrical point. A mutual admittance between the two branches is required where

$$Y_n = \frac{\nu D}{\Delta x \Delta y}$$

This mutual admittance requires an essentially perfect transformer for its realization, bringing to three the number of such

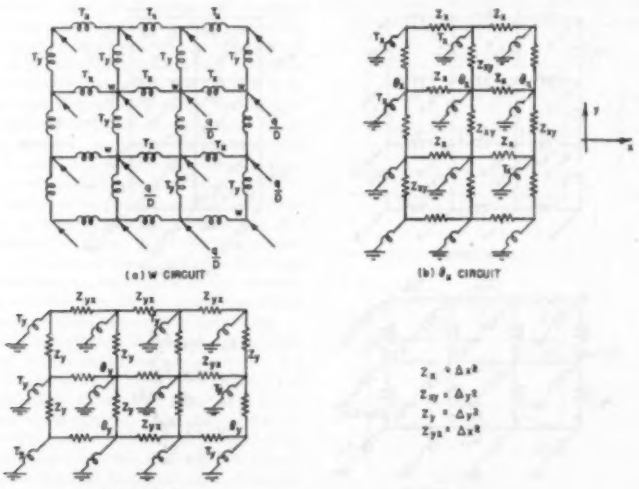

Fig. 3 Dynamic Analogy for Constant-Thickness Plate

transformers required per cell. In practice it is expedient to convert this mutual admittance to a mutual impedance with accompanying modifications in Z_x and Z_y. The impedances required may be summarized as follows

$$Z_x = \frac{1}{1-\nu^2}\frac{\Delta x^2}{D}$$

$$Z_y = \frac{1}{1-\nu^2}\frac{\Delta y^2}{D}$$

$$Z_m = \frac{\nu}{1-\nu^2}\frac{\Delta x\,\Delta y}{D}$$

$$Z_{xy} = \frac{1}{1-\nu}\frac{\Delta y^2}{D}$$

$$Z_{yx} = \frac{1}{1-\nu}\frac{\Delta x^2}{D}$$

Fig. 4 shows the network for a variable-thickness plate. In this network the currents in the slope circuits are proportional to the moments, and the currents in the w-circuit are proportional to the shears

$$\text{Current in } Z_x = \frac{M_x}{\Delta x}$$

$$\text{Current in } Z_y = \frac{M_y}{\Delta y}$$

$$\text{Current in } Z_{xy} = \frac{M_{xy}}{\Delta y}$$

$$\text{Current in } Z_{yx} = \frac{M_{yx}}{\Delta x}$$

$$\text{Current in } x\text{-branch of } w \text{ circuit} = \frac{Q_x}{\Delta x}$$

$$\text{Current in } y\text{-branch of } w \text{ circuit} = \frac{Q_y}{\Delta y}$$

We see that all of the quantities of physical interest are available in the electrical analogy.

The variable-thickness-plate analogy can be easily extended to include anisotropic plates. For such a plate four constants instead of two are needed to define the elastic properties of the material (4). In terms of these four constants the equation of the plate may be written as

$$\frac{\partial}{\partial x}\left\{\frac{\partial}{\partial x}\left[D_x\frac{\partial \theta_x}{\partial x} + D_1\frac{\partial \theta_y}{\partial y}\right] + \frac{\partial}{\partial y}\left[2D_{xy}\frac{\partial \theta_x}{\partial y}\right]\right\} + \frac{\partial}{\partial y}\left\{\frac{\partial}{\partial y}\left[D_y\frac{\partial \theta_y}{\partial y} + D_1\frac{\partial \theta_x}{\partial x}\right] + \frac{\partial}{\partial x}\left[2D_{yx}\frac{\partial \theta_y}{\partial x}\right]\right\} = q \quad \ldots\ldots [20]$$

This equation is entirely similar in form to Equation [19]. Referring to Fig. 3, we see that the self-admittance of the Z_x and Z_y branches are $D_x/(\Delta x^2)$ and $D_y/(\Delta y^2)$ respectively, that the self-admittance of the Z_{xy} and Z_{yx} branches are $2D_{xy}/(\Delta y^2)$ and $2D_{yx}/(\Delta x^2)$, respectively, and that the mutual admittance between the Z_x and Z_y branches is $D_1/(\Delta x\,\Delta y)$.

Method of Applying Boundary Conditions

Two boundary conditions must be applied along each edge of an elastic plate. A general result of the application of the principle of virtual work is that along any edge one condition from each of the following two groups must apply

Group 1

$$w = w_0 \quad \ldots\ldots [a]$$

$$Q_n + \frac{\partial M_{tn}}{\partial t} = R_0 \quad \ldots\ldots [b]$$

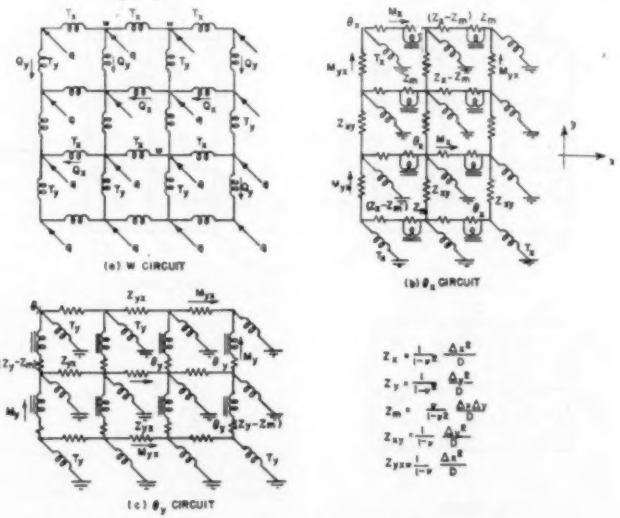

Fig. 4 Dynamic Analogy for Variable-Thickness Plate

Group 2

$$\frac{\partial w}{\partial n} = \theta_0 \quad \ldots\ldots [c]$$

$$M_n = M_0 \quad \ldots\ldots [d]$$

n is the co-ordinate normal to the edge, and t is the co-ordinate parallel to the edge. The combination [a], [c] gives the boundary conditions of a clamped edge, while the combination [a], [d] with $M_0 = 0$ refers to a simply supported edge. For an edge that is insufficiently clamped, a linear combination of [c] and [d] can be applied, in addition to [a]. The boundary conditions of a free or elastically supported edge are given by the combination [b], [d]. Along a line of symmetry the combination [b], [c] applies with R_0 and θ_0 equal to zero, and the further derivable condition that M_{tn}, the twisting moment, is equal to zero.

This grouping of the boundary conditions corresponds to the division into a deflection and slope circuits in the electrical analogy. The quantities involved in Group 1 are represented by the currents and voltages in the deflection network, while the quantities in Group 2 are analogous to the currents and voltages in the slope circuits. One may expect, therefore, that these conditions can be imposed on the network in a natural way.

Before examining in detail the manner in which these boundary conditions can be applied to the electrical analogy, we shall develop a general intuitive approach to the problem.

The boundary-condition equations as summarized are the consequences of constraints on the plate or of changes in its elastic properties. For instance, a free edge can be described completely by saying that there are no constraints on the edge, and that the stiffness and load equal zero beyond the edge. This type of physical description can be used directly in the derivation of an electrical analogy. In the variable-thickness analogy, the value of each impedance depends only on the local value of the stiffness constant. It may be expected, therefore, that for points one or two cells beyond a free edge, these impedances will vanish. A more precise expression of this idea leads to the correct analogy.

Up to this point the network impedances have been considered as lumped elements without attaching any particular geometrical significance to their location. For the discussion of boundary conditions the network impedances must be regarded as distributed elements. For example, along an edge where the slope θ_x is constrained to zero, all impedances in the θ_x-circuit should be grounded at the points where they cross the edge. A part of an impedance element is retained proportionally to the portion of its length interior to the plate. The transformer primaries of the deflection circuit should similarly be considered as distributed coils and grounded at the point where the coil crosses the edge. The part of the winding extending beyond the edge cannot be omitted. From the discussion of beams, the value of the transformer primary winding depends only on Δx, the cell size, and not on the elastic properties of the plate. If transformer primary windings are to be omitted for points beyond the edge, this must be deduced from the conditions on other parts of the network. The transformer secondary windings are intimately associated with the nodes of the slope circuits and cannot be distributed.

It has been said that the admittances in the slope circuits are proportional to the local values of the stiffness constant. To give precision to this statement, each impedance element will have assigned to it an element of area with sides Δx and Δy, centered at the mid-point of the element. The value of the admittance of the element will be calculated from the average value of the stiffness constant taken over this area. If this area is crossed by a free edge, for example, the admittance of the element will be proportional to the fraction of area interior to the plate.

The justification of this method of calculating impedances when sharp discontinuities are present rests on the verification of the resulting networks by means of the mathematical boundary conditions, and, when this is impossible, on the experimental results obtained from the network. A sharp distinction should be made between boundary conditions arising from constraints and boundary conditions arising from discontinuities in the elastic properties of the plate.

Boundary Conditions for a Rectangular Plate

The analogy developed in the section on Constant-Thickness Plate can be used only for a constant-thickness plate with a combination of simply supported and clamped edges. If the edge $x = \text{const}$ is clamped, the constraints require that $w = 0$ and $\theta_x = 0$ along the edge. As a consequence of the first condition θ_y also equals zero along this edge. These conditions can be imposed upon the network by grounding the deflection and slope networks where they cross the boundary, as discussed in the previous section. No difficulty is encountered in clamping an edge not parallel to a co-ordinate axis, since θ_x and θ_y must still be zero.

If the edge $x = \text{const}$ is simply supported, the mathematical boundary conditions are

$$w = 0$$

$$M_x = -D\left(\frac{\partial^2 w}{\partial x^2} + \nu\frac{\partial^2 w}{\partial y^2}\right) = 0 \quad \ldots\ldots [21]$$

As a consequence of the first condition $\partial w/\partial y = 0$ and $\partial^2 w/\partial y^2 = 0$ so that by the second condition $\partial^2 w/\partial x^2 = 0$ also. In the constant-thickness-plate analogy, the current in Z_x is proportional to $\partial^2 w/\partial x^2$. Consequently a Z_x-branch that crosses a simply supported edge is left open. The w and θ_x-circuits are grounded where they cross a simply supported edge. Fig. 5 shows the method of representing simply supported and clamped edges, when they coincide with nodes of the w-circuit.

Clamped and simply supported edges are represented in the variable-thickness analogy in exactly the same way. To represent a free edge, the analogy for a variable-thickness plate must be used, even though the plate may be uniform.

The physical conditions along a free edge are the absence of

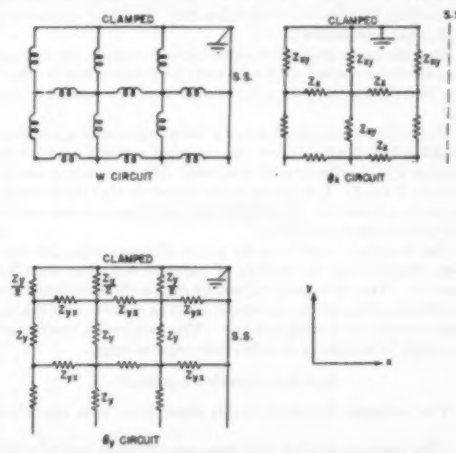

Fig. 5 Clamped and Simply Supported Edges for Constant-Thickness Plate

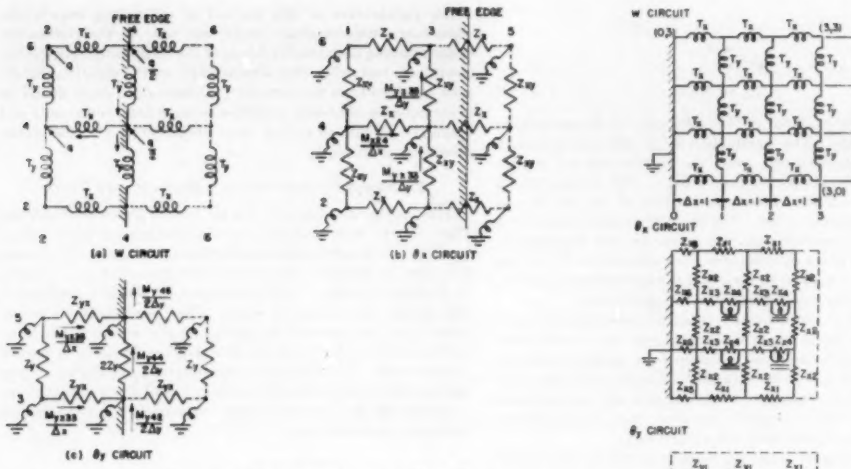

FIG. 6 VARIABLE-THICKNESS PLATE ANALOGY AND FREE EDGE

any constraints and the vanishing of the stiffness constant for points beyond the edge. Applying these conditions to the circuit in Fig. 6, we reason that $(Z_y)_5$, $(Z_x)_6$, $(Z_{xx})_6$, and $(Z_{xy})_5$ can be left out. The numerical subscripts refer to the value of x.

Since $(Z_{xx})_6$ and $(Z_y)_6$ are left out, there can be no current in the y-branches of the w-circuit along $x = 6$, and these branches can be left out. Since there is no load at $x = 6$, no current can flow in the x-branches of the w-circuit at $x = 5$. This means that no current flows into the nodes of the θ_x-circuit through the transformer secondaries. Consequently, no current flows in $(Z_x)_4$ and these impedances can be left out. Half of the area associated with $(Z_y)_4$ is beyond the edge, so that the impedance of these branches should be doubled. Furthermore, since there is no current in $(Z_x)_4$, the mutual impedance between the two circuits can be omitted. (This is not the same thing as omitting the mutual admittance, a condition that would be appropriate if $(Z_x)_4$ had been shorted.)

Since the load vanishes for points beyond the edge, the average load density is one half the load density for points inside the plate. The load currents for points on the edge should be reduced by one half.

The networks resulting from the foregoing reasoning are illustrated in Fig. 7 which shows the complete network used in the solution of a cantilever-plate problem. The impedances are defined in Table 1. It is shown in the Appendix that the free-edge network satisfies the finite-difference equivalent of the mathematical boundary conditions.

The boundary conditions for a free diagonal edge also have been obtained by the method of physical reasoning described here (5). They have been verified by means of the mathematical conditions, although the agreement is not as perfect as for the free edge parallel to a co-ordinate axis. This verification becomes exceedingly laborious for an arbitrarily oriented edge.

THE SOLUTION OF PROBLEMS[4]

The analogies described in this paper have been applied to the solution of a few problems on the Cal Tech electric-analog computer. At the present time this computer contains approximately 80 each of inductors, capacitors, and resistors, and 25 transformers. The only elements with imperfections that need to be considered are the transformers. In connection with an earlier study on beam-vibration analysis (1), it was shown that

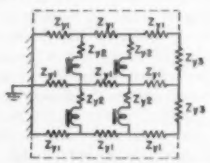

FIG. 7 NETWORK FOR SOLUTION OF RECTANGULAR CANTILEVER-PLATE PROBLEM

TABLE 1 DATA FOR ELECTRICAL ANALOGY OF RECTANGULAR CANTILEVER PLATE

$\Delta x = 1 \qquad \Delta y = 1 \qquad \nu = 0.30$

$D = 0.005$ for static loads
$D = 2.5$ for dynamic loads

$$Z_{x1} = \frac{2\,\Delta x^3}{D\,(1-\nu^2)} = \frac{2.25}{D}$$

$$Z_{x2} = \frac{\Delta y^3}{D\,(1-\nu)} = \frac{1.43}{D}$$

$$Z_{x3} = \frac{\Delta x^3}{D\,(1-\nu^2)} - \frac{\nu\,\Delta x \Delta y}{D\,(1-\nu^2)} = \frac{0.77}{D}$$

$$Z_{x4} = \frac{\nu\,\Delta x \Delta y}{D\,(1-\nu^2)} = \frac{0.33}{D}$$

$$Z_{x5} = \frac{\Delta x^3}{D\,(1-\nu^2)} = \frac{1.125}{D}$$

$$Z_{x6} = \frac{\Delta x^3}{2D} = \frac{0.50}{D}$$

$$Z_{y1} = \frac{\Delta x^3}{D\,(1-\nu)} = \frac{1.43}{D}$$

$$Z_{y2} = \frac{\Delta y^3}{D\,(1-\nu^2)} - \frac{\nu\,\Delta x \Delta y}{D\,(1-\nu^2)} = \frac{0.77}{D}$$

$$Z_{y3} = \frac{2\,\Delta y^3}{D\,(1-\nu^2)} = \frac{2.25}{D}$$

[4] The examples included here were investigated as part of a contract with the Air Materiel Command and are published with their permission.

the finite leakage and magnetizing impedances of the transformers can lead to appreciable errors in the determination of natural frequencies of vibration. This conclusion also holds for the elastic plate analogy.

With the 25 transformers available, it was possible to set up a plate with a maximum of twelve nodes and consequently only plates with simple shapes could be investigated. The following specimens, all of uniform thickness, were studied:

1 Rectangular plate—all edges simply supported.

2 Rectangular plate—all edges built-in.

3 Square plate, one edge built-in, three edges free (cantilever plate).

4 Cantilever plate swept back at an angle of 45 deg.

In each case influence coefficients were calculated for concentrated loads at each node; deflections and bending moments were measured for various distributed loads; and the normal modes of vibration for a uniform mass loading were determined. In this paper detailed results will be given only for the square cantilever plate, the other cases being of less general interest.

The cantilever plate and its electrical analogy are shown in Fig. 7. The co-ordinate system used in the tables of deflections, slopes, and moments is shown. Poisson's ratio for the plate is $\nu = 0.30$. The transformer secondary windings coupling the slope circuits with the deflection circuit are omitted for clarity, as are the load currents in the deflection circuit. In the slope circuits, Z_{x1}, Z_{x2}, Z_{x4}, Z_{y1}, and Z_{y2} are calculated from the formulas given in Fig. 4 for the general interior point; while the rest of the impedances, Z_{x1}, Z_{x3}, Z_{x5}, and Z_{y3} have special values because of their proximity to the edges of the plate. The values of all of the impedances are given in Table 1. Two values of the stiffness constant D are given in Table 1 because resistors were used in the slope impedances for static loads and inductors were used for dynamic loads. When the value of D for dynamic loads is inserted in the impedance formulas, the numerical value of these inductors is obtained.

Influence coefficients were calculated for the twelve nodes of the deflection circuit by inserting a constant alternating-current (10 ma) into each node in succession and measuring the voltages at all twelve points. The results are given in Table 2, in dimensionless form.

TABLE 2 INFLUENCE COEFFICIENTS, k_{ij}, FOR A SQUARE CANTILEVER PLATE

$$w_i = k_{ij}\frac{Pja^2}{D}$$

Load applied / Deflection measured at	(1, 0)	(2, 0)	(3, 0)	(1, 1)	(2, 1	(3, 1)	(3, 2)
(1, 0)	0.051	0.073	0.091	0.024	0.046	0.064	0.041
(2, 0)	0.073	0.197	0.280	0.048	0.135	0.215	0.157
(3, 0)	0.090	0.278	0.522	0.071	0.222	0.400	0.306
(1, 1)	0.024	0.048	0.072	0.027	0.046	0.067	0.050
(2, 1)	0.045	0.134	0.221	0.046	0.133	0.214	0.189
(3, 1)	0.064	0.214	0.400	0.067	0.212	0.400	0.350
(1, 2)	0.011	0.029	0.049	0.017	0.037	0.059	0.067
(2, 2)	0.026	0.089	0.164	0.037	0.111	0.189	0.213
(3, 2)	0.041	0.155	0.306	0.058	0.189	0.352	0.400
(1, 3)	0.002	0.011	0.024	0.011	0.029	0.041	0.064
(2, 3)	0.011	0.053	0.112	0.029	0.090	0.157	0.214
(3, 3)	0.023	0.111	0.237	0.049	0.164	0.306	0.400

Influence coefficients have been obtained for the square cantilever plate at the Defense Research Laboratory of the University of Texas both by direct experiment and by analytical calculation (6). Fig. 8 presents a comparison of the analog-computer solution with experimental results for a concentrated corner load.

In Table 3 results are given for a uniformly distributed edge load. Currents in the slope circuits corresponding to the bending moments were measured in this case. The twisting moment can be measured in both circuits, thus providing a direct check on the network. Since the twisting moments are small for a uniform edge load, the percentage agreement between the two values is not particularly good. It will be noticed that all quantities that should be identical by reason of symmetry show good agreement.

For the determination of the normal modes of vibration, inductors were substituted for the resistors in the slope circuits and capacitors were connected from the nodes of the deflection circuit to ground, in order to represent the mass of each cell. A voltage source from a variable-frequency oscillator was then connected to one of the nodes of the deflection circuit and the frequency varied until the current fed into the network was a minimum. This resonance condition corresponds to a minimum force for a given deflection. The frequency of the oscillator was recorded and the voltages at the 12 nodes of the deflection circuit were measured. In this way the first five normal modes of vibration were determined, Fig. 9.

At the Defense Research Laboratory of the University of Texas, the normal mode frequencies for a square cantilever plate have

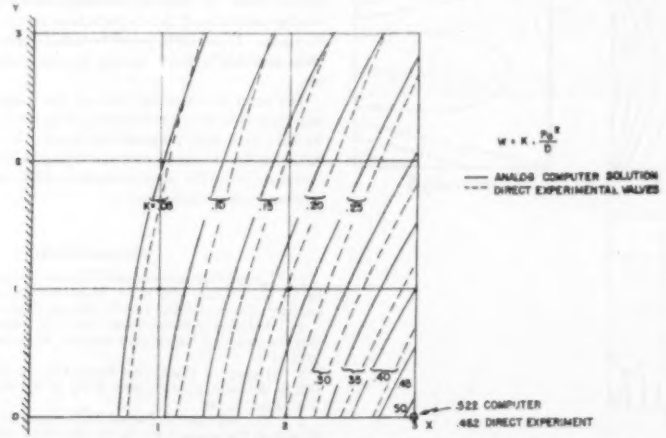

FIG. 8 CONSTANT INFLUENCE COEFFICIENT LINES FOR CONCENTRATED CORNER LOAD

TABLE 3 RESULTS FOR UNIFORM EDGE LOAD

$D = 0.500$ $\nu = 0.3$ $a = 3$

Loads — 1.000 were applied at (3,1) and (3,2)
Loads — 0.500 were applied at (3,0) and (3,3)

This represents uniform edge load equal to 1.000 per unit length of edge

Deflections and slopes

x	y	w	x	y	$\theta_x = \frac{\partial w}{\partial x}$	x	y	$\theta_y = \frac{\partial w}{\partial y}$
1	0	2.95	0.5	0	2.97	1	0.5	0.460
2	0	10.3	1.5	0	7.36	2	0.5	0.455
3	0	19.8	2.5	0	9.53	3	0.5	0.348
1	1	3.38	0.5	1	3.30	1	1.5	0.008
2	1	10.8	1.5	1	7.35	2	1.5	0.009
3	1	20.25	2.5	1	9.42	3	1.5	0.008
1	2	3.38	0.5	2	3.31	1	2.5	−0.454
2	2	10.8	1.5	2	7.35	2	2.5	−0.462
3	2	20.25	2.5	2	9.43	3	2.5	−0.353
1	3	2.95	0.5	3	2.96			
2	3	10.3	1.5	3	7.36			
3	3	19.9	2.5	3	9.52			

MOMENTS

Two values of twisting moments are given. They were measured independently in the network. Sign of the moments was not measured

Bending moments								Twisting moments M_{xy}	
x	y	M_x	M_y	x	y	M_x	M_y	x	y	measured in θ_x-circuit	measured in θ_y-circuit
0.25	0	2.614	0	0.25	2	3.35	0	0.5	0.5	0.119	0.159
1.00	0	1.964	0	1.00	2	2.05	0.43	1.5	0.5	0.022	0.009
2.00	0	0.986	0	2.00	2	1.016	0.104	2.5	0.5	0.045	0.040
0.25	1	3.24	0	0.25	3	2.614	0	0.5	1.5	0.004	0.004
1.00	1	2.07	0.420	1.00	3	1.960	0	1.5	1.5	0.002	0.001
2.00	1	1.014	0.102	2.00	3	0.992	0	2.5	1.5	0.001	0.003
3.00	0	0	0	3.00	2	0	0.154	0.5	2.5	0.122	0.154
3.00	1	0	0.154	3.00	3	0	0	1.5	2.5	0.023	0.006
								2.5	2.5	0.050	0.038

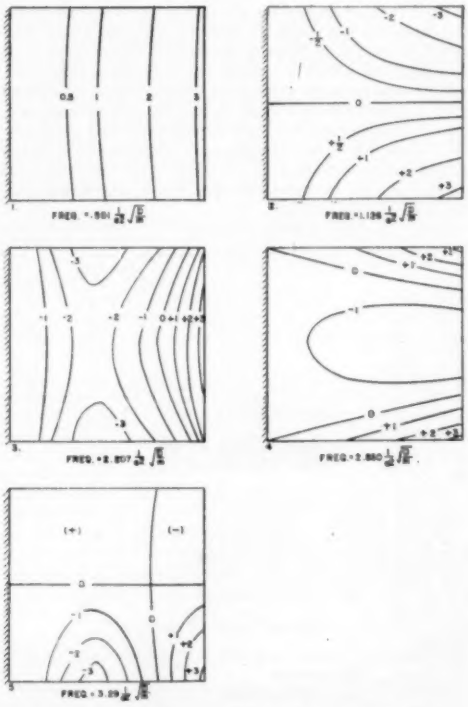

FIG. 9 NORMAL MODES OF SQUARE CANTILEVER PLATE

been measured experimentally for the two lowest modes and calculated theoretically for the five lowest modes (7). The frequency for the lowest mode as given by the analog computer is 8.2 per cent below the experimental value while the computer value for the second (torsional) mode is 17.2 per cent below the experimental value. The theoretical calculations for the higher modes indicate that the analog-computer values for these frequencies are even more in error. The mode-shape data are in considerably better agreement.

Errors in the normal mode frequencies are due primarily to the approximations inherent in the finite-difference method. The errors from this source are inversely proportional to the total number of cells in the network representation of the plate, and it is estimated that at least 10 times as many cells as were used in these tests would be necessary to reduce these errors to a satisfactory level. L. Brillouin (8) suggests methods by which quantitative estimates of the magnitude of errors from this source may be made. It should be possible to add a correction term based on these methods to the frequency measured on the analog computer.

The error in frequency due to the magnetizing and leakage impedances of the transformers can be eliminated by using transformers with high permeability cores. An experimental design indicates that the ratio of magnetizing to leakage inductance can be raised from the present value of 2500 to more than 100,000 without unreasonable expense.

BIBLIOGRAPHY

1 "Beam Vibration Analysis With the Electric-Analog Computer," by G. D. McCann and R. H. MacNeal, JOURNAL OF APPLIED MECHANICS, Trans. ASME, vol. 72, March, 1950, pp. 13–26.

2 "Analyses of Skew Slabs," by V. P. Jensen, University of Illinois, Engineering Experiment Station, Bulletin No. 332, September, 1941.

3 "Theory of Plates and Shells," by S. Timoshenko, McGraw-Hill Book Company, Inc., New York, N. Y., 1940, p. 88.

4 Ibid., p. 188.

5 "The Solution of Partial Differential Equations by Means of Electrical Networks," by R. H. MacNeal, PhD thesis, California Institute of Technology, Pasadena, Calif., 1949.

6 "Experimental Values of Deflection, Stresses and Influence Coefficients for a Thin Square Plate Fixed Along One Edge," by J. W. Dalley, Defense Research Laboratory Report No. 189, University of Texas, Austin, Texas, Nov. 5, 1948.

7 "Free Vibration Characteristics of Rectangular Cantilever Plates," by M. V. Barton, Defense Research Laboratory Report No. 212, University of Texas, Austin, Texas, May 24, 1949.

8 "Wave Propagation in Periodic Structures," by L. Brillouin, McGraw-Hill Book Company, Inc., New York, N. Y., 1946.

Appendix

Verification of Boundary Conditions for a Free Edge

Fig. 10 shows the location of the points where the moments are defined in the neighborhood of a boundary point (4,4). The quantities M_{x64}, M_{y055}, and M_{y056} are fictitious. By eliminating

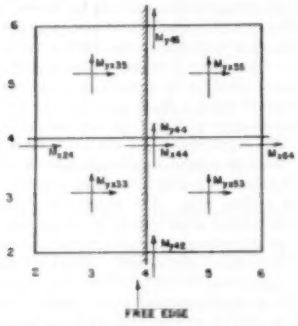

Fig. 10 Geometrical Distribution of Moments Near Free Edge

them from the boundary-condition equations, a single equation is obtained that the real moments must satisfy. In terms of the moments the differential equation is

$$\frac{\partial^2 M_x}{\partial x^2} + 2\frac{\partial^2 M_{xy}}{\partial x \partial y} + \frac{\partial^2 M_y}{\partial y^2} = q \quad \ldots\ldots [22]$$

and the boundary condition equations are

$$\left.\begin{aligned} M_x &= 0 \\ \frac{\partial M_x}{\partial x} + 2\frac{\partial M_{xy}}{\partial y} &= 0 \end{aligned}\right\} \text{ at } x = 4 \quad \ldots\ldots [23]$$

The finite-difference equivalent of Equation [22] is

$$\frac{M_{x64} - 2M_{x44} + M_{x24}}{\Delta x^2} + 2\frac{M_{y055} - M_{y053} + M_{y033} - M_{y035}}{\Delta x \Delta y} + \frac{M_{y06} - 2M_{y04} + M_{y02}}{\Delta y^2} = q_{44} \quad \ldots\ldots [24]$$

The finite-difference equivalents of Equation [23] are

$$M_{x44} = 0 \quad \ldots\ldots [25]$$

and

$$\frac{M_{x66} - M_{x26}}{2\Delta x} + \frac{M_{y056} + M_{y055} - M_{y033} - M_{y035}}{\Delta y} = 0 \quad \ldots\ldots [26]$$

Multiply Equation [26] by $2/\Delta x$, and subtract from Equation [24]. Then utilizing Equation [25]

$$\frac{M_{x24}}{\Delta x^2} + 2\frac{M_{y033} - M_{y035}}{\Delta x \Delta y} + \frac{M_{y06} - 2M_{y04} + M_{y02}}{2\ \Delta y^2} = q_{44} \quad \ldots\ldots [27]$$

It will now be shown that this equation is satisfied by the free-edge network. In Fig. 6 the currents in the slope circuits are written in terms of the moments. The dotted circuit elements are ficticious. In the θ_y-circuit the current in the branch (4,4) is one half of normal because, as shown earlier, the impedance of this branch must be doubled.

Referring to the w-circuit we see that

$$(i_T)_{24} + (i_T)_{42} - (i_T)_{43} = \frac{q_{44}}{2} \quad \ldots\ldots [28]$$

The currents in the transformer primaries are related to the moments as follows

$$(i_T)_{24} = \frac{1}{\Delta x}\left(\frac{M_{x24}}{\Delta x} + \frac{M_{y033}}{\Delta y} - \frac{M_{y035}}{\Delta y}\right) \quad \ldots\ldots [29]$$

$$(i_T)_{42} = \frac{1}{\Delta y}\left(\frac{M_{y02}}{2\Delta y} - \frac{M_{y04}}{2\Delta y} + \frac{M_{y033}}{\Delta x}\right) \quad \ldots\ldots [30]$$

$$(i_T)_{43} = \frac{1}{\Delta y}\left(\frac{-M_{y06}}{2\Delta y} + \frac{M_{y04}}{2\Delta y} + \frac{M_{y035}}{\Delta x}\right) \quad \ldots\ldots [31]$$

Substituting these terms into Equation [28] gives Equation [27] identically. Thus the network in Fig. 7 is verified.

The Dynamics of the Buckling of Elastic Columns[1]

By N. J. HOFF,[2] BROOKLYN, N. Y.

The motion of a perfectly elastic initially slightly curved column is calculated when one of its ends is displaced axially at a constant speed in a perfectly rigid testing machine. A nondimensional quantity Ω is defined which depends only upon the slenderness ratio of the column and the ratio of the velocity of the propagation of sound in its material to the speed of the testing machine. Two elastic columns are dynamically similar if Ω and the initial deviations from straightness are the same for both of them. The dynamic transverse deflections of the column lag behind the static values at the outset and overshoot them later. At an advanced stage of the loading the dynamic deflections can be represented as oscillations superimposed upon the static deflections. The axial compressive force in the column increases proportionately to the displacement of the loading head of the testing machine in the first phase of the loading. When the deflections become large, the compressive force increases at a reduced rate, reaches a maximum, and finally begins to oscillate about the Euler load. The maximum force recorded on the testing machine can be a multiple of the Euler load when Ω and the initial deviations from straightness are small. At ordinary speeds and with the usual inaccuracies of routine testing the maximum load should differ little from the Euler load.

Introduction

In the classical theory of elasticity the stability of an elastic body subjected to given constant loads is investigated through the device of assuming an infinitesimal disturbance in the geometry of the equilibrium configuration of the elastic body. When the cause of the disturbance is removed, the body resumes its original shape, possibly after some vibrations, provided the loads are smaller than their critical values. If these values are exceeded, deviations from the equilibrium configuration increase indefinitely. Consequently, in the limiting case, namely, when the critical loads are applied to the body there must exist patterns of deviations from the equilibrium shape which are neither increased nor decreased. This means that equilibrium is possible with deflected shapes differing from the original equilibrium configuration. The critical loads can therefore be found as the loads under which equilibrium can be maintained not only in the original configuration but also in configurations adjacent to it and differing from it only by infinitesimal quantities.

This approach to the problem of stability cannot be maintained for elastic systems that are nonlinear or for systems that develop permanent deformations through plasticity or creep under sufficiently large loads. It was suggested by the author at a Symposium on Engineering Structures held at Bristol University[3] that the stability of such systems be investigated by assuming a finite disturbance and following up the ensuing motion by means of the dynamic equations of motion. The concept of a static stability is thereby replaced by dynamic stability considerations. A system is stable if within a reasonable time it returns to a configuration satisfactorily close to the original configuration of equilibrium. The exact meaning of the words "reasonable" and "satisfactory" must be defined in each case individually.

A certain arbitrariness is thus introduced into the definition of the theoretical critical load. The experimental buckling load has always been defined in an equally arbitrary manner. With columns it is usually taken as the maximum load registered by the testing machine in a buckling test. There is no fundamental reason for the belief that the critical load of the classical theory and the maximum load measured in a buckling test should be identical. It is true, of course, that good agreement has been found between the Euler load and the maximum loads recorded in column tests carried out with elastic columns on commercial testing machines, and it is even possible to extend this range of correlation to columns failing at stresses exceeding the elastic limit. But the definition fails completely in the case of flat elastic plates subjected to edgewise compression which are known to carry loads amounting to multiples of the theoretical critical loads. This has led experimental investigators to defining the buckling load of plates on the basis of load-strain and load-deflection diagrams. There are a number of such definitions[4] in use today and the buckling loads obtained from them for the same test specimen differ considerably.

A column test is a dynamic process in which the column fails while the load is being increased. The classical buckling load is derived from considerations of the properties of the equilibrium under constant loads. Consequently, the conditions on which the theory of stability is based differ fundamentally from those under which buckling tests are undertaken, and there is no obvious connection between the experimental failing load and the theoretical buckling load. Better correlation between theory and experiment can be expected only if the buckling test itself is examined analytically.

In the present paper the behavior of an elastic column compressed in a commercial testing machine is calculated with the aid of the dynamic equations of motion. The testing machine is assumed to be perfectly rigid and its moving head descends with

[1] The investigation presented in this paper was carried out under contract with the Office of Naval Research of the U. S. Navy.

[2] Professor of Aeronautical Engineering, Polytechnic Institute of Brooklyn. Mem. ASME.

Presented at the Annual Conference of the Applied Mechanics Division, Purdue University, Lafayette, Ind., June 22–24, 1950, of The American Society of Mechanical Engineers.

Discussion of this paper should be addressed to the Secretary, ASME, 29 West 39th Street, New York, N. Y., and will be accepted until April 10, 1951, for publication at a later date. Discussion received after the closing date will be returned.

Note: Statements and opinions advanced in papers are to be understood as individual expressions of their authors and not those of the Society. Manuscript received by the Applied Mechanics Division, December 14, 1949. Paper No. 50—APM-23.

[3] "Dynamic Criteria of Buckling," by N. J. Hoff, Research, Engineering Structures Supplement, Butterworths Scientific Publications, Ltd., London, England, and Academic Press, Inc., New York, N. Y., 1949, p. 121.

[4] "The Development of a Technique for Testing Stiff Panels in Edgewise Compression," by N. J. Hoff, B. A. Boley, and J. M. Coan, Proceedings of the Society for Experimental Stress Analysis, Addison-Wesley Press, Inc., Cambridge, Mass., vol. 5, 1948, p. 14.

a uniform velocity. The column is of uniform cross section, and it has a slight initial curvature of sinusoidal shape. The ideally straight column can be approximated by decreasing arbitrarily the amplitude of the initial deviations from the straight line.

Basic Equations

If the element of a column, Fig. 1, bounded by two cross sections a distance dx apart is isolated, its equation of motion in the axial direction can be written in the form

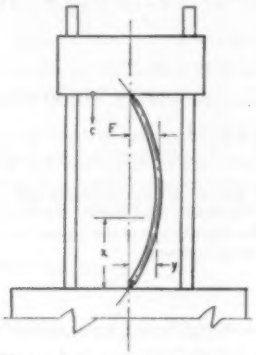

Fig. 1 Column in Testing Machine

$$(\partial^2 u/\partial t^2) = (E/\mu)(\partial^2 u/\partial x^2) \ldots\ldots\ldots\ldots\ldots [1]$$

where E is Young's modulus, μ the mass of a unit volume of the material, u the x-displacement of a section originally a distance x from the origin, and t is time.[5]

The transverse motion of the element is governed by the equation

$$EI(\partial^4 y/\partial x^4) + (\partial/\partial x)[P(\partial y/\partial x)] + \mu A(\partial^2 y/\partial t^2) = 0 \ldots [2]$$

where y is the transverse deflection, EI the bending rigidity, A the cross-sectional area, and P the compressive force in the particular section of the column.[6]

Since

$$P = -EA(\partial u/\partial x) \ldots\ldots\ldots\ldots\ldots\ldots\ldots [3]$$

Equations [1] and [2] are connected by Equation [3].

Solution of these simultaneous equations with prescribed boundary and initial conditions is difficult. Fortunately, changes in the end displacement of the column cause pressure waves to travel along the axis of the column with a velocity

$$a = (E/\mu)^{1/2} \ldots\ldots\ldots\ldots\ldots\ldots\ldots [4]$$

This amounts to about 200,000 ips for aluminum or steel. With a column of 20 in. length, a pressure wave travels from the moving head to the fixed platen and back again in 2×10^{-4} sec. The effect upon the lateral motion of the consequent variations in compressive force along the column is therefore negligible when the period or the duration of the lateral motion is large as compared to 2×10^{-4} sec. In such cases the transverse motion can be calculated from Equation [2] with no regard to Equation [1], and an average value, which is a function of time alone, can be assumed for P along the column.

[5] "The Theory of Sound," by Lord Rayleigh, first American edition, Dover Publications, New York, N. Y., vol. 1, 1945, p. 245.

[6] Ibid., p. 297.

Column With Slight Initial Curvature

When the column is slightly curved in its original natural state, the first term in Equation [2] must be replaced by the expression $EI[\partial^4(y - y_0)/\partial x^4]$, where y_0 stands for the initial and y for the total deflection. The other two terms are not changed by the initial curvature, but a suitable expression must be derived and substituted for P in the second term of the equation.

With a perfectly straight column in a perfectly rigid testing machine, the compressive load is a linear function of the displacement of the moving head. If this is descending with a uniform velocity c from the unloaded position, the strain is

$$-\epsilon_0 = ct/L$$

where L is the initial distance between the end points of the column. When the column is slightly bent at the outset, the bending increases as the moving head descends with a consequent relief in the compressive strain. The relief is equal to the difference between the end-point distances in the initial and final curved states divided by the initial distance

$$-\epsilon_1 = (1/2L)\int_0^L [(\partial y/\partial x)^2 - (\partial y_0/\partial x)^2]\,dx$$

The compressive force in the bar can, therefore, be written as

$$P = (EA/L)\left\{ct - (1/2)\int_0^L [(\partial y/\partial x)^2 - (\partial y_0/\partial x)^2]dx\right\} \ldots [5]$$

where EA is the rigidity of the column in compression. Equation [2] becomes

$$EI[\partial^4(y - y_0)/\partial x^4] + (EA/L)\left\{ct - (1/2)\int_0^L [(\partial y/\partial x)^2 - (\partial y_0/\partial x)^2]dx\right\}(\partial^2 y/\partial x^2) + \mu A(\partial^2 y/\partial t^2) = 0 \ldots\ldots [6]$$

In this investigation the rigidities EA and EI are considered constant, and the initial deflected shape is assumed as

$$y_0 = a \sin(\pi x/L) \ldots\ldots\ldots\ldots\ldots\ldots [7]$$

Substitution of this expression for y_0 in Equation [6] and the assumption

$$y = F \sin(\pi x/L) \ldots\ldots\ldots\ldots\ldots\ldots [8]$$

where F is a function of time alone, yield

$$\left\{EI(\pi/L)^4(F - a) - (EA/L)\left[ct - (L/4)(\pi/L)^2(F^2 - a^2)\right](\pi/L)^2 F + \mu A(\partial^2 F/\partial t^2)\right\} \sin(\pi x/L) = 0 \ldots\ldots [9]$$

As this equation must be satisfied identically for every value of x, the expression in braces must vanish. Use of the notation

$$\epsilon_E = \pi^2(\rho/L)^2 \qquad \Omega = \pi^2\epsilon_E{}^2(E/\mu c^2) \ldots\ldots [10]$$

$$\xi = (1/\epsilon_E)(ct/L)$$

$$F/\rho = f \qquad a/\rho = e$$

where ρ is the radius of gyration of the cross section, leads to

$$f'' + \Omega[(1 - \xi)f - e + (1/4)f^3 - (1/4)e^2 f] = 0 \ldots [11]$$

The primes denote differentiation with respect to the nondimensional time parameter ξ. The initial conditions are

$$f = e \quad df/dt = 0 = df/d\xi, \text{ when } t = 0 \ldots\ldots [12]$$

After similar transformations Equation [5] can be written as

$$P/P_E = \xi - (1/4)(f^2 - e^2) \ldots\ldots\ldots\ldots [13]$$

Motion Below Euler Displacement

When both the initial deviations from straightness and the total deflections are small, the terms containing f^3 and e^2f may be neglected in Equation [11]. One obtains

$$f'' + \Omega(1 - \xi)f = \Omega e \quad \ldots\ldots [14]$$

and if the new nondimensional time parameter

$$z = 1 - \xi \quad \ldots\ldots [14]$$

is introduced

$$f'' + \Omega z f = \Omega e \quad \ldots\ldots [15]$$

where the primes denote differentiation with respect to z. This is an inhomogeneous Bessel-type equation. Below the Euler displacement, $z > 0$, that is, as long as the shortening ct of the distance between the end points of the column caused by the motion of the head of the testing machine is smaller than the length L multiplied by the Euler strain ϵ_E, the complementary solution of differential Equation [13] is[7]

$$f_c = Af_{c1} + Bf_{c2} = Az^{1/2}J_{1/3}[(2/3)\Omega^{1/2}z^{3/2}] + Bz^{1/2}J_{-1/3}[(2/3)\Omega^{1/2}z^{3/2}] \quad \ldots\ldots [16]$$

where A and B are constants of integration, and J stands for the Bessel function. A particular solution is[8]

$$f_p(z) = (\Omega e/W)[f_{c2}(z)\int_0^z f_{c1}(s)ds - f_{c1}(z)\int_0^z f_{c2}(s)ds] \ldots [17]$$

with W the Wronskian of the two solutions

$$W = f_{c1}f_{c2}' - f_{c2}f_{c1}'$$

It can be shown[9] that the Wronskian of the two solutions of Equation [13] must be a constant

$$W = -1/[\Gamma(2/3)\Gamma(4/3)] = -3/[\Gamma(1/3)\Gamma(1 - 1/3)] = -(3/\pi)\sin(\pi/3) = -3\sqrt{3}/2\pi \quad \ldots\ldots [18]$$

The displacement is given by

$$f = Af_{c1} + Bf_{c2} + f_p \quad \ldots\ldots [19]$$

and the velocity is

$$v = -(c/L\epsilon_E)(df/dz) = -(c/L\epsilon_E)f' \quad \ldots\ldots [20]$$

It follows from Equation [17] that

$$df_p(z)/dz = (\Omega e/W)[f_{c1}'(z)\int_0^z f_{c2}(s)ds - f_{c2}'(z)\int_0^z f_{c1}(s)ds] \ldots [21]$$

where the prime indicates differentiation with respect to z. Moreover

$$f_{c1}' = \Omega^{1/2}zJ_{-1/3}[(2/3)\Omega^{1/2}z^{3/2}] \quad \ldots\ldots [22]$$

$$f_{c2}' = -\Omega^{1/2}zJ_{1/3}[(2/3)\Omega^{1/2}z^{3/2}] \quad \ldots\ldots [23]$$

Thus the initial conditions can be written in the form

$$AJ_{1/3}[(2/3)\Omega^{1/2}] + BJ_{-1/3}[(2/3)\Omega^{1/2}] = (2\pi/3\sqrt{3})\Omega e\left\{J_{-1/3}[(2/3)\Omega^{1/2}]\int_0^z s^{1/2}J_{1/3}[(2/3)\Omega^{1/2}s^{3/2}]ds - J_{1/3}[(2/3)\Omega^{1/2}]\int_0^z s^{1/2}J_{-1/3}[(2/3)\Omega^{1/2}s^{3/2}]ds\right\} + e = R_1 \ldots [24]$$

$$A\Omega^{1/2}J_{-1/3}[(2/3)\Omega^{1/2}] - B\Omega^{1/2}J_{1/3}[(2/3)\Omega^{1/2}] = -(2\pi/3\sqrt{3})\Omega^{1/2}e\left\{J_{1/3}[(2/3)\Omega^{1/2}]\int_0^z s^{1/2}J_{1/3}[(2/3)\Omega^{1/2}s^{3/2}]\,ds + J_{-1/3}[(2/3)\Omega^{1/2}]\int_0^z s^{1/2}J_{-1/3}[(2/3)\Omega^{1/2}s^{3/2}]ds\right\} = R_2 \ldots [25]$$

The denominator determinant of the equations is

$$D = -J_{1/3}\Omega^{1/2}J_{1/3} - J_{-1/3}\Omega^{1/2}J_{-1/3} = -3\sqrt{3}/(2\pi) \ldots [26]$$

Hence

$$A = \{+\Omega^{1/2}J_{1/3}[(2/3)\Omega^{1/2}]R_1 + J_{-1/3}[(2/3)\Omega^{1/2}]R_2\}\,[2\pi/(3\sqrt{3})] \ldots\ldots [27]$$

$$B = \{-J_{1/3}[(2/3)\Omega^{1/2}]R_2 + \Omega^{1/2}J_{-1/3}[(2/3)\Omega^{1/2}]R_1\}\,[2\pi/(3\sqrt{3})] \ldots\ldots [28]$$

Of particular interest are the deflection and velocity at the moment when the loading head reaches the Euler displacement, that is, when the displacement of the loading head is L times the Euler strain. At that moment

$$z = 0$$

and

$$f(0) = B3^{1/3}[\Omega^{-1/3}/\Gamma(2/3)] = 1.065\,\Omega^{-1/3}B \ldots\ldots [29]$$

$$v(0) = -(c/L\epsilon_E)\,A(1/3)^{1/3}[\Omega^{1/3}/\Gamma(4/3)] = -0.776(c/L\epsilon_E)\Omega^{1/3}A \quad \ldots\ldots [30]$$

As A and B are proportional to e and depend in a transcendental manner on Ω, the deflection and the velocity at the Euler displacement are also proportional to e. This is true only because the deflections were assumed small enough to neglect the nonlinear terms in e and f in Equation [11].

A numerical example was worked out, with slide-rule accuracy, to illustrate the theory. The buckling index Ω was chosen as 2.25 so as to obtain unity for the maximum value of the argument

$$\varphi_{max} = (2/3)\,\Omega^{1/2} = 1$$

Tables[10] yield the values

$$J_{-1/3}(1) = 0.18834 \qquad J_{-1/3}(1) = 0.60689$$
$$J_{1/3}(1) = 0.73088 \qquad J_{2/3}(1) = 0.59795$$

The integration was carried out with the aid of the series

$$\int s^{1/2}J_{1/3}[(2/3)\Omega^{1/2}s^{3/2}]ds = \Omega^{-1/2}\int J_{1/3}(\varphi)\,d\varphi = 2\Omega^{-1/2}\sum_{p=0}^{\infty} J_{(4/3)+2p}(\varphi) \ldots [31a]$$

$$\int s^{1/2}J_{-1/3}[(2/3)\Omega^{1/2}s^{3/2}]ds = \Omega^{-1/2}\int J_{-1/3}(\varphi)d\varphi = 2\Omega^{-1/2}\sum_{p=0}^{\infty} J_{(2/3)+2p}(\varphi) \ldots [31b]$$

with

$$\varphi = (2/3)\Omega^{1/2}s^{3/2}$$

and of the recursion formula

$$J_{n+1} = 2(n/\varphi)J_n - J_{n-1}$$

with $\varphi = 1$. Summations yield

[7] "Tables of Functions," by Eugen Jahnke and Fritz Emde, American edition, Dover Publications, New York, N. Y., 1943, p. 147.

[8] "Differential Equations," by L. R. Ford, McGraw-Hill Book Company, Inc., New York, N. Y., 1933, p. 76.

[9] "Applied Bessel Functions," by F. E. Relton, Blackie and Son, Ltd., London, England, and Glasgow, Scotland, 1946, p. 50.

[10] The Computation Laboratory of the National Applied Mathematics Laboratories, National Bureau of Standards, Tables of Bessel Functions of Fractional Order, Columbia University Press, New York, N. Y., 1949.

$$(1/2)\int_0^1 J_{-1/3}(\varphi)d\varphi \cong 0.635$$

$$(1/2)\int_0^1 J_{1/3}(\varphi)d\varphi \cong 0.309$$

With these values the right-side members of Equations [24] and [25] become

$$R_1 = 0 \qquad R_2 = -1.66e$$

Equations [27] and [28] yield

$$A = -1.21e \qquad B = 1.46e$$

Finally, Equations [29] and [30] become

$$f(0) = 1.36e \qquad v(0) = 1.08\,(ce/La_E)$$

Small Deflections Beyond Euler Displacement

When the time parameter ξ is greater than unity and both e and f are small as compared to unity, omission of the nonlinear terms from Equation [11] and introduction of the notation

$$\zeta = \xi - 1 \qquad [32]$$

result in the differential equation

$$f'' - \Omega\zeta f = \Omega e \qquad [33]$$

The solution of the homogeneous equation can be written as

$$f_c = A'f_{c1} + B'f_{c2} = A'\zeta^{1/2}I_{1/3}[(2/3)\Omega^{1/2}\zeta^{3/2}] + B'\zeta^{1/2}I_{-1/3}[(2/3)\Omega^{1/2}\zeta^{3/2}] \qquad [34]$$

where A' and B' are constants of integration, and I stands for the modified Bessel function. The differential coefficient of f_c with respect to ζ is

$$f_c' = A'f_{c1}' + B'f_{c2}' = A'\Omega^{1/2}\zeta I_{-2/3}[(2/3)\Omega^{1/2}\zeta^{3/2}] + B'\Omega^{1/2}\zeta I_{2/3}[(2/3)\Omega^{1/2}\zeta^{3/2}] \qquad [35]$$

At the Euler displacement, that is, when $\zeta = 0$, the values of the two independent solutions and of their derivatives are

$$\left.\begin{aligned} f_{c1} &= 0 & f_{c2} &= 3^{1/3}[\Omega^{-1/6}/\Gamma(2/3)] \\ f_{c1}' &= (1/3)^{1/3}[\Omega^{1/6}/\Gamma(4/3)] & f_{c2}' &= 0 \end{aligned}\right\} \qquad [36]$$

The particular solution can be given in the form

$$f_p(\zeta) = (\Omega e/W)\,[-f_{c1}(\zeta)\int_0^\zeta f_{c2}(s)ds + f_{c2}(\zeta)\int_0^\zeta f_{c1}(s)ds] \qquad [37]$$

where W is the Wronskian of the two solutions

$$W = f_{c1}f_{c2}' - f_{c2}f_{c1}'$$

As the Wronskian is a constant it can be calculated from the values of the functions and their derivatives at $\zeta = 0$, which are given in Equations [36]. One obtains

$$W = -1/[\Gamma(2/3)\Gamma(4/3)] \cong -0.828 \qquad [38]$$

The solution of the inhomogeneous differential equation is

$$f = A'f_{c1} + B'f_{c2} + f_p \qquad [39]$$

This represents the deflection of the mid-point of the column. Its velocity is

$$v = (c/La_E)\,(df/d\xi) = \sqrt{\Omega}\,(c/La_E)\,[A'f_{c1}' + B'f_{c2}' + f_p'] \qquad [40]$$

where

$$f_p'(\zeta) = (\Omega e/W)\,[-f_{c1}'(\zeta)\int_0^\zeta f_{c2}(s)ds + f_{c2}'(\zeta)\int_0^\zeta f_{c1}(s)ds] \qquad [41]$$

The constants of integration are determined from the initial conditions. It must be stipulated that the deflection and the velocity at $\zeta = 0$ be the same as those obtained earlier for $\xi = 0$. If the values are again denoted by $f(0)$ and $v(0)$ one has

$$\left.\begin{aligned} A' &= 3^{1/2}\Gamma(4/3)\Omega^{-1/6}(La_E/c)\,v(0) \\ B' &= (1/3)^{1/2}\Gamma(2/3)\Omega^{1/6}f(0) \end{aligned}\right\} \qquad [42]$$

These constants of integration can be expressed by means of the constants that obtain below the Euler displacement. Substitution in Equations [29] and [30] yields

$$A' = -A \qquad B' = B \qquad [43]$$

The solution is valid provided the nonlinear terms are small as compared to the linear ones in Equation [11]. One might stipulate, for instance, that the nonlinear terms should not amount to more than $2^1/_2$ per cent of the value of the linear ones. In the form of an equation

$$(1/4)f(f^3 - e^3)/(\zeta f + e) \leq 0.025 \qquad [44]$$

If the corresponding values of ζ and (f/e) are known from the solution, Equation [44] can be used to determine the eccentricity e that causes an error of $2^1/_2$ per cent. A form of Equation [44] suitable for such computations is

$$e^3 = (1/10)\,\frac{\zeta(f/e) + 1}{(f/e)\,[(f/e)^3 - 1]} \qquad [45]$$

When (f/e) and $\zeta(f/e)$ are large as compared to unity, the formula simplifies to

$$e^3 = (1/10)\zeta/(f/e)^3 \qquad [45a]$$

The numerical example of the preceding section was continued beyond the Euler displacement. With

$$A' = -A = 1.21e \qquad B' = B = 1.46e$$

graphical integration of the expressions contained in Equation [37] and substitutions yield the following simultaneous values

$$\zeta = 0.1 \quad f = 1.5e \quad f' = 1.326e$$

At this stage of the loading, the error caused by the omission of the nonlinear terms in Equation [11] amounts to $2^1/_2$ per cent if the amplitude of the original deviations from the straight-line shape is one quarter of the radius of gyration of the section. This can be ascertained by substituting the values in Equation [44]. Consequently, the modified Bessel function solution ceases to be valid at this stage of loading if $e = 0.25$. From this point on a new solution of Equation [11] is needed.

Solution by Power Series

When the deflection f is large, the terms containing f^3 and e^3f must not be disregarded in Equation [11]. As the expression in brackets in Equation [11] is an analytic function of ξ and f at all points except infinity, the solution is also analytic and can be represented by the convergent power series[11]

$$f = a_0 + a_1x + a_2x^2 + a_3x^3 + \cdots \qquad [46]$$

where

$$x = \xi - T \qquad [46a]$$

and $\xi = T$ is any point except infinity.

Substitution of f from Equation [46] into Equation [11] and the requirement that coefficients of each power of x vanish in the resulting equation yield the following expressions for a_2, a_3, and so on

[11] "Differential Equations," by L. R. Ford, McGraw-Hill Book Company, Inc., New York, N. Y., 1933, p. 183.

$$a_2 = (\Omega/2)\,[e - Ca_0 - (1/4)a_0^3] \quad [47a]$$

$$a_3 = (\Omega/6)\,[a_0 - Ca_1 - (3/4)a_0^2 a_1] \quad [47b]$$

$$a_4 = (\Omega/12)\,[a_1 - Ca_2 - (3/4)\,(a_0^2 a_2 + a_1^2 a_0)] \quad [47c]$$

$$a_5 = (\Omega/20)\,[a_2 - Ca_3 - (1/4)\,(a_1^3 + 3a_0^2 a_3 + 6a_0 a_1 a_2)] \quad [47d]$$

The nth coefficient is

$$a_n = [\Omega/n(n-1)]\,[a_{n-3} - Ca_{n-2} - (1/4)\sum_{i=0}^{n-2}\sum_{j=0}^{n-2} a_i a_j a_{n-2-i-j}] \quad [48]$$

In these equations

$$C = 1 - T - (1/4)e^2 \quad [49]$$

The values of the first two coefficients, namely, a_0 and a_1, must be determined from the initial conditions prevailing when $\xi = T$. At that time, from Equation [46]

$$f = a_0 \quad \text{and} \quad f' = a_1$$

Moreover, the velocity of the mid-point of the column is

$$v = (c/L_{\mathcal{E}})f'$$

If the deflection and the velocity of the mid-point are prescribed at $\xi = T$, the foregoing equations suffice to determine all the coefficients of the expansion.

The series solution is naturally valid for small as well as large values of f. It does not lend itself so easily to the drawing of general conclusions in regard to the motion of the column as do the Bessel-function solutions given earlier. For this reason, and because it usually converges slowly, the series solution should be used only in that realm of ξ where other solutions are not available.

The numerical example is now continued from the point where the Bessel function solution began to become inaccurate. For an eccentricity $e = 0.25$ the pertinent values are

$$\xi = 0.1 \quad \xi = T = 1.1 \quad f = 0.375 \quad f' = 0.3313$$

Consequently

$$a_0 = 0.375 \quad a_1 = 0.3313 \quad C = -0.115625$$

Evaluation of the coefficients given in Equations [47] and substitutions in Equation [46] yield

$$f = 0.375 + 0.3313x + 0.315x^2 + 0.142x^3 + 0.0569x^4 + 0.0280x^5 + 0.00467x^6 - 0.000800x^7 - 0.00111x^8 - 0.00102x^9 - 0.000560x^{10} - 0.000248x^{11} - 0.0000971x^{12} - \ldots$$

Differentiation gives

$$f' = 0.3313 + 0.630x + 0.426x^2 + 0.2276x^3 + 0.14x^4 + 0.02802x^5 - 0.005600x^6 - 0.00888x^7 - 0.00918x^8 - 0.00560x^9 - 0.002728x^{10} - 0.0011652x^{11} - \ldots$$

The series was used to calculate numerical values up to $\xi = 2.1$. Beyond this value of the independent variable the series was too slowly convergent and was replaced by new expansions. Altogether, four different values of T were used for successive expansions, until the following numerical values were obtained

$$\xi = 3.54 \qquad f = 3.25 \qquad f' = -2.0$$

Solution Based on Static Deflection Curve

It was observed that at large values of ξ the dynamic deflection curve can be represented as small oscillations superimposed upon the static deflections. With a vanishing acceleration Equation [11] can be solved for ξ

$$\xi = 1 - (e/f_0) + (1/4)f_0^2[1 - (e/f_0)^2] \quad [50]$$

where the subscript zero indicates that the solution corresponds to zero acceleration. When the expression

$$f = f_0 + \eta \quad [51]$$

where η is the small deviation of the dynamic displacement from the static value, is substituted in Equation [11], and Equation [50] is duly considered, the following equation is obtained

$$f_0'' + \eta'' + \Omega[(1 - \xi)\eta + (3/4)f_0^2\eta + (3/4)f_0\eta^2 + (1/4)\eta^3 - (1/4)e^2\eta] = 0 \quad [52]$$

Whenever the ratio of the nonlinear terms to the linear ones

$$E = [(3/4)f_0\eta + (1/4)\eta^2]/[1 - \xi + (3/4)f_0^2 - (1/4)e^2] \quad [53]$$

is small as compared to unity, Equation [52] can be written in the linearized form

$$\eta'' + \Omega[1 - (1/4)e^2 - \xi + (3/4)f_0^2]\eta = -f_0'' \quad [54]$$

In this equation the independent variable is ξ and the primes denote differentiation with respect to ξ. Since Equation [50] contains a convenient expression for ξ in terms of f_0, while no simple expression is available for f_0 in terms of ξ, f_0 is chosen as the new independent variable. With

$$d\eta/d\xi = (d\eta/df_0)\,(df_0/d\xi) \quad [55a]$$

$$d^2\eta/d\xi^2 = (d^2\eta/df_0^2)\,(df_0/d\xi)^2 + (d\eta/df_0)\,(d^2f_0/d\xi^2) \quad [55b]$$

$$df_0/d\xi = 2f_0^2/(f_0^2 + 2e) \quad [56a]$$

$$d^2f_0/d\xi^2 = -4f_0^2(f_0^2 - 4e)/(f_0^2 + 2e)^3 \quad [56b]$$

Equation [54] becomes

$$\eta'' - (1/f_0)\,[(f_0^2 - 4e)/(f_0^2 + 2e)]\eta' + (\Omega/8)\,(1/f_0^2)\,(f_0^2 + 2e)^2\eta = (1/f_0)\,(f_0^2 - 4e)/(f_0^2 + 2e) \quad [57]$$

where the independent variable is f_0 and the primes indicate differentiation with respect to f_0. When e is small as compared to f_0^2 Equation [57] can be written in the form

$$\eta'' - [(1/f_0) - (6e/f_0^4)]\eta' + (\Omega/8)\,[f_0^4 + 6fe]\eta = (1/f_0) - (6e/f_0^4) \quad [58]$$

Finally, when

$$(6e/f_0^2) << 1 \quad [59]$$

Equation [58] simplifies to

$$\eta'' - (1/f_0)\eta' + (\Omega/8)f_0^4\eta = (1/f_0) \quad [60]$$

where f_0 is the independent variable. This is a Bessel type differential equation whose solution can be written in the form

$$\eta = A\eta_{a1} + B\eta_{a2} + \eta_p \quad [61]$$

with the complementary solutions

$$\eta_{a1} = f_0 J_{1/3}[(1/3)\,(\Omega/8)^{1/2}f_0^3] \quad [62a]$$

$$\eta_{a2} = f_0 J_{-1/3}[(1/3)\,(\Omega/8)^{1/2}f_0^3] \quad [62b]$$

The particular solution is

$$\eta_p = -\eta_{a1}\int(\eta_{a2}/f_0 W)\,df_0 + \eta_{a2}\int(\eta_{a1}/f_0 W)df_0 \quad [63]$$

where W is the Wronskian of the two complementary solutions

$$W = \eta_{a1}\eta_{a2}' - \eta_{a2}\eta_{a1}'$$

Differentiation of Equations [62] yields

$$(d\eta_{a1}/df_0) = \eta_{a1}' = (\Omega/8)^{1/3} f_0^3 J_{-1/3}[(1/3)(\Omega/8)^{1/3} f_0^3] \ldots [64a]$$

$$(d\eta_{a2}/df_0) = \eta_{a2}' = -(\Omega/8)^{1/3} f_0^3 J_{1/3}[(1/3)(\Omega/8)^{1/3} f_0^3] \ldots [64b]$$

Substitution gives

$$W = -(3\sqrt{3}/\pi) f_0 \ldots [65]$$

Hence the particular solution becomes

$$\eta_p = [\pi/(3\sqrt{3})]\,[f_0 J_{1/3}[(1/3)(\Omega/8)^{1/3} f_0^3 \int (1/f_0) J_{-1/3}[(1/3)(\Omega/8)^{1/3} f_0^3]\,df_0 - f_0 J_{-1/3}[(1/3)(\Omega/8)^{1/3} f_0^3 \int (1/f_0) J_{1/3}[(1/3)(\Omega/8)^{1/3} f_0^3]\,df_0] \ldots [66]$$

The numerical example was continued from the stage of loading characterized by the values of ξ, f, and f' given at the end of the preceding section. Substitution in Equation [50] shows that the point represented by these values of ξ and f lies on the static deflection curve. Consequently $\eta = 0$. This is one of the initial conditions to be used in determining the constants of integration. The other is obtained from the rate of change of η with f_0

$$\left.\begin{aligned} d\eta/df_0 &= d(f - f_0)/df_0 = (df/df_0) - 1 \\ &= (df/d\xi)\,(d\xi/df_0) - 1 \end{aligned}\right\} \ldots [67]$$

From Equation [50]

$$d\xi/df_0 = (e/f_0^3) + (1/2) f_0 \ldots [68]$$

The numerical values obtained at the end of the preceding section were

$$\xi = 3.54 \quad f_0 = f = 3.25 \quad (df/d\xi) = -2.0$$

Substitution in Equation [68] yields

$$d\xi/df_0 = 1.65$$

Hence

$$d\eta/df_0 = -4.3$$

With $(1/3)(\Omega/8)^{1/3} = 0.177$ and $f_0 = 3.25$, the argument of the Bessel functions is 6.07 at the transition from the power-series solution to the Bessel-function solution. Tables of Bessel functions give the values

$$J_{1/3}(6.07) = 0.01207 \quad J_{-1/3}(6.07) = 0.286$$

$$J_{-1/3}(6.07) = 0.3236 \quad J_{1/3}(6.07) = -0.1437$$

With these values one obtains

$$\eta_{a1} = 0.0392 \quad \eta_{a2} = 0.929$$

$$\eta_{a1}' = 5.87 \quad \eta_{a2}' = 2.61$$

Thus the initial conditions are

$$0.0392\,A + 0.929\,B = 0$$

$$5.87\,A + 2.61\,B = -4.3$$

The solution of these two simultaneous equations is

$$A = -0.747 \quad B = 0.0307$$

Again, graphic integration had to be carried out to obtain the particular solution. Its contribution to the total deflections was found to be negligibly small. This is due in part to the fact that in the integrands of the particular solution the Bessel functions are divided by f_0 while the complementary solutions are multiplied by f_0, and the values of f_0 range from 3.25 to 5.0. Inequality [59] is satisfied by the solution. On the other hand, E in Equation [53] is not very small in the neighborhood of $f_0 = 3.25$. In that vicinity, therefore, the solution is only a first approximation. Nevertheless it fully represents the important features of the motion of the column. With a smaller speed of loading the approximation would be good throughout.

Discussion of Results

The deflections of the mid-point of the column calculated in the numerical example are shown in Fig. 2. Fig. 3 represents the variation of the axial load as computed from Equation [13]. The behavior of an elastic column during a compression test can be discussed with the aid of these graphs on the basis of the equations derived in the preceding sections.

Two perfectly elastic columns are dynamically similar when compressed in a rigid testing machine whose moving head is displaced at a constant speed if the nondimensional buckling index Ω is the same for both. This requirement is sufficient only when the displacements are small. For dynamic similarity at large displacements, the initial deviation from straightness must also be the same. The buckling index, as defined in Equations [10], is proportional to the square of the velocity a of the propagation of sound in the material of the column, as can be seen from a comparison of Equations [10] with Equation [4]. It is inversely proportional to the sixth power of the slenderness ratio of the column and to the square of the velocity of the loading head

$$\Omega = \pi^2 (a/c)^2 (\rho/L)^6 \ldots [69]$$

The equation shows that the value chosen for Ω in the numerical example, namely, 2.25, can be realized if a 10-in-long column of $^3/_{32}$-in. × $^3/_{32}$-in. rectangular cross section, whose slenderness ratio is 370, is compressed with a loading velocity of 0.256 ips. The validity of the theory can be checked by taking the square root of each member of Equation [69]

$$\Omega^{1/2} = \pi^4 (a/c)\,(\rho/L)^3 = 2\pi^2 (\rho/L)\,(a\epsilon_E/2c)$$

Since $L\epsilon_E/c$ is the time necessary for the loading head to reach the Euler displacement, and $2L/a$ is the time required for a pressure wave to start from the moving head, arrive at the fixed platen, and return again through the column to the moving head, the ratio of the two quantities, $a\epsilon_E/2c$, is clearly the number N of round trips the pressure wave can make from the beginning of the loading until the Euler displacement is reached. Solution of the preceding equation for N yields

$$N = (1/2\pi^2)\,(L/\rho)\Omega^{1/2} \ldots [70]$$

With the values of the numerical example $N = 28$, and thus the assumption of a uniform axial force along the column appears to be warranted.

The numerical example represents the very rapid loading of a very slender column. A slenderness ratio of (1/4)370 = 92.5 and a loading-head velocity of (1/10)0.256 = 0.0256 ips would be more usual in a column test. In such a case Equations [69] and [70] would give $\Omega = 922{,}000$ and $N = 4560$.

In the first phase of the loading, before the moving head reaches the Euler displacement, the solution of the differential equation consists of Bessel functions with real argument. Consequently, the column must undergo oscillations. As the distance between consecutive zeros of the Bessel function is close to π, the number of oscillations is the range of the argument divided by π. Consequently, the total number n of oscillations from the beginning of the loading until the Euler displacement is reached is

$$n \leqq (2/3\pi)\Omega^{1/2} \ldots [71]$$

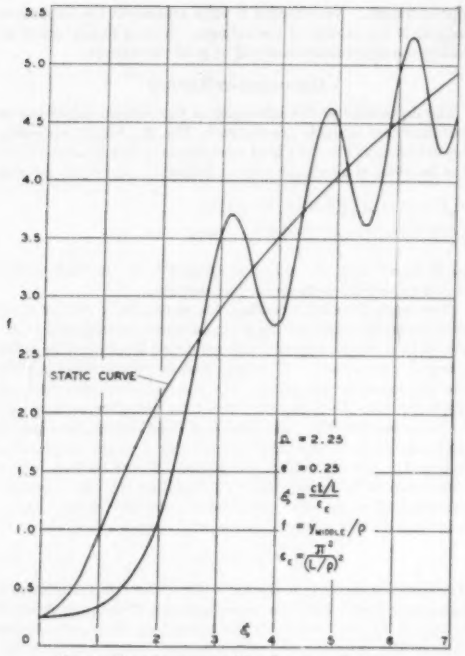

FIG. 2 DEFLECTIONS OF MID-POINT OF COLUMN

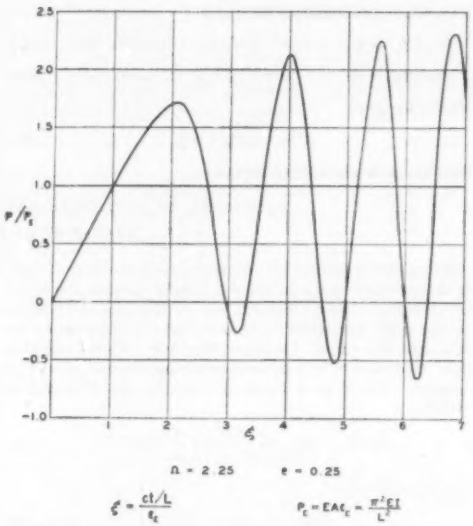

FIG. 3 VARIATION OF COMPRESSIVE FORCE IN COLUMN

In the numerical example $\Omega = 2.25$ and thus the plot of deflections does not show any vibrations. With the more usual arrangement for a column test represented by $\Omega = 922{,}000$, the total number of oscillations would be 204. Because of the small amplitudes, the oscillations would not be easily detected.

During a rapid loading the transverse motion of the elements of the column is retarded by the inertia of their masses. For this reason the dynamic deflections lag behind the values that correspond to infinitely slow loading. In the example, the dynamic deflection is 1.36ϵ at the Euler displacement while the static deflection is 4ϵ. The lag increases rapidly as the initial deviation from straightness decreases. For instance, at the Euler displacement the static deflection is 36ϵ when $\epsilon = 0.01$, as compared to the dynamic value of 1.36ϵ. The lag also increases with decreasing Ω.

Column tests are often interrupted for readings and adjustments. After the testing machine is stopped, the column eventually assumes its static-deflection position. When the loading is resumed, the column has to be accelerated from this deflected position and reaches the Euler displacement with less lag than in an uninterrupted loading.

Beyond the Euler displacement the solution is represented by modified Bessel functions, and the deflections increase monotonically. Depending upon the initial deflections and the value of Ω, the deflections sooner or later become so large that the small-deflection theory loses its validity. Up to this point the axial force in the column increases linearly since the nonlinear terms in Equation [13] are negligibly small. When Ω and ϵ are small, the axial force may well reach values which are multiples of the Euler load.

In the third phase of the loading, the deflections can be represented by power series in the nondimensional time parameter. In the first expansion of the numerical example the first negative coefficient is the ninth coefficient of the series, indicating that the monotonic increase in deflections represented by the modified Bessel function solution is continued for a while in this phase of the loading. At large values of the independent variable, the negative coefficients of the higher powers become effective and oscillations develop. The mass of the column is now accelerated sufficiently in the transverse direction to catch up with the static deflections. As a matter of fact, the inertia forces make the column overshoot the static deflections with a consequent drop in the compressive axial force below the Euler value.

The ensuing vibrations can be represented by Bessel functions of the static deflection superimposed upon the static deflection. In the numerical example the axial compressive force reaches the value $1.725P_E$ before it begins to decrease. The first minimum of the force is $-0.25P_E$ which is a tensile force. This cannot be realized in an ordinary column test but is feasible if the ends of the column are pivoted about pins rigidly attached to the testing machine. With lower speeds of loading the vibrations would be much less violent.

Evaluation of Stress Distribution in the Symmetrical Neck of Flat Tensile Bars[1]

By JULIUS ARONOFSKY,[2] DALLAS, TEXAS

The local strains and the strain distribution in the necks of two flat tensile specimens have been measured. A strain-hardening function for the material was obtained from the results of tension tests on round bars. This strain-hardening function and the measured strains are used to determine the stress distribution in the neck. Good agreement between the calculated and the measured fracture load was obtained.

Introduction

THE tension test has been used for many years as an important tool for evaluating the physical properties of metals. The tests usually are performed with round, flat, or tubular specimens, and the results are used to predict the strength of structural members under various conditions of combined stress. There are several phases of the tension test, however, that are not so well understood and which warrant further study. Local necking (previous to fracture) in the tension test of a round bar is a well-known phenomenon, but no rigorous theory has been offered as yet which explains this process (1–4).[3]

If a circular specimen of a ductile material is loaded in a testing machine, the tensile load will reach its maximum value at the instant that the uniform extension ceases. At this point the test piece will begin to neck, and the load on the specimen will decrease as the neck develops. The state of stress will change gradually from uniaxial tension to a complex condition of triaxial stress. Also the stress-strain relationship becomes much more complicated in the neck due to the rotation of the principal directions of both the stresses and strains. Some approximate solutions to the problem of stress analyses in the neck of round bars have been developed by the following investigators.

Siebel (5) developed an equation of equilibrium for the curved elements of material in the neck but did not consider the double curvature of the elements, and simplified his solution by considering it as a plane problem. Then Bridgman (6) arrived at more accurate conclusions by taking into consideration the double curvature of the material elements. More recently, Davidenkov and Spiridonova (7) developed a simple theory which is similar to Bridgman's theory but with more experimental justification. Most investigators determined only the distribution of the stresses in the minimum section of the neck; but the theory, when consequently developed, may permit the determination of stress distributions in the entire necked portion of the round bar. Some additional experimental work has been done by Parker, Davis, and Flanigan (8), and their results at least are in qualitative agreement with the theories of Bridgman, and Davidenkov and Spiridonova.

In this investigation, at the suggestion of Dr. Nadai, the more complex problem of analyzing the stresses in the neck of a flat bar was treated by making use of the information developed for the round bar and a knowledge of the strain distribution for the flat bar. The method applied herein assumes that (*a*) the flat bar deformed symmetrically around a section perpendicular to the axis of the bar; (*b*) the distribution of the permanent strains near the minimum section and the strain-hardening function for the metal have been determined from experiments; and (*c*) the ratios of width to thickness are not too small and not too large.

Theory for Computation of Stresses at Fracture for Round Bar

Before discussing the stress distribution in a flat bar, a brief description will be given of the method used for evaluating the stresses in the neck of a round tensile bar. The problem of determining the stress distribution in the neck is complex, as there is a triaxial stress condition with rotation of the principal axis. The following approximate theory has been developed by Davidenkov and Spiridonova (7) in which they describe the stress distribution on the minimum section of the neck of a round bar. They found experimentally that the radial strain $\bar{\epsilon}_r$, is equal to the tangential strain $\bar{\epsilon}_t$, and that both values are the same throughout the minimum section for a given stage of development of the neck. Let

δ_a = true principal stress in axial direction
δ_r = true principal stress in radial direction
δ_t = true principal stress in tangential direction
$\bar{\epsilon}_a, \bar{\epsilon}_r, \bar{\epsilon}_t$ = principal natural strains
τ_{oct} = octahedral shear stress
$\bar{\gamma}_{oct}$ = octahedral unit shear
r = radial distance in minimum section of neck
ρ = radius of curvature of longitudinal fiber element in neck
R = radius of curvature of contour of neck
a = radius of minimum section
$\text{avg } \sigma_a$ = average true axial stress = $\dfrac{\text{load}}{A}$
A = area of minimum section

The principal natural strains in the minimum section are

$$\bar{\epsilon}_r = \bar{\epsilon}_t = -\frac{\bar{\epsilon}_a}{2} = \text{const} \quad \ldots\ldots\ldots\ldots [1]$$

One of the known laws of plasticity is expressed by

$$\frac{\delta_a - \delta_r}{\bar{\epsilon}_a - \bar{\epsilon}_r} = \frac{\delta_a - \delta_t}{\bar{\epsilon}_a - \bar{\epsilon}_t} = \frac{\delta_r - \delta_t}{\bar{\epsilon}_r - \bar{\epsilon}_t} = K(\text{const}) \quad \ldots\ldots [2]$$

Davidenkov and Spiridonova did not concern themselves with the validity of Equation [2]. They did point out that this equa-

---

[1] This work represents part of a thesis submitted to the University of Pittsburgh as part of the requirements for the degree of Doctor of Philosophy.

[2] Senior Research Engineer, Magnolia Petroleum Company; formerly, Westinghouse Research Laboratories, East Pittsburgh, Pa. Jun. ASME.

[3] Numbers in parentheses refer to the Bibliography at the end of the paper.

Contributed by the Applied Mechanics Division and presented at the Annual Meeting, New York, N. Y., November 26–December 2, 1950, of The American Society of Mechanical Engineers.

Discussion of this paper should be addressed to the Secretary, ASME, 29 West 39th Street, New York, N. Y., and will be accepted until April 10, 1951, for publication at a later date. Discussion received after the closing date will be returned.

Note: Statements and opinions advanced in papers are to be understood as individual expressions of their authors and not those of the Society. Manuscript received by the Applied Mechanics Division, March 15, 1950. Paper No. 50—A-14.

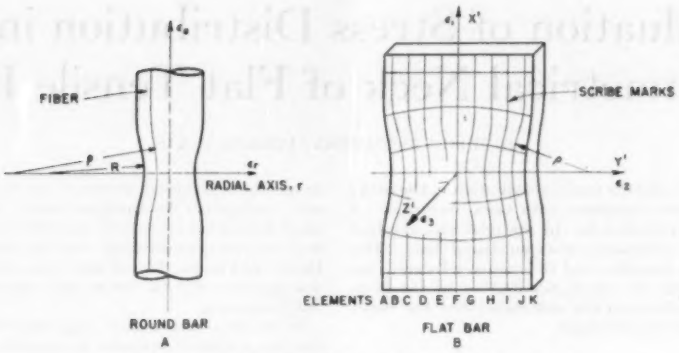

FIG. 1 SCHEMATIC VIEW OF NECK OF ROUND AND FLAT BARS

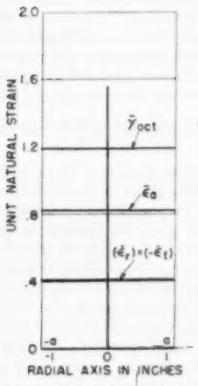

FIG. 2 STRAIN DISTRIBUTION IN NECK OF ROUND BAR NO. 11

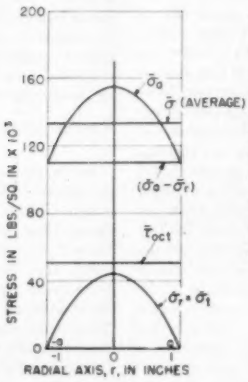

FIG. 3 STRESS DISTRIBUTION IN NECK OF ROUND BAR NO. 11

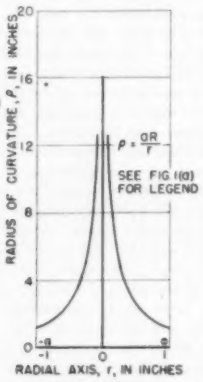

FIG. 4 CHANGE IN RADIUS OF CURVATURE IN NECK OF ROUND BAR NO. 11

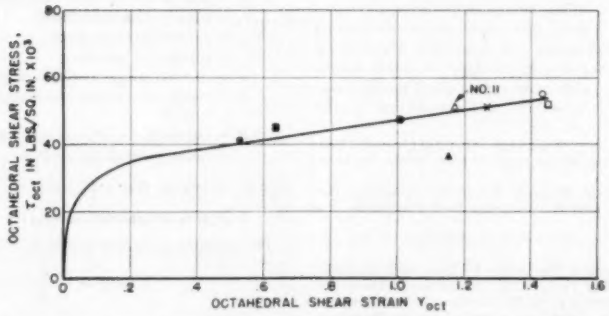

FIG. 5 OCTAHEDRAL SHEAR STRESS VERSUS OCTAHEDRAL SHEAR STRAIN FOR ROUND-BAR SERIES

tion has not been proved experimentally as being fully accurate (9). They justified their use of this flow condition simply by assuming it can be employed at least as a first approximation. The restrictions of the validity of this flow condition for flat bars will be discussed later.

Equations [3] and [4] follow from Equations [1] and [2]

$$\delta_r = \delta_t \quad [3]$$

$$S_0 = \delta_a - \delta_t = \text{const} \quad [4]$$

The equilibrium condition of the stresses in the axial direction in the neck is expressed by

$$\text{Axial load} = \int\int \delta_a \, dA \quad [5]$$

It is assumed that the curvature $1/\rho$ (of the principal stress trajectories of the stress σ_a) is proportional to the radius r, along the minimum section of the neck, Fig. 1(*A*)

$$\frac{1}{\rho} = \frac{r}{aR} \quad [6]$$

Davidenkov and Spiridonova checked this assumption experimentally by measuring the radius of curvature ρ of the fibers on an etched longitudinal section of the neck.

The radial equilibrium condition of an element in the neck is expressed by using as curvilinear co-ordinates the orthogonal system of the trajectories of principal stresses

$$\frac{d\delta_r}{dr} = \frac{\delta_a - \delta_r}{\rho} = \frac{S_0}{aR} \quad [7]$$

Integrating Equation [7] along the symmetry plane or in the minimum cross section leads to

$$\delta_a = S_0\left(1 + \frac{a^2 - r^2}{2Ra}\right) \quad [8]$$

which indicates how the axial stress δ_a varies along the minimum section of the neck with r.

The octahedral shear stress is

$$\bar{\tau}_{oct} = \frac{1}{3}\sqrt{(\delta_a - \delta_r)^2 + (\delta_r - \delta_t)^2 + (\delta_t - \delta_a)^2} = \frac{0.47\ (\text{avg}\ \delta_a)}{1 + \frac{a}{4R}} \quad [9]$$

and the octahedral unit shear

$$\gamma_{oct} = \frac{2}{3}\sqrt{(\bar{\epsilon}_a - \bar{\epsilon}_r)^2 + (\bar{\epsilon}_r - \bar{\epsilon}_t)^2 + (\bar{\epsilon}_t - \bar{\epsilon}_a)^2} = \sqrt{2}\,\bar{\epsilon}_a \quad [10]$$

Equations [9] and [10] serve for calculating $\bar{\tau}_{oct}$ and γ_{oct} in the minimum section.

The foregoing equations were utilized for calculating the stress and strain distribution in the minimum section at fracture of round bar No. 11 which is from the same heat of steel as the flat bars. The data for bar No. 11 were taken from a paper by J. Miklowitz (10). The natural strain distribution along the minimum section for round bar No. 11 is shown in Fig. 2. As was stated in Equation [1], the strains are uniform along the minimum section. The distribution of stresses at fracture is given in Fig. 3. The stresses σ_a, σ_r, and σ_t have a parabolic form with a maximum at the center of the minimum section ($r = 0$), and δ_a is much larger than either δ_r or δ_t. Also $\bar{\tau}_{oct}$ is constant throughout the minimum section. In Fig. 4 the radius of curvature of the fibers ρ is plotted against the radial axis r of the minimum section. According to Equation [6], the radius of curvature ρ is expressed by a hyperbola in function of r with the smallest value of ρ at the boundary ($r = a$) and an infinite value at the center of the minimum section ($r = 0$).

Strain-Hardening Function

The strain-hardening function which connects the octahedral shearing stress $\bar{\tau}_{oct}$, with the octahedral unit shear, γ_{oct}, has been described by A. Nadai (11) and may be expressed by the following equations

$$\bar{\tau}_{oct} = F(\gamma_{oct}) \quad [11]$$

It is herewith assumed that (*a*) the elastic portions of the strains are small and can be neglected, (*b*) that the principal directions of stress coincide with the principal directions of strain in the minimum section of the neck, and (*c*) that the flow condition expressed by Equation [2] may be used. Several investigators (12) have shown experimentally that a ductile steel, under biaxial states of stress, will follow the strain-hardening function Equation [11] for various conditions of combined stress. The assumption is made, therefore, that the strain-hardening function which applies in elements of a bar in the minimum section of a round bar also will hold for the material elements in the minimum section of a flat bar. In Fig. 5 the octahedral shearing stress is plotted against the octahedral shearing strains for the round bar series previously described (10). The curve represented in Fig. 5 was used in analyzing the stresses in flat bars 6A and 10A.

Flat-Bar Theory

Description of Strain Measurements in Flat Bars. A series of flat-bar tension tests (13) was previously carried out in order to investigate the influence of size and shape of the specimen on the mode of yielding and fracture. The grid pattern used for strain measurements is shown in Figs. 1(*B*) and 13. It was put on the specimen mechanically with the use of a scriber. The strain distribution in the neck for specimens 6A and 10A was taken from the foregoing report and was utilized to evaluate the stress distribution in the minimum section at fracture. Let ϵ_1 denote the local conventional strain in the axial direction, ϵ_2 the strain in the lateral direction parallel to the width of the bar, and ϵ_3 the strain in the direction parallel to the thickness of the bar (see the schematic sketch in Fig. 1*B*). The strain in the axial direction ϵ_1 was calculated from ϵ_2 and ϵ_3 by use of the equation expressing the volume constancy

$$\epsilon_1 = \frac{1}{(1 + \epsilon_2)(1 + \epsilon_3)} - 1$$

The value for the local strain in the width direction is given by the relation

$$\epsilon = \frac{dy' - dy}{dy}$$

where dy' is the strained value of the original element dy. The strain ϵ_3 was calculated using the entire thickness of the bar as the element. This strain is given by $\epsilon_3 = (h - h_0)/h_0$, where h is the strained value of the original thickness h_0. The original dimensions of the two flat bars are as follows:

Specimen	6A	10A
Gage length, in.	22.50	37.50
Width (b_0), in.	4.50	7.50
Thickness (h_0), in.	0.75	0.75
Ratio $\left(\frac{b_0}{h_0}\right)$	6	10

The distribution of conventional strains in the minimum section for specimen 6A is given in Fig. 6. The plotted points are

at the intersection of the longitudinal elements with the minimum section of the neck.

Analysis of Stresses at Fracture in Two Flat Bars. The stress distribution in the flat bar can be evaluated by utilizing the foregoing information on the round-bar analysis.

Only the minimum section of the neck will be considered for evaluating stresses. The following assumptions are made:

1 Since the distorted grid pattern on both sides of the minimum section appears in first approximation as orthogonal, it is assumed that the principal directions have rotated to coincide with the grid lines. Obviously, the principal directions in the minimum section do not rotate due to symmetry.[4]

2 The general strain-hardening function determined from a tensile test made with a round bar also holds for the elements of a flat bar.

3 The principal stress in the thickness direction σ_3, is assumed to vanish throughout the thickness.[5]

A glance at Fig. 6 shows that the strains in the thickness direc-

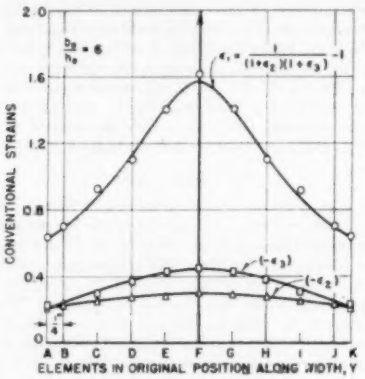

FIG. 6 VARIATION OF CONVENTIONAL STRAINS IN MINIMUM SECTION AT FRACTURE OF FLAT BAR 6A

tion ($\bar{\epsilon}_3$) are larger than the strains in the width direction ($\bar{\epsilon}_2$) in the minimum section. Hence, the symmetry of the strains in the round bar ($\bar{\epsilon}_r = \bar{\epsilon}_t$) does not hold for the flat bar, and a different method of analysis must be developed.

Symbols:

$\bar{\sigma}_1, \bar{\sigma}_2, \bar{\sigma}_3$ = true principal stresses
$\epsilon_1, \epsilon_2, \epsilon_3$ = principal conventional strains
$\bar{\epsilon}_1, \bar{\epsilon}_2, \bar{\epsilon}_3$ = principal natural strains
$\bar{\gamma}_{12}, \bar{\gamma}_{23}, \bar{\gamma}_{31}$ = principal natural unit shears
$\bar{\tau}_{12}, \bar{\tau}_{23}, \bar{\tau}_{31}$ = principal shear stresses

The logical approach to writing a relation between the stresses and strains is to start with the natural strain rates

$$\frac{\frac{d\bar{\epsilon}_1}{dt} - \frac{d\bar{\epsilon}_2}{dt}}{\bar{\sigma}_1 - \bar{\sigma}_2} = \frac{\frac{d\epsilon_2}{dt} - \frac{d\epsilon_3}{dt}}{\bar{\sigma}_2 - \bar{\sigma}_3} = \frac{\frac{d\bar{\epsilon}_3}{dt} - \frac{d\bar{\epsilon}_1}{dt}}{\bar{\sigma}_3 - \bar{\sigma}_1} = K' \quad \ldots [12a]$$

This equation is a generalization of the flow condition which was proposed originally by Saint Venant in his theory of the plastic deformation of ductile metals (1871). In Saint Venant's theory the rates of strains were assumed to be infinitesimals. For a finite distortion we may presume logically that the true strain rates can be substituted for the former ones. Thus $(d\bar{\epsilon})/(dt)$ may be substituted for $(d\epsilon)/(dt)$ where $\bar{\epsilon}$ is $\bar{\epsilon} = \ln(1 + \epsilon)$.

Equation [12a] could be written in the form

$$\left.\begin{aligned} \frac{d\bar{\epsilon}_1}{dt} &= \frac{d\phi}{dt}\left[\bar{\sigma}_1 - \frac{\bar{\sigma}_2 + \bar{\sigma}_3}{2}\right] \\ \frac{d\bar{\epsilon}_2}{dt} &= \frac{d\phi}{dt}\left[\bar{\sigma}_2 - \frac{\bar{\sigma}_3 + \bar{\sigma}_1}{2}\right] \\ \frac{d\bar{\epsilon}_3}{dt} &= \frac{d\phi}{dt}\left[\bar{\sigma}_3 - \frac{\bar{\sigma}_1 + \bar{\sigma}_2}{2}\right] \end{aligned}\right\} \quad \ldots [12b]$$

or in the form

$$\left.\begin{aligned} d\bar{\epsilon}_1 &= d\phi\left[\bar{\sigma}_1 - \frac{\bar{\sigma}_2 + \bar{\sigma}_3}{2}\right] \\ d\bar{\epsilon}_2 &= d\phi\left[\bar{\sigma}_2 - \frac{\bar{\sigma}_3 + \bar{\sigma}_1}{2}\right] \\ d\bar{\epsilon}_3 &= d\phi\left[\bar{\sigma}_3 - \frac{\bar{\sigma}_1 + \bar{\sigma}_2}{2}\right] \end{aligned}\right\} \quad \ldots [12c]$$

where $d\bar{\epsilon}_1$, $d\bar{\epsilon}_2$, and $d\bar{\epsilon}_3$ are the increments of the principal natural strains. In a rigorous solution these relations would have to be integrated step by step.

The preceding equations can be integrated when the principal stresses $\bar{\sigma}_1$, $\bar{\sigma}_2$, $\bar{\sigma}_3$ change in such a manner that the ratios $\bar{\sigma}_2/\bar{\sigma}_1$, $\bar{\sigma}_3/\bar{\sigma}_1$ are kept constant during the increase of the stresses and strains. Equations [12c] then will integrate into

$$\left.\begin{aligned} \bar{\epsilon}_1 &= \phi\left[\bar{\sigma}_1 - \frac{\bar{\sigma}_2 + \bar{\sigma}_3}{2}\right] \\ \bar{\epsilon}_2 &= \phi\left[\bar{\sigma}_2 - \frac{\bar{\sigma}_3 + \bar{\sigma}_1}{2}\right] \\ \bar{\epsilon}_3 &= \phi\left[\bar{\sigma}_3 - \frac{\bar{\sigma}_1 + \bar{\sigma}_2}{2}\right] \end{aligned}\right\} \quad \ldots [12d]$$

where ϕ is a variable quantity, or in the form

$$\left.\begin{aligned} \bar{\gamma}_{12} &= (\bar{\epsilon}_1 - \bar{\epsilon}_2) = \frac{3}{2}\phi\,(\bar{\sigma}_1 - \bar{\sigma}_2) = 3\phi\,\bar{\tau}_{12} \\ \bar{\gamma}_{23} &= (\bar{\epsilon}_2 - \bar{\epsilon}_3) = \frac{3}{2}\phi\,(\bar{\sigma}_2 - \bar{\sigma}_3) = 3\phi\,\bar{\tau}_{23} \\ \bar{\gamma}_{31} &= (\bar{\epsilon}_3 - \bar{\epsilon}_1) = \frac{3}{2}\phi\,(\bar{\sigma}_3 - \bar{\sigma}_1) = 3\phi\,\bar{\tau}_{31} \end{aligned}\right\} \quad \ldots [13]$$

Although the condition that $\bar{\sigma}_2/\bar{\sigma}_1$ and $\bar{\sigma}_3/\bar{\sigma}_1$ remain constant is not satisfied in general in the material elements on both sides of the minimum cross section since the lateral components of stress develop quite gradually, in a first approximation, use of the Equations [12d] was made by assuming that they may express at least averaging conditions in a similar manner, as in the theory of partial yielding of bodies (heavy-walled cylinders) in which use of such relations was made with good results by several investigators. Let the octahedral shear stress be

$$\bar{\tau}_{oct} = \frac{2}{3}\sqrt{\bar{\tau}_{12}^2 + \bar{\tau}_{23}^2 + \bar{\tau}_{31}^2} \quad \ldots [14]$$

[4] The first crack starts at the center of the minimum section and then propagates along it. During the formation of the rupture surface, the elements of the bar adjoining it deform plastically. This additional permanent distortion is not considered.

[5] The size and effect of σ_3 is assumed to be negligible, because it is known that σ_3 must be zero at the surfaces, and because the thickness of the model is small in comparison to the other dimensions

and the octahedral shearing strain

$$\gamma_{oct} = \frac{2}{3}\sqrt{\gamma_{12}^2 + \gamma_{23}^2 + \gamma_{31}^2} \quad \ldots\ldots [15]$$

In accordance with what has just been stated, from Equations [13], [14], and [15]

$$\gamma_{oct} = 3\phi\tau_{oct}; \text{ or } \phi = \frac{\gamma_{oct}}{3\tau_{oct}} \quad \ldots\ldots [16]$$

From Equations [16] and [13]

$$\left.\begin{aligned} \gamma_{12} &= \frac{1}{2}\frac{\gamma_{oct}}{\tau_{oct}}(\sigma_1 - \sigma_2) \\ \gamma_{23} &= \frac{1}{2}\frac{\gamma_{oct}}{\tau_{oct}}(\sigma_2 - \sigma_3) \\ \gamma_{31} &= \frac{1}{2}\frac{\gamma_{oct}}{\tau_{oct}}(\sigma_3 - \sigma_1) \end{aligned}\right\} \quad \ldots\ldots [17]$$

Rewriting Equations [17] and neglecting σ_2

$$\left.\begin{aligned} \sigma_1 &= -2\frac{\tau_{oct}}{\gamma_{oct}}\gamma_{31} \\ \sigma_2 &= -2\frac{\tau_{oct}}{\gamma_{oct}}\gamma_{23} \\ \sigma_3 &= 0 \end{aligned}\right\} \quad \ldots\ldots [18]$$

Thus the stress distribution in the minimum section can be evaluated from Equations [18].

Fig. 7 shows the principal natural strains plotted as a function of the distorted co-ordinate of points along the minimum section y' for flat bar 6A. The plotted points are at the intersection of the distorted longitudinal elements with the minimum section (Fig. 13). The natural unit shears and the octahedral shearing strains are plotted against the y'-co-ordinate for bar 6A in Fig. 8. In Fig. 9 the octahedral shearing stress and the principal stresses are plotted against the y'-axis. The octahedral shearing stress was determined from the strain-hardening function in Fig. 5 and the normal stresses were calculated from Equations [18].

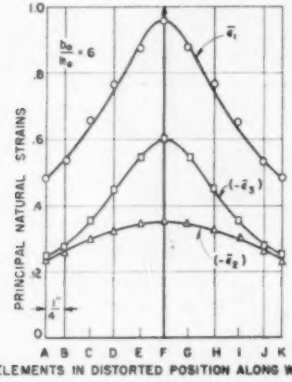

FIG. 7 VARIATION OF PRINCIPAL NATURAL STRAINS IN MINIMUM SECTION AT FRACTURE OF FLAT BAR 6A

The fracture load for bar 6A was calculated by evaluating graphically the integral

$$\text{Load} = \int\int \bar{\sigma}_1(y', z')dy'dz' \quad \ldots\ldots [19]$$

where y' and z' are the distorted co-ordinates of points in the width and thickness direction (see the schematic sketch in Fig. 1). The minimum cross section of the neck at fracture of specimen 6A was divided into 28 small increments of area (Fig. 9). The average load for each small area was calculated and then summed over the entire cross section. The calculated fracture load was 182,000 lb, whereas the observed fracture load in the testing machine was 178,000 lb. The calculated fracture load,

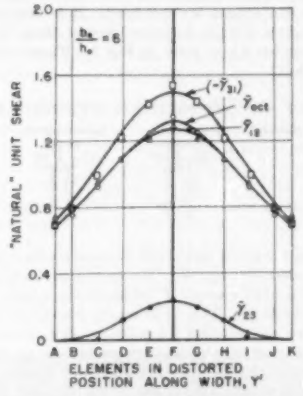

FIG. 8 VARIATION OF NATURAL UNIT SHEARS IN MINIMUM SECTION AT FRACTURE OF FLAT BAR 6A

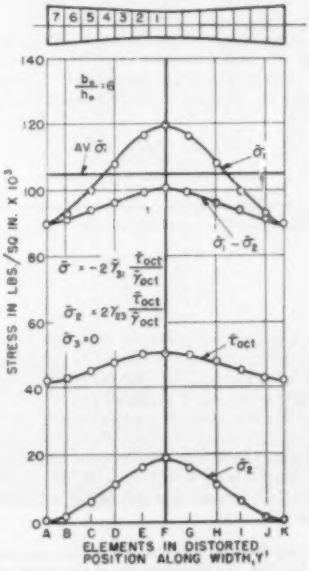

FIG. 9 DISTRIBUTION OF STRESSES IN MINIMUM SECTION AT FRACTURE OF FLAT BAR 6A

therefore, was 2.2 per cent higher than the observed fracture load for bar 6A.

The same procedure was used in computing the stress distribution for specimen 10A. The load at fracture again was calculated by integrating graphically Equation [19] from the curves in Fig. 10. The calculated fracture load was 278,000 lb, whereas the observed load was 302,000 lb. Therefore, the calculated fracture was 7.9 per cent lower than the observed fracture load for bar 10A.[4]

The basic restriction for the validity of Equations [12*d*] is that the ratio of the principal stresses σ_2/σ_1 will remain constant as the stresses and strains are increased. It is desirable then to check the values of σ_2/σ_1 for some element along the minimum section of flat bar 6A as given in Fig. 9. These data are compiled in Table 1.

TABLE 1 RATIO OF PRINCIPAL STRESSES IN BAR 6A

Longitudinal element, in.	Axial stress, σ_1, psi	Lateral stress, σ_2, psi	Ratio σ_2/σ_1
F	120×10^3	19.5×10^3	0.163
E	115.3	16.2	0.141
D	107.5	11.3	0.105
C	100.5	6.1	0.0606
B	92.8	1.5	0.0162
A	89.2	0	0

It is evident that the ratio σ_2/σ_1 remains constant only for the boundary elements *A* and *K*. The maximum deviation of σ_2/σ_1 occurs at the axial element *F* which changes from 0 to 0.163 as the neck develops. This deviation for element *F* is represented in Fig. 16 by constructing the plasticity ellipses for a material exhibiting strain-hardening and observing how far the point *F'* has drifted from the σ_1-axis. If the element *F* (axis of the bar) were subjected to pure axial tension, then the point *F* at fracture necessarily would be located on the σ_1-axis. The conclusion then is that Equations [12*d*] may be used as a first approximation, since the ratio σ_2/σ_1 remains practically constant.

Satisfying the Equilibrium Condition. Since the stress distributions in Figs. 9 and 10 were evaluated from the experimentally observed values of the strains, it is desirable to investigate whether the equilibrium equation of the stresses in the direction of the width of the bar has been satisfied. For an element of volume near the minimum section, the equilibrium equation is expressed by

$$\frac{d\sigma_2}{dy'} = \frac{\sigma_1 - \sigma_2}{\rho} \quad \ldots\ldots [20]$$

Where ρ is the radius of curvature of a longitudinal grid line (see Fig. 1*B*). Rewriting Equation [20], we get

$$\rho = \frac{\sigma_1 - \sigma_2}{\frac{d\sigma_2}{dy'}} \quad \ldots\ldots [21]$$

This equation can be used to calculate the value of the radius of curvature ρ (assuming that the stresses σ_1 and σ_2 were known), as given in Figs. 9 and 10. The calculated ρ then was compared with the radius of curvature measured from the photos in Figs. 13 and 14. For this purpose it was necessary to differentiate graphically the σ_2 curve (Figs. 9 and 10) to obtain values for the slope ($d\sigma_2/dy'$). The change in ρ along the minimum section at fracture for bar 6A is plotted in Fig. 11. Both the calculated values of ρ and the measured ρ are plotted along the minimum section at fracture.

[4] It is believed that due to the local distortion near the shear-type fractures in bar 10A, the measurements of the strains and measurements of the radii of curvatures were less exact than in the case of bar 6A in which the fracture surface was more sharply defined.

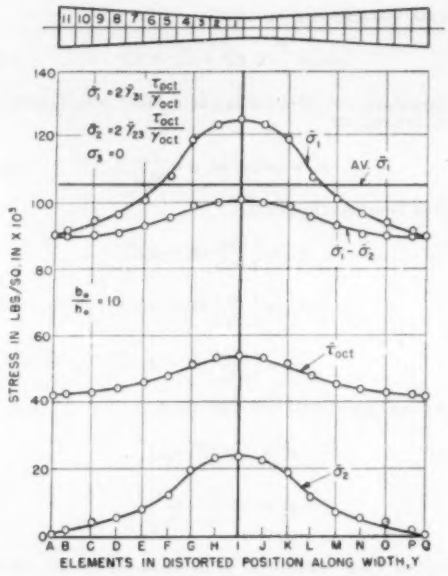

FIG. 10 DISTRIBUTION OF STRESS IN MINIMUM SECTION AT FRACTURE OF FLAT BAR 10A

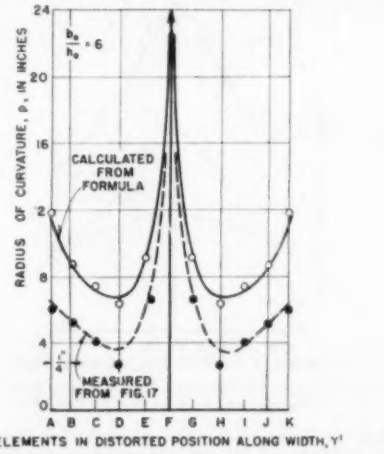

FIG. 11 CHANGE IN RADIUS OF CURVATURE ALONG MINIMUM SECTION AT FRACTURE OF FLAT BAR 6A

It is quite interesting to point out that the minimum value of the radius of curvature ρ is not obtained at the bar profile or the outer surface (as in the case of a round bar), but approximately halfway between the axis of the bar and outer surface in the width direction. In Fig. 12 the measured ρ is plotted along the minimum section for bar 10A at an intermediate stage of necking. The object of plotting ρ at an intermediate stage was to show that the minimum value of ρ again is approximately

halfway between the center axis of the bar and outer surface in the width direction.

Accuracy in Measuring ϵ and ρ. A glance at Fig. 11 shows that there is considerable difference in the calculated ρ and the ρ measured from the photographs. This difference probably is due to the difficulties in (*a*) measuring ρ from an enlarged photograph, and (*b*) calculating ρ from Equation [21], due to the graphical differentiation of the σ_x-curve.

The strain measurements, however, are comparatively accurate as they were made directly on the specimen with the aid of a scale divided in hundredths of an inch and by a micrometer. The accuracy of the strain measurements at fracture depends somewhat on the type of fracture. For instance, the fracture surface of bar 10A (Fig. 14) was irregular, due to the tearing action that separated the two halves of the bar which did not fit together after fracture, so that it was difficult to make the measurements. The stress distribution at an intermediate stage, therefore, would be more accurate than at fracture. It would have been desirable to calculate the stress distribution for bar 10A at the intermediate stage as shown in Fig. 15. The load at this intermediate stage was 315,000 lb as compared to the fracture load of 302,000 lb.

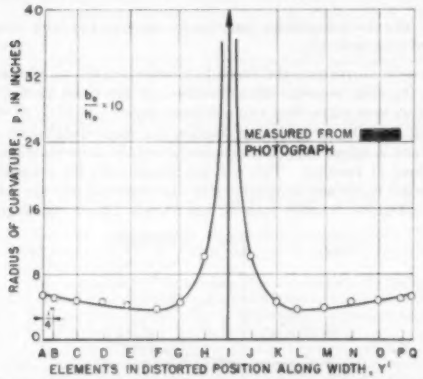

FIG. 12 CHANGE IN RADIUS OF CURVATURE ALONG MINIMUM SECTION AT INTERMEDIATE STAGE OF FLAT BAR 10A

COMPARISON OF ROUND AND FLAT BARS

A comparison is made of the stress distribution in the round and flat bars. The octahedral shear stress $\bar{\tau}_{oct}$, is constant along the minimum section of the round bar, Fig. 3, while $\bar{\tau}_{oct}$ varies along the minimum section of the flat bars. For both bars 6A and 10A, the maximum value of $\bar{\tau}_{oct}$ was found at the center of the minimum section ($y' = 0$). Furthermore, there appears an inflection point in the curves for the flat bars while there is no inflection point in the $\bar{\tau}_{oct}$-curve of the round bar.

The octahedral shear stress $\bar{\tau}_{oct}$ for the round bar is 51,600 psi, and the maximum $\bar{\tau}_{oct}$ for the flat bars 6A and 10A is 52,500 psi and 54,500 psi, respectively. The axial stress curve σ_a is repre-

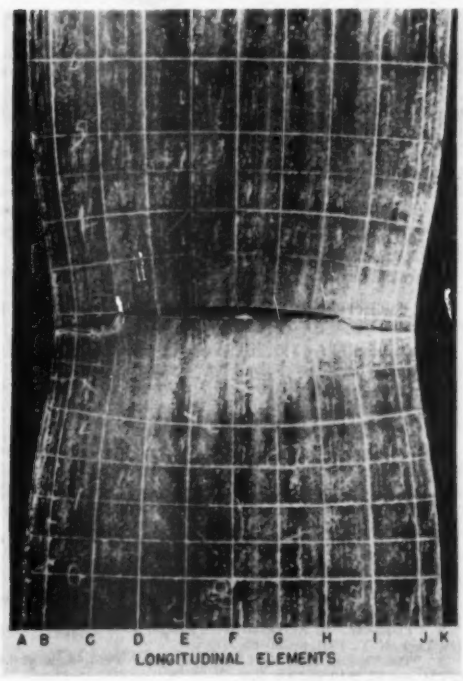

FIG. 13 ENLARGED PROFILE OF NECK AT FRACTURE OF FLAT BAR 6A

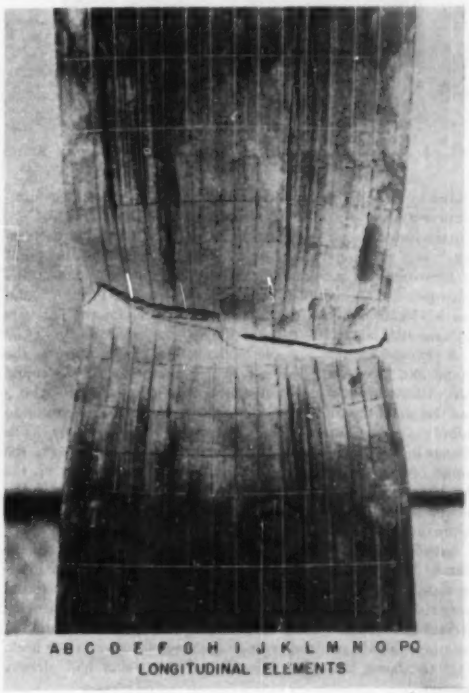

FIG. 14 ENLARGED PROFILE OF NECK AT FRACTURE OF FLAT BAR 10A

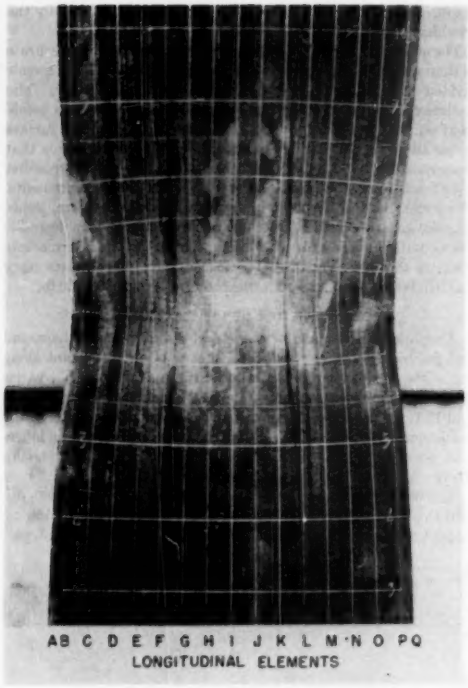

FIG. 15 ENLARGED PROFILE OF NECK AT INTERMEDIATE STAGE OF FLAT BAR 10A

sented by a parabola with a maximum at the center of the minimum section ($r = 0$) for the round bar. The flat bars also have a maximum axial stress ϑ_1 at the center ($y' = 0$) and a decreasing ϑ_1 as y' increases. The ϑ_1 curves also have an inflection point at approximately the same distance as the inflection point on the $\bar{\tau}_{oct}$-curve. The maximum axial tensile stress ϑ_a for the round bar is 155,500 psi, and the maximum stress σ_1 for the flat bars 6A and 10A is 120,500 psi and 125,800 psi, respectively.

A comparison also is made of the radius of curvature in the round and flat bars. The radius of curvature ρ for the round bar varies with the radial distance r as a hyperbola. Also ρ has the smallest value at the boundary ($r = a$) and increases to infinity at the center of the minimum section ($r = 0$). The change in the radius of curvature for the flat bars is similar to the round bar except that an analytic minimum of ρ occurs for the flat bar which is not located at the boundary. The dip in the ρ-curves and the inflection point in the stress curves occur at approximately the same distance along the y'-axis.

In order to show that the dip in the ρ-curve does not form at the instant when the fracture occurs, ρ was measured at an intermediate stage of necking before any cracks had yet formed and were visible (see Fig. 15 and the curve in Fig. 12). The necking process in wide flat bars is more complex than that in a round bar because a highly strained cross-shaped region forms in the neck. Fig. 15 shows that this cross-shaped depression had already formed.

CONCLUSIONS

The stress distribution in the minimum section at fracture has been analyzed for two flat bars having the ratios of width to thickness equal to 6 (bar 6A) and 10 (bar 10A). The method which was used may be applied for determining the stress distribution in the minimum section at any given stage prior to fracture during the necking of a flat bar provided:

1 Measurements are taken to determine the strain distribution.

2 The strain-hardening function for the steel has been determined experimentally.

In order to evaluate the stress distribution for the bars 6A and 10A, the data on strain measurements and the strain-hardening function were taken from two published papers (10, 13). It was shown that the method of evaluating the stress distribution in flat bars in a first approximation permitted the determination of the load at fracture. This was calculated from the stress-distribution curve and compared with the observed fracture load. The calculated fracture load for bar 6A was 2.2 per cent higher

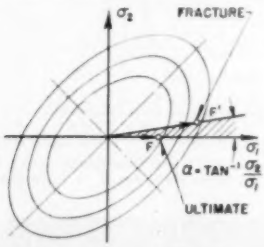

FIG. 16 PLASTICITY ELLIPSES FOR A STRAIN-HARDENING MATERIAL SHOWING HOW POINT F MOVES TO F' AT FRACTURE IN σ_1, σ_2 PLANE

than the observed fracture load, and the calculated load for bar 10A was 7.9 per cent lower than the observed fracture load.

Also the distribution of the axial and lateral principal stresses ϑ_1 and ϑ_2 could be computed in the minimum section of wide flat bars at fracture. The maximum values of axial stress for a 0.20 per cent C steel causing fracture were found to be as follows:

(*a*) In a round bar of 3 in. diam, max $\vartheta_a = 155{,}000$ psi
(*b*) In a flat bar of $b_0/h_0 = 6$, max $\vartheta_1 = 120{,}500$ psi
(*c*) In a flat bar of $b_0/h_0 = 10$, max $\vartheta_1 = 125{,}800$ psi

But the maximum value of octahedral shear stress causing fracture were as follows:

(*a*) In a round bar of 3 in. diam, max $\bar{\tau}_{oct} = 51{,}600$ psi.
(*b*) In a flat bar $b_0/h_0 = 6$, max $\bar{\tau}_{oct} = 52{,}500$ psi
(*c*) In a flat bar $b_0/h_0 = 10$, max $\bar{\tau}_{oct} = 54{,}500$ psi

ACKNOWLEDGMENT

Acknowledgment is due to Dr. Nadai for suggesting the undertaking of the work and for his guidance throughout the investigation. Acknowledgment also is given to the David Taylor Model Basin and to the Westinghouse Research Laboratories for permission to publish these results.

BIBLIOGRAPHY

1 "Elemente der Technologischen Mechanik," by P. Ludwik, Julius Springer, Berlin, Germany, 1909.
2 "Plasticity," by A. Nadai, McGraw-Hill Book Company, Inc., New York, N. Y., 1931, pp. 80–85.
3 "The Tension Test," by C. W. MacGregor, Proceedings of the ASTM, vol. 40, 1940, pp. 508–534.
4 "The True Stress-Strain Tension Test—Its Role in Modern Materials Testing," by C. W. MacGregor, *Journal of The Franklin Institute*, vol. 238, 1944, pp. 111–135, 159–176.

5 "Formänderungsfestigkeit und Spannungsverteilung im eingeschnürten Stabe," by E. Siebel, Werkstoffausschussbericht No. 71 des Verbandes deutscher Elektrotechniker Düsseldorf, *Stahl und Eisen*, 1925.

6 "The Stress Distribution at the Neck of a Tension Specimen," by P. W. Bridgman, Trans. ASM, vol. 42, 1944, pp. 553–572.

7 "Analysis of the State of Stress in the Neck of a Tension Test Specimen," by N. N. Davidenkov and N. I. Spiridonova, Proceedings of the ASTM, vol. 46, 1946, pp. 1147–1158.

8 "A Study of the Tension Test," by E. R. Parker, H. E. Davis, and A. E. Flanigan, Proceedings of the ASTM, vol. 46, 1946, pp. 1159–1174.

9 "Increase of Stress With Permanent Strain and Stress-Strain Relations in the Plastic State for Copper Under Combined Stresses," by E. A. Davis, *Journal of Applied Mechanics*, Trans. ASME, vol. 65, 1943, p. A-187.

10 "Influence of the Dimensional Factors on Mode of Yielding and Fracture in Medium-Carbon Steel—II, the Size of the Round Tensile Bar," by J. Miklowitz, *Journal of Applied Mechanics*, Trans. ASME, vol. 72, 1950, pp. 159–168.

11 "Plastic Behavior of Metals in the Strain-Hardening Range—Part I," by A. Nadai, *Journal of Applied Physics*, vol. 8, 1937, pp. 205–213.

12 "Yielding and Fracture of Medium-Carbon Steel Under Combined Stress," by E. A. Davis, *Journal of Applied Mechanics*, Trans. ASME, vol. 67, 1945, p. A-13.

13 "The Influence of the Dimensional Factors on the Mode of Yielding and Fracture in Medium-Carbon Steel—I, the Geometry and Size of the Flat Tensile Bar," by J. Miklowitz, *Journal of Applied Mechanics*, Trans. ASME, vol. 70, 1948, pp. 274–287.

14 "The Flow of Metals Under Various Stress Conditions," by A. Nadai, James Clayton Lecture, Proceedings of The Institution of Mechanical Engineers, London, England, vol. 157, 1947, pp. 121–160.

15 "Theory of Plates and Shells," by S. Timoshenko, McGraw-Hill Book Company, Inc., New York, N. Y., 1940, p. 359.

16 "Drang und Zwang—Part II," by A. Föppl and S. Föppl, J. Edwards, Ann Arbor, Mich., 1948, p. 4.

Appendix

Thin-Walled Tubular Specimen—An Ideal Tension Specimen for Studying the Strain-Hardening Function of a Metal

As the analysis of the distribution of the stresses after necking started in a solid round bar has shown, several assumptions had to be introduced for determining the radial and tangential stresses in the neck. As A. Nadai (14) remarked, some of these difficulties may be eliminated by using a hollow cylindrical specimen in a tension test instead of a solid round bar.

A thin-walled hollow cylinder may thus be considered an ideal tension specimen because the strain-hardening function $\tau_{oct} = F(\gamma_{oct})$ may be determined without resorting to superficial or arbitrary special assumptions.

Suppose that a series of snapshots is taken of the minimum section region to supply consecutive values of the radius of curvature ρ, and the outside radius a, at the minimum section (Fig. 20). The initial values are ρ', a' and the initial wall thickness h'.

Let ϑ_z, ϑ_r, and ϑ_t represent the principal stress directions as shown in Fig. 17. Assume that the radial stress ϑ_r and the bending stresses may be neglected for a thin-walled tube.

The static equations in the neck are

$$\left.\begin{aligned} \vartheta_r &= 0 \\ \frac{\vartheta_z}{\rho} + \frac{\vartheta_t}{a} &= 0 \end{aligned}\right\} \quad \ldots\ldots\ldots\ldots\ldots [29]$$

The latter equation is known as the membrane equation from the theory of thin curved shells and is derived in several textbooks (15).

From equilibrium condition

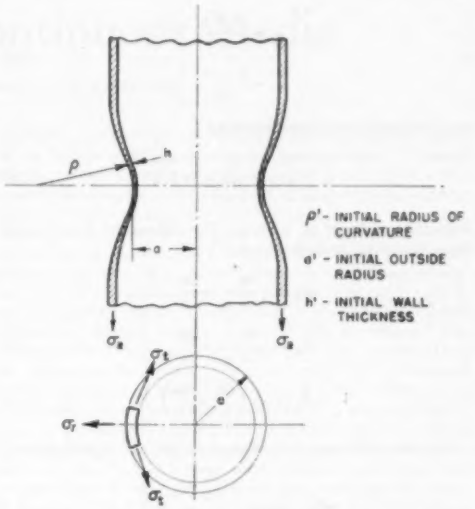

Fig. 17 Direction of Principal Stresses in Neck of Hollow Cylinder Under Tension Load

$$\vartheta_z = \frac{P}{2\pi a h} \quad \ldots\ldots\ldots\ldots\ldots [30]$$

where P is the tensile load. Equation [29] may be written in the form

$$\vartheta_t = -\frac{a}{\rho}\,\vartheta_z \quad \ldots\ldots\ldots\ldots\ldots [31]$$

where ρ is considered negative and a is positive for the saddle-type surface.

Equation [31] shows that in general the ratio of stresses ϑ_t/ϑ_z does not remain constant, so it is preferable to use the stress-strain relation in the differential form (14)

$$\left.\begin{aligned} di_z &= d\phi\left[\vartheta_z - \frac{\vartheta_r + \vartheta_t}{2}\right] \\ di_r &= d\phi\left[\vartheta_r - \frac{\vartheta_z + \vartheta_t}{2}\right] \\ di_t &= d\phi\left[\vartheta_t - \frac{\vartheta_z + \vartheta_r}{2}\right] \end{aligned}\right\} \quad \ldots\ldots\ldots [32]$$

where di_z, di_r, di_t are increments of principal natural strains.

Substituting Equation [31] in Equations [32]

$$\left.\begin{aligned} di_z &= \frac{d\phi}{2}\,[2 + a/\rho] \\ di_r &= \frac{d\phi}{2}\,[1 - a/\rho] \\ di_t &= -\frac{d\phi}{2}\,[2a/\rho + 1] \end{aligned}\right\} \quad \ldots\ldots\ldots [33]$$

The conventional strains are

$$\left.\begin{aligned} \epsilon_t &= \frac{a - a'}{a'} \\ \epsilon_r &= \frac{h - h'}{h'} \end{aligned}\right\} \quad \ldots\ldots [34]$$

and the natural strains are defined as

$$\left.\begin{aligned} \bar{\epsilon}_t &= \ln(1 + \epsilon_t) = \ln a/a' \\ \bar{\epsilon}_r &= \ln(1 + \epsilon_r) = \ln h/h' \\ \bar{\epsilon}_z &= -(\bar{\epsilon}_t + \bar{\epsilon}_r) \end{aligned}\right\} \quad \ldots\ldots [35]$$

from the constancy of volume. The differential strains come from differentiating Equations [35]

$$\left.\begin{aligned} d\bar{\epsilon}_t &= \frac{d\epsilon_t}{1 + \epsilon_t} = \frac{da}{a} \\ d\bar{\epsilon}_r &= \frac{d\epsilon_r}{1 + \epsilon_r} = \frac{dh}{h} \\ d\bar{\epsilon}_z &= -\left(\frac{da}{a} + \frac{dh}{h}\right) \end{aligned}\right\} \quad \ldots\ldots [36]$$

Equation [37] comes from Equations [36] and Equations [33]

$$\frac{d\bar{\epsilon}_t}{d\bar{\epsilon}_r} = \frac{da/a}{dh/h} = \frac{\left(2\frac{a}{\rho} - 1\right)}{\left(1 - \frac{a}{\rho}\right)} \quad \ldots\ldots [37]$$

which reduces to

$$\frac{dh}{h} = \frac{\rho - a}{2a + \rho} \cdot \frac{da}{a} \quad \ldots\ldots [38]$$

Integrating Equation [38], we have

$$\ln \frac{h}{h'} = \int_{a'}^{a} \frac{\rho - a}{2a + \rho} \cdot \frac{da}{a} \quad \ldots\ldots [39]$$

The thickness h can be determined by integrating Equation [39] graphically, since successive values of the radius of curvature ρ and the outside radius a are known from the series of snapshots.

Hence, from Equations [30] and [39], the state of stress is known up to the instant in which fracture occurs.

The octahedral shear stress and unit shear become

$$\bar{\tau}_{oct} = \frac{P}{2\pi ah} \frac{\sqrt{2}}{3} \sqrt{\left(\frac{a}{\rho}\right)^2 + \left(\frac{a}{\rho}\right) + 1} \quad \ldots\ldots [40]$$

and

$$\bar{\gamma}_{oct} = \frac{2}{3}\sqrt{\left[\ln\left(\frac{a'}{a}\right)^2 \frac{h'}{h}\right]^2 + \left[\ln \frac{a}{a'} \frac{h'}{h}\right]^2 + \left[\ln\left(\frac{h}{h'}\right)^2 \frac{a}{a'}\right]^2} \quad \ldots\ldots [41]$$

The strain-hardening function $\bar{\tau}_{oct} = F(\bar{\gamma}_{oct})$ can now be plotted from Equations [40] and [41], and could replace the curve in Fig. 5. It would be of interest to conduct a tubular tension test in this manner and compare the strain-hardening function of the tubular test with that of the solid circular test.

Shakedown in Continuous Media[1]

By P. S. SYMONDS,[2] CAMBRIDGE, ENGLAND

A new and simpler proof is given for a theorem due to Melan concerning the conditions under which an elastic-plastic body will "shake down" i.e., reach a residual stress state on which only elastic stresses are superimposed for all further variations of the surface loading stresses within limits prescribed at surface points. The theorem is applied to discuss the case of a circular bar subjected to an axial force and a torsional moment which vary independently between given limits. Relations to previous work on trusses and rigid frames are discussed briefly.

Introduction

PREVIOUS papers (1, 2, 3)[3] have dealt with methods for the analysis of elastic-plastic structures such as trusses and rigid frames. One important problem which was considered was that of determining whether a given structure, subjected to a set of "load components" each of which may be varied independently of the others between prescribed extreme values, will eventually shake down. By this term is meant that plastic flow ultimately ceases, and, in particular, in no part of the structure is there set up a cycle of plastic flow. If this were the case the material would be damaged severely after relatively few cycles, and the structure could not be considered "safe" under the given extreme values of the load components. This condition of shakedown, therefore, provides a criterion of failure which may be used in the analysis and design of structures subjected to several independent loads, and which may be considered as a more realistic basis for design than that of the conventional methods which assume failure to occur when a critical elastic stress is attained. It should be emphasized, however, that what is attempted is only to introduce a more realistic criterion of failure than that of elastic design methods; in many cases entirely different conditions, such as maximum deformations, or fatigue, are the controlling factors in design.

The typical structure considered in reference (1) was a plane pin-jointed truss with load components consisting of a set of independently variable forces applied to the pins. Considerable insight into the nature of the problem and suitable methods of attacking it was gained by the use of certain geometrical concepts. For a truss of n bars the state of stress could be represented by a point in an n-dimensional Euclidean space, the n rectangular Cartesian co-ordinates being proportional to the forces in the n bars. The sets of linear equations of equilibrium and of compatibility, together with the yield conditions,[4] govern the motion of the "stress point" as the external load is varied. Although the geometrical concepts are highly suggestive and afford a convenient terminology, in the analysis of particular trusses (of many bars) recourse must be had to algebraic methods.

In (1) a simple proof was given for a "shakedown theorem," stated first by Bleich (4) in a more restricted form, which could be made the basis for analysis of structures having any number of members. Applications of this theorem have been made in (2) and (3) to continuous beams and to rigid frames. Before stating the theorem certain terms will first be defined. The "elastic stresses" corresponding to any given set of external loads are defined as the stresses in the bars computed by standard elastic methods, i.e., assuming each bar to behave elastically at all stresses. (A set of elastic stresses is of course fictitious if some of the values fall outside the actual yield limits in tension or compression. In such a case certain bars flow plastically, and the actual set of stresses corresponding to the final load values depend on the yield values and also on the precise history of loading.) Now suppose, after bringing the load components to certain values (and producing a definite state of stress in the truss), all of the load components are reduced to zero in such a way that the stresses in all bars are maintained within their elastic ranges. This is defined as an "unloading process," and, in general, when it has been completed there will be a definite state of permanent deformation and a corresponding set of "residual stresses" in the bars. Obviously, from the definitions, the residual stresses, corresponding to any set of actual stresses produced by a given loading program, can be calculated by subtracting from the stress in each bar the elastic stress corresponding to the given final load value.

The definition of shakedown which was given earlier implies that the structure ultimately reaches a state of residual stresses such that all further changes of the load components, between their respective extreme values, produce only elastic changes of stresses and deformations. This will be termed a shakedown state of residual stress, or simply a "shakedown state." Now the essential content of the shakedown theorem is this: If any set of residual stresses can be found such that the addition of elastic stresses calculated for all possible load combinations results in stresses which do not violate the yield conditions, then the structure eventually will shake down. It will not, in general, shake down to a unique state independent of the loading program. However, the theorem shows that if any residual-stress state exists, satisfying the conditions of a shakedown state, the structure will find its way to some shakedown state. This theorem reduces the analysis of a particular structure under a system of load components with given extreme values to the investigation of a system of linear algebraic inequalities. If this system possesses at least one solution, then shakedown occurs; if there is no solution, then shakedown cannot occur. These systems of inequalities can be investigated without difficulty by the methods presented in (3).

[1] These results were obtained in course of research conducted under Contract N7onr-358 sponsored jointly by the Office of Naval Research and the Bureau of Ships, Navy Department.

[2] On leave from Brown University; now at Engineering Department, Cambridge University, England.

[3] Numbers in parentheses refer to the Bibliography at the end of the paper.

Contributed by the Applied Mechanics Division and presented at the Annual Meeting, New York, N. Y., November 26–December 1, 1950, of The American Society of Mechanical Engineers.

Discussion of this paper should be addressed to the Secretary, ASME, 29 West 39th Street, New York, N. Y., and will be accepted until April 10, 1951, for publication at a later date. Discussion received after the closing date will be returned.

Note: Statements and opinions advanced in papers are to be understood as individual expressions of their authors and not those of the Society. Manuscript received by the Applied Mechanics Division, September 2, 1949. Paper No. 50—A-17.

[4] The assumption of ideally plastic behavior was made in (1) and (2); each bar has a yield stress in tension and in compression, and flow continues indefinitely when the stress is held constant at either of these values. In (3), dealing especially with rigid frames, a more realistic moment-curvature relation was assumed, of the "limited strain-hardening" type.

Shakedown Theorem for Continuous Media

A typical problem of an elastic-plastic body which must be treated as a continuum rather than a structure is that of a bar subjected to an axial force and a twisting moment. If these two loads can vary independently between given limits, the question arises whether the bar will shake down to some state of residual stress, on which only elastic stresses are imposed thereafter, or whether plastic flow at some points may continue indefinitely, alternating in sign with suitable reversals of the loads.

The concepts of stress-space geometry can be extended to continuous media letting a state of stress (six functions of position throughout a given body) be represented by a point in an appropriate function-space. It is possible that the use of these geometrical concepts in the discussion of elastic-plastic bodies will prove to be of value similar to that in the case of purely elastic bodies (5), although there seems little hope of establishing approximation methods having anything like the simplicity of those which are available in theory of elasticity. Instead of pursuing this line of attack, the present paper will be concerned with a proof of the shakedown theorem for elastic-plastic bodies, and an application of this theorem to the problem of a bar under independently variable axial force and twisting moment.

The only paper previously published on problems of continuous media subjected to loading of the type considered here seems to be one of E. Melan (6). In Melan's paper a theorem of uniqueness of solution is proved as well as a theorem of shakedown. Melan's proofs made use of integral equations involving certain "influence functions" which relate the permanent strains to the residual stresses. No applications of the theorems were considered by Melan. The proof of the shakedown theorem to be given in the present paper is simpler and more direct than Melan's, and the application to the problem of a bar under simultaneous axial and torsional loads is apparently the first attempt to apply the theorem in a specific problem.

Let σ_{ij}, ϵ_{ij} denote the stress and strain components, respectively; the subscripts i, j take the values 1, 2, 3, and refer to the three co-ordinate axes. The "stress deviator" s_{ij} has components defined by

$$s_{ij} = \sigma_{ij} - \frac{1}{3}\,\delta_{ij}\,\sigma_{pp} \qquad [1]$$

where $\delta_{ij} = 1$ for $i = j$, and $\delta_{ij} = 0$ for $i \neq j$; and $\sigma_{pp} = \sigma_{11} + \sigma_{22} + \sigma_{33}$, using the summation convention on repeated suffixes.[6] Now the effect of changes in the external loads is to produce certain increments of the stresses and the strains, say, $\Delta\sigma_{ij}$ and $\Delta\epsilon_{ij}$. It is convenient to introduce the rates of change $\dot{\sigma}_{ij}$, $\dot{\epsilon}_{ij}$ defined in the usual way as the limits of the quotients $\Delta\sigma_{ij}/\Delta t$, $\Delta\epsilon_{ij}/\Delta t$ as $\Delta t \to 0$, where t stands for time or possibly some monotonic function of time. It is simplest to think of the "rates" $\dot{\sigma}_{ij}$, $\dot{\epsilon}_{ij}$ as merely a convenient notation for infinitesimal increments $d\sigma_{ij}$, $d\epsilon_{ij}$.

It will be assumed that the strain rates depend on the stress rates and the existing state of stress in the following manner

$$\dot{\epsilon}_{ij} = \frac{1}{2G}\left[\dot{s}_{ij} + \frac{2G}{9K}\,\delta_{ij}\dot{\sigma}_{pp}\right] + \dot{\epsilon}_{ij}{}^{p} \qquad [2]$$

In this expression the first two terms represent the usual elastic strain rate; G and K are the elastic moduli of shear and of compressibility, respectively. The last term represents the plastic (permanent) strain rate, and is assumed governed by the following law

$$\dot{\epsilon}_{ij}{}^{p} = \lambda s_{ij} \qquad [3]$$

where

$$\lambda = \begin{cases} 0 \text{ if } s_{ij}s_{ij} < 2k^2, \quad \text{or} \quad s_{ij}s_{ij} = 2k^2,\ s_{ij}\dot{s}_{ij} < 0 \\ \dfrac{s_{ij}\dot{\epsilon}_{ij}{}^{p}}{2k^2} > 0 \text{ if } s_{ij}s_{ij} = 2k^2,\ s_{ij}\dot{s}_{ij} = 0 \end{cases}$$

The Mises yield criterion is thus assumed to hold. The constant k is the yield stress in pure shear. It is noteworthy that when plastic flow occurs, the parameter λ is positive, since $s_{ij}\,\dot{\epsilon}_{ij}{}^{p}$ is the rate at which plastic work is done, and this is a positive quantity.

With every state of stress σ_{ij}, reached after some loading program (which, in general, produces some plastic flow), can be associated two other states of stress, namely, an "elastic-stress state" $\sigma_{ij}{}^{*}$, and a "residual-stress state" ρ_{ij}. By the elastic stress state $\sigma_{ij}{}^{*}$, corresponding to a given state of external loads, is meant the system of stresses that would be reached if the material were perfectly elastic at all stresses. The residual-stress state ρ_{ij}, corresponding to a given state of stress σ_{ij}, means the system of stresses which exists after the body is unloaded from the external loads which produced σ_{ij}; in an unloading process all of the external loads are reduced to zero in such a way that no additional plastic flow occurs ($\dot{\epsilon}_{ij}{}^{p} = 0$ everywhere). Since the changes in stress which result from an unloading process are $-\sigma_{ij}{}^{*}$, the residual stresses are given by

$$\rho_{ij} = \sigma_{ij} - \sigma_{ij}{}^{*} \qquad [4]$$

Alternatively, one can think of any stress state σ_{ij} as consisting of an elastic stress state $\sigma_{ij}{}^{*}$ corresponding to the values of the external loads (independent of the previous history of loading) superimposed on a residual stress state ρ_{ij} which satisfies equilibrium with zero external loads, and which depends upon the state of permanent deformation of the body, and hence upon the history of loading. Corresponding to any residual-stress state ρ_{ij}, there is a residual stress deviator r_{ij}, equal to

$$r_{ij} = \rho_{ij} - \frac{1}{3}\,\delta_{ij}\,\rho_{pp} \qquad [5]$$

Now by definition a body is said to have "shaken down" if it has arrived at a state of residual stress such that thereafter all allowed combinations of the external load components produce only elastic increments of stress and strain. Thus if $\sigma_{ij}{}^{*}$ represents any elastic-stress state which the external loads can produce, and if $\bar{\rho}_{ij}$ is a shakedown state of residual stress, then the corresponding stress deviators $s_{ij}{}^{*}$ and $\bar{r}_{ij}$ satisfy the following relation

$$(\bar{r}_{ij} + s_{ij}{}^{*})\,(\bar{r}_{ij} + s_{ij}{}^{*}) \leq 2k^2 \qquad [6]$$

The shakedown theorem for continuous media may be expressed by the statement: "If any residual stress state $\bar{\rho}_{ij}$ can be found which satisfies the equations of equilibrium under zero external loads and satisfies the shakedown criterion [6], for all values of the external loads, then the body will shake down to some residual stress state $\bar{\rho}_{ij}'$, not necessarily the same as $\bar{\rho}_{ij}$." The value of the theorem, as will appear from the example to be given, lies in the fact that the analysis of a body under a set of external load components which vary arbitrarily between prescribed limits is reduced to an investigation of the conditions under which a "solution" of inequalities [6] can exist.

The following proof appears to be simpler than Melan's since it does not require the consideration of the "influence coefficients" which relate the residual stresses to an existing state of permanent strains. Let us suppose that there exists at least one residual-stress state $\bar{\rho}_{ij}$ whose deviator $\bar{r}_{ij}$ satisfies the "shakedown con-

[6] Any subscript which appears twice in a term is given in turn the values 1, 2, 3 and the results are added; for example, $s_{ij}s_{ij} = s_{11}s_{11} + s_{12}s_{12} + s_{13}s_{13} + s_{21}s_{21} + s_{22}s_{22} + s_{23}s_{23} + s_{31}s_{31} + s_{32}s_{32} + s_{33}s_{33}$.

dition" [6]. Let σ_{ij} denote the actual state of stress in the body at any instant, under any arbitrary (permissible) set of load components, and after any arbitrary loading program. Corresponding to σ_{ij} there is a certain residual stress-state $\rho_{ij} = \sigma_{ij} - \sigma_{ij}^{\circ}$ and residual stress deviator r_{ij}. Now let V denote the total volume of the body and form the following integral

$$E(\bar{\rho}_{ij}, \rho_{ij}) = \int_V \left[(\bar{r}_{ij} - r_{ij})(\bar{r}_{ij} - r_{ij}) + \frac{2}{9}\frac{G}{K}(\bar{\rho}_{pp} - \rho_{pp})^2 \right] dV \quad \ldots\ldots [7]$$

E is a positive definite functional form vanishing only when $\bar{\rho}_{ij} = \rho_{ij}$; it is the elastic-strain energy corresponding to the system of stresses $\bar{\rho}_{ij} - \rho_{ij}$ to within a factor $4G$. The proof of the theorem now consists simply of showing that ρ_{ij} always approaches $\bar{\rho}_{ij}$ in the sense that E always decreases (if yielding occurs) or remains constant (if no yielding occurs). But since E is positive definite, it can decrease at most until it reaches the value zero, when no further change can occur. In general, however, E reaches a constant value different from zero, since the shakedown state which is reached in general is not unique, but depends on the loading program.

The rate of change of E, corresponding to changes of ρ_{ij} is, by differentiation of Equation [7], equal to

$$\dot{E} = -2\int_V \left[\bar{r}_{ij} - r_{ij} \right)\dot{r}_{ij} + \frac{2}{9}\frac{G}{K}(\bar{\rho}_{pp} - \rho_{pp})\dot{\rho}_{pp} \Big] dV \ldots [8]$$

The rates $\dot{\rho}_{ij}$ are supposed to be produced by some arbitrary (permissible) change of the state of loading. Equation [8] will now be transformed by means of the principle of virtual work. Let σ_{ij}' and σ_{ij}'' denote any two systems of stresses, both of which satisfy the equations of equilibrium throughout the interior of the body, and are in equilibrium with the same surface stresses wherever these are specified by the given state of loading. Further, let $\dot{\eta}_{ij}$ denote any system of strain rates which satisfy the equations of compatibility everywhere, and in addition correspond to displacement rates which vanish at any surface points where the displacements are specified. Then the "principle of virtual work" states

$$\int_V (\sigma_{ij}' - \sigma_{ij}^{\circ})\dot{\eta}_{ij}\, dV = 0 \quad \ldots\ldots [9]$$

(This result is easily proved by an application of the divergence theorem taking account of the properties of σ_{ij}', σ_{ij}'', and $\dot{\eta}_{ij}$ just defined.)

In particular, let us take $\sigma_{ij}' = \bar{\rho}_{ij}$, and $\sigma_{ij}'' = \rho_{ij}$, the latter being the actual residual stresses at some instant, as defined for Equation [7]. Moreover, let $\dot{\eta}_{ij} = \dot{\epsilon}_{ij}$, the actual strain rates corresponding to some arbitrary change of the system of external loads. Then, using the stress-strain Equation [2], Equation [9] becomes

$$\int_V (\bar{\rho}_{ij} - \rho_{ij})\left[\dot{s}_{ij} + \frac{2G}{9K}\delta_{ij}\dot{\sigma}_{pp} + 2G\,\dot{\epsilon}_{ij}^{\,p} \right] dV = 0 \ldots [10]$$

We can write the actual stress rates as

$$\dot{\sigma}_{ij} = \dot{\sigma}_{ij}^{\circ} + \dot{\rho}_{ij};\quad \dot{s}_{ij} = \dot{s}_{ij}^{\circ} + \dot{r}_{ij} \quad \ldots\ldots [11]$$

where $\dot{\sigma}_{ij}^{\circ}$ and $\dot{\rho}_{ij}$ are the elastic- and residual-stress rates, respectively, and $\dot{s}_{ij}^{\circ}$, $\dot{r}_{ij}$ the corresponding deviations. Then Equation [10] becomes

$$\int_V (\bar{\rho}_{ij} - \rho_{ij})\left[\dot{s}_{ij}^{\circ} + \dot{r}_{ij} + \frac{2G}{9K}\delta_{ij}(\dot{\sigma}_{pp}^{\circ} + \dot{\rho}_{pp}) + 2G\,\dot{\epsilon}_{ij}^{\,p} \right] dV = 0 \ldots\ldots [12]$$

However, note that

$$\frac{1}{2G}\left[\dot{s}_{ij}^{\circ} + \frac{2G}{9K}\delta_{ij}\dot{\sigma}_{pp}^{\circ} \right]$$

stands for the system of strains corresponding to the elastic stresses $\dot{\sigma}_{ij}^{\circ}$, and hence is a compatible system which satisfies Equation [9]. After using this fact, and writing ρ_{ij}, $\bar{\rho}_{ij}$ in terms of the corresponding deviations, Equation [12] becomes

$$\int_V \left[\bar{r}_{ij} - r_{ij} + \frac{1}{3}\delta_{ij}(\bar{\rho}_{pp} - \rho_{pp}) \right]\left[\dot{r}_{ij} + \frac{2G}{9K}\delta_{ij}\dot{\rho}_{pr} + 2G\,\dot{\epsilon}_{ij}^{\,p} \right] dV = 0$$

Since

$$\delta_{ij}r_{ij} = \delta_{ij}\dot{r}_{ij} = \delta_{ij}\dot{\epsilon}_{ij}^{\,p} = 0$$

this reduces to

$$\int_V \left[(\bar{s}_{ij} - r_{ij})(\dot{r}_{ij} + 2G\dot{\epsilon}_{ij}^{\,p}) + \frac{2G}{9K}(\bar{\rho}_{pp} - \rho_{pp})\dot{\rho}_{pp} \right] dV = 0 \quad \ldots\ldots [13]$$

Combining this with Equation [8], we obtain the important result

$$\dot{E} = 4G\int_V (\bar{r}_{ij} - r_{ij})\,\dot{\epsilon}_{ij}^{\,p}\, dV \quad \ldots\ldots [14]$$

Obviously, if no plastic flow occurs anywhere, (i.e., $\dot{\epsilon}_{ij}^{\,p} = 0$) then $\dot{E} = 0$. However, we can now show that at all points where plastic flow is occurring (i.e., $\dot{\epsilon}_{ij}^{\,p} \neq 0$) the quantity $(\bar{r}_{ij} - r_{ij})\dot{\epsilon}_{ij}^{\,p}$ is negative, if $\bar{r}_{ij}$ is a shakedown state, and $\dot{\epsilon}_{ij}^{\,p} = \lambda s_{ij}$, according to Equation [3]. To prove this, let us assume the contrary, namely, that at some point

$$(\bar{r}_{ij} - r_{ij})\,\dot{\epsilon}_{ij}^{\,p} > 0 \quad \ldots\ldots [15]$$

Since $\lambda > 0$ this implies that $(\bar{r}_{ij} - r_{ij})s_{ij} > 0$ or

$$(\bar{r}_{ij} + s_{ij}^{\circ} - r_{ij} - s_{ij}^{\circ})s_{ij} > 0$$

where s_{ij}° is the elastic-stress deviation corresponding to the existing stress deviations s_{ij}. This, in turn, implies

$$(\bar{r}_{ij} + s_{ij}^{\circ})s_{ij} > s_{ij}s_{ij} = 2k^2$$

Now since $s_{ij}s_{ij} \geq 0$, this inequality means that also

$$[(\bar{r}_{ij} + s_{ij}^{\circ})s_{ij}]^2 > (s_{ij}s_{ij})^2 \quad \ldots\ldots [16]$$

But Cauchy's inequality (7) states that for any set of numbers $a_k, b_k, k = 1, \ldots n$

$$\left(\sum_{k=1}^{n} a_k^2\right)\left(\sum_{k=1}^{n} b_k^2\right) \geq \left(\sum_{k=1}^{n} a_k b_k\right)^2$$

the equality sign holding only when $a_k = \alpha b_k$ for all k. Accordingly, if [16] is true, then also

$$[(\bar{r}_{ij} + s_{ij}^{\circ})(\bar{r}_{ij} + s_{ij}^{\circ})]s_{ij}s_{ij} > (s_{ij}s_{ij})^2$$

Dividing through by $s_{ij}s_{ij} = 2k^2$, we have finally

$$(\bar{r}_{ij} + s_{ij}^{\circ})(\bar{r}_{ij} + s_{ij}^{\circ}) > 2k^2$$

But this contradicts the initial hypothesis that $\bar{r}_{ij}$ is a shakedown state and satisfies Inequality [6] for all s_{ij}°. Hence the Assumption [15] is false, and we conclude that throughout the body

$$(\bar{r}_{ij} - r_{ij})\dot{\epsilon}_{ij}^{\,p} \leq 0 \quad \ldots\ldots [17]$$

This proves that $\dot{E} \leq 0$, or, in words, if plastic flow occurs anywhere E decreases, while if no plastic flow occurs at any point E remains constant. This establishes the shakedown theorem stated earlier.

Application of the Shakedown Theorem

Consider a circular bar subjected to an axial force F and a torsional moment M which may have any values within specified limits

$$\left.\begin{aligned} F_{\min} \leq F \leq F_{\max} \\ M_{\min} \leq M \leq M_{\max} \end{aligned}\right\} \quad \ldots\ldots\ldots\ldots [18]$$

The state of stress is defined by the values of the axial stress σ and shear stress τ tangent to circles with center at the axis. The elastic stresses are

$$\sigma^e = F/A, \; \tau^e = rM/I_p \quad \ldots\ldots\ldots\ldots [19]$$

where r is the radial co-ordinate, A is the area and I_p is the polar moment of inertia. The yield condition is

$$\frac{1}{3}\sigma^2 + \tau^2 \leq k^2 \quad \ldots\ldots\ldots\ldots [20]$$

We may now introduce residual stresses $\bar{\sigma}, \bar{\tau}$. Since these are functions of r only, they satisfy the differential equations of equilibrium identically. They must also be in equilibrium with zero values of F and M, i.e.

$$\int_A \bar{\sigma}\, dA = 0; \quad \int_A \bar{\tau}\, r dA = 0 \quad \ldots\ldots\ldots\ldots [21]$$

Now if the bar can shake down, there exists a pair of functions $\bar{\sigma}, \bar{\tau}$ such that for all values of r the following inequality is satisfied

$$\frac{1}{3}\left(\bar{\sigma} + \frac{F}{A}\right)^2 + \left(\bar{\tau} + \frac{rM}{I_p}\right)^2 \leq k^2 \quad \ldots\ldots\ldots\ldots [22]$$

The investigation of the possibility of shakedown under given loads is thus reduced to investigating whether it is possible to find $\bar{\sigma}, \bar{\tau}$ satisfying the "shakedown condition" [22], and the equilibrium requirements [21]. This is facilitated by introducing dimensionless quantities

$$\bar{\sigma}_1 = \bar{\sigma}/k, \; \bar{\tau}_1 = \bar{\tau}/k, \; \alpha = F/kA, \; \beta = M/kI_p$$

and taking the radius of the bar as unity. Then [22] becomes

$$\frac{1}{3}(\bar{\sigma}_1 + \alpha)^2 + (\bar{\tau}_1 + r\beta)^2 \leq 1 \quad \ldots\ldots\ldots\ldots [23]$$

where

$$0 \leq r \leq 1$$

$$\frac{F_{\min}}{kA} = \alpha_2 \leq \alpha \leq \alpha_1 = \frac{F_{\max}}{kA}$$

$$\frac{M_{\min}}{kI_p} = \beta_2 \leq \beta \leq \beta_1 = \frac{M_{\min}}{kI_p}$$

$\bar{\sigma}_1$ and $\bar{\tau}_1$ must also satisfy the following equations

$$\int_0^1 \bar{\sigma}_1\, r dr = 0; \quad \int_0^1 \bar{\tau}_1\, r^2\, dr = 0 \quad \ldots\ldots\ldots\ldots [24]$$

Under any given loading, specified by α and β, the values of $\bar{\sigma}_1$ and $\bar{\tau}_1$ which allow the yield condition to be satisfied at any point r are related by Equation [23]. Taking $\bar{\sigma}_1$, $\bar{\tau}_1$ as rectangular axes, the points with co-ordinates $(\bar{\sigma}_1, \bar{\tau}_1)$ satisfying Equation [23] lie on or inside an ellipse of semiaxes $\sqrt{3}$ and 1 and with center at $(-\alpha, -r\beta)$. As the state of loading changes, the ellipse translates, its center remaining on or within the rectangle bounded by the lines $\bar{\sigma}_1 = -\alpha_1, \bar{\sigma}_1 = -\alpha_2, \bar{\tau}_1 = -r\beta_1, \bar{\tau}_1 = -r\beta_2$. A necessary condition (but not a sufficient one) for shakedown to occur is that at each value of r there is an area common to every position of the ellipse.

Fig. 1 illustrates the use of the yield ellipses. In Fig. 1(*a*) are shown the four ellipses with centers at points corresponding to the four extreme load values taking $r = 1$. With the ranges of α and β as shown there is a region common to all the ellipses shaded in the figure. Figs. 1(*b*) and (*c*) show the common areas of the yield ellipses when r is taken as 0.5 and 0, respectively. In order for shakedown to occur it is also necessary that $\bar{\sigma}_1$ and $\bar{\tau}_1$ satisfy Equations [24]. In the example shown in Fig. 1 the only allowed values of $\bar{\sigma}_1$ at $r = 1$ are negative, while those of $\bar{\tau}_1$ at the same point are positive. Therefore, before it can be concluded that shakedown will occur it must be shown that at least one pair of functions $\bar{\sigma}_1(r)$ and $\bar{\tau}_1(r)$ can be constructed from the allowed points such that Equations [24] are satisfied. It is clear that shakedown is impossible if the ellipses in their most remote positions (centers at α_1, β_1 and α_2, β_2) have no point in common, and thus one condition for shakedown to be possible is that

$$\frac{1}{3}\left(\frac{\alpha_1 - \alpha_2}{2}\right)^2 + \left(\frac{\beta_1 - \beta_2}{2}\right)^2 \leq 1 \quad \ldots\ldots\ldots [25]$$

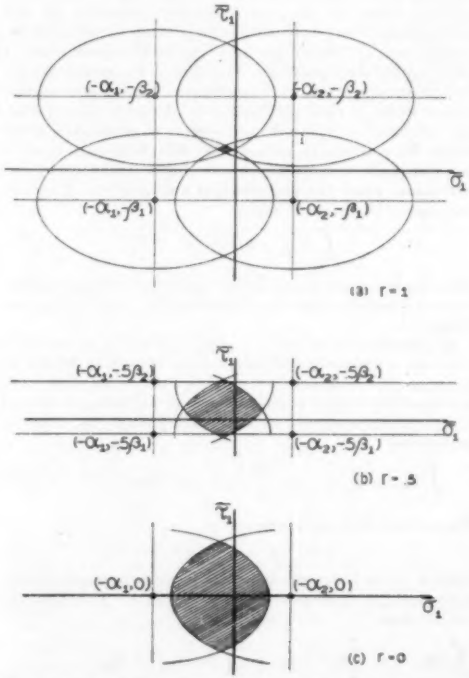

Fig. 1 Diagrams Illustrating Allowed Values of Residual Stresses $\bar{\sigma}_1$, $\bar{\tau}_1$ for Shakedown of a Circular Bar Subjected to Independently Variable Axial Force and Twisting Moment

In addition, limits on α and β which are set by the requirement that plastic collapse does not occur are

$$|\alpha| \leq \sqrt{3}, \quad |\beta| \leq \frac{4}{3} \ldots\ldots\ldots\ldots\ldots [26]$$

In the case when the axial and torsional loads have positive and negative values of equal magnitude, say

$$\alpha_1 = -\alpha_2 = m; \quad \beta_1 = -\beta_2 = n,$$

then Equation [25] yields

$$\frac{1}{3} m^2 + n^2 \leq 1 \ldots\ldots\ldots\ldots\ldots [27]$$

In this case, therefore, the condition for shakedown to be impossible is merely that the elastic stresses cause the yield stress to be exceeded at any point. Moreover, in this case it is obvious that shakedown must occur if the load limits are such that Equation [27] is satisfied. This is a trivial result, however, since Equation [27] is merely the condition that no plastic flow occurs.

The more interesting cases are those in which plastic flow does occur, but in which there is a possibility of shakedown (Inequalities [25] and [26] are satisfied). The case of equal positive and negative limits for the axial force is one for which the conditions under which shakedown will definitely occur can be given explicitly. If the limits on the axial force are specified by $\alpha_1 = -\alpha_2 = \alpha_0$, and the numerically greater limit of the torsional moment is specified by β_0, then the relation between α_0 and β_0, such that shakedown will occur, is the following

$$\beta_0 \leq \frac{4}{3} \sqrt{1 - \frac{1}{3} \alpha_0^2} \ldots\ldots\ldots\ldots\ldots [28]$$

The range of the torsional moment, specified by $\beta_1 - \beta_2 = \beta_0 + \beta_0'$, say, must be such that Equation [25] is also satisfied. If it is, then satisfaction of Equation [28] indicates that shakedown will occur. As a numerical example, suppose $\alpha_0 = 0.9$; then shakedown will occur if

$$\beta_0 \leq 1.14, \quad \beta_0' \leq 0.57$$

Thus in this case the bar would carry "safely" a torsional moment which exceeds the maximum elastic moment by about 14 per cent.

In the general case when none of the positive and negative load limits are equal, then satisfaction of Equation [28], taking α_0 as the numerically greater limit, is not enough to insure that shakedown will occur; however, shakedown is impossible if Equation [28] is not satisfied. A trial-and-error numerical procedure would determine whether shakedown will actually occur in a given case.

Conclusions

The shakedown theorem proved is of theoretical interest since it shows, for example, that if an elastic-plastic body shakes down under some particular program of loading, it will ultimately shake down under any loading program (in which the individual load components are held within their prescribed limits). It may also possibly provide the simplest basis for the plastic design of members subjected to several independent loads which vary arbitrarily between given extreme values. However, the example which has been given shows that the application of the theorem even in a simple problem is much more complicated than is the application of the corresponding theorem to a structure such as a truss or frame. Explicit statements of conditions under which shakedown will occur probably can be given for special loading conditions in many problems, as was found to be the case in the combined torsion-tension problem treated as an example.

BIBLIOGRAPHY

1 "Elastic-Plastic Analysis of Structures Subjected to Loads Varying Arbitrarily Between Prescribed Limits," by P. S. Symonds and W. Prager. ASME Paper No. 49—A-13. To be published in the Journal of Applied Mechanics.

2 "The Behavior of Continuous Beams and Plane Frames Under Repeated Loading," by B. G. Neal, Technical Report A11-32 to Office of Naval Research by Graduate Division of Applied Mathematics, Brown University, Providence, R. I.

3 "The Calculation of Failure Loads on Plane Frames Under Arbitrary Loading Programs," by P. S. Symonds and B. G. Neal, to be published in the *Journal of The Institution of Civil Engineers*, vol. 35, 1950–1951.

4 "Über die Bemessung statisch unbestimmter Stahltragwerke unter Berucksichtigung des elastisch-plastischen Verhaltens des Baustoffes," by Hans Bleich, *Der Bauingenieur*, vol. 13, no. 19/20 May 6, 1932, pp. 261–267.

5 "Approximations in Elasticity Based on the Concept of Function Space," by W. Prager and J. L. Synge, *Quarterly of Applied Mathematics*, vol. 5, 1947, pp. 241–269.

6 "Der Spannungszustand eines "Hencky-Mises'schen" Kontinuums bei veraenderlicher Belastung," by E. Melan, *Sitzungsberichte der Akademie der Wissenschaften in Wien*, vol. 147, 1938, pp. 73–87.

7 "Methoden der Mathematischen Physik," by R. Courant and D. Hilbert, Julius Springer, Berlin, Germany, vol. I, 1931, p. 2.

Solution to the Rolling Problem for a Strain-Hardening Material by the Method of Discontinuities[1]

By ALICE WINZER,[2] PROVIDENCE, R. I.

The problem of drawing and rolling of a thin plastic sheet between cylindrical guides was investigated recently by H. I. Ansoff, under the assumption that the material is in a state of plane plastic flow and obeys the Saint Venant-Mises yield condition (1, 2).[3] He determined the stress distribution along the sheet by the method of characteristics and also by the method of discontinuity surfaces and found good agreement between these results as well as with experimental data. Since the computations required for the discontinuous solution are considerably less laborious than those necessary for the continuous solution, the same type of problem, but now under the assumption that the material displays strain-hardening, will be analyzed by the method of discontinuities. It seems reasonable to expect that the results so found constitute a close approximation to results based upon a continuous solution.

Basic Equations—Ideal Plasticity

IF THE x, y-plane is the plane in which plastic flow occurs, then the state of stress is completely determined once the normal stresses σ_x and σ_y and the shearing stress $\tau_{xy} = \tau$ are known where σ_x, σ_y, and τ are functions of x and y only. These quantities must satisfy the equations of equilibrium

$$\left.\begin{aligned} \frac{\partial \sigma_x}{\partial x} + \frac{\partial \tau}{\partial y} &= 0 \\ \frac{\partial \sigma_y}{\partial y} + \frac{\partial \tau}{\partial x} &= 0 \end{aligned}\right\} \quad \ldots\ldots\ldots\ldots\ldots [1]$$

and the yield condition

$$(\sigma_x - \sigma_y)^2 + 4\tau^2 = 4k^2$$

The stresses may be represented in the form

$$\left.\begin{aligned} \sigma_x &= k(2\omega + \sin 2\theta) \\ \sigma_y &= k(2\omega - \sin 2\theta) \\ \tau &= -k \cos 2\theta \end{aligned}\right\} \quad \ldots\ldots\ldots\ldots\ldots [2]$$

With this substitution, the yield condition is identically satisfied and the equilibrium equations become the equations of the characteristics. In Equations [2]

$$\omega = \frac{\sigma_x + \sigma_y}{4k}$$

and θ is the angle between the negative y-axis and the characteristics which coincide with the slip lines.

Now consider the projection AB of an arbitrary surface element in the plastic field separating two elementary rectangles, Fig. 1.[4] In order that this be in equilibrium, the normal stress

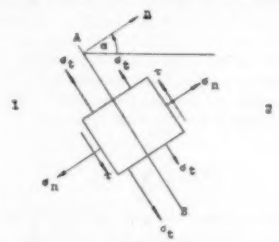

FIG. 1

and the shear stress acting across the line element must be continuous; however, the normal stress acting along this separating surface may be discontinuous. If the normal to the surface forms an angle α with the positive x-direction, then the stresses acting on it are given by

$$\left.\begin{aligned} \sigma_n &= k[2\omega + \sin 2(\theta - \alpha)] \\ \sigma_t &= k[2\omega - \sin 2(\theta - \alpha)] \\ \tau &= -k \cos 2(\theta - \alpha) \end{aligned}\right\} \quad \ldots\ldots\ldots\ldots\ldots [3]$$

Equilibrium demands that $\sigma_{n_1} = \sigma_{n_2}$ and $\tau_1 = \tau_2$ where the subscripts 1 and 2 denote the two regions separated by the surface. Such a discontinuity surface shall be referred to as a shock.

Rolling Problem for a Strain-Hardening Material—Determination of Stresses and Velocities

Consider now the problem of the rolling of a fully plastic sheet between two cylindrical surfaces. Let the circular trace of the rollers be approximated by a succession of chords, and assume that the field of plastic flow may be represented by n regions of constant state (in each such region the stresses are constant), separated by shocks as indicated in Fig. 2. It is assumed that the yield condition is satisfied in each constant-state region but, since the material undergoes strain-hardening, the yield constant k varies from region to region. Let its value in the nth region be denoted by k_n. Continuity across a shock requires that

---

[1] The results presented in this paper were obtained in the course of research conducted under Contract N7onr-358 sponsored jointly by the Office of Naval Research and the Bureau of Ships. The paper constitutes part of a thesis submitted in partial fulfillment for the PhD degree at Brown University.

[2] Graduate Division of Applied Mathematics, Brown University.

[3] Numbers in parentheses refer to the Bibliography at the end of the paper.

Presented at the Annual Conference of the Applied Mechanics Division, Purdue University, Lafayette, Ind., June 22–24, 1950, of The American Society of Mechanical Engineers.

Discussion of this paper should be addressed to the Secretary, ASME, 29 West 39th Street, New York, N. Y., and will be accepted until April 10, 1951, for publication at a later date. Discussion received after the closing date will be returned.

Note: Statements and opinions advanced in papers are to be understood as individual expressions of their authors and not those of the Society. Manuscript received by the Applied Mechanics Division, September 2, 1949. Paper No. 50—APM-19.

[4] For further details, see Bibliography, ref. (3).

$$k_n[2\omega_n + \sin 2(\theta_n - \alpha)] = k_{n+1}[2\omega_{n+1} + \sin 2(\theta_{n+1} - \alpha)] \quad [4a]$$

and

$$k_n \cos 2(\theta_n - \alpha) = k_{n+1} \cos 2(\theta_{n+1} - \alpha) \quad [4b]$$

where α is the angle between the shock and the negative y-axis. In particular, consider the plastic region divided into seven ($n = 1, 2, \ldots, 7$) constant-state regions.

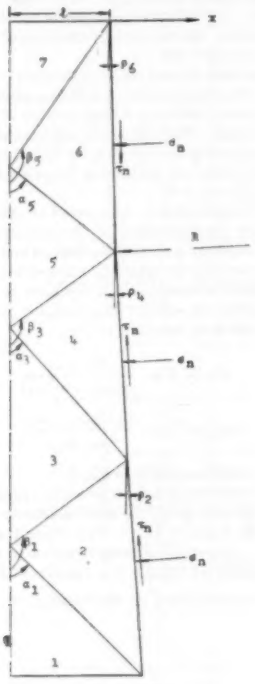

FIG. 2

It is assumed that the entrance and exit sections are free from normal pressure; further, due to symmetry, the shearing stress vanishes along the center line. These conditions are satisfied if

$$\omega_1 = \omega_7 = -1/2 \quad [5a]$$

and

$$\theta_1 = \theta_2 = \theta_3 = \theta_7 = \frac{3\pi}{4} \quad [5b]$$

Application of Equation [4b] to two successive regions, together with Equation [5b] yields

$$2\alpha - \cos^{-1}\left(-\frac{k_1}{k_2}\sin 2\alpha\right) = 2\beta - \cos^{-1}\left(-\frac{k_2}{k_3}\sin 2\beta\right) \quad [6]$$

where $(\beta - \alpha)$ is the angle between two shocks one of which is the reflection of the other off the center line, Fig. 2. Equation [6] is satisfied by the relation

$$\frac{\sin 2\alpha}{\sin 2\beta} = \pm\frac{k_2}{k_1}, \qquad \left(\frac{k_2}{k_1} = \frac{k_3}{k_2}\right) \quad [7]$$

On the basis of the geometry of the problem, the minus sign in Equations [7] gives the desired relation. Note that in the perfectly plastic case ($k_1 = k_2$), two such reflective shocks must be inclined at $\pi/2$ (reference 5), which agrees with the result obtained from Equations [7]. Elimination of the quantities ω_n in Equation [4a], together with Equations [5] and [7] yields

$$\frac{1 - \frac{k_1}{k_7}}{1 + \frac{k_6}{k_7}} + \frac{k_2}{k_6}g(\alpha_1) + \frac{k_4}{k_6}g(\alpha_3) + g(\alpha_5) = 0 \quad [8]$$

where

$$g(\alpha_n) = -\frac{k_n}{k_{n+1}}\cos 2\alpha_n + \sin\left[\cos^{-1}\left(-\frac{k_n}{k_{n+1}}\sin 2\alpha_n\right)\right]$$

$$= -\frac{k_n}{k_{n+1}}\cos 2\alpha_n + \cos 2\beta_n$$

by Equations [7]. Corresponding to any α there are two possible β satisfying Equations [7], symmetric about $3\pi/4$. The geometry of the problem determines the proper choice of β.

Now consider the conditions along the surface of the guides. Denote the angle between the boundary and the negative y-axis by $\rho_m << 1$. Then the angle between the slip lines and the boundary will be $\pi - \theta_m + \rho_m$, where θ_m is the angle between the slip line and the negative y-axis in region m. Since ρ_m is small, the shearing stress τ_n along the boundary will be small compared to k_m. For the case of a smooth boundary (i.e., $\tau_n = 0$), $\pi - \theta_m + \rho_m = \pi/4$. Hence for τ_n small, $\pi - \theta_m + \rho_m = \pi/4 + \delta_m$, where δ_m is a small angle. Let us apply the Coulomb friction law along the guides, i.e., shearing stress directly proportional to normal stress. Then

$$\left.\begin{aligned} |\tau_n| &= |f\sigma_n| \quad \text{for} \quad |f\sigma_n| < k \\ |\tau_n| &= k \quad \text{for} \quad |f\sigma_n| \geq k \end{aligned}\right\} \quad [9]$$

where f is the coefficient of friction.

Along the boundary

$$\sigma_{n_m} = k_m[2\omega_m + \sin 2(\theta_m - \rho_m)] = k_m[2\omega_m - \cos 2\delta_m]$$

$$\tau_{n_m} = -k_m \cos 2(\theta_m - \rho_m) = k_m \sin 2\delta_m$$

Assuming a reversal of shearing stress along the guides, Fig. 2, the friction law yields

$$\frac{-k_m \sin 2\delta_m}{k_m[2\omega_m - \cos 2\delta_m]} = f \text{ for } m = 2, 4, \text{ and } \frac{k_6 \sin 2\delta_6}{k_6[2\omega_6 - \cos 2\delta_6]} = f \quad [10]$$

These relations reduce to

$$\left.\begin{aligned} \delta_2 &= -\varphi = \frac{1}{2}\cos^{-1}\left[\frac{f}{\sqrt{1+f^2}}\,2\omega_2\right] \\ \text{and} \\ \delta_6 &= \varphi = \frac{1}{2}\cos^{-1}\left[\frac{f}{\sqrt{1+f^2}}\,2\omega_6\right] \end{aligned}\right\} \quad [11]$$

where φ is given by

$$\sin 2\varphi = \frac{1}{\sqrt{1+f^2}}$$

and the sign must be chosen such that δ is small. The angle

which the boundary makes with the negative y-axis is then given by

$$\left.\begin{aligned}\rho_m &= \delta_m + \theta_m + \frac{\pi}{4} + l\pi, \quad (l = \pm 1, \pm 2, \ldots)\\ &= \delta_m + (\alpha + \beta)_{m-1} + l\pi\end{aligned}\right\} \quad [12]$$

since $\theta_m = \alpha_{m-1} + \beta_{m-1} - \pi/4$ from Equation [4b]. The quantities ω_m are given by Equation [4a]. The problem now reduces to finding three shock angles α_1, α_2, α_3 such that Equation [8] is satisfied, and furthermore that the resulting ρ in Equations [12] satisfies the geometrical condition that $0 < \rho_6 < \rho_4 < \rho_2$. The chords thereby determined should approximate a circle as closely as possible.

Numerical Results

The rolling problem has been solved for the particular case $f = 0.2$, $(k_{n+1})/(k_n) = 1.05$. Equations [12] then reduce to

$$\rho_2 = -39°21' \pm \frac{1}{2}\cos^{-1}\left\{0.19612[-0.95238 + g(\alpha_1)]\right\} + \alpha_1 + \beta_1 + n_1\pi$$

$$\rho_4 = -39°21' \pm \frac{1}{2}\cos^{-1}\left\{0.19612\,[-0.86384 + 1.8594\,g(\alpha_1) + g(\alpha_2)]\right\} + \alpha_2 + \beta_2 + n_2\pi$$

$$\rho_6 = \quad 39°21' \pm \frac{1}{2}\cos^{-1}\left\{0.19612\,[-1.05\,[1 + g(\alpha_2)]]\right\} + \alpha_3 + \beta_3 + n_3\pi$$

where the choice of sign and n_1, n_2, n_3 (integers) is such that the resulting ρ is physically reasonable.

The simultaneous solution of these equations and Equation [8] is shown in the nomograph, Fig. 3.[6] Of all possible solutions the one which gives a polygon which best approximates the circular trace of the guides was chosen, namely, $\alpha_1 = 45°13'$ ($\beta_1 = 126°7'$, $\rho_2 = 4°4'$), $\alpha_2 = 41°$ ($\beta_2 = 125°17'$, $\rho_4 = 2°47'$), $\alpha_3 = 50°30'$ ($\beta_3 = 145°24'$, $\rho_6 = 1°1'$). With this result the values of all the θ and ω were computed from Equations [4], and the stresses from Equations [3]. The stress distribution is shown in Fig. 4. The thickness reduction of the sheet is found to be about 20 per cent; the ratio of half-thickness of sheet to radius of rollers (l/R) is about 1/80.

If one requires that the end points of the approximating chords fall on a circle rather than as close to a circle as possible, one could not divide the plastic field into a fixed number of constant-state regions at the outset. The solution would have to proceed from the exit section, placing the end point of each chord on the circle by an iterative scheme and continuing the process to a region in which $\omega = -1/2$, i.e., $\sigma_y = 0$.

The velocity distribution is determined completely once the shock angles and the inclination of the boundary are known. The velocity is constant in each of the regions and directed along the center line and the boundary in successive regions. From the condition that the normal velocity must be continuous across a shock, one can find the velocity distribution in the entire plastic field for a given entrance velocity V_1; then

$$V_{2n} = V_{2n-1}\frac{\sin\alpha_{2n-1}}{\sin(\alpha_{2n-1} - \rho_{2n})}$$

$$V_{2n+1} = V_{2n}\frac{\sin(\beta_{2n-1} - \rho_{2n})}{\sin\beta_{2n-1}}$$

The numerical results are shown in Fig. 5.

Since a point of reversal of shear stress was assumed along the boundary, i.e., at some point, the relative velocity between roller and sheet is zero, $V_{\text{roller}} = (V_4 + V_6)$. Once the velocities are determined, the corresponding stress-strain curve can be plotted. The jump of tangential velocity is a measure of the strain rate;

[6] For details on construction, see Bibliography, ref. (6).

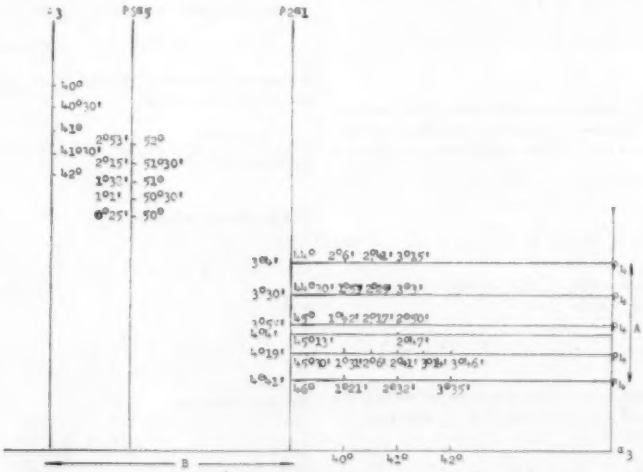

Fig. 3 Use of Nomograph

(Choose α_1 and α_2 on A-scale such that corresponding ρ_3 and ρ_5 satisfy $\rho_5 < \rho_3$. Use a straightedge line up α_1 and α_2 on B-scale and find corresponding α_3. The choice is acceptable if the corresponding $0 < \rho_6 < \rho_5$.)

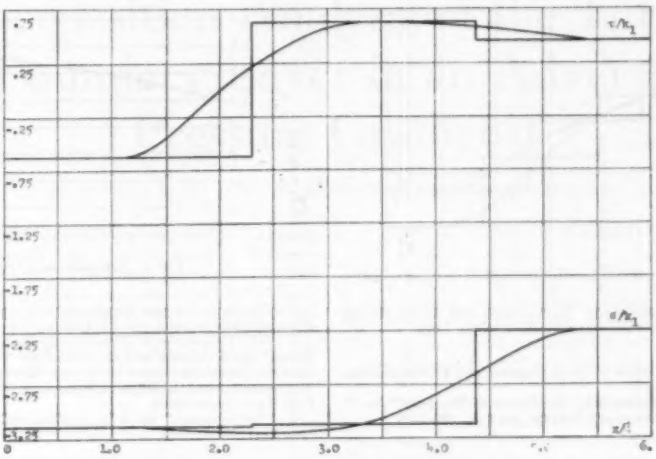

FIG. 4(a) STRESS DISTRIBUTION ALONG BOUNDARY
(Curves fitted to computed, piecewise constant, stresses.)

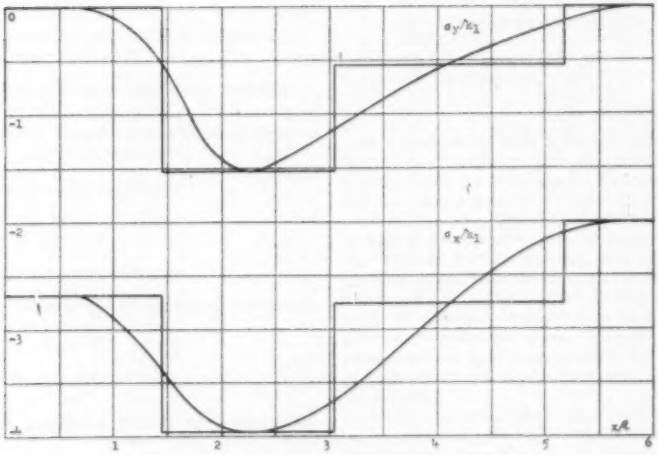

FIG. 4(b) STRESS DISTRIBUTION ALONG CENTER LINE

the variation of this quantity versus the nondimensional k_n (equivalent to nondimensional octahedral shearing stress) is indicated in Fig. 6, the stress-strain curve.

CONCLUSION

The method of discontinuities is applied to the rolling problem for a strain-hardening material. The corresponding stress-strain curve cannot be determined until the problem is completed, although it is given at the outset for any actual problem. Hence one would have to apply the method a number of times for different ratios k_{n+1}/k_n and various shock angles until one could deduce from the data used a stress-strain curve which coincides with the given one, or arrive at the given curve by an interpolative scheme. Alternatively, starting with the given stress-strain curve, the value of k_{n+1}/k_n and the values of the shock angles are immediately determined (though not uniquely) and must be such as to satisfy Equations [8] and [12].

BIBLIOGRAPHY

1 "The Forming of a Thin Plastic Sheet Between Fixed Cylindrical Surfaces," by H. I. Ansoff, Technical Report no. 23, Contract N7onr-358, Brown University (Graduate Division of Applied Mathematics) and the Office of Naval Research and Bureau of Ships, U. S. Navy Department.

2 "The Rolling of a Thin Sheet Between Cylindrical Rolls With Coulomb Friction," by H. I. Ansoff, Technical Report no. 25, Contract N7onr-358, Brown University (Graduate Division of Applied

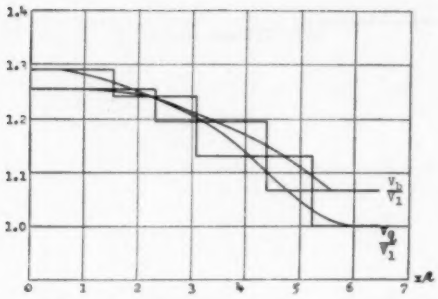

FIG. 5 VELOCITY DISTRIBUTION: V_b/V_1—VELOCITY ALONG BOUNDARY, V_c/V_1—VELOCITY ALONG CENTER LINE

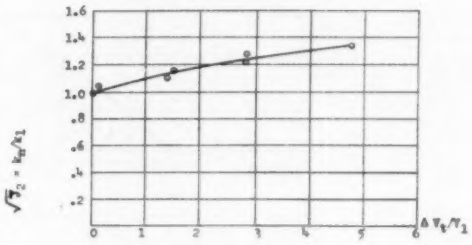

FIG. 6 STRESS-STRAIN CURVE

Mathematics) and the Office of Naval Research and Bureau of Ships, U. S. Navy Department.

3 "Discontinuous Solutions in the Theory of Plasticity," by W. Prager, R. Couvant Anniversary Volume, 1948, pp. 289–300.

4 "Plasticity for the Aerodynamicist," by W. Prager, *Journal of Aeronautical Sciences*, vol. 15, 1948, pp. 253–262.

5 "The Interaction of Discontinuity Surfaces in Plastic Fields of Stress," by A. Winzer and G. F. Carrier, Technical Report no. 9, Contract N7onr-358, Brown University (Graduate Division of Applied Mathematics) and the Office of Naval Research and Bureau of Ships, U. S. Navy Department.

6 "Nomography," by A. S. Levens, John Wiley & Sons, Inc., New York, N. Y., 1948.

A Superposition Analysis of the Turbulent Boundary Layer in an Adverse Pressure Gradient[1]

By DONALD ROSS[2] and J. M. ROBERTSON,[3] STATE COLLEGE, PA.

As an interim solution to the problem of the turbulent boundary layer in an adverse pressure gradient, a superposition method of analysis has been developed. In this method, the velocity profile is considered to be the result of two effects: the wall shear stress and the pressure recovery. These are superimposed, yielding an expression for the velocity profiles which approximate measured distributions. The theory also leads to a more reasonable expression for the wall shear-stress coefficient.

Nomenclature

The following nomenclature is used in the paper:

A = boundary-layer parameter, coefficient of pressure term in velocity relation

$AR = \left(\frac{D}{D_0}\right)^2$ = diffuser area ratio

b = half-width of a two-dimensional diffuser, at station x

b_0 = initial value of b (at $x = 0$)

$c_f = \frac{\tau_0}{{}^1/_2 \rho u_1^2}$ = wall shear stress, or skin-friction coefficient

$c_f' = \frac{\tau_0}{{}^1/_2 \rho (u_1')^2}$ = wall shear-stress coefficient in terms of effective velocity

$C_p = \frac{p - p_0}{{}^1/_2 \rho U_0^2}$ diffuser pressure coefficient

D = diameter of conical diffuser, at station x

D_0 = initial value of D (at $x = 0$)

$H = \frac{\delta^*}{\theta}$ = boundary-layer shape parameter

L = effective length of straight pipe preceding start of diffuser

p = pressure in diffuser at station x

p_0 = initial value of p (at $x = 0$)

$\mathrm{R}_\theta = \frac{u_1 \theta}{\nu}$ = momentum-thickness Reynolds number

$\mathrm{R}_\theta' = \frac{u_1' \theta}{\nu}$ = effective momentum-thickness Reynolds number

u = x-component velocity in diffuser at any point

$u_* = \sqrt{\frac{\tau_0}{\rho}}$ = wall shear-stress velocity

u_1 = maximum velocity outside of boundary layer, at station x

u_1' = effective value of u_1 defined by Equation [6]

U_0 = average velocity at start of diffuser

x = distance in direction of flow along diffuser or surface

y = normal distance from wall

α = two-dimensional diffuser half-angle

β = total angle of conical diffuser

δ = boundary-layer disturbance thickness

δ^* = boundary-layer displacement thickness

$\theta = \int_0^\delta \left(1 - \frac{u}{u_1}\right) \frac{u}{u_1} \, dy$ = boundary-layer momentum thickness

κ = von Kármán turbulence constant

ν = fluid kinematic viscosity

ρ = fluid density

τ = shear stress

τ_0 = wall shear stress

Introduction

As a result of the work of Prandtl, von Kármán, and others, the turbulent boundary layer in a uniform or nearly uniform pressure region can be analyzed. The boundary-layer thickness and the velocity profile in the layer at any location also can be predicted reliably. However, when the boundary layer is in a pressure gradient there seems to be no adequate means of analysis. Thus the flow of a boundary layer into an adverse pressure gradient, although a common type of incompressible, turbulent-boundary-layer motion, is not predictable. This type of flow occurs in diffusers, along airfoil surfaces, and along the after portions of streamlined bodies. In these cases it is desirable to predict the occurrence of separation as well as the rate of boundary-layer growth and the distribution of velocity in the layer at any location.

Usually the pressure distribution along a surface is known or can be estimated with sufficient precision to allow a successive approximations type of solution to be used. The growth of the boundary layer can be found from the von Kármán momentum equation if the shapes of the velocity profiles are known. Therefore the problem reduces to the prediction of the changes in the velocity profile which occur as the flow proceeds into the high-pressure region. Various researchers have shown that the profiles can be characterized by single form parameters. However, attempts to correlate these parameters with local flow conditions have not been particularly successful. The methods of Buri (1)[4] and Gruschwitz (2) have only limited application and do not appear to be fundamentally sound (3, 4). The analyses presented by von Doenhoff and Tetervin (4) and by Garner (5) are based on empirical relations for the rate of change of the velocity

[1] Work done under Navy Contract NOrd 7958, in connection with the diffuser design for the new water tunnel at The Pennsylvania State College.

[2] Associate Professor of Engineering Research, Ordnance Research Laboratory, Pennsylvania State College.

[3] Professor of Engineering Research, Ordnance Research Laboratory, Pennsylvania State College. Mem. ASME.

Presented at the Heat Transfer and Fluid Mechanics Institute, Los Angeles, Calif., June 28–30, 1950, of The American Society of Mechanical Engineers.

Discussion of this paper should be addressed to the Secretary, ASME, 29 West 39th Street, New York, N. Y., and will be accepted until April 10, 1951, for publication at a later date. Discussion received after closing date will be returned.

Note: Statements and opinions advanced in papers are to be understood as individual expressions of their authors and not those of the Society. Manuscript received by ASME Applied Mechanics Division on October 11, 1950.

[4] Numbers in parentheses refer to the Bibliography at the end of the paper.

form parameter and appear to be more successful. However, these analyses still involve unjustifiable assumptions concerning the boundary shear stress.

During the course of a study of diffuser flow (6, 7, 8), in connection with the design of a large water tunnel (9), a superposition method of analysis was developed. This method assumes that the form of the velocity profile is the result of two effects, one associated with the wall shear stress and the other with the pressure recovery. Besides yielding an equation which approximates measured velocity profiles, the theory leads to a more reasonable expression for the wall shear-stress coefficient.

Rationale

A boundary layer is the result of the diffusion of shearing motions into the flowing stream from the boundary surface where they originate. These motions are carried downstream as they diffuse outward, so that at any station, the flow conditions are a function of the previous history of the flow as well as the local conditions. For the case of flow with zero or small pressure gradients, the velocity function and the wall shear stress do not vary significantly in the direction of flow, and one can correlate the turbulence, and hence the shear and velocity distributions, with local conditions. However, when the flow conditions vary, as in a diffuser or along an airfoil surface, this simple correlation does not hold. In this case, motions in the outer boundary-layer region are governed by the previous history of the flow, while near the solid surface, local conditions control. Thus one is led to the concept that the outer shape of the velocity profile is associated with the space history, while the inner shape is associated with the local wall shear stress.

A study of the velocity distributions measured by Nikuradse (10), Fig. 1, reveals the existence of two regions in which the form of the velocity distributions are different. In the region near the wall the velocity curves for the eight convergences and divergences are functionally similar, while in the outer regions the curves become linear with markedly different slopes. These slopes are greater for the larger angles of divergence. The same general characteristics were observed in the experimental diffuser studies (7) carried out in connection with the water-tunnel design, as may be seen in Fig. 2. It seems logical, therefore, to

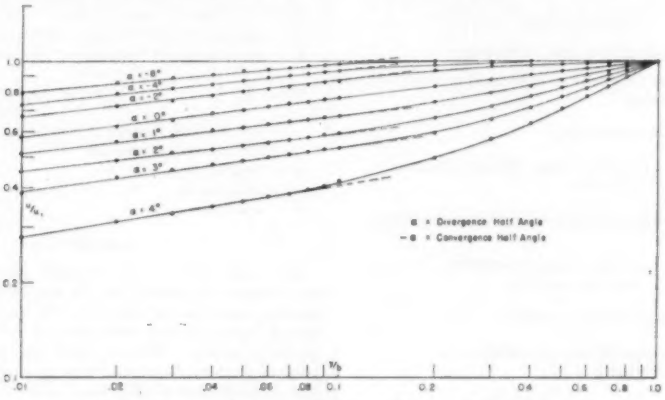

Fig. 1 Nikuradse's Results Plotted on Log-Log Co-Ordinates

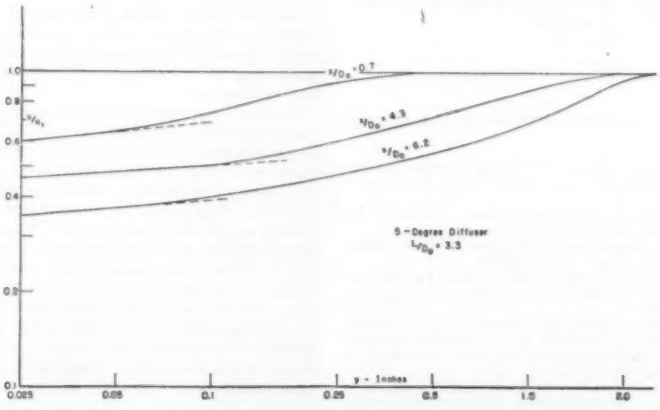

Fig. 2 Measured Velocity Profiles in 5-Deg Conical Diffuser, Preceded by an Entrance Length of 3.3 Diam

treat the general case involving a pressure gradient as a superposition of a frictional velocity distribution and an additional term. The frictional term should have the same form as it has for the case of negligible pressure gradient, while the other term should depend on the pressure gradient and pressure regain. Thus the idea of superposition leads to an equation for the velocity distribution of the form:

$$u = u_{friction} + u_{pressure} \quad [1]$$

That this approach leads to useful conclusions is shown by the fact that when the straight channel velocity distribution ($\alpha = 0$) is subtracted from the velocity distributions obtained by Nikuradse, Fig. 1, in expanding channels the remaining "pressure terms" are approximately linear functions of the distance from the wall.

For limited ranges of Reynolds numbers the friction term can be approximated by a power law; but, in order to make the expression more general, and to obtain better applicability at the higher Reynolds numbers, the Prandtl-von Kármán logarithmic relation is used. A study of Fig. 1 suggests that the effective maximum velocity for the friction component differs from the actual maximum velocity of the boundary layer. The effective value for divergences is less than u_1 and decreases with increasing angle of divergence, while, for convergences, the opposite conditions apply. Calling the effective maximum velocity u_1', the friction velocity term may be written

$$u_{friction} = u_1' + \frac{u_*}{\kappa} \ln \frac{y}{\delta} \quad [2]$$

where the turbulence constant κ, has the value of 0.40, and u_* is the square root of the kinematic wall shear stress

$$u_* = \sqrt{\frac{\tau_0}{\rho}} = u_1 \sqrt{\frac{c_f}{2}} \quad [3]$$

The form of the pressure term could be taken as a general power series; however, analysis of Nikuradse's data shows that the effect is predominantly linear and is zero at the wall. The pressure term is expressed as

$$u_{pressure} = A\, u_1 \frac{y}{\delta} \quad [4]$$

Combining Equations [2], [3], and [4], the general equation for the velocity distribution is

$$\frac{u}{u_1} = \frac{u_1'}{u_1} + \frac{1}{\kappa} \sqrt{\frac{c_f}{2}} \ln \frac{y}{\delta} + A \frac{y}{\delta} \quad [5]$$

This equation contains three coefficients which must be evaluated. The coefficient of the logarithmic term depends upon the wall shear-stress coefficient, which is discussed in the next section. The other two coefficients are functions of the pressure and are related. The local velocity must equal the maximum velocity when $y = \delta$, hence

$$1 = \frac{u_1'}{u_1} + A \quad [6]$$

Taking A as the pressure component parameter, Equation [5] can be written

$$\frac{u}{u_1} = 1 - A + \frac{1}{\kappa} \sqrt{\frac{c_f}{2}} \ln \frac{y}{\delta} + A \frac{y}{\delta} \quad [7]$$

In this equation the value of the parameter A indicates the relative influence of the pressure on the velocity distribution. Its value ranges from zero for negligible pressure effect to nearly unity. When A is zero, the expression reduces to the usual logarithmic velocity law.

Wall Shear Stress

The principle of superposition leads to a method of evaluating the wall shear stress in terms of standard relations. As previously noted, the flow near the wall is governed by the effective maximum velocity u_1' rather than the actual maximum velocity u_1. Therefore the wall shear stress is expressed by the relation

$$\tau_0 = c_f'\, {}^1/_2\, \rho u_1'^2 = \frac{c_f'}{2} \rho u_1^2 (1 - A)^2 \quad [8]$$

where c_f', is the effective wall shear-stress coefficient, which is independent of the pressure effects. If Equation [8] is compared with the usual definition of the wall shear-stress coefficient c_f, there results the following relation for c_f

$$c_f = c_f' (1 - A)^2 \quad [9]$$

The value of c_f' may be obtained from any one of the usual formulas for the skin friction, by using u_1' instead of u_1 in evaluating the Reynolds number of the boundary-layer thickness (expressions involving R_x are inapplicable). Thus the Squire and Young (11) relation becomes

$$c_f' = [4.16 \log_{10} (4.075\, R_\theta')]^{-2} \quad [10]$$

where $R_\theta' = u_1'\theta/\nu$ is the Reynolds number, defined in terms of the momentum thickness and the effective velocity.

A rough check of the validity of Equation [9] was made by use of the data obtained at the National Bureau of Standards on the shear distribution in a boundary layer on the suction surface of a simulated airfoil (12). The comparison between the experimental wall shear-stress determinations, the Squire and Young

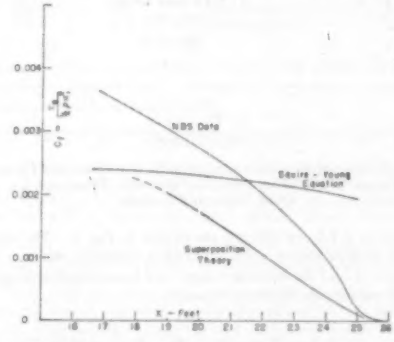

Fig. 3 Comparison of Superposition-Theory Wall Shear-Stress Predictions With NBS Measurements

relation with R_θ computed from u_1, and the superposition theory is shown in Fig. 3.[5] The superposition-theory curve has the same form as the experimental curve, but the magnitudes are about 40 per cent too low. As the experimental values were obtained by extrapolating hot-wire data, they may contain a systematic error.[6] That this may be so can be seen from the

[5] In obtaining the superposition-theory curve, A was estimated from the experimental values of H using an expression obtained from the velocity distribution Equation [8]. The values of c_f', needed in this expression, were evaluated with the aid of Equation [10].

[6] Another possible explanation of this disagreement is that surface roughness may have been sufficient to influence the wall friction.

fact that at the 17-ft station, the pressure gradient is zero, and the Squire and Young relation should give the correct coefficient. In any case, it is seen that the superposition theory is superior in predicting the form of the variation of wall shear stress.

Comparison With Velocity Profiles

The primary test of the superposition theory lies in its comparison with measured velocity profiles. For this purpose, three of the traverses obtained in the diffuser studies (7) at various

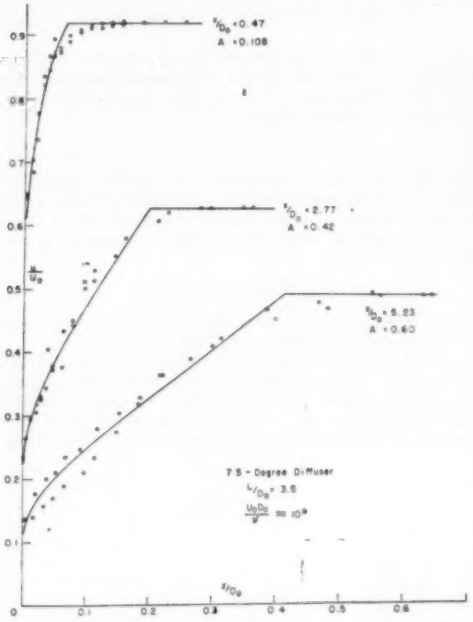

Fig. 4 Comparison of Superposition-Theory Velocity Profiles With Those in a 7.5-Deg Conical Diffuser, Preceded by a 3.5 Diam Entrance Length

locations in a 7.5-deg diffuser are shown in Fig. 4. The superposition profiles shown were obtained by suitable choice of the parameter A and the boundary-layer thickness δ for introduction into the velocity-distribution equation

$$\frac{u}{u_t} = 1 - A + \frac{1 - A}{\kappa}\sqrt{\frac{c_f'}{2}}\ln\frac{y}{\delta} + A\,\frac{y}{\delta} \quad \ldots\ldots [11]$$

Although there are some small systematic divergences, the theory is seen to yield a good fit to the experimental points. The greatest divergence occurs at the outer edge of the boundary layer, where the equation yields a sharp termination to the layer. This discrepancy is also characteristic of most velocity-distribution laws for zero pressure gradient. As equally good agreement is obtained in fitting Nikuradse's data, the superposition theory appears to yield a satisfactory expression for the velocity profiles in both two and three-dimensional diffusers.

Empirical Relations for A

This superposition theory does not yield an analytic expression for A in terms of the boundary-layer flow conditions, and it is thus necessary to obtain empirical relations. Using the data from the diffuser studies (8), one such relation has been obtained for conical diffuser flow. In these tests the pressure and velocity conditions were measured at several stations in 5, 7.5, and 10-deg diffusers preceded by 3.5, 6.3, and 10.3-diam effective lengths of straight pipe. The range of entrance-pipe Reynolds numbers was 0.5 to 2.5 $\times$ 10^5. As the parameter A is the coefficient of the pressure term, it appeared logical to correlate its values with the pressure recovery in the diffuser, expressed as the coefficient

$$C_p = \frac{p - p_0}{\frac{1}{2}\rho\, U_0^2}$$

It was found that A is also a function of both diffuser angle and entrance conditions, these two factors having equal influence; the best correlation of data was found using the product of these two factors to the 0.37 power. Fig. 5 is a plot of the experimental values of A, divided by $[(L/D_0)\beta]^{0.37}$ as a function of C_p. Values of A for all Reynolds numbers were averaged, as no systematic variation with this factor could be found. The final scatter was still about 10 per cent of the average values, and the scatter of the average values about the curve in Fig. 5 is somewhat larger than desired.

The data shown in Fig. 5 suggest that it is not the local pressure gradient, but the cumulative effect of the pressure gradient, which governs the shape of the velocity profile. As C_p is determined by the diffuser-diameter ratio and the pressure efficiency, and, as the latter does not vary greatly, A can be correlated directly with the diffuser geometry. Therefore, $A/[(L/D_0)\beta]^{0.37}$ is plotted as a function of the area ratio in Fig. 6. This plot may be used to estimate A when the pressure coefficient is not known.

To confirm for two-dimensional diffuser flow the variation in A, shown in Fig. 6, the values of A determined from Nikuradse's tests have also been plotted. As β is proportional to the pressure gradient in a three-dimensional diffuser, an analysis of the pressure gradients in two and three-dimensional diffusers indicates that β/D_0 should be replaced by $\alpha/(2b_0)$ for two-dimensional diffusers. The value of L/b_0 was estimated to be about 3 from the geometry of Nikuradse's apparatus. The plotted points are seen to follow the same curve as do the other data.

Separation

The main objective of an analysis of the development of a boundary layer in an adverse pressure gradient is the prediction of the occurrence of separation. The value of the parameter A forms a convenient indicator of the proximity of separation. A study of Equations [9] and [11] suggests that at separation A is close to unity. Thus for $A = 1$, Equation [9] yields a wall friction coefficient of zero, and Equation [11] gives a linear velocity profile with zero apparent wall velocity. These two conditions are characteristic of incipient separation.

In certain of the diffuser tests (7), incipient separation was noted near the ends of the diffusers. The observations and corresponding values of A are summarized in Table 1, where it is seen that separation was not noted for A below 0.74 and was noted for A above 0.83. A good criterion for incipient separation is therefore $A = 0.8$. A review of Nikuradse's work indicates that separation occurred for approximately the same value in his experiments, although some asymmetry was noted for lower values of A.

Applications and Limitations

The superposition theory for the velocity distributions of turbulent boundary layers in adverse pressure gradients is based

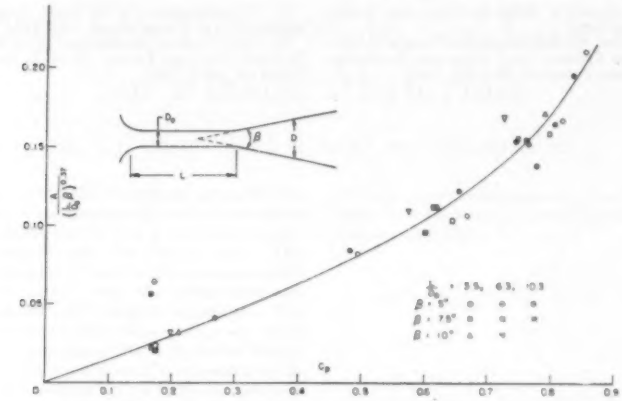

FIG. 5 BOUNDARY-LAYER PARAMETER AS A FUNCTION OF PRESSURE COEFFICIENT, PIPE-ENTRANCE LENGTH, AND DIFFUSER ANGLE

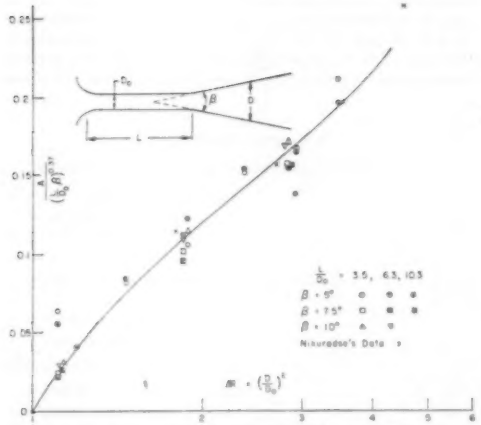

FIG. 6 BOUNDARY-LAYER PARAMETER AS A FUNCTION OF DIFFUSER-AREA RATIO, PIPE-ENTRANCE LENGTH, AND ANGLE

on the concept that a pressure term is added to the effective flat-plate velocity distribution. This theory yields an adequate expression for the velocity profiles and depicts the variation in the wall shear stress. An empirical relation has been found for the variation of A, the coefficient of the pressure component, in diffuser flow. With the momentum equation, this analysis should enable one to predict the flow conditions in a diffuser and to determine the likelihood of separation.

The superposition theory is limited in its usefulness as it does not derive from considerations of the details of the actual turbulent motions. Thus the derivatives of the velocity profiles lead to unreasonable variations in the shear stress and the mixing length across the boundary layer. While giving the general form of velocity distributions, the superposition equation does not in itself lead to a method for the determination of the basic parameter. The empirical relations for each of the various applications may have to be determined separately. Thus, in its present state, the superposition theory appears to be only a useful interim approach.

TABLE 1 INCIPIENT SEPARATION

Run	R_0	Comments	A
7½-deg diffuser	$L/D_0 = 10.4$	$D/D_0 = 1.68$	$AR = 2.83$
M93	0.8×10^6	Slightly unsymmetrical	0.80
D73	1.2	Normal	0.81
M90	1.2	Slightly unsymmetrical	0.68
M71	1.5	Just separated	0.74
P2	1.5	Normal	0.83
D74	1.95	Normal	0.77
P3	2.0	Normal	0.82
M91	2.05	Normal	0.74
10-deg diffuser	$L/D_0 = 6.4$	$D/D_0 = 1.68$	$AR = 2.83$
E39	0.5×10^6	Normal	0.71
E40	0.5	Almost separated	0.82
E41	0.85	Just separated	0.88

BIBLIOGRAPHY

1 "A Method of Calculation for the Turbulent Boundary Layer With Accelerated and Retarded Basic Flow," by A. Buri, thesis No. 652, 1931, Federal Technical College, Zurich, Switzerland; Trans. in RTP Translation No. 2073, British Ministry of Aircraft Production.

2 "Die Turbulente Reibungsschicht in Ebener Strömung bei Druckabfall und Druckanstieg," by E. Gruschwitz, *Ingenieur-Archiv*, vol. 2, 1931, pp. 321–346.

"The Process of Separation in the Turbulent Friction Layer," by E. Gruschwitz, *Zeitschrift für Flugtechnik und Motorluftschiffahrt*, vol. 23, June 14, 1932, pp. 308–312. Trans. in NACA Technical Memo 699, 1933.

3 "On the Separation of Turbulent Boundary Layers," by H. Peters, *Journal of the Aeronautical Sciences*, vol. 3, 1935, pp. 7–12.

4 "Determination of General Relations for the Behavior of Turbulent Boundary Layers," by A. E. von Doenhoff and N. Tetervin, NACA Report No. 772, 1943.

5 "The Development of Turbulent Boundary Layers," by H. C. Garner, British ARC R&M No. 2133, 1944.

6 "Water Tunnel Diffuser Flow Studies—Part I—Review of Literature," Ordnance Research Laboratory Report, Serial No. NOrd 7958–139, May 16, 1949.

7 "Water Tunnel Diffuser Flow Studies—Part II—Experimental Research," Ordnance Research Laboratory Report, Serial No. NOrd 7958–143, July 8, 1949.

8 "Water Tunnel Diffuser Flow Studies—Part III—Analytical Research," Ordnance Research Laboratory Report.

9 "Hydrodynamic Design of the 48-Inch Water Tunnel at The Pennsylvania State College," by D. Ross, J. M. Robertson, and

R. B. Power, Trans. The Society of Naval Architects and Marine Engineers, vol. 56, 1948, pp. 5–29.

10 "Untersuchungen über die Strömungen des Wassers in Konvergenten und Divergenten Kanalen," by J. Nikuradse, *Forschungsarbeiten des Vereines Deutscher Ingenieure*, Heft 289, 1929.

11 "The Calculation of the Profile Drag of Airfoils," by H. B. Squire and A. D. Young, British ARC R&M No. 1838, 1938.

12 "Some Recent Contributions to the Study of Transition and Turbulent Boundary Layers," by H. L. Dryden, NACA Technical Note 1168, April, 1947.

Pressure Distribution in the Calendering of Plastic Materials

By J. T. BERGEN[1] and G. W. SCOTT, JR.,[1] LANCASTER, PA.

In the calendering, or rolling, of a plastic material into sheet form by passing it between parallel rolls, hydrostatic pressure is exerted against the surface of the roll throughout the region of contact with the plastic mass. This pressure has been measured by means of a pressure-sensitive cylinder, inserted in the body of a 10-in-diam roll, together with high-speed oscillographic technique. The materials which were calendered consisted of a resin which exhibited flow properties characteristic of a viscous liquid, and several filled plastic compositions of commercial interest. Pressure maxima ranging up to 8000 psi were observed. Comparison of experimental results with theoretical expressions for pressure distribution, as given by several authors, indicates that the equation derived by Gaskell quite satisfactorily predicts the results for the case of the viscous liquid. The commercial plastics were found to exhibit pressure-distribution characteristics which were perceptibly different from those of the viscous liquid. Certain limitations of Gaskell's treatment of nonviscous materials prevent its application to these experimental results.

Nomenclature

The following nomenclature is used in the paper:

R = roll radius
U = peripheral roll speed
$2l_0$ = roll separation
$\delta = \sqrt{2l_0/R}$
ρ = length of arc subtended by some angle θ
$\xi = x/\sqrt{2Rl_0}$
μ = viscosity coefficient
τ = shear stress

Subscripts:

L = entrance of calender "wedge"
1 = point of maximum pressure
E = exit of calendered sheet

Introduction

THE term "calendering" is taken to denote the process of forming a mass of plastic material, of indefinite shape, into a sheet by passing it between parallel rollers rotating in opposite directions. A similar process is that denoted as "milling," in which the sheet of plastic material is allowed to wrap around either or both rolls so that it is passed between them repeatedly. A recent comprehensive survey of the machinery employed for these processes is given by Kullgren (1).[2] The process is illustrated in Fig. 1.

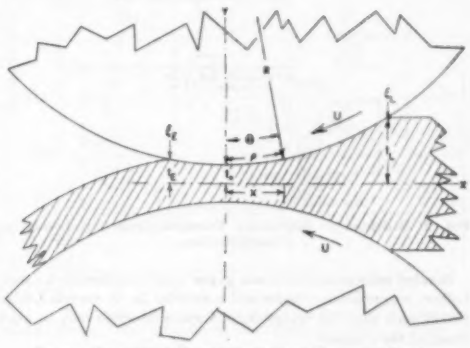

FIG. 1 GEOMETRIC CONFIGURATION OF CALENDER ROLLS

The rolls are presumed to be of great length with respect to the distance $2l_0$ between them. Their rotation causes a thin wedge of the plastic material to be drawn between them with a compressive force which commences at the boundary l_L corresponding to x_L. After passing through the minimum clearance between the rolls, the material continues to occupy the gap between them for some distance x_E, finally leaving the rolls as a continuous sheet with a thickness equal to $2l_E$.

This idea of the calendering process, taken from Gaskell (2) presumes essentially that the material behaves as a viscous liquid, or at least that viscous flow plays a major role in the origin of forces developed in the calender nip. Gaskell arrives at an analytical expression for the pressure against the roll surface as a one-dimensional function of the co-ordinate x, Fig. 1. It has been possible to measure this pressure distribution experimentally[3] both for a material which appears to be a viscous liquid and for several plastic materials which are of commercial importance. These experimental results are compared with Gaskell's theory which is cited, and certain characteristics of the behavior of the plastic materials are noted.

Experimental Apparatus

The method employed to measure the pressure exerted against the roll surface by the plastic mass corresponds in principle to that used by Lueg (3) to measure the forces encountered in the rolling of metals. A pressure-sensitive device was inserted in the roll body in a manner illustrated in Fig. 2. The force acting upon

---

[1] Research Laboratories, Armstrong Cork Company.

Contributed by the Applied Mechanics Division and presented at the Annual Meeting, New York, N. Y., November 26–December 1, 1950, of THE AMERICAN SOCIETY OF MECHANICAL ENGINEERS.

Discussion of this paper should be addressed to the Secretary, ASME, 29 West 39th Street, New York, N. Y., and will be accepted until April 10, 1951, for publication at a later date. Discussion received after the closing date will be returned.

NOTE: Statements and opinions advanced in papers are to be understood as individual expressions of their authors and not those of the Society. Manuscript received by ASME Applied Mechanics Division, May 19, 1950. Paper No. 50—A-34.

[2] Numbers in parentheses refer to the Bibliography at the end of the paper.

[3] This research was carried out in conjunction with a project which was completed by Gaskell and other members of the staff of Brown University and was sponsored by the Armstrong Cork Company.

the area m is proportional to the electric signal carried through the slip rings to suitable amplifying and recording equipment.

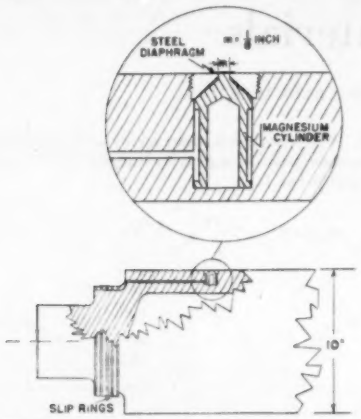

FIG. 2 METHOD OF MOUNTING PRESSURE-SENSITIVE INSERT IN CALENDER ROLL

Bonded resistance-wire strain gages[4] were mounted on a small, hollow, magnesium cylinder and connected in an electric bridge circuit such that the bridge output was a function only of axial strain of the cylinder.

The bridge output was filtered, amplified through a two-stage amplifier, and impressed upon one of the galvanometers of a photographic recording magnetic oscillograph.[5] Null balance was obtained by connecting resistance and capacitance components in parallel with suitable arms of the bridge. The cylinder was calibrated prior to insertion into the roll cavity by applying axial dead-weight load in a vertical jig, noting the deflection of the galvanometer. Upon mounting the cylinder in the roll body, a static load was applied through a lever arm and small rubber pad resting upon the shim-steel diaphragm. By varying the equilibrium roll temperature the temperature-response curve of the pressure-sensing cell was established.

Timing of the oscillograph trace was accomplished conveniently by referring to the 1000-cycle per second (cps) carrier wave, which was found upon comparison with the 60-cycle line frequency to be accurate within 2 or 3 cycles per sec. In order to relate the timing lines to some point in a fixed co-ordinate system, a switch was caused to trip at the instant the center of the pressure cell passed the plane of roll centers. This induced an interruption of the trace of a second galvanometer which furnished a reference point from which to measure time, and thus distance, on the pressure trace. Knowing the speed of rotation of the roll, it was possible, by counting peaks of the carrier wave of the oscillograph trace, to relate the observed pressure to the corresponding distance along the roll arc from the plane of roll centers.

It is desirable to measure pressure as a function of the distance x in Fig. 1, whereas the method just described yields pressure as a function of ρ in Fig. 1. It is evident from the figure that

$$x = [R - (t - t_0)] \sin\theta \cong R \sin\theta; \quad \rho = R\theta$$

since in the first expression $(t - t_0) \ll R$. In these experiments θ is never larger than about 0.2 radians, and the assumption that $\sin\theta = \theta$ introduces a maximum error of less than 1 per cent. Therefore x is taken to be equal to ρ in reporting experimental data.

Roll speed was determined by means of a recording tachometer calibrated daily with a revolution counter and stop watch. Roll temperature was measured with a surface pyrometer which could be read to 1 F. The accuracy of the pyrometric system was established by cooling the roll slowly until a haze of dew appeared on its surface; the pyrometer reading agreed with the psychrometrically determined dew point within 1 F. Likewise the roll was heated slowly until a thin band of wax, previously frozen onto the roll surface, was observed to melt and become transparent. The temperature at which the wax was observed, by means of the surface pyrometer, to melt on the roll agreed within 2 F with the capillary melting point of 170 F.

Roll separation $2l_0$ was determined by passing rubber stock through the rolls in such a way that a portion of the length of roll was unoccupied by the stock. A short length of solder wire was passed through the section of the calender unoccupied by the stock. The thickness of the solder measured with a dial micrometer was taken to be equal to $2l_0$ and was reproducible to ± 0.001 in.

EXPERIMENTAL PROCEDURE

Upon establishment of desired temperature, roll speed, and roll separation, the plastic material in question was introduced to the calender in the form of sheets, layers of sheets or granules, or was allowed to wrap around one or both of the rolls as in the milling process. When the calendering process appeared to be stable, usually after the first revolution or so of sheet rolling, or within 5 or 10 sec after forming the "wrap" when milling, three or more pressure traces were obtained for successive rotations of the roll. These traces were found to agree within experimental error if sufficiently stable conditions of calendering had been established. Upon completion of the oscillograms the sheet was removed from the rolls if necessary, and the roll temperature was checked. Owing to the short duration of the test, the roll temperature was found not to increase more than about 3 or 4 F in the worst case, and usually the change was less than 1 F.

The different roll temperatures and roll separations used for the various materials examined were chosen to enable the material to be calendered under conditions approaching those used commercially, and to obtain pressure within the range defined by the limitations of the experimental equipment.

A typical oscillographic trace is shown in Fig. 3. The amplitude of the nth cycle of the carrier wave was measured to ± 0.01 in. for successive values of n, taking n to be zero at the instant of interruption of the auxiliary trace. Wave amplitude was expressed as pressure by means of the pressure-cell calibration described previously. The distance x from the plane of roll centers ($n = 0$) may be computed by means of the relationship

$$x = \frac{Un}{1000}$$

The peripheral roll speed U is denoted by suitable units, and positive values of x lie to the right of $n = 0$ in the figure. Further, x is most conveniently expressed in the dimensionless form used by Gaskell (2)

$$\xi = x/\sqrt{2Rl_0}$$

Owing to the small increments in ξ between successive cycles, the data are virtually continuous, and individual points are not

[4] SR-4, Type CB-11, manufactured by Baldwin Locomotive Works, Philadelphia, Pa.

[5] Type PA, manufactured by Westinghouse Corporation, Pittsburgh, Pa.

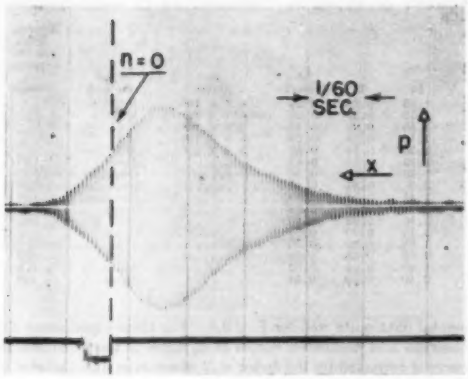

FIG. 3 TYPICAL OSCILLOGRAM OF PRESSURE DISTRIBUTION IN CALENDERING A VISCOUS LIQUID
(Experiment No. 4.)

indicated in the graphical pressure-distribution curves presented in this paper.

PRESSURE DISTRIBUTION IN CALENDERING OF A VISCOUS LIQUID

The material chosen to represent a viscous liquid was a plasticized thermoplastic resin. The flow properties were examined by means of a coaxial falling-cylinder viscometer described by Traxler and Schweyer (4) for the purpose of measuring the flow properties of asphaltic bitumens. The relationship of shear rate to shear stress was linear over the range 0–10 psi with a viscosity, at 95 F, computed to be 3.2×10^9 poises. This material was allowed to band onto the calender rolls so that it was milled in the sense previously described. Upon adjusting the conditions of calendering suitably, the pressure distribution was recorded oscillographically. The results are given in Fig. 4, where p is expressed as a function of the dimensionless length ξ.

Included in the figure are the solutions of the expressions for pressure distribution given by Gaskell (2), Ardichvili (5), and Eley (6), which are as follows, referring to Fig. 1 for notation

Gaskell

$$p = \frac{3\mu U}{4t_0\delta}\left\{\left[\frac{-1+\xi^3-5\xi_1^2-3\xi_1^3\xi^2}{(1+\xi^3)^2}\right]\right.$$

$$\left.\xi - \left(\frac{1+3\xi_1^2}{1+\xi_1^2}\right)\xi_1 + (1-3\xi_1^2)(\tan^{-1}\xi + \tan^{-1}\xi_1)\right\} \quad \ldots [1]$$

Ardichvili

$$p' = 4\mu U\sqrt{R}\,\frac{\sqrt{t-t_0}}{t^2} \quad \ldots [2]$$

Eley

$$p'' = 8\mu U\tan\theta/t^2 \quad \ldots [3]$$

The latter two equations were transformed from terms in t into terms in ξ by the approximation pointed out by Gaskell

$$t = t_0(1+\xi^2)$$

If we assume as a further approximation that $R - (t - t_0) \cong R$, it follows from simple geometric considerations that the equations of Ardichvili and Eley may be reconciled so that

$$p'/p'' = R/2\sqrt{2}$$

For a given radius of the rolls, these solutions thus differ only by a constant factor. In Fig. 4 the two curves are rendered identical merely by choosing two different values of μ so that the calculated and experimental values of maximum pressure agree.

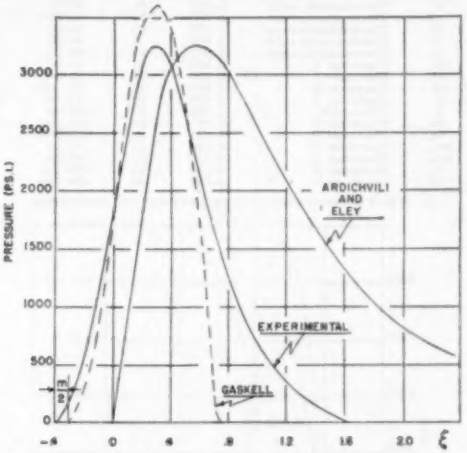

FIG. 4 PRESSURE DISTRIBUTION FOR CALENDERING A THERMOPLASTIC RESIN, COMPARED WITH SOLUTIONS OF SEVERAL EQUATIONS

The viscosity μ for the Gaskell equation was chosen so that the solution for $\xi = 0$ yielded a value of p identical with the corresponding experimental value. The curve in this region is sufficiently linear to render the average value of pressure, observed experimentally, very nearly equal to the mathematical point value. This viscosity is termed for convenience the "effective" viscosity μ_e. Likewise, the observed value of ξ_1, for which p is a maximum, was used as the second parameter in the Gaskell equation.

The Gaskell equation appears to represent the experimental data quite satisfactorily for $\xi < 0.6$. It will be noted that the observed value of ξ_E (exit plane) is about 0.1 greater than the computed value. This is almost exactly the error pointed out by Lueg (3) being equal to $m/2$, where m is the diameter of the pressure-diaphragm (equal to 0.25 in terms of ξ). Applying this correction, we find that $\xi_1 = \xi_E$ experimentally as predicted by the Gaskell equation.

The divergence of the Gaskell equation from observed data for $\xi > 0.6$ lies in the fact[5] that no rational choice for ξ_1 may be deduced from physical considerations. In Equation [1], ξ_1 is found merely to be one of the roots for $p = 0$, and hence does not represent an arbitrary boundary value.

In Table 1 appear values of μ_e for the viscous liquid which range between 10^9 and 10^8 poises. These values differ appreciably from the viscosity coefficient computed from data obtained with the Traxler viscosimeter as 3.2×10^9 poises. This discrepancy may be better understood when it is noted that the maximum shear rate encountered in the calender may be 10^7 times that obtained in the viscometer. The curvature of the rheological diagram may be quite pronounced over such a range of shear rate.

In Fig. 5 appear the pressure-distribution curves for several values of roll separation, $2t_0$. In each case the solution of the Gaskell equation (shown by dashed lines) represents the experi-

[5] Pointed out by Gaskell, private communication.

TABLE 1 SUMMARY OF EXPERIMENTAL DATA FOR MEASUREMENT OF PRESSURE DISTRIBUTION IN CALENDERING OF PLASTICS

Experiment no.	Material	$2h_0$, in.	U ips	Roll temp., deg F (1)[a]	Stock temp., deg F	ξ_L	ξ_1	ξ_E ($-m/2$)	μ_0, poises	Feed method	Approx. filler per 100 parts of resin
10	Thermoplastic resin	0.035	10	80/80	...	1.63	0.28	0.29	4.7×10^5	Mill	...
4	Thermoplastic resin	0.050	10	80/80	...	1.50	0.30	0.30	4.4×10^5	Mill	...
13	Thermoplastic resin	0.075	10	80/80	...	1.50	0.32	0.32	2.8×10^5	Mill	...
5	Thermoplastic resin	0.050	5	80/80	...	1.50	0.28	0.29	9.9×10^5	Mill	...
6	Thermoplastic resin	0.050	20	80/80	...	1.50	0.29	0.29	1.8×10^5	Mill	...
27	Elastomer L	0.050	20	80/80	80	1.38	0.30	0.45	.....	Sheet	180
42	Elastomer L	0.050	20	80/140	80	1.80	0.32	0.36	.....	Granules	180
46	Elastomer L	0.035	20	80/140	80	2.0	0.34	0.40	.....	Granules	180
47	Elastomer L	0.075	20	80/140	80	1.45	0.31	0.30	.....	Granules	180
51	Filled resin	0.050	20	120/80	200	1.8	0.16	0.38	.....	Sheet	300
36	Elastomer V	0.025	20	200/200	...	3.50	0.32	0.40	.....	Mill	110
88	Elastomer V	0.025	20	200/200	200	1.35	0.20	0.28	.....	Sheet	110
201	Elastomer N	0.040	20	100/80	...	1.85	0.32	0.30	.....	Mill	225
204	Elastomer N	0.040	20	100/80	80	2.65	0.38	0.36	.....	Sheet	225
71	Elastomer P	0.035	20	180/130	80	1.85	0.20	0.32	.....	Mill	120
74	Elastomer P	0.035	20	180/130	...	3.40	0.50	0.51	.....	Sheet	120

[a] (1) Refers to temperature of forward and rear roll, respectively.

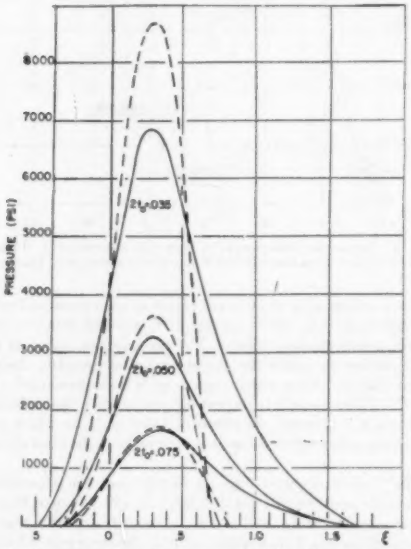

FIG. 5 EFFECT OF ROLL SEPARATION $2h_0$ UPON PRESSURE DISTRIBUTION IN CALENDERING A THERMOPLASTIC RESIN (Computed curve is represented by the dashed line.)

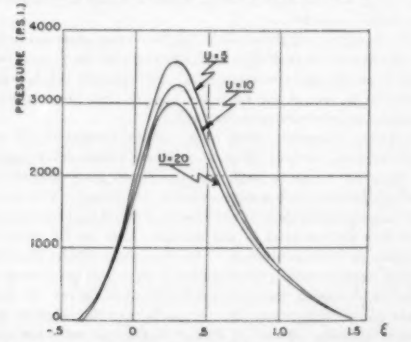

FIG. 6 EFFECT OF ROLL SPEED U ON PRESSURE DISTRIBUTION IN CALENDERING A THERMOPLASTIC RESIN

mental data quite well for $\xi < 0.6$. For these experiments the observed and calculated values of ξ_E agree if the experimental curve is corrected by the factor $m/2$ where m is the diameter of the pressure diaphragm.

The increasing discrepancy in maximum pressure between the observed and calculated curves as $2h_0$ becomes smaller may be attributed to the fact that the cell used to measure pressure actually integrates and averages the pressure exerted on the thin steel diaphragm. At ξ_1, where p passes through a maximum, the observed pressure should be less than the computed pressure because of this effect. The discrepancy should diminish as $2h_0$ is made larger, since the diameter of the diaphragm in terms of ξ is an inverse function of t_0.

Also, according to Equation [1] the pressure is a direct function of U, the peripheral speed of the roll. The observed pressure-distribution curves, Fig. 6, covering a fourfold range of U, actually exhibit a slightly diminishing pressure with increasing U. The entrance ξ_L and exit ξ_E remain remarkably constant as does the shape of the curve. Evidently the combined coefficient μU in Equation [1] plays the role of a constant [viz. Ardichvili (5)], with the viscosity diminishing in proportion to increased speed, due no doubt to higher temperature associated with greater energy dissipation as U is increased. The effect of energy dissipation upon the pressure-distribution curve has been considered by Finston.[7] He found that, for the region between ξ_1 and ξ_E, the distortion of the curve by localized thermal effects was slight.

EFFECT ON PRESSURE DISTRIBUTION OF ADDING SOLID FILLERS TO A VISCOUS LIQUID

Since the experimental pressure distribution for the viscous liquid previously described was in good agreement with the Gaskell equation for the most part, it was of interest to examine the effect of large additions of solid filler in the amounts met with commercially. Using the same conditions of calendering as for Fig. 4, the pressure-distribution curve in Fig. 7 was obtained. From the experimental values of ξ_1 and t_0 for the filled resin, the theoretical curve from Equation [1] was computed, using the same technique of curve fitting as that employed for Fig. 4. This curve is represented by the dashed line. Finally, the experimental curve for the unfilled resin is included for comparison, being represented by the broken line.

The curve computed from Equation [1] quite obviously fails to agree with the experimental data whereas in the case of the unfilled resin the agreement was acceptable. Likewise of course the curves for the filled and unfilled resins are not alike. Evidently the presence of fillers brings about nonviscous behavior to the extent that the assumptions associated with viscous liquids no longer apply. Whether the departure from viscous behavior

[7] M. Finston, doctoral thesis, Brown University, 1949.

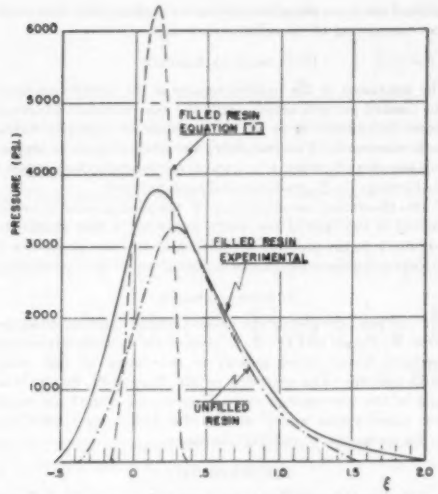

FIG. 7 COMPARISON OF PRESSURE-DISTRIBUTION CURVE IN CALENDERING A FILLED THERMOPLASTIC RESIN WITH THAT OF THE UNFILLED RESIN AND THE CURVE COMPUTED FROM EQUATION [1]

may be attributed to structural viscosity, thixotropy, slip between the material and the roll surface, or thermal effects cannot be stated. It is not likely that the latter effect is appreciable, since it was not found to cause such divergence in the case of the unfilled resin. Unpublished data indicate that the rheological diagram (shear rate as a function of shear stress) is markedly curved. Hence it may be concluded that structural viscosity and slip account for most of the nonviscous behavior of the filled resin.

In the derivation of the hydrodynamic functions for the calendering process the assumption has been made that the plastic mass is incompressible. In order to examine this assumption the following simple experiment was performed:

By means of a steel piston moving within a cylinder, sealed with a thin rubber diaphragm, it was possible to subject a known volume of sample to a pressure of about 150 atm. The results are given in Table 2, together with results for pure compounds.

TABLE 2 COMPRESSIBILITY OF FILLED ELASTOMER COMPARED TO PURE LIQUIDS BETWEEN 40 AND 120 ATMS

Material	—Compressibility ($\Delta V/V$ per atm)— Observed	From Perry*
Distilled water	56×10^{-6}	Ca 46×10^{-6}
Distilled water	56×10^{-6}	Ca 46×10^{-6}
Abstract of ethanol	105×10^{-6}	Ca 86×10^{-6}
Elastomer + wood-flour filler	66×10^{-6}	....
Elastomer + inorganic filler	86×10^{-6}	....

* "Chemical Engineers Handbook," by J. H. Perry, McGraw-Hill Book Company, New York, N. Y., 1950, p. 209.

Since the compressibility even of the material containing wood flour is of the order of magnitude of that of water, it seems justifiable to consider it "incompressible" in the ordinary sense.

PRESSURE DISTRIBUTION IN CALENDERING OF SEVERAL COMMERCIAL FILLED PLASTICS

Plastic materials are often supplied to the calender in the form of granules which are consolidated and rolled out to form a sheet by the calender. The results of a series of experimental determinations of the pressure distribution for such a process are given in Fig. 8. It is to be noted that ξ_1 is practically independent of $2t_0$, although this is not so for ξ_2 and ξ_L. The fit of these data to the Gaskell equation is much less satisfactory than for the viscous liquid (thermoplastic resin), as evidenced by the discrepancy between ξ_1 and ξ_2, Table 1.

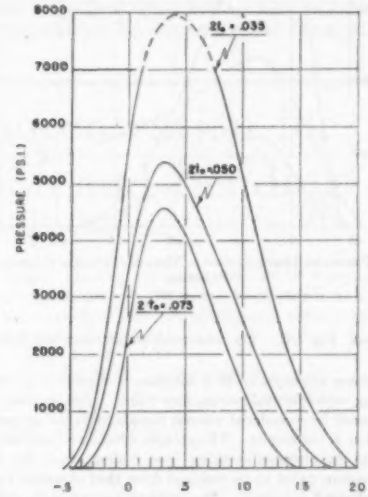

FIG. 8 EFFECT OF ROLL SEPARATION ON PRESSURE DISTRIBUTION IN CALENDERING ELASTOMER GRANULES

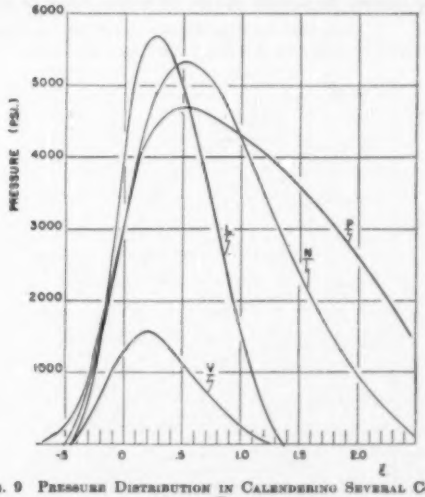

FIG. 9 PRESSURE DISTRIBUTION IN CALENDERING SEVERAL COMPOUNDED PLASTICS

(V = expt. 58; L = expt. 27; N = expt. 204; P = expt. 74. Materials fed as sheets.)

Other compounded elastomers were employed both in the form of sheets which were reduced in thickness, Fig. 9, and in the mill-

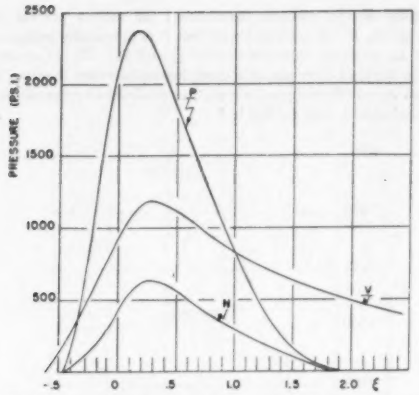

FIG. 10 PRESSURE DISTRIBUTION IN MILLING SEVERAL COMPOUNDED PLASTICS
(V = expt. 36; N = expt. 201; P = expt. 71.)

ing process, Fig. 10. The observed parameters are listed in Table 1.

In all cases attempts to fit a solution of Equation [1] to the data using experimental parameters failed. Hence these materials cannot be considered viscous liquids in so far as pressure distribution is concerned. Thixotropic effects are undoubtedly present, as the repeated shearing upon milling causes the shape of the pressure curve to be changed from that observed for the material sheared only once. The previous history of the samples for more than a few minutes has been ignored in this comparison. The role of thermal effects accompanying energy dissipation, and of slip between the material and the roll surface cannot be distinguished one from the other; the latter undoubtedly does occur in the calendering of viscoelastic materials.

DISCUSSION OF RESULTS

The treatment of the hydrodynamics of the calendering process by Gaskell predicts satisfactorily the experimentally observed pressure distribution in so far as the choice of boundary conditions is concerned. Unfortunately, no rational choice of the entrance boundary ξ_L when $p = 0$ was possible, and a disagreement exists between the ξ_L predicted and that observed.

If the theoretical consideration of calendering were to be reexamined in the light of the results presented in this discussion, an approach to the problem of establishing the flow properties of non-Newtonian materials should lie within the realm of possibility.

ACKNOWLEDGMENT

The authors take pleasure in acknowledging their indebtedness to Prof. W. Prager and Dr. R. E. Gaskell for valuable advice and suggestions which aided greatly in the course of this work. Thanks also are to be extended to Mr. Robert W. Snyder who helped in the construction of equipment and carried out much of the experimental work; and to the Armstrong Cork Company for permission to publish this paper.

BIBLIOGRAPHY

1 "Modern Calender Processing Equipment," by G. V. Kullgren, *India Rubber World*, vol. 120, 1949, pp. 323 and ff.

2 "The Calendering of Plastic Materials," by R. E. Gaskell, Trans. ASME, vol. 72, 1950, pp. 334–336.

3 "Spannungsverteilung und Werkstoffluss in Walzspalt," by W. Lueg, *Stahl und Eisen Jahrg.*, vol. 14, 1933, pp. 346–352.

4 "Measurement of High Viscosity—A Rapid Method," by R. N. Traxler and H. E. Schweyer, Proceedings of the American Society for Testing Materials, vol. 36, 1936, pp. 518–529.

5 "Versuch der rationalen Bestimmungen der Bombierung von Kalanderwalzen," by G. Ardichvili, *Kautschuk*, vol. 14, 1938, pp. 23–25 and 41–45.

6 "Theory of Rolling Plastics. I. Calculation of Roll Pressure," by D. D. Eley, *Journal of Polymer Science*, vol. 1, 1946, pp. 529–534.

Design Data

It is important that the data contained in technical papers be made readily available to designing engineers. In order to satisfy these needs of industry, this section of the Journal includes a concise presentation of data and information drawn chiefly from papers previously published by the Applied Mechanics Division of The American Society of Mechanical Engineers.

Factors of Stress Concentration for Slotted Bars in Tension and Bending[1]

By M. M. FROCHT[2] and M. M. LEVEN[3]

Definition of k

FACTORS of stress concentrations have been determined photoelastically for slotted bars subjected to pure tension and to pure bending. A slot is defined as a rectangle with semicircular ends.

In the curves here presented the factor of stress concentration, k, is defined by the expression

$$k = \frac{\sigma_{\text{maximum in bar}}}{\sigma_{\text{nominal at section through slot}}} \quad [1]$$

Tension. For pure tension

$$\sigma_{\text{nominal}} = P/A$$

where

P = applied axial load

A = net cross-sectional area at transverse section through slot

In the case of pure tension the maximum stress is always found at the roots of the semicircular grooves of the slot.

The curves in Figs. 1 and 2 give k as a function of r/d and h/r.

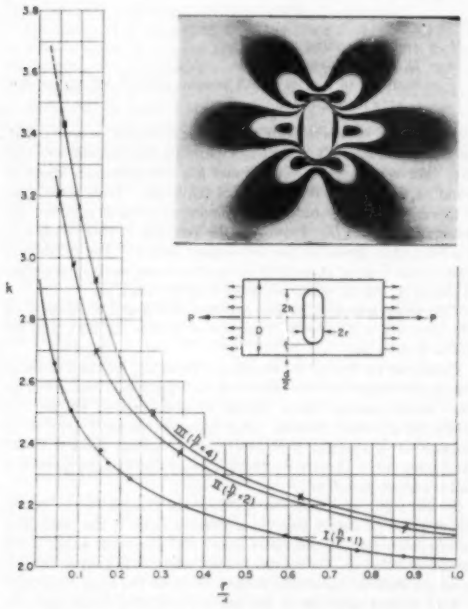

Fig. 1 Slotted Bars in Tension; k Versus r/d

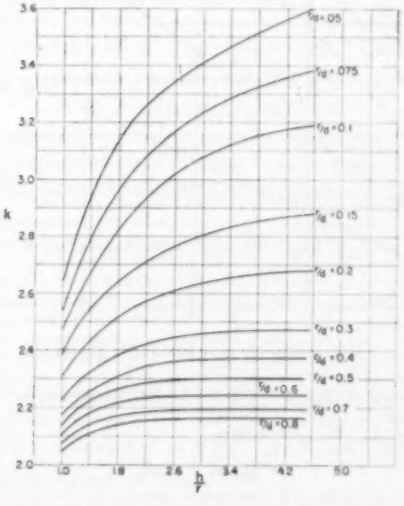

Fig. 2 Slotted Bars in Tension; k Versus h/r

[1] This work was done when both authors were at the Carnegie Institute of Technology, Pittsburgh, Pa.

[2] Research Professor of Mechanics, Illinois Institute of Technology, Chicago, Ill. Mem. ASME.

[3] Westinghouse Research Laboratories, East Pittsburgh, Pa.

Note: Statements and opinions advanced in papers are to be understood as individual expressions of their authors and not those of the Society. Manuscript received by ASME Applied Mechanics Division, July 11, 1950.

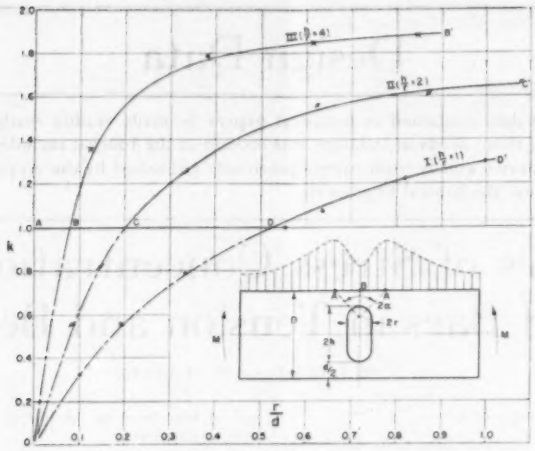

FIG. 3 SLOTTED BARS IN BENDING; k VERSUS r/d

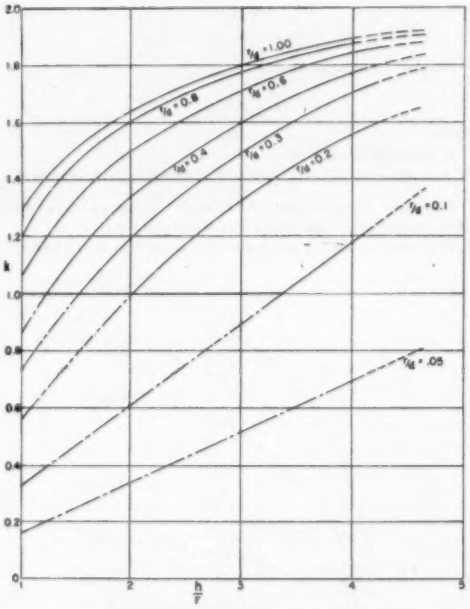

FIG. 4 SLOTTED BARS IN BENDING; k VERSUS h/r

The range of r/d is from 0.05 to 1.0, approximately, for h/r equal 1, 2, and 4.

Bending. For pure bending

$$\sigma_{\text{nominal}} = Mc/I$$

where

M = applied bending moment
$2c = D$, depth of beam, Fig. 3
I = moment of inertia about neutral axis of net transverse area through slot

In using the curves relating to bending it should be noted that the maximum stress is not always found on the boundary of the slot. For certain values of r/d and h/r the maximum stress is found on the straight outer edges of the beam. Tests show that in this case the magnitude of the maximum stress is equal to the nominal stress Mc/I. However, the position of this stress differs from that given by the elementary theory. The maximum stress is not located at point B of the transverse section but rather at points A, Fig. 3, which are defined by the angle α.

This angle seems to be independent of r/d and a function of h/r. For $h/r = 1$, $\alpha = 30°$; for $h/r = 2$, $\alpha = 32° 30'$; and for $h/r = 4$, $\alpha = 35°$.

Comments on Curves for Bending. Referring to the curves in Fig. 3, the values of k corresponding to Equation [1] are given by the "solid" curves which consist of a horizontal branch followed by a curved branch. For example, curve I ($h/r = 1$) consists of a straight part A-D and a curved portion D-D'. Similarly, curve II ($h/r = 2$) consists of the straight part A-C and a curved part C-C'.

If the value of k falls on the straight branch of the curve, where $k = 1$, it means that the maximum stress in the beam is at points A on the extreme outer fiber. On the other hand, if the values of k fall on the curved branch where k is greater than 1, it means that the maximum stresses occur on the roots of the slot.

The dashed portions of the curves, O-B, O-C, O-D, give the values of k_1 which represent the ratio of the maximum stress on the boundary of the slot to the nominal stress in the section through the slot, i.e.

$$k_1 = \frac{\sigma_{\text{maximum on slot}}}{\sigma_{\text{nominal at section through slot}}}$$

For factors of stress concentration greater than one $k_1 = k$.

Discussion

Bending Vibrations of a Pipe Line Containing Flowing Fluid[1]

R. L. Bisplinghoff.[2] The authors should be commended for indicating a relatively simple plan of solution to a problem, which at first glance seems quite complicated. The fact that the significant effects of the internal flow apparently can be expressed by the simple expression of force per unit length of $-\sigma(\partial^2 z)/(\partial x\, \partial t)$ leaves the problem linear and thereby tractable. The power-series approximation of the deformed pipe illustrates how a solution of acceptable accuracy in an engineering problem can be obtained often with less labor by approximate methods than by the classical methods which usually come to one's mind at first. A solution of the Bernoulli-Euler beam equation containing an internal damping term according to Stokes' law also has been discussed by Sezawa in 1927, and more recently by Mindlin, Stubner and Cooper and Stowell, Schwartz and Houboldt. Although this damping term is not the same as that considered by the authors, Sezawa's work indicates a solution to a similar problem.

The last part of the paper, in which the traveling-wave point of view is adopted, is particularly illuminating in that it shows mathematically and discusses physically why standing waves are not possible. This conclusion of course can be drawn tentatively at the outset because of the existence of a damping term in the system. It is interesting to speculate on the importance of adding a term arising from the rotary motion of the fluid. This term, which would be proportional to the time derivative of the rate of change of curvature along the beam, would be of less importance than the term already considered but probably of greater importance than the Sezawa damping term already given considerable attention.

W. H. Hoppmann, 2nd.[3] The authors have presented a study of an interesting problem and have developed a differential equation which appears to have considerable importance for its description. However, the writer wishes to submit an objection to the use of the term "damping," applied to the resistance to vibration caused by change of momentum of the fluid in a direction perpendicular to the length of the pipe. Forces arising from this cause will resist vibrations of the pipe but only because the internal surface of the pipe imposes compressive forces upon the fluid to constrain it to move in the changing direction of the pipe.

It appears that one may consider a damping force, however, because of the relative transverse velocities of the fluid and this force would be given by $\mu\, (\partial^2 Z)/(\partial x\, \partial t)$ where μ is a viscosity coefficient. In this case it would be proper to speak of viscous damping. It is assumed that the authors ignored these forces because they are probably too small for practical consideration.

It is stated that supports are spaced about 66 ft apart and that they are assumed to be of the hinged type. This assumption appears to be reasonable but the writer cannot agree with the treatment of the pipe as if it were only a single span. The frequencies and shapes for each span of a multispan beam are radically different from those of a single span.

It would be very interesting if the authors could find an opportunity to test a model pipe line in a wind tunnel and measure the vibration characteristics when a fluid is flowing through it.

Authors' Closure

The authors wish to express their appreciation to Professors Bisplinghoff and Hoppmann for several most instructive comments and suggestions. It certainly does appear that the importance of viscous-damping, structural-damping, and rotary-inertia terms to solutions of the pipe-line vibration equation should be fully investigated. The latter two effects were considered during detailed analysis of the problem but were omitted in the interests of simplicity and to emphasize what is believed to be the primary influence of the fluid flow.

It is agreed that the word "damping" is perhaps a poor choice to describe the transfer of energy from the pipe motion to the fluid. It was of course used loosely for lack of a better concise term. The authors concur with Professor Hoppmann, who is better qualified than they to write on the subject of multispan beams, that any possible asymmetry of support, inequality of support distance, and so on, will have a severe effect on the mode shapes and frequency. However, it was assumed on the basis of observation that alternate spans moved oppositely to one another and were hinged to the supports. Under these conditions there must be complete antisymmetry and the structural boundary conditions on any one span consist of zero deflection and bending moment at its extremities. This is in analogy with a single simply supported span.

The authors wish to call attention to an error in column 1, page 231, of the original paper: in the first two places where the symbol δ_f appears, its sign should be changed.

A Mechanical Analyzer for Computing Transient Stresses in Airplane Structures[1]

Walter Ramberg.[2] The authors are to be congratulated for extending Dr. Biot's attractive torsion-pendulum analogy to obtain directly the transient response to a forcing function of fixed shape in space (e.g., impact at a fixed point) of a linear elastic system simultaneously in as many as three natural modes. The writer was especially pleased by the ingenious application of wire strain gages to record the forcing function as well as the response.

It is to be hoped that this highly flexible analyzer is to be used in future investigations of transient response. In particular, the writer would be interested in the authors' views on using the analyzer for determining the convergence of the response in terms of the natural modes, and also the response over a long period including several cycles of the fundamental mode. The solution of this latter problem for different cams representing forcing functions of different shape in time and for different rates of rotation

[1] By Holt Ashley and George Haviland, published in the September, 1950, issue of the Journal of Applied Mechanics, Trans. ASME, vol. 72, pp. 229–232.

[2] Associate Professor of Aeronautical Engineering, M.I.T., Cambridge, Mass.

[3] Associate Professor of Mechanical Engineering, The Johns Hopkins University, Baltimore, Md. Mem. ASME.

[1] By R. L. Bisplinghoff, T. H. H. Pian, and L. I. Levy, published in the September, 1950, issue of the Journal of Applied Mechanics, Trans. ASME, vol. 72, pp. 310–314.

[2] Physicist, National Bureau of Standards, Department of Commerce, Washington, D. C. Mem. ASME.

of the cam would provide a check on the assumption of Biot and Bisplinghoff's statistical method,[3] that the maximum resultant response can be estimated by adding maximum responses in each mode without regard to phase.

It would be especially worth while to include cams for a forcing function which alternates in sign to represent antisymmetrical forcing functions.[4] The consideration of response over a long period makes it more important to include the effect of damping. Have the authors given any thought to the inclusion of damping in the analyzer to approximate the damping present in an actual structure?

R. H. Scanlan.[5] The problem which the authors solve is a trying one in the aircraft-engineering design office. They are to be lauded for their success in bringing it neatly under control.

If every engineering office were equipped with efficient machine computers of effectiveness beyond that of the usual key-driven calculator, it is possible that the present paper would not have had to be written. The authors have merely provided a particular mechanical analog machine to solve one type of linear dynamics problem, the mathematical solution of which is well known. A differential analyzer could easily handle such a problem, and in fact has done so.[6] Application of linear difference equation techniques would make it amenable to punch-card computation also.

However, the real point of building such a machine is to solve rapidly an important problem which recurs more and more frequently. Unfortunately, there do not happen to be as yet enough general analog computers available for use on such recurrent problems. Thus the authors' machine has its place and its uses, and its popularity should increase. The writer is of the hope that the machine can be made available to the industry for routine use so that its effectiveness can be high.

The question whether the machine or hand computation procedures should be used is the usual economic one. The writer happens to have had the experience of planning to use the authors' machine but found that hand computations, of a somewhat simplified nature, were proceeding so rapidly that adequate results were available in time without the machine. However, if plans to use the machine had been made from the very outset of his particular project, there is no doubt that more extensive results, with a number of variations of key parameters, could have been obtained, and that they would have lent more value to the project.

A hand-computing approach which is of value requires the Fourier analysis of the forcing function. Then the separate analytical portions of the solution are given mathematically and merely added directly. Analog machines are in existence for making the initial Fourier analysis quickly. Again, speed, availability, cost are the prime factors governing choice of method.

As to particular engineering aspects of the problem which the authors' machine solves, the following may be commented:

The old practice of neglecting mode phasing was undoubtedly poor (ultraconservative) and certainly unwarranted. The authors have correctly eliminated this fault.

Upon conversation with Dr. Pian at one time, the writer discussed with him the possibility of including damping into the system. If this idea has been pursued, how has it been carried out in the machine? Specifically, could correct values of structural (nonviscous) damping as well as aerodynamic damping be included, if desired?

It should be mentioned again perhaps that the present and several other current solutions to the landing-load problem are essentially empirical in that certain specific forms of the landing force-time curves are assumed a priori. The actual interaction between oleo strut (or hull in water) and elastic airplane is not simulated, but typical operational test results are substituted for the loading function.

It would appear that a project of considerable interest could be developed around the more rational setting up of loading devices for the authors' present apparatus. For example, a device to simulate dynamically an actual water landing or oleo strut plus tire compression would be of value. This is a nonlinear problem but within range of present techniques, both analytical[6] (to some extent, at least), and experimental. If developed to this point, the superiorities of this analog machine over the theoretical approach would be greatly increased because of extreme complexities in the theoretical hydrodynamics of the forcing function.

Authors' Closure

Dr. Ramberg and Professor Scanlan's comments are greatly appreciated. The authors wish to state in reply that a damping device has been installed in the analyzer. It was felt that effects of both structural and aerodynamic damping could be approximated by means of equivalent viscous damping. A mechanical damper utilizing the shearing resistance of a high-viscosity fluid was attached to one component of the analyzer. No attempt was made to simulate the coupling of the modes due to damping.

Crushing of Aluminum Tubes Under Hydrostatic and Localized Pressure[1]

Marshall Holt.[2] The author has made a contribution to engineering literature in making these test data available. It appears, however, that in the analysis of the data and in the correlation with both Sturm's and Timoshenko's theories he has overlooked the significance of the term E, modulus of elasticity. One should not expect either theory to give computed values in agreement with test results when the stresses are above the elastic stress range. In all but three of the tests reported the computed hoop stress is greater than 12,000 psi. Although the mechanical properties of the actual material used are not given, it is quite probable that the elastic limit is not this high. Therefore one must use the value of the effective modulus rather than that of the initial modulus, or in this case 10,000,000 psi. The tangent modulus or slope of the stress-strain curve is satisfactory for some stability problems, and perhaps it is in this case also. This problem has been discussed by Sturm and O'Brien.[3]

It should be pointed out that for long tubes which buckle into two lobes Equations [1] and [2] of the paper are practically identical. It is noticed that the computed collapsing pressures of the two largest tubes having a wall thickness of 0.020 in. are somewhat less than the corresponding test results. Nothing is said of the precision with which the thicknesses were measured, but, by means of the rewritten Equations [1] or [2], one can deduce from

[3] Reference (1) of the paper.

[4] "The Dynamic Response of a Simple Elastic System to Antisymmetric Forcing Functions Characteristic of Airplanes in Unsymmetric Landing Impact," by J. B. Woodson, Journal of Applied Mechanics, Trans. ASME, vol. 71, 1949, pp. 310–316.

[5] Associate Professor of Aeronautical Engineering, Rensselaer Polytechnic Institute, Troy, N. Y.

[6] "An Analytical Theory of Landing Shock Effects on an Airplane Considered as an Elastic Body," by E. C. Keller, Journal of Applied Mechanics, Trans. ASME, vol. 66, 1944, p. A-219.

[1] By E. Creuts, published in the September, 1950, issue of the Journal of Applied Mechanics, Trans. ASME, vol. 72, pp. 324–326.

[2] Senior Research Engineer, Engineering Design Division, Aluminum Research Laboratories, New Kensington, Pa.

[3] "Computed Strength of Vessels Subjected to External Pressure," by R. G. Sturm and H. L. O'Brien, Trans. ASME, vol. 69, 1947, pp. 353–358.

the test results that the 1-in. tube must have had a wall thickness of 0.024 in., and the 0.75-in. tube had a wall thickness of 0.0214 in.

Empirical equations, in general, are dangerous because they are so often misapplied. In this case it should be borne in mind that the equation deduced by the author is applicable to material having mechanical properties the same as those of the material used in these tests and should not be used for high-strength aluminum alloys.

The impression is given in the paper that aluminum alloys do not follow the laws of elasticity whereas steel does. The basis for this probably lies in the fact that the stresses in the steel specimens were elastic and those in the aluminum specimens were above the elastic stress range for that particular alloy and temper. The fallacy arises from the misapplication of the laws of elasticity and not from any peculiarity of aluminum as such.

A Method for Determining Mode Shapes and Frequencies Above the Fundamental by Matrix Iteration[1]

J. B. Duke.[2] The revival of interest in matrix methods of representation of arrays of simultaneous equations opens anew a discussion of the practical difficulties encountered with such methods. The discussion presented in the paper is a valuable contribution to the subject of practical application of matrix methods in the solution of engineering problems. However, the paper does not point out accurately the restrictions which are imposed on the method of sweeping.

These lie primarily in the specific condition of orthogonality between modes stated in Equation [2] of the paper, which is repeated here for continuity

$$\sum_i m_i \phi_i^{(r)} A_i^{(r+1)} = 0$$

$$\sum_i \sum_j m_{ij} \phi_i^{(r)} A_i^{(r+1)} = 0$$

This orthogonality condition, upon which the sweeping method is based, follows from a consideration of the classical form of the characteristic equation for an array of equations with an arbitrary parameter. Consider the following

$$(\lambda I - u)k = 0$$

or

$$\kappa(\lambda I - u) = 0$$

where

λ = frequency parameter
I = unit matrix
u = dynamic matrix
k = modal column of section displacement, moment, or shear, etc., coefficients
κ = modal row

It is a well-known theorem of matrix algebra which states

$$\kappa_p k_q = 0$$

or the orthogonality condition between modes p and q. In order for κ, the modal row, to have a simple relation to the modal column k, the u-matrix must be the product of two nonsingular symmetrical matrices. If

$$u = [D_{ij}]\,[m_{ij}]$$

then

$$(\lambda I - [D_{ij}]\,[m_{ij}])k = 0$$

$$k'(\lambda I - [m_{ij}]'[D_{ij}]') = 0$$

(Primes indicate transposed matrices.)

It follows immediately

$$k'(\lambda I - [m_{ij}]'[D_{ij}]'[m_{ij}][m_{ij}]^{-1}) = 0$$

or

$$k'[m_{ij}]\,(\lambda I - u) = 0 = \kappa(\lambda I - u)$$

$$\kappa = k'[m_{ij}]$$

$$\kappa_p k_q = k_p'[m_{ij}]k_q = 0$$

Since the method of sweeping states as a postulate that this condition must be true, a large class of problems are not adaptable to this method.

Several alternative methods have been outlined in the literature.[3,4,5] That of Hotelling shows how the characteristic polynomial in λ may be generated from consideration of the diagonal elements of successive powers of the dynamic matrix. It is objectionable for practical use, except in cases where the entire frequency spectrum is desired. Extreme care must be exercised in the evaluation of each coefficient of the polynomial equation.

Aitken presents a general method by which the dominant mode of the characteristic matrix may be removed by a simple algebraic process. The desired condition is

$$\mu_2 = \mu_1 - A$$

$$\kappa_1 \mu_2 = 0$$

$$\mu_2 k_1 = 0$$

After some algebra, $A = \lambda_1(k_1\kappa_1)/(\kappa_1 k_1)$, and it is easily shown that the μ_2-matrix has the same latent row and column vectors as the original matrix with the dominant mode removed. In the case where κ is a simple function of k, this reduces to the method of sweeping. This process is the least susceptible to loss of significant figures, but it requires twice the calculation effort, in the general case, for both the modal row and the modal column must be calculated for each mode.

The latter objection may be removed by a simple extension of the Frazer, Duncan, Collar[5] method, and one may proceed from eigenvalue to eigenvalue with only the calculation of the latent column vector. Supplementing paragraph 4.18 of the Frazer, Duncan, Collar reference;[5] note that

$$\kappa_s \omega = \kappa_1 \frac{\kappa_{rs}}{\kappa_{r1}}$$

Let r_s be a modal row of $v\,(s = 1)$ and set

$$r_s = \frac{\kappa_s}{\kappa_{r1}} + a_s$$

---

[1] By H. I. Flomenhoft, published in the September, 1950, issue of the Journal of Applied Mechanics, Trans. ASME, vol. 72, pp. 249–256.

[2] Analytical Engineer, Hamilton Standard Propellers, East Hartford, Conn.

[3] "Some New Methods in Matrix Calculation," by Harold Hotelling, *Annals of Mathematical Statistics*, vol. 14, March, 1943.

[4] "Studies in Practical Mathematics—Part II," by A. C. Aitken, Proceedings of the Royal Society of Edinburgh, vol. 57, 1937, pp. 269–304.

[5] "Elementary Matrices," by R. A. Frazer, W. J. Duncan, and A. R. Collar, Cambridge University Press, 1946, pp. 143–145.

where a_s is to be determined. Then

$$\lambda_s \frac{\kappa_s}{\kappa_{rs}} + \lambda_s a_s - \frac{\kappa_s}{\kappa_{rs}} v - a_s v = 0$$

But

$$\kappa_s v = \kappa_s u - \kappa_s u \omega$$
$$= \lambda_s \kappa_s - \lambda_s \kappa_1 \frac{\kappa_{rs}}{\kappa_{r1}}$$

Hence

$$\lambda_s a_s + \lambda_s \frac{\kappa_1}{\kappa_{r1}} - a_s u = 0$$

$$a_s = -\frac{\kappa_1}{\kappa_{r1}}$$

and

$$r_s = \frac{\kappa_s}{\kappa_{rs}} - \frac{\kappa_1}{\kappa_{r1}}$$

This does not provide an explicit solution for κ_s in terms of r_s and κ_1. Consider

$$r_s = c\left(\frac{\kappa_s}{\kappa_{rs}} - \frac{\kappa_1}{\kappa_{r1}}\right)$$

where c is a constant to be determined.
Now

$$\frac{\kappa_s}{\kappa_{rs}} (\lambda_s I - u) = 0$$

$$\left(\frac{r_s}{c} + \frac{\kappa_1}{\kappa_{r1}}\right)(\lambda_s I - u) = 0$$

$$\frac{r_s}{c} (\lambda_s I - u) + (\lambda_s - \lambda_1) \frac{\kappa_1}{\kappa_{r1}}$$

This represents an array of simultaneous equations, only one of which needs to be considered

$$\frac{r_s}{c} (\lambda_s - u_{ir}) + (\lambda_s - \lambda_1) \frac{\kappa_1}{\kappa_{r1}}$$

so

$$c = \frac{r_s [u_{ir}]}{\lambda_s - \lambda_1}$$

and

$$\frac{\kappa_s}{\kappa_{rs}} = \frac{\kappa_1}{\kappa_{r1}} - \frac{(\lambda_1 - \lambda_s) r_s}{r_s (u_{ir})}$$

With this relation, or a similar one for the modal columns, one may calculate successive eigenvalues and true vectors for any matrix, and complete generality may be observed.

In each of the foregoing methods, the tacit assumption has been that the roots are real and distinct. A considerable complication arises in cases of complex or multiple roots.

The subject of accuracy has been carefully avoided for it is the writer's belief that none of the foregoing methods will provide sufficient accuracy for the calculation of many modes unless extreme care is exercised at each step. The use of computing machines alleviates this condition somewhat, but does not remove the difficulty entirely. In some cases, where a very high mode is desired, it is possible to alter the dynamic matrix in such a way as to shift the axis of the roots so that the highest root appears first. This is accomplished by adding a scalar factor to the diagonal elements, and avoids the necessity of reciprocation.

Consider

$$(\lambda I - u + fI)k = 0 = (\lambda_m I - u_m)k_m$$

where f may be any number greater than one half the difference between the estimated values of the first and last roots.
Then

$$\lambda = \lambda_m - f$$
$$k = k_m$$

By judicious choice of the factor f, it is sometimes possible to get at a higher mode without too many reductions of the dynamic matrix, and to attain greater accuracy as a result.

In the approach to a large-scale problem, probably the most desirable technique would be that of generating the characteristic polynomial and solving this equation for specific desired roots. A recent paper[6] appears to offer a most promising technique for doing this without the numerical difficulties encountered by other methods.

A. C. Gilbert[7] and K. B. Gillmore.[8] The author's work in bringing to light a little-known method for alleviating the tedious calculations necessary to obtain higher roots beyond the fundamental should be commended. The writers found, however, in applying the method that it did not produce accurate results. It seems our problem, which incidentally merely involved seven degrees of freedom, was the exception that disproves the rule. It was found that the columns were being swept from right to left instead of from left to right as dictated in the paper. Rows and columns were reorganized but to no avail. Apparently, as predicted by the author, this proved a constant source of error.

The problem was solved when the writers resorted to the method to be explained. It might be noted that accuracy of the succeeding method is quite good. As with the paper, the method probably could be found in any of the numerous classic texts on the subject of matrix analysis. Basically it is similar to the author's method but its application is slightly different. The writers wish to bring it to light as to comparative method, not as a replacement.

If the problem is such that the columns may be swept from left to right as dictated by the author's method, then his method would be the most expedient. But if such is not the case in that the columns cannot be swept as prescribed then the following method is advised:

Basic Method. It will be assumed that the dynamic matrix of the structure has been computed and that the system is of the form

$$[y^{(1)}] = \omega^{(1)2} [B^{(1)}] [y^{(1)}] \quad \ldots\ldots\ldots\ldots\ldots\ldots [1]$$

where

- y is column modal matrix
- ω is natural frequency, otherwise known as dominant root of matrix
- B is dynamic matrix consisting of mass matrix, multiplied by influence coefficient matrix or $[M][\delta_{ij}]$
- (1) is superscript indicating that quantity is associated to the (1) th mode

---

[6] "An Iteration Method for the Solution of the Eigenvalue Problem of Linear Differential and Integral Operators," by Cornelius Lanczos, National Bureau of Standards, Institute for Numerical Analysis, Los Angeles, Calif.

[7] Vibration Engineer, Piasecki Helicopter Corporation, Morton, Pa. Jun. ASME.

[8] Design Engineer, Piasecki Helicopter Corporation.

and that there are no repeated roots. It is well known that, associated with each root of the dynamic matrix, there is a row matrix which is designated the characteristic row. Furthermore, if an arbitrary row is used to premultiply the dynamic matrix, then by matrix iteration the arbitrary row will converge to the fundamental characteristic row, and the root will be the dominant root. This is a convenient check on the validity of the root (fundamental root) found by premultiplying the dynamic matrix by a column matrix to determine the root as well as the modal shape. (The convergent column matrix is known as the modal column.)

Once the dominant root of the dynamic matrix has been found, the remaining roots can be obtained successively in order of magnitude by constructing auxiliary matrices which contain all the latent roots except those already obtained. If $\omega^{(1)}$ is the dominant root of a dynamic matrix $[B^{(1)}]$, and if $[K^{(1)}]$ is the characteristic row obtained by matrix iterative premultiplication of $[B^{(1)}]$, then if $K_i^{(1)}$ is the maximum element of the characteristic row matrix, a matrix $[C^{(1)}]$ may be defined as a square matrix which has $K^{(1)}/K_i^{(1)}$ for its ith row and its remaining rows zero. The matrix $[B^{(2)}]$ which contains all the latent roots except the dominant may be written as

$$[B^{(2)}] = [B^{(1)}][I - C^{(1)}] = [B^{(1)}]\begin{bmatrix} 1 & 0 & \cdots & 0 \\ 0 & 1 & \cdots & 0 \\ \cdot & & & \cdot \\ \cdot & & & \cdot \\ \cdot & & & \cdot \\ \cdot & & & \cdot \\ -\frac{K_{i1}^{(1)}}{K_{in}^{(1)}} & -\frac{K_{i2}^{(1)}}{K_{in}^{(1)}} & \cdots & 0_n \end{bmatrix} \quad \ldots [2]$$

where I is the unit matrix (unit diagonal). This is proved in any of the classic texts on matrix algebra from the generalized orthogonality condition for matrices.

Thus it might be stated that, to obtain higher roots of a matrix, it is necessary to obtain a row matrix $[K]$ by iterative premultiplication, and with this row matrix construct a sweeping matrix which is premultiplied by the dynamic matrix to obtain the modified dynamic matrix which contains all the latent roots exclusive of the previous roots.

With the method presented one does not need to rearrange the rows or columns to suit any array, but merely assume an arbitrary row and premultiply the dynamic matrix to obtain a characteristic row matrix. The dominant root obtained in the first iteration for the fundamental mode should check the root obtained by the row premultiplication. Thus a convenient check is provided.

Alternative Derivation of Characteristic Row. In a conservative system, oscillating in simple harmonic motion in a normal mode, a method similar to the one outlined by the author may be used to obtain the characteristic row, but it must undergo the premultiplication also. It does provide a short cut and speed convergence. If $[K^{(r)}]$ is the characteristic row for the rth root and $[y^{(s)}]$ is the modal column for the sth root then the generalized orthogonality condition for any matrix is

$$[K^{(r)}][y^{(s)}] = 0 \; (r \neq s) \ldots\ldots\ldots\ldots\ldots [3]$$

The orthogonality condition for antisymmetrical "free-free" modes

$$[y^{(r)}][M][y^{(s)}] = 0 \ldots\ldots\ldots\ldots\ldots [4]$$

or for symmetrical free-free modes

$$[(y - y_0)^{(r)}][M][y^{(s)}] = 0 \ldots\ldots\ldots\ldots [5]$$

Therefore, apart from a constant factor (for antisymmetrical free-free modes)

$$[K^{(r)}] = [y^{(r)}][M] \ldots\ldots\ldots\ldots\ldots [6]$$

If any nonzero element in the row matrix $[K^{(r)}]$ is equal to the identical element in the row matrix $[y^{(r)}][M]$, then each element in one is equal to its corresponding element in the other. Also, if one is normalized by dividing through by a nonzero element and the other is normalized by dividing through by the element in the same position, then the normalized matrices are equal. Thus if $[y^{(r)}][M]$ is written as

$$[m_1 y_1^{(r)} \quad m_2 y_2^{(r)} \quad m_3 y_3^{(r)} \ldots\ldots m_n y_n^{(r)}] \ldots\ldots [7]$$

then $[K^{(r)}]$ may be written directly. This characteristic row should then be premultiplied by the original dynamic matrix to insure greater accuracy of the row matrix. Obtaining a final $[K^{(r)}]$ the dynamic matrix exclusive of the dominant root may be found

$$[B^{(s)}] = [B^{(r)}][I - C^{(r)}] \ldots\ldots\ldots\ldots [8]$$

The rows and columns of the original dynamic matrix need not be rearranged but may be used directly as calculated.

Accelerating Convergence. Convergence of the characteristic row may be accelerated by realizing that the root, which is the normalizing value $K_{in}^{(r)}$, must be equal to the latent root calculated by column multiplication for the frequency and modal column. Thus, if convergence appears, after two or three iterations, to be approaching the proper value for $K_{in}^{(r)}$ then convergence may be accelerated by multiplying the characteristic row by the ratio of the normalizing value $K_{in}^{(r)}$ to the dominant latent root found by iterating the original dynamic matrix.

Author's Closure

Mr. Duke describes very concisely the fundamental principles on which most methods for obtaining higher modes are based. The orthogonal relationship of κ and k provides convenient equations for introducing into the dynamic matrix the constraints necessary to cause convergence to other than the dominant modes. As Mr. Duke demonstrates, when the two symmetrical matrices whose product forms the dynamic matrix are known, it is not necessary to perform successive premultiplication to obtain the modal row, since $\kappa = k'[m_{ij}]$. This is described in detail in the discussion by Messrs. Gilbert and Gillmore in their "Alternative Derivation of Characteristic Row." Of course, for modes higher than the second, a number of orthogonality conditions of the general form $k_y'[m_{ij}]k_y = 0$ must be solved simultaneously to obtain the characteristic row. The tables presented in the paper have been considered to provide a reasonably efficient means for accomplishing this.

It is worth noting that the conditions $\kappa = k'[m_{ij}]$ and $u = [D_{ij}][m_{ij}]$ imply that symmetrical matrices, D and m, can be derived for any matrix, u. There are $n^2 + n$ unknowns in D and m, where n is the order of each matrix, and the same number of algebraic equations result from the two matrix equations. There-

fore there is theoretically a unique solution for D and m. In practice, this is extremely difficult to carry out and hardly worth the effort.

The two symmetrical matrices are known for typical engineering problems, such as determining the mode shapes and frequencies of an elastic structure, or using the normal-mode approach to couple the effects of separate degrees of freedom. It is for these cases that the procedure outlined in the paper was intended.

It is difficult to understand the inaccuracies encountered by Messrs. Gilbert and Gillmore in applying the method to their specific problem, particularly since the method they resorted to successfully is theoretically equivalent to the one described in the paper. Perhaps the setup of the problem is inconsistent with the application of the tables. This might be easily straightened out by a recheck of the numerical example.

Stability of Flow in a Rocket Motor[1]

H. I. Ansoff.[2] From a mathematical point of view we are confronted with a special case of the following problem: To determine the stability of solutions of the differential equation

$$\sum_{k=0}^{n} a_k \frac{d^k x(t)}{dt^k} = \sum_{k=0}^{m} b_k \frac{d^k x(t-\tau_k)}{dt^k}$$

where $n < m$, τ_k, a_k, and b_k are constants (some a_k and b_k may be zero). Physically, this is a general feedback problem with constant time lag.

It may be worth while to discuss the applicability of the methods of the present paper to this general problem.

Application of Method 1 appears to involve solution of a differential equation for each interval following the first. For $n > 1$ such procedure is clearly very cumbersome; particularly so, since no information is obtained about the stability of the system as a function of the parameters.

The method of separation of the real and imaginary parts of the characteristic equation (Method 3 of the present paper) tends to become cumbersome for $n > 2$.[3]

If the inversion of the Laplace transform (Method 2) is accomplished by the method of residues, direct information is obtained about the stability of a system. Unfortunately, the number of residues is infinite in this problem.

Referring specifically to the present problem, it should be remarked that, the system being linear, it is sufficient to define initial conditions at $t = 0$ and $t < 0$ (or better at $t = -\alpha$) and that a prescription of a disturbing function over $-\alpha < t < 0$ merely supplies that initial condition.

The final method using the Cauchy-Rouche theorem is the only one here which permits determination of the stability of solutions with relative ease. For a given set of parameters it is always possible to plot the characteristic equation of a system in the $f(z)$-plane, and thus to determine whether the equation has roots with positive real parts. However, it is frequently desirable to determine relations between the parameters of the system which would guarantee stability. This can be done without plotting $f(z)$ in the λ-plane. Thus, if we have to study the behavior of

$$f(z) = B + z + He^{-z}$$

Letting $z = i\beta$, we can write

$$f(i\beta) = \frac{1}{B + i\beta}\left(1 + \frac{H}{[B^2 + \beta^2]^{1/2}} e^{-i[\beta + \tan^{-1}\beta/B]}\right)$$

Hence $f(i\beta)$ will not vanish if only

$$\frac{H}{[B^2 + \beta^2]^{1/2}} < 1; \quad \text{or } B > H$$

which is a sufficient condition for stability obtained in the paper under discussion.

Similarly consider

$$f(z) = z^2 + Mz + N + e^{-z}(Sz + T)$$

Since $z^2 + Mz + N$ will have no roots with positive real parts we can write

$$f(z) = \left(1 + e^{-z}\frac{Sz + T}{z^2 + Mz + N}\right)\frac{1}{(z^2 + Mz + N)}$$

Again, letting $z = i\beta$ and simplifying, we are led to the conclusion that $f(i\beta)$ will have no roots in the right half-plane if the equation

$$\frac{S^2\beta^2 + T^2}{(N - \beta)^2 + \beta^2 M^2} = 1$$

has no real roots. Elementary operations will lead to a pair of conditions on S, T, N, and M which will guarantee stability of the system.

The severe drawback of the results obtained here lies in the fact that only sufficient (but not necessary) conditions have been obtained. Further analysis of the characteristic equation along similar lines sometimes leads to closed forms for both necessary and sufficient conditions.

M. Yachter.[4] This paper appears rather simple, but this simplicity is somewhat deceiving. In reality the phenomenon of "chugging" in a rocket chamber is a very complex one and depends upon a number of processes so far only superficially understood. Among these one may mention the hydrodynamics, the impingement and atomization of the jets, and the chemical-reaction process.

The simplicity of this paper arises from the introduction of, what may appear at first, an artificial quantity, the time lag ($\mathcal{L}$) between the flow rate and the rate of pressure build-up, or, what is essentially the same thing, the time lag between the liquid flow rate and the burning rate. Upon reflection it will be seen that this time lag has really a simple physical meaning. It is nothing else but the time it takes a liquid particle, once it leaves the injector, to go through the process of impingement, atomization, and final conversion into gas. It is assumed of course that this time is the same for all particles and does not change with time. The notion of such a time lag, as introduced by the authors, turns out to be a fruitful and far-reaching one for problems of this nature.

The question now is: How can this quantity be determined? It is clear that this time delay depends upon the very complicated jet hydrodynamics and chemical-reaction processes already referred to, and an analytical treatment of these phenomena is not a simple matter at all. Furthermore, from considerations, which will be discussed presently, it appears that this time lag is usually of the order of a few milliseconds. Hence a direct experimental determination of such a small time lag would require rather delicate experimental technique.

Fortunately, it turns out that this time quantity can be ex-

[1] By D. F. Gunder and D. R. Friant, published in the September, 1950, issue of the Journal of Applied Mechanics, Trans. ASME, vol. 72, pp. 327–333.

[2] Associate Mathematician, The Rand Corporation, Santa Monica, Calif. Jun. ASME.

[3] See, for example, "Self-Excited Oscillations in Dynamical Systems," by N. Minorsky, Journal of Applied Mechanics, Trans. ASME, vol. 64, 1942, p. A-65.

[4] Engineer, The M. W. Kellogg Company, Jersey City, N. J.

pressed theoretically in terms of two other quantities, one of which is given by the particular design of the system and the other one being an experimental quantity which can be, and has been, determined, for a number of cases, in a relatively simple manner and with reasonable accuracy. This quantity is the frequency of oscillation of the chamber pressure during "chugging."

In order to shorten this discussion as much as possible, detailed derivations will be omitted, but the following can be proved:

Let

ω = frequency of oscillation of chamber pressure during chugging in radians per sec (as obtained from records)

$$t_0 = \frac{1}{\omega} \text{ sec}$$

$$t_p = \frac{A_T l}{A_2 C^*}, \text{ sec}$$

A_T = nozzle throat area

A_2 = pipe area

l = length of pipe

and

$$C = \gamma \left(\frac{2}{1+\gamma}\right)^{\frac{\gamma+1}{2(\gamma-1)}} C^*$$

or

$$C^* = \sim \frac{4}{3} C \quad \text{for} \quad \gamma = 1.25 - 1.35$$

with C being the speed of sound at nozzle throat.

Then

$$p^*_{CR} = \left(\frac{2\Delta p}{p_{CS}}\right)_{CR} = \sqrt{1 - \left(\frac{t_p}{t_0}\right)^2} \quad \ldots\ldots\ldots [1]$$

and

$$\frac{\pi}{2} \leq \frac{\alpha}{t_0} = \tan^{-1}\left(-\frac{t_p}{t_0}\right) \leq \pi \quad \ldots\ldots\ldots [2]$$

For an injector pressure drop Δp such that

$$p^* = \frac{2\Delta p}{p_{CS}} < p^*_{CR}$$

the burning is unstable.

From the records it was found that ω varied somewhere between 500 and 1000 radians per sec. So that from Equation [2] herewith, the range of α would be 1.5 to 6 millisec.

In general

$$\alpha = \sim 2t_0$$

and in most cases investigated α = 2–4 millisec.

Consider now Equation [1] of this discussion: This equation indicates that for $t_p = t_0$, the system is stable no matter how small the injector pressure drop may be. For a typical case we may take

$$\frac{A_T}{A_2} = 1, C^* = 4000 \text{ fps}, t_0 = 0.0003 \text{ sec}$$

then

$$l = \frac{A_2}{A_T} C^* t_0 = 4000 \times 0.003 = 12 \text{ ft}$$

Now an examination of Equation [5] of the paper shows that the main effect in reducing the p^*_{CR} arises from the acceleration term dV'/dt. Indeed, if the accelerations in the pipe are neglected, then it will be found from Equation [5] that $p^*_{CR} = 1$, that is, the required injector pressure drop for stability must not be less than $^1/_2$ the chamber pressure.

Accordingly, it is found from Equation [1] in this discussion that the accelerations that would be set up in a 12-ft pipe when chugging starts would be sufficient to eliminate this phenomenon altogether even if the injector pressure drop to chamber pressure ratio is very small.

Now, this is a very strange result. Indeed, if this theoretical result was even approximately true, chugging in rocket chambers would never even show up, since there is always that much of effective pipe length in any rocket-motor system. Unfortunately, the known facts do not at all correspond to this theoretical result. Why is this so? Undoubtedly, if the chamber-pressure oscillations could really induce the proper accelerations over the entire pipe length as assumed in this paper, which for a pipe diameter of, say, $1^1/_2$ in. would amount to a length of 100 diam, then the oscillations would die out and chugging would not occur. Apparently, something else intervenes which limits the effect of the pressure oscillations only to the immediate neighborhood of the chamber, say, to a neighborhood of only 10 pipe diam. If this is so, then Equation [1] of this discussion shows that this reduced effective pipe length has only a moderate effect on the critical injector pressure drop, and this result does seem to correspond to the known facts.

Exactly what it is which prevents the effect of the chamber-pressure oscillations to be felt further upstream in the pipe is not really known. But theoretical considerations lead to the supposition that the pressure oscillations are accompanied by alternate expansions and contractions of the jet areas so that the jets themselves act as storage areas while the flow in almost the entire pipe length, except in the immediate neighborhood of the injectors, is quite steady.

Now, however, how about the chamber itself acting as a storage element? In this paper the storage capacity of the chamber was neglected altogether. Yet the oscillations occur right in the chamber itself, and it would appear that the characteristics of the chamber (i.e., its storage capacity) should play a dominant role. Upon analysis, this turns out to be the case. Accordingly, the results of an analysis which take into account the chamber characteristics but neglects altogether the pipe effect will be given. This analysis again is based upon the introduction of a time delay between the flow and burning rates. Again, in order not to lengthen this discussion unduly, all mathematical details are omitted, but the following results have been derived in a company report.[5]

Let

$t_0 = 2L^*/C^*$ = characteristic chamber time constant, i.e., the fundamental resonance period of a one-dimensional closed pipe of length L^* in which the speed of propagation of small disturbances is C^*, where L^* = ratio of chamber volume up to nozzle throat to nozzle throat area

$C^* = \sim 4/3C$ as already defined, C being the sound speed at throat

$t_0 = 1/\omega$ sec, where ω = frequency of oscillation of chamber pressure in radians per sec, as already defined, and as obtained from film records

$$p^* = \frac{2\Delta p}{p_{CS}}$$

Δp = injecture pressure drop

[5] "Dynamics of a Rocket Motor," by M. Yachter and H. Waldinger, The M. W. Kellogg Report No. SPD 241 (restricted).

p_{cs} = steady-state chamber pressure
$p_{CR}{}^*$ = value of p^* such that for $p^* < p_{CR}{}^*$ chugging occurs
α = time delay between liquid flow and burning rates

Then

$$p_{CR}{}^* = \frac{1}{\sqrt{1 + \left(\frac{t_e}{t_0}\right)^2}} \quad [3]$$

$$\frac{\pi}{2} \leq \frac{\alpha}{t_0} = \tan^{-1}\left(-\frac{t_e}{t_0}\right) \leq \pi \quad [4]$$

$$\frac{\Delta\omega}{\omega} = \frac{\frac{p_{CR}{}^*}{p^*} - 1}{1 + \frac{\alpha}{t_e} + \left(\frac{\alpha}{t_e}\right)^2 + \left(\frac{\alpha}{t_0}\right)^2} \quad [5]$$

$$\frac{\bar{t}}{t_e} = \frac{1 + \frac{\alpha}{t_e} + \left(\frac{\alpha}{t_e}\right)^2 + \left(\frac{\alpha}{t_0}\right)^2}{\left(1 + \frac{1}{p_{CR}{}^{2*}}\frac{\alpha}{t_e}\right)\left|\frac{p^*_{CR}}{p^*} - 1\right|} \quad [6]$$

where $\Delta\omega$ = change in frequency of oscillation in chamber due to change in injector pressure drop, in the neighborhood of, and below, the critical injector pressure drop; $\bar{t}$ = "decay" time for disturbances to damp out to $1/e$ of initial magnitude, in the neighborhood of, and above, the critical injector pressure drop.

Equation [5], herewith, is of importance; for, strictly speaking, Equations [3] and [4] are true only just when instability occurs. At this point the amplitudes of the chamber-pressure oscillations are small, and it would be difficult to estimate the frequency from the records. On the other hand, when $p^* < p_{CR}{}^*$ and the amplitudes have built up already so that the frequency can be estimated, then this frequency is no more the theoretical one to be used in Equations [3] and [4]. However, a numerical check of Equation [5] shows that the change in frequency ought to be rather small, and this fact has also been verified from a number of film records.

Equation [6] of this discussion can be used in order to estimate the amount of damping existing in the system in the neighborhood of instability. Two typical runs with pressure oscillations recorded on films are chosen for illustration:

(1) p_{CS} = 380 psia, L^* = 50 in. = 4.16 ft; C^* = 4400 fps; ω = 750 radians per sec (from films).

We have

$$t_e = \frac{2 \times 4.16}{4400} = 0.00189 \text{ sec}$$

$$t_0 = \frac{1}{750} = 0.00133 \text{ sec}; \quad \frac{t_e}{t_0} = 1.43$$

$$\text{Theoretical } p^*_{CR} = \frac{1}{\sqrt{1 + (1.43)^2}} = 0.574$$

The experimental value of p^*_{CR} occurred between 0.53 and 0.63 with an average of 0.58. This close agreement is, of course, purely coincidental

$$\frac{\alpha}{t_0} = \tan^{-1}(-1.43) = 2.18$$

$$\alpha = 2.18 \times 0.00133 = 0.00288 \text{ sec}$$

Thus, α = ~ 3 milliseconds; $\frac{\alpha}{t_e} = 1.52$

(a) Suppose p^* decreased to $(2/3)p^*_{CR}$ so that

$$\frac{p^*_{CR}}{p^*} = \frac{3}{2}$$

Then

$$\frac{\Delta\omega}{\omega} = \frac{\frac{3}{2} - 1}{1 + 1.52 + (1.52)^2 + (2.18)^2} = 0.052$$

∴Change in frequency is only 5 per cent.

(b) Suppose now that p^* is increased to $(4/3)p^*_{CR}$.

Then

$$\frac{\bar{t}}{t_e} = \sqrt{\left[1 + \frac{1.52}{(5.74)^2}\right]\left|\frac{3}{4} - 1\right|} = 9.35$$

and

$$\bar{t} = 0.0178 \text{ sec}$$

(2) p_{CS} = 1040 psia; L^* = 47 in.; C^* = 3500 fps; ω = 1130 radians per sec (from film records).

We have

$$t_0 = \frac{1}{1130} = 0.000884 \text{ sec}$$

$$t_e = \frac{2 \times \frac{47}{12}}{3500} = 0.00224 \text{ sec}$$

$$\text{Theoretical } p_{CR}{}^* = \frac{1}{\sqrt{1 + \left(\frac{0.00224}{0.000884}\right)^2}} = 0.366$$

The experimental value of p^*_{CR} was about 0.27. This would indicate a p^* well in the unstable range. As a matter of fact the records for this case already show considerable amplitudes.

Finally

$$\frac{\alpha}{t_0} = \tan^{-1}\left(-\frac{0.00224}{0.000884}\right) = 1.95$$

$$\alpha = 1.95 \times 0.000884 = 0.00173 = 1.73 \text{ millisec}$$

It must be emphasized again that Equation [3] of this discussion is not a formula which can always be used a priori, inasmuch as t_0 is an experimental quantity, which depends upon the hydrodynamics of the jets, the reaction process, etc., just as much as the time delay α does. What has been achieved is the substitution of a quantity (α) which can hardly be determined in any direct manner, in terms of a quantity (ω) which can be determined experimentally with reasonable accuracy.

If the geometry of the injectors, say, of a new design corresponds reasonably well to that of an earlier design for which ω (or α) is already known, then the effect of L^* or C^* or both of the new design on $p_{CR}{}^*$ can be estimated, assuming ω to be the same as for the old design. On the other hand, if the geometry of the injectors is radically changed, then ω may also change radically. Thus it was found that a chamfer versus sharp corners at the injector entrance has a marked effect in reducing the required p^*_{CR} for stability. Accordingly Equation [3] of this discussion should be regarded as only partly theoretical.

An Investigation of Ejector Design by Analysis and Experiment[1]

WALTON FORSTALL, JR.[2] On a problem, hitherto explored mainly by the experimental method, the authors have brought to bear two powerful analytical tools; the phenomenological approach and one-dimensional analysis. Taken together, these avoid the necessity of looking into the internal details of the mixing process, yet results computed by this method approach measured data so closely that differences can be allowed for by experimentally determined coefficients. This is a tremendous step forward from earlier dependence upon purely empirical design.

However, admiration for the neatness of the analytical attack should not be allowed to obscure the labor involved in the preparation of this paper. Even with one-dimensional analysis, the working equations are quite complex, so that the work required to compute Figs. 10 and 11 of the paper is simply enormous. It is characteristic of the authors that they do not stop with the analysis, but present their readers with the computations as well. And finally, as a third contribution, the paper represents many hours of painstaking work involved in obtaining experimental results.

When so much is presented in the scope of a single paper, the authors' skill in succinct composition is impressive. At what point compressed presentation ceases to be a virtue is a matter of personal opinion, but the writer feels that Fig. 5 of the paper and its discussion would be improved by somewhat less crowding. There is so much information packed into Fig. 5 that a good deal of reader effort is required to separate the various cases and visualize the physical model for each. It is interesting to note that for the constant-pressure case, point C corresponds to a zero-velocity secondary moving across an infinite area, resulting in a finite secondary flow.

It is hoped that this work will be continued and that more information, both analytical and experimental, can be obtained on the influence of length-diameter ratios and on the optimum entrance shape for constant-pressure mixing.

A. H. SHAPIRO.[3] The striking result of this investigation is the degree to which the performance of jet pumps may be predicted by a simple one-dimensional analysis which takes no account of wall friction forces in the mixing tube.

Two empirical facts were brought out by the authors for the constant-area mixing tube; (1) the "best length" of mixing tube for subsonic streams is about 8 diameters, and (2) the measured maximum pressure is only a few per cent less than the pressure calculated by the one-dimensional analysis without wall friction.

An experimental investigation by Szynkiewicz and Tierney[4] of the constant-area mixing tube of a water-to-water jet pump led to the conclusions that (1) the "best length" of mixing tube is about 6 to 8 diameters, and (2) the measured maximum pressure rise varies between 93 and 98 per cent of the pressure rise calculated by a one-dimensional analysis without wall friction. These results were obtained over a range of flow ratios (secondary to primary) from 0.3 to 2.6, and over a range of area ratios (mixing tube to primary nozzle) from 100 to 1000.

That these empirical rules are so similar for such different fluid combinations as air-air and water-water suggests that they may be useful working rules for other fluid combinations. Furthermore, the marked similarity in results for very different types of fluids is strong evidence to the effect that the mixing process is controlled by high-intensity turbulence.

AUTHORS' CLOSURE

Professor Forstall's generous remarks cannot be answered with entire satisfaction. The discussion of Fig. 5 was presented in an attempt to provide a framework within which the empirical and analytical material of the paper could be correlated. Rather than exceed the limits on length of papers usually prescribed by the ASME Applied Mechanics Division the exposition of Fig. 5 was kept brief, perhaps to a degree not welcome to the reader.

Professor Shapiro's account of thesis work on a water-water ejector, which was carried out under his direction, is most welcome. It serves to indicate how widely the one-dimensional analysis can be successfully applied. The data from this thesis on mixing length and pressure rise are consistent with the observations recorded in this paper and in reference (2).

Elastic-Plastic Analysis of Structures Subjected to Loads Varying Arbitrarily Between Prescribed Limits[1]

GEORGE WINTER.[2] The chief merit of this paper, it seems to the writer, rests in Equation [21], that is, in the formulation of Bleich's theorem of shakedown as a system of simultaneous inequalities. It is hoped that the use of such mathematical systems for structures of various types will be "spelled out" in later papers, as promised by the authors. In this respect, treatments as easily visualized and understood as that given for the continuous beam by F. Bleich[3] will be preferred by structural engineers to a purely mathematical presentation. For this same reason the authors' formulation of this problem in terms of an n-dimensional space does not seem to add too much to a structural understanding of performance.

One fact should be emphasized which follows very clearly from this paper, even though it was known ever since Bleich, father and son, gave their treatment of the shakedown problem. The more extreme proponents of "limit or plastic design" advocate as one of the substantial, practical advantages of the method the fact that it abolishes elastic analysis and supplants it by the much simpler and shorter analysis of the limit state on a purely plastic basis. This claim is quite justified if the structure is subject only to one set of loads with fixed ratios of intensities of the various load components such that all of them can change only simultaneously and in the same proportion. Structures of this kind, however, are rare. In most practical cases the type of loading is that considered in this paper, where various components can vary independently. In this case the determination of shakedown requires a purely elastic analysis of the usual type and complexity for the extreme values of each component load. It is in this manner that the authors' σ_i or F. Bleich's σ_i are determined. From the viewpoint of simplicity of analysis nothing is gained, therefore, by supplanting elastic by plastic-strength criteria. To be

---

[1] By J. H. Keenan, E. P. Neumann, and F. Lustwerk, published in the September, 1950, issue of the JOURNAL OF APPLIED MECHANICS, Trans. ASME, vol. 72, pp. 299–309.

[2] Associate Professor of Mechanical Engineering, Carnegie Institute of Technology, Pittsburgh, Pa. Jun. ASME.

[3] Associate Professor of Mechanical Engineering, M.I.T., Cambridge, Mass. Mem. ASME.

[4] "Characteristics of an Ejector Mixing Tube of Constant Area," by A. J. Szynkiewicz and W. D. Tierney, BS thesis in Department of Mechanical Engineering, M.I.T., 1944.

[1] By P. S. Symonds and W. Prager, published in the September, 1950, issue of the JOURNAL OF APPLIED MECHANICS, Trans. ASME, vol. 72, pp. 315–323.

[2] Head, Department of Structural Engineering, Cornell University, Ithaca, N. Y.

[3] Reference (1) of paper.

sure, this is only one feature entering the problem, and it is in no way denied that the plastic analysis gives more realistic information on the actual strength of the structure than current elastic methods, provided assumptions are reasonably satisfied. However, based upon the evidence of the present paper, it seems appropriate to contradict this frequently made claim of extreme simplicity, a claim which is bound to appeal to many designers.

The application of this method to indeterminate trusses stands or falls depending upon whether or not the behavior depicted in Fig. 1 of the paper can be expected of all members of the truss. As to mild-steel tension members, there is little doubt that this assumed behavior is a rather close approximation of actual performance. In the Appendix justified doubt is expressed as to its applicability to compression members. The authors' term "yield force," as referred to compression members, seems somewhat ambiguous since in the accepted sense it would mean the capacity of the member if the unit stress equals the yield point. For compression members, of course, the extreme value $-Y_c'$ to be used in such determinations is the critical buckling load rather than the yield-stress load. The question then becomes that of determining whether a compression member subject to its critical load can maintain this load with increasing deformation over a sufficient range so that its behavior can be regarded as approaching that of Fig. 1.

For very slender compression members (with large L/r or, more precisely, when the critical stress is a small fraction of the yield stress) there is little doubt that the answer is affirmative. Such members approach the behavior of Eulerian elasticas, that is, they maintain a practically constant critical load over a rather large range of deformation. For ideal elastica the load would eventually increase, while for ordinary structural truss members the slenderness is hardly ever large enough for this to occur so that, at very large deformations, the load drops off eventually. Unfortunately, such large slenderness ratios rarely occur in engineering structures. In fact, members with such high L/r-ratios are generally uneconomical since their useful strength, as determined by the critical stress, is far below the strength of the material as given by the yield stress.

It is for this reason that in most trusses the slenderness of the compression members is in an intermediate range such that their elastic critical stress (i.e., computed on the basis of constant Young's modulus), is of the general order of the yield point. The real critical stress for such members is that defined by the tangent modulus, as was shown by Shanley.

The load-deformation relation of compression members in this slenderness range has been investigated rather extensively, by von Kármán, Chwalla, Jezek, and others, both for idealized stress-strain diagrams of the type of Fig. 1, and for real materials with strain hardening. In a recent doctoral thesis at Cornell University, Miss A. Y. Lee analyzed the case for a material with the characteristics of the authors' Fig. 7. All these investigations (including those which account for strain hardening) show that after the maximum load is reached with relatively small deformation, the load begins immediately to decrease with increasing deformation in a manner that does not exhibit any sizable range of constant load.[4] Few tests are known to the writer which deal with this feature, but those that have come to his attention confirm the stated behavior.[5] In addition, most of these analyses are carried out with such rigor as to leave little doubt as to their reliability.

It must be said, therefore, that except for the rather unusual case of trusses all of whose compression members have very large slenderness ratios, the assumptions in Fig. 1 will not be satisfied by practical trusses containing compression members. For this reason the writer believes that the principles of plastic analysis are of little value for the design of statically indeterminate truss structures and that attention more advantageously may be concentrated on structures primarily subject to flexure, such as continuous beams and rigid frames.

T. M. Charlton.[6] The writer is particularly interested in the section of the paper which deals with theorems for the "Elastic-Plastic Analysis of Structures." The Haar-Kármán principle seems to be identical with Engesser's principle of stationary complementary energy for the particular type of problem under consideration (although the latter is more general). The authors will, no doubt, recall that the complementary energy principle is restricted to systems of such a type that the principle of superposition is applicable to the displaced form over the working range. This is due to the basis of the principle being the principle of virtual work for finite displacements. The writer would be glad to have the authors' comments concerning this identity, and also upon the suitability of the complementary energy method for the elastic-plastic analysis of structures. Incidentally, it seems to the writer that the complementary energy principle is in fact based upon "conservation" of complementary energy.

Have the authors any knowledge of the practical effect of assuming the idealized force-extension diagram shown in Fig. 1 of the paper, and which is commonly employed in elastic-plastic analysis?

Such a discontinuous curve makes the application of the principle of stationary potential energy (which insures equilibrium) to this kind of problem extremely difficult. (Since energy is, in one sense, a mathematical concept, the application of this principle is valid in the nonconservative plastic range provided that a given static loading system is applied only.) If the necessary characteristics could be expressed by a continuous function, it seems as though some analytical simplification would be afforded.

Authors' Closure

The authors are in complete agreement with Professor Winter's remark to the effect that shakedown analysis does not possess the extreme simplicity of limit analysis but is, in fact, more complicated than purely elastic analysis. On the other hand, it furnishes more realistic information than do analyses based on the assumption either of proportional loading or of purely elastic behavior. As regards the geometric discussion of the problem in n-dimensional space, the authors did not suggest this as a method to be adopted in practical structural analysis. However, the geometric approach has proved valuable in so far as it suggested a number of results which could then be proved analytically. Finally, the authors agree with Professor Winter's remarks concerning the difficulties created by the presence of compression members, and are grateful to him for supplementing the brief discussion in the paper. They would emphasize again that the "truss" discussed in the paper is to be considered as a simple model of a structure with well-defined elastic-plastic behavior, rather than a physical truss with members exhibiting real elastic-plastic properties. The theorems obtained for this simple model can be translated into terms appropriate to other structures such as rigid frames and to continuous media.

The most useful applications of the shakedown theorem are to continuous beams and rigid frames (1,2).[7] Methods have now been

[4] See, for example, "Theory of Elastic Stability," by S. Timoshenko, McGraw-Hill Book Company, Inc., New York, N. Y., 1936, Figs. 38 and 39. The deformations plotted there are lateral deflections which can easily be translated into axial shortening in an approximate way by assuming the deflection curve to be a sine wave.

[5] See, for example, "Theory of Limit Design," by J. A. Van den Broek, John Wiley & Sons, Inc., New York, N. Y., 1948, p. 85.

[6] Merz and McLellan, Carliol House, Newcastle upon Tyne, England

[7] Numbers in parentheses refer to References at end of this closure.

developed for the numerical solution of the shakedown problem for general framed structures (1, 2). These are based on a form of the shakedown theorem applicable especially to rigid frames (3); the physical interpretation of the shakedown theorem is particularly interesting (4). Although the methods described require an elastic analysis as a preliminary step, the shakedown analysis proper can be made quite speedily as compared with the elastic analysis. The fact remains that the need for an elastic analysis not only makes the solution more laborious than the limit analysis appropriate to proportional loading, but effectively eliminates the possibility of adapting the shakedown theorems to direct design. The simplicity of limit analysis is one of its most attractive features, since this greatly facilitates the proportioning of a structure for minimum weight. It is therefore a matter of practical interest to investigate how much lower are the load limits set by the shakedown analysis than are those set by the most dangerous combination of loads, supposing these are applied in fixed ratios. A number of portal frame-type structures have been analyzed, and the results obtained so far indicate that the safe load using the shakedown criterion is rarely more than about 20 per cent less than that calculated on the limit load basis. It is to be hoped, therefore, that the greater simplicity of the limit-load method of design can be taken advantage of in most practical cases, with a shakedown analysis required only as a final check in cases of structures subjected to especially severe conditions of variable loading.

Concerning the identity between the Haar-Kármán principle and Engesser's principle of minimum complementary energy, suggested by Mr. Charlton, the authors agree that the Haar-Kármán principle is, in fact, the form of Engesser's more general theorem which is appropriate to trusses consisting of ideal elastic-plastic members when the program of loading is such as to exclude temporary unloading of individual members. This restriction is much more severe than might appear at first glance, because even under proportional loading of a truss, temporary unloading can occur in some of its members. Despite the limitations of the theorem, useful applications of it can be made to simple structures. Great caution must be exercised, however, concerning the application of the principle to stress analysis in an elastic-plastic continuum or in a structure other than a simple truss or rigid frame. It was from such an unjustified application that H. Hencky (5) derived the first stress-strain relations of the "deformation type." Recent discussion of these stress-strain relations has shown that they are acceptable only in exceptional circumstances (6).

The practical effect of assuming the idealized force-extension diagram for trusses has been discussed by Chwalla (7), among others. Finally, stress-strain relations representing a continuous transition from the elastic to the plastic state have been considered by W. Prager (8) in the hope of simplifying the stress analysis in the plastic range. Unfortunately, this hope did not prove to be justified.

REFERENCES

1 "A Review of Methods for the Plastic Analysis of Rigid Frames," by P. S. Symonds, Summary Report All-86/86 of Brown University to ONR, Contract N7 onr-358, Providence, R. I., May, 1950.

2 "The Calculation of Failure Loads on Plane Frames Under Arbitrary Loading Programs," by P. S. Symonds and B. G. Neal, *Journal of The Institution of Civil Engineers*, London, England, vol. 35, 1950–1951, pp. 41–61.

3 "Plastic Collapse and Shakedown Theorems for Structures of Strain-Hardening Material," by B. G. Neal, *Journal of the Aeronautical Sciences*, vol. 17, 1950, pp. 297–307.

4 "The Basic Theorems in the Plastic Theory of Structures," by P. S. Symonds, *Journal of the Aeronautical Sciences*, Readers' Forum, vol. 17, 1950, pp. 669–670.

5 "Zur Theorie Plastischer Deformationen und der hierdurch im Material hervorgerufenen Nachspannungen," by H. Hencky, *Zeitschrift fur Angewandte Mathematik und Mechanik*, vol. 4, 1924, pp. 323–334.

6 See, for instance, "Theory of Plastic Flow Versus Theory of Plastic Deformation," by W. Prager, *Journal of Applied Physics*, vol. 19, 1948, pp. 540–543.

7 "Three Contributions to the Problem of Load Carrying Capacity of Statically Indeterminate Steel Frames," by E. Chwalla, Publication of International Association of Bridge and Structural Engineering, Zurich, Switzerland, vol. 2, 1933–1934, pp. 96–125.

8 "On Isotropic Materials With Continuous Transition From Elastic to Plastic State," by W. Prager, Proceedings of Fifth International Congress of Applied Mechanics, Cambridge, Mass., 1938, pp. 234–237.

Critical Load of Columns of Varying Cross Section[1]

E. D'APPOLONIA.[2] By means of the Laplace transform, the author has developed an interesting procedure for the determination of the critical load of columns of varying cross section. However, as the author points out, for columns with four or more varying sections, the numerical solution for the critical load becomes tedious and long. Mention is made of the fact that a numerical method of tabular computation would be preferable for cases where $n > 4$. It seems to the writer that a numerical method would be preferable even for the cases when $n < 4$. The problems solved by the author involve only simple transcendental equations. For the cases dealing with unequal lengths of varying cross section, the transcendental equations obviously are more involved and, consequently, the solutions more tedious.

A numerical procedure and tabular scheme presented by N. M. Newmark[3] enables one to carry out a solution for the type of column problems under discussion in a simple direct manner. For example, the results of a numerical solution for column No. 1,

TABLE 1 CRITICAL LOAD FOR COLUMN NO. 1, FIG. 2 OF PAPER

Segments	Critical load
$\lambda = l/3$	$3.54\ EI_1/l^2$
$\lambda = l/6$	$3.42\ EI_1/l^2$
$\lambda = l/12$	$3.43\ EI_1/l^2$

Fig. 2 of the paper, are given in Table 1. The values are the results of two trials, where in the first trial the assumed shape of the deflected column was taken as a sine curve. Further, it can be seen that for such simple problems, exceedingly good results can be obtained even with few subdivisions of the span length. For example, considering only two points on the column, or for $\lambda = l/3$, the computed critical load differed by only 3.2 per cent of that given by the author.

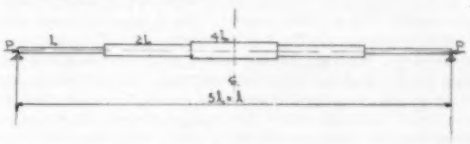

FIG. 1

To indicate the simplicity of the numerical technique, the critical load for the five-section column shown in Fig. 1 of this discus-

[1] By W. T. Thomson, published in the June, 1950, issue of the JOURNAL OF APPLIED MECHANICS, Trans. ASME, vol. 72, pp. 132–134.

[2] Assistant Professor of Civil Engineering, Carnegie Institute of Technology, Pittsburgh, Pa.

[3] "Numerical Procedure for Computing Deflections, Moments, and Buckling Loads," by N. M. Newmark, Trans. American Society of Civil Engineers, vol. 100, 1943, pp. 1161–1234.

sion was determined. For purposes of computation, the column length was divided into 10 equal segments. As a first trial, a sine-curve distribution was assumed for the column deflection and the critical load given by Equation [1] is the result of the second trial

$$P_{CR} = 21.3\frac{EI_0}{l^2} \quad \ldots\ldots\ldots\ldots\ldots\ldots\ldots\ldots [1]$$

The Flow and Fracture of a Brittle Material[1]

I. Cornet[2] and R. C. Grassi.[3] The author is to be congratulated on the valuable contribution he has made to the study of flow and fracture. The experimental measurement of the three principal strains independently, which he has achieved by his excellent experimental design and technique, and the demonstration that the assumption of incompressibility of plastic deformation is clearly violated in all the specimens in which a complete strain study was made, will no doubt have far-reaching effects on future studies of flow and fracture. The extension of data to the compression-compression quadrant and the strain data themselves are noteworthy contributions. The data of this paper will surely provide a basis for future analyses and further contributions to knowledge.

Materials of very limited ductility offer certain advantages in studying fracture laws. The virtual elimination of necking permits greater assurance in determining the state of stress at fracture; it also reduces strain-hardening effects. Brittle materials, such as cast iron, do present problems owing to stress concentrations and residual stresses attributed to microcracks or the presence of a second phase. Also, materials which are brittle in tension may exhibit appreciable ductility in compression or under combined stresses. In general, however, the characteristics of low-ductility materials will make them valuable subjects for the study of fracture laws, and the present study indicates that the same characteristics will make them useful for studies of flow, but careful measurement of small strains will be required.

In 1948, Grassi and Cornet[4] noted that "cast iron could be considered as a material composed of a matrix of carbon steel with interspersed graphite." They postulated that "under comparatively low tensile stresses, the graphite flakes would give rise to sharp notches which grow to cause brittle failure." It is gratifying that within so short a time, this model has been given quantitative formulation and that it is soon to be presented by J. C. Fischer.

It is interesting to compare the data for the tension-compression regions (Fig. 5, Coffin's paper;[1] Fig. 3, paper of Grassi and Cornet,[4] reproduced in Fig. 1 of this discussion). The agreement is excellent. We hope that the author will be able to add to his data for the tension-compression quadrant, and particularly for ratios of axial to tangential stress from -2.7 to $-\infty$ in which it was noted[4] that appreciable deformation existed. It is understood that such data are difficult to obtain where local ductility or bulging occurs. From the data, it would appear that the actual stresses at fracture lie along a vertical line for ratios of axial to tangential stress ranging from 0 to -1.0, and from there to the state of pure compressive stress, the actual fracture stresses are not on a straight line.

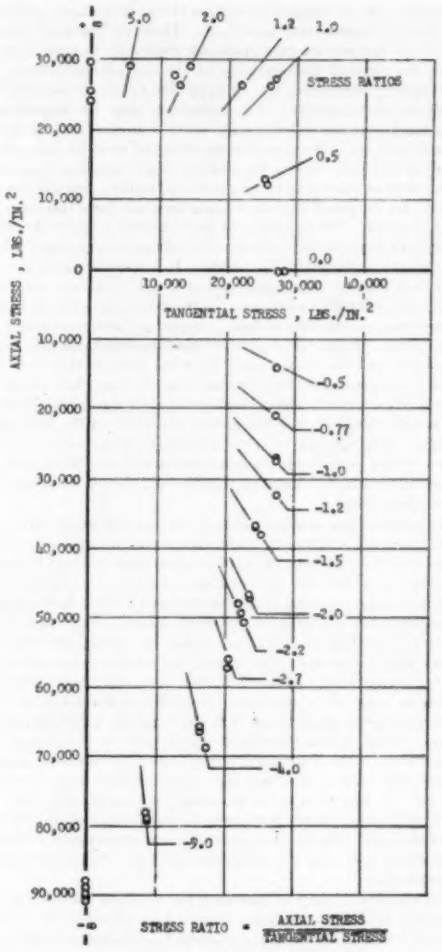

Fig. 1 True Stress at Fracture for Various Stress Ratios, Gray Cast Iron[4]

Strains for states of stress in tension-tension and part of the tension-compression quadrant are small, less than 1 per cent, and the nominal stress is approximately equal to the true stress. This is in agreement with the earlier study noted.[4]

In his last conclusion, the author points out that during unloading from plastic compression, the geometry of the crack shape is changed, and there is an opening of cracks parallel to the stress direction. From this, it may be expected that a bar of cast iron which has been subjected to plastic compression would exhibit changes in notch-bar impact or transverse bend tests. Are there any data on such tests?

---

[1] By L. F. Coffin, Jr., published in the September, 1950, issue of the Journal of Applied Mechanics, Trans. ASME, vol. 72, pp. 233–248.

[2] Assistant Professor of Mechanical Engineering, University of California, Berkeley, Calif.

[3] Assistant Professor of Mechanical Engineering, University of California, Berkeley, Calif. Mem. ASME.

[4] "Fracture of Gray-Cast-Iron Tubes Under Biaxial Stresses," by R. C. Grassi and I. Cornet, Journal of Applied Mechanics, Trans. ASME, vol. 71, 1949, pp. 178–182.

C. W. MacGregor.[6] It is a great deal of satisfaction to the writer that this particular research project on the behavior of a brittle material under the action of combined stresses, conducted in our laboratories, has reached the stage where the results could be published. The writer has long felt the need for such work since it became quite obvious to him many years ago that the commonly accepted laws of plastic flow could not be applied at all to a brittle material. This was made clear when attempts were made a long time ago to construct an effective stress-effective strain curve for cast iron, based upon a few simple combined stress tests. The author's tests have further emphasized this and they go a long way toward clearing up the problem. Much further work needs to be done, however, and additional experimental projects along this line are now under way in our laboratories.

In connection with the interpretation of the results of the present tests, the author has assumed the presence of a residual stress σ_0 (due to the difference in thermal coefficients of expansion of the graphite and the iron during solidification) and a stress-concentration factor k, due to the graphite plates. The same values of σ_0 and k are assumed to operate during the entire flow process up to and including fracture. In a notched tensile bar of a homogeneous and isotropic metal which is subjected to an axial load, two effects are generally present, namely (1) constraint (due to the local combined stress system), and (2) stress concentration. In addition, residual stresses may be present due to some cause. It is commonly accepted that as plastic flow sets in, this serves to reduce or eliminate entirely both the original stress concentration and the original residual-stress system. Indeed, it has been shown that residual stresses do not affect material properties if flow can take place.

Consequently, the writer wonders if the tests results cannot be interpreted completely from a consideration of the constraint effects of the notches produced by the graphite flakes rather than by considering a constant stress-concentration factor and a constant residual-stress system as maintaining throughout the flow process. Since very appreciable plastic flow occurs as evidenced by the author's test results, it would appear that the constraint effect of the notches (brought about by the local combined stress system at the notch) is probably the only one left.

E. B. Shand.[6] The analytical methods developed by the author to determine the effects of combined stresses on cast iron appear to correlate well with experimental results. These methods should prove valuable in such stress problems. The question raised in this discussion is whether a material such as cast iron can be considered representative of brittle bodies in general, and specifically of what might be expected in the case of a vitreous material such as glass, which is perhaps our nearest approach to an ideal brittle body.

As noted by Bridgman,[7] a brittle material is one which fractures without previous plastic deformation. The author's data show conclusively that cast iron exhibits a very definite plastic flow before rupture occurs, so that cast iron cannot be regarded as a true brittle body. In the case of glass, fine fibers broken in tension under stresses of the order of 1,000,000 psi show no perceptible indications of necking-in or other deformation, and the fracture origin is in a plane normal to the stress axis. This general characteristic of failure in tension is also shown by the tests of Bridgman,[7] as well as Gurney and Rowe[8] made on glass rods under combined stresses. In the case of Bridgman's tests, some specimens showed multiple fractures which divided the test rods into laminar disks.

The author has used the shear-energy theorem as a criterion of the critical stress in cast iron, modified to take into consideration the stress concentrations resulting from the presence of graphite flakes. This criterion may also apply to truly brittle bodies of crystalline structure, which fail as a result of a shear stress across a plane through the crystal lattice. There are, however, reasons to believe that they do not apply to amorphous bodies such as glass which have no lattice structure and fail in tension rather than in shear. For such bodies, the breaking stress under simpler conditions of loading is identified most closely with the maximum principal tensile stress, although other components undoubtedly have modifying effects as surmised by Bridgman[7] and indicated analytically by Griffiths[9] and Orowan.[10] Orowan has developed a criterion of failure for isotropic brittle materials under biaxial stress similiar to but not identical with that of Coffin.

Gurney and Rowe[8] found that the average tensile component of breaking stress differed very little regardless of whether the tests were made in simple bending of rods, or in tension with high radial components of compression. Bridgman's results are somewhat more difficult to evaluate, because they represent unique tests (tests on a single specimen), and also because the wide differences in the superposed tensile stresses result largely from differences in test techniques. A similar range of results can be obtained from simple bending tests on glass rods by varying the test techniques, particularly with respect to the preparation of the specimens.

It is characteristic of fracture in glass that failure originates at the surface, either in some flaw which is inherent in the material (Griffiths flaw), or resulting from accidental injury. The magnitudes of such flaws vary greatly so that the range of breaking stresses resulting from tests on a series of similar specimens will be quite broad—often from 2:1 or even 3:1—so that the strength of the glass is reduced to a matter of probability. This effect is characteristic of a truly brittle body, because there is no plastic flow before failure to relieve the high stress concentrations at the inner extremities of the flaws. The stress-concentration factors of accidental flaws in glass may reach values of the order of several hundred as noted by the author. This effect of very high stress-concentration factors in reducing the useful strength of the material can be compared with the effect of dislocations in the lattice of crystalline materials which permits flow under stresses; which represent only an extremely small fraction of the theoretical shear strength of the material.

The foregoing discussion is intended to point out that wide differences exist in the mechanism of failure among bodies ordinarily classified as "brittle," and that the conclusions derived from the study of one of these may not be valid for another brittle body of widely different characteristics.

Author's Closure

The author wishes to thank Professors Cornet, Grassi, and MacGregor, and Mr. Shand for their most stimulating discussions

---

[6] Professor of Applied Mechanics, Head, Materials Division, Department of Mechanical Engineering, Massachusetts Institute of Technology, Cambridge, Mass. Mem. ASME.

[6] Staff Sales Engineer, Corning Glass Works, Corning, N. Y. Mem. ASME.

[7] "The Effect of Hydrostatic Pressure on the Fracture of Brittle Substances," by P. W. Bridgman, *Journal of Applied Physics*, vol. 18, 1947, p. 246.

"Effect of Hydrostatic Pressure on Plasticity and Strength," by P. W. Bridgman, *Research*, London, England, vol. 2, December, 1949, p. 550.

[8] "Fracture of Glass Rods in Bending and Under Radial Pressure," by C. Gurney and P. W. Rowe, Royal Aircraft Establishment Reports and Memoranda No. 2284, November, 1945.

[9] "The Theory of Rupture," by A. A. Griffiths, Proceedings of the First International Congress for Applied Mechanics, Delft, Holland, 1924, part 1, p. 55.

[10] "Fracture and Strength of Solids," by E. Orowan, The Physical Society, London, Reports on Progress in Physics, vol. 12, 1948, 1949 p. 185.

to this paper. They have brought forth several interesting points which should help considerably to clarify the problem.

Referring to the discussion of Professors Cornet and Grassi, the author is grateful for their kind remarks concerning the experimental aspects of this investigation. It is felt that brittle materials will play an ever-increasing role in our technology, and it is hoped that experimental techniques similar to those used in the present work on cast iron will have an important bearing on the understanding of these materials. The author is in complete agreement with the writers concerning the experimental advantages of using brittle substances in the study of fracture laws. The development of reliable strain-measuring devices, such as the resistance-wire strain gage, have rendered the brittle material into an extremely fruitful substance for future research. Investigations into fracture of ductile materials under combined stresses might well be undertaken from this point of view where brittleness may be brought about by low temperature, heat-treatment, or some prior cold-working operation.

The author has not performed any tests on changes in notch sensitivity in cast iron produced by prior deformation, and this might prove to be an interesting and worth-while investigation. It is to be noted, as pointed out in the paper, that prior compression substantially improved the ductility in tension for a single test, but this was not explored further.

In reply to the remarks of Professor MacGregor, the author would like to point out that, as applied in the paper, the stress-concentration factor of $k = 3$ is indeed a constraint effect. By the mechanism described, as load is applied, very high local stresses at the edges of the graphite plates are relieved by plastic flow without gross plastic flow occurring in the steel matrix. The stress-concentration factor can be calculated when the general state of stress throughout the matrix has reached the level of extending the plastic flow completely across the section between adjacent plates. The mechanism is much the same as that of a bar in tension with deep sharp edge notches, or the truncated-wedge problem of Prandtl where the wedge angle is 180 deg. Here, for complete yielding at the notch cross section or the wedge face, the normal stress is $\sigma = \sigma_0(1 + \pi/2)$ where σ_0 is the yield stress of the matrix material in simple tension. The use of $k = 3.0$ rather than $k = 2.57$ is introduced for simplicity and for better experimental fit.

Without question, the residual stress developed by the graphite flakes through the mismatch in thermal expansions of the graphite and steel would be relieved if considerable plastic flow occurred. However, as the plastic strains at fracture in the tension-tension region and portions of the tension-compression region are the same order of magnitude as the elastic strains at fracture (see Fig. 23 of the paper), the residual stress developed by the flakes cannot be excluded. To simplify the picture, these stresses are considered to be constant.

Mr. Shand has presented an interesting summary of the work on fracture in glass. It should be pointed out that the flow and fracture mechanism described in the paper was intended only for crystalline materials and would have little significance in glass. Owing to the extreme viscosity at room temperature, viscous flow (which is the only mechanism of permanent deformation available to glass), proceeds at such low rates that for normal rates of testing the substance acts in a completely brittle way. Under these circumstances, the stress concentrations caused by flaws completely dominate the fracture picture, and effects of combined stress are negligible. It is interesting to speculate whether the fracture picture is comparable to crystalline structures when loading rates on glass under combined stress are of the same order of magnitude as the viscous rate of flow for glass at room temperature. This might be investigated at some elevated temperature where the rates involved are reasonable. The author is not aware that any such work has ever been done, however.

Torsion of Noncylindrical Shafts of Circular Cross Section[1]

H. Poritsky.[2] It is gratifying to see the appearance of further examples of solutions of stress problems which can be determined with relatively little analytical complication.

The authors are probably aware of the fact that in addition to the formulation of stress problems in shafts of circular symmetry in terms of the angular displacement ϵ, these problems may also be formulated in terms of a stress function ψ. These two functions are related to each other by means of the following equations[3]

$$\frac{\partial \psi}{\partial r} = r^2 \frac{\partial \epsilon}{\partial z}, \quad \frac{\partial \psi}{\partial z} = -r^2 \frac{\partial \epsilon}{\partial r}$$

When the stress function ψ is used the boundary conditions are considerably simplified by being replaced merely by the condition ψ = const over the portion of the boundary which is free from stress. Thus the numerical evaluation of certain integrals involving Bessel functions could be eliminated.

The authors may be interested in a paper by the writer[4] which includes examples involving superposition of product solutions along the line contemplated by the authors, particularly toward the case of an increase of shaft radius. Of general interest also is a powerful method utilizing a definite integral formulation of solutions, involving an arbitrary analytic function of a complex variable.

Authors' Closure

The authors regret not having quoted Love's solution by a stress function. It appears only in the fourth edition, which was the reason that we forgot about it. However, it does not make our solution superfluous, since our solution leads to different classes of the shape of the generatrix.

The difference in numerical work seems not so great as Dr. Poritsky thinks, if one compares the one-term solutions of both methods, as follows

$$\text{Love}^5 = Z = \frac{1}{k} \ln \frac{C}{A^2 r^2 J_2(kr)}$$

$$\text{The authors} = Z = -\int \frac{J_1(kr)}{J_2(kr)}\, dr \ldots\ldots [14]$$

Apparently the two results are not reducible to each other and lead two different shapes.

After completing our paper we worked at another method of solution by transformation of the differential equation of the boundary condition to an exact equation. This was also men-

[1] By H. J. Reissner and G. J. Wennagel, published in the September, 1950, issue of the Journal of Applied Mechanics, Trans. ASME, vol. 72, pp. 275–282.

[2] Consulting Engineer, General Electric Company, Schenectady, N. Y. Mem. ASME.

[3] "A Treatise on the Mathematical Theory of Elasticity," by A. E. H. Love, fourth edition, Cambridge University Press, 1927, p. 327.

[4] "Stress Fields of Axially Symmetric Shafts in Torsion and Related Fields," by H. Poritsky, presented in June, 1949, at the Third Symposium for Applied Mathematics of the American Mathematical Society.

[5] Reference (5) of the paper, p. 275.

tioned in the discussion after presentation. The development showed that this method contains Love's solution, but leads to some more general solutions, as we hope to show in the continuation of our paper.

We are certainly interested in the manuscript of Dr. Poritsky's paper, which came to our knowledge as late as at the day of the presentation of our paper. It is written at a high mathematical level and might lead to other new results.

Book Reviews

Gas Turbines With Constant-Pressure Combustion

GASTURBINEN MIT GLEICHDRUCKVERBRENNUNG. By Rudolf Friedrich. Publisher, G. Braun, Karlsrue, Baden, Germany, 1949. Cloth, 6 × 8½ in., 144 pp., 120 illustrations, 5 tables, index, bibliography, cardboard cover 8.80 Dm, cloth 10.80 Dm.

REVIEWED BY ADOLF EGLI[1]

THIS small book is the first of a series of volumes on turbo machines planned to be brought out by the publisher. The series is to cover water turbines, steam turbines, gas turbines, wind turbines, centrifugal pumps, blowers and compressors, ship screws, air screws, and hydraulic transmissions.

The present volume is a concise and well co-ordinated introduction to the field of gas turbines. It is obviously addressed primarily to engineering students of the undergraduate level and will also be useful to professional engineers of other fields who wish to get a general picture of the most important ideas and problems involved in the development of gas turbines.

The essential features of the basic working cycles are first discussed, requiring some knowledge of thermodynamics of a perfect gas. The principal elements, i.e., compressor, combustor, turbine, and heat exchanger, are then treated individually whereby the salient points of operating characteristics and design are described in a qualitative manner.

A rather primitive chapter on high-temperature materials follows. About half of the book is devoted to descriptions of representative gas-turbine designs whereby the continental developments, especially those of the Swiss firms, are given predominance.

Chapter 1 deals with the general aspects of the cycle. Chapters 2 and 3 discuss in detail the efficiency of a gas turbine; the question of the reheat coefficient is treated very thoroughly. Chapter 4 deals with air compression with or without intercooling; the theoretically best intercooling conditions are discussed. Chapter 5 covers the simple cycle without heat exchange or reheat, chapter 6 the cycle with reheat, chapter 7 the cycle with heat exchange, and chapter 8 the cycle with heat exchange and reheat.

Chapters 9 and 10 deal with low-pressure cycles, that is, those in which the turbine works between atmospheric pressure and a vacuum provided by a compressor exhausting in the atmosphere, the fluid being cooled between turbines and compressor. Chapter 11 briefly compares the open, closed, and semiclosed cycles, without discussing the engineering factors which might direct the choice to one of them. Chapter 12 deals with gas-turbine cycles compounded with Diesel, free-piston and steam cycles, and chapter 13 with gas-turbine cycles compounded with refrigeration or heating; these two chapters are rather sketchy considering the importance of these compounded cycles and the wealth of information that can be obtained on them by thermodynamics alone.

The book, particularly the first eight chapters, is the work of an intelligent man who has thought deeply about his subject; many remarks and viewpoints are original and interesting. Unfortunately, the author has considered efficiency the sole standard of merit in a cycle; no weight has been given to work done per pound of fluid. The conclusions reached in this way are lopsided; the work per pound of fluid determines the size and cost of the machine and is just as important as maximum efficiency. It is, for instance, often better to choose compression ratios for maximum work rather than for maximum efficiency; the more so as maximum work is obtained at lower compression ratios than maximum efficiency, with consequent gain in weight and cost and with an increase in component efficiencies which, in practice, entails a greater thermal efficiency. If the author had considered the work per pound of fluid, he probably would not have given so much space to the low-pressure cycles.

The work is essentially theoretical in character: its chief merit is to stimulate thought on thermodynamic cycles. It is, therefore, a pleasant surprise to find an excellent large-scale enthalpy-entropy chart and an explanation for its use in an appendix. The chart is printed in two colors, with the constant volume lines in red; it is referred to 1 kilogram-molecule of air or combustion gas, a special scale being provided to correct the enthalpy and temperature values according to the air-fuel ratio. This chart is very similar in principle to the excellent Lutz and Wolf charts that could be obtained in Germany before the war; it covers pressures from 0, 1 to 100 atmospheres, and temperatures from 0 C to 950 C. Unfortunately 0 C is too high for aircraft turbine work. But on the whole this chart is extremely useful; it would be nice if the publisher were to sell it separately.

Gas-Turbine Cycles

THERMODYNAMIQUE DE LA TURBINE À GAZ. (Actualités Scientifiques et Industrielles 1072.) By P. Chambadal, preface by C. Monteil. Hermann et Cie, Editeurs, Paris, France, 1949. Paper, 6½ × 10 in., diagrams, charts, tables, 315 pp., 1700 fr.

REVIEWED BY P. F. MARTINUZZI[2]

THIS work deals almost exclusively with the thermodynamic aspect of several gas-turbine and compounded cycles. No description or discussion of machines or components is given. Even subjects lending themselves to theoretical treatment, such as gas dynamics applied to compressors and turbines or heat transmission in heat exchangers are either omitted or mentioned incidentally.

[1] Professor of Mechanical Engineering, Towne Scientific School, University of Pennsylvania, Philadelphia, Pa. Mem. ASME.

[2] Professor of Mechanical Engineering, Cornell University, Ithaca, N.Y. Mem. ASME.

Stability Problems of Elastostatics

STABILITÄTSPROBLEME DER ELASTOSTATIK. By A. Pflüger. Springer-Verlag, Berlin, Göttingen, Heidelberg, Germany, 1950. Cloth, 6½ × 9¾ in., 389 figs., 76 graphs, references, index, viii and 339 pp., Dm 34.50.

REVIEWED BY A. L. NADAI[3]

THE author states in the preface that in the last ten to fifteen years the stability problem in engineering construction and machine design has developed into a special branch of statics and theory of elasticity which has reached a certain maturity in the mathematical treatment of such questions. In his opinion some of these stability problems can be considered as a special branch of the theory of finite elastic strains; attention being devoted not only to a determination of the critical loads but also to the second-order terms in the expressions of the strains in the distorted shapes of the bodies beyond the critical range. The critical buckling loads are also computed by means of the energy method under reference to investigations by K. Marguerre and by R. Kappus. In an introductory chapter the instability of the equilibrium of two elastic bars, hinged together at a flat obtuse angle, which may snap beyond the line connecting their outer-end points under a certain transversal load applied at the center joint, serves the author as an example in which instability is reached after a succession of similar states of equilibrium. This is contrasted with the known case of the buckling of a straight beam under a compression force representing the other prototype of instability, namely, the case when under an increasing load, at a certain load, a new state of equilibrium (in a bent form of the bar) becomes possible and a new solution develops from the one which was originally considered.

A major part of the book deals with the derivation of expressions for the components of strains and stresses in which second-order terms are included in spite of the fact that the lateral deflections of bars and of flat plates after buckling are considered to remain infinitesimal. The corresponding expressions for the strain energy are developed and the first and second variations of it computed. Elaborate new ways are also considered of introducing certain unusual types of components of strain and of stress, particularly for states of plane stress, in which account is taken of the infinitesimal differences between the abscissas, measuring the position of a point on the axis of bars, or on the middle plane of plates, in the direction of the axis or middle plane, in the distorted and in the unstrained original condition of bodies and of the changes in length of the arc elements of the elastic lines or elastic surfaces which are hereby caused. This may make the book difficult reading for American engineers not familiar with this way of dealing with finite strains. This reviewer believes that the second-order correction terms required could have been derived in a much simpler and in a clearer way from the general theory of finite homogeneous strains.

The value of the book is greatly enhanced, however, by a valuable appendix of 86 pages containing a unique, detailed collection of formulas for the buckling of straight columns under various conditions of loading and support of curved beams, of frames, of flat, rectangular, and circular plates, and of cylindrical shells. Many diagrams are also included representing buckling forces in their dependency on slenderness ratios, on ratios of width to height in rectangular plates, etc. Inelastic buckling has been only very briefly treated; recent American work on this subject has apparently not as yet become known in Germany.

[3] Consulting Mechanical Engineer, Westinghouse Research Laboratories, East Pittsburgh, Pa. Mem. ASME.

The Properties of Metallic Materials at Low Temperatures

THE PROPERTIES OF METALLIC MATERIALS AT LOW TEMPERATURES. By P. Litherland Teed. Vol. I. (A Series of Monographs on Metallic Materials published under the authority of The Royal Aeronautical Society.) John Wiley & Sons, Inc., New York, N. Y., 1950. Cloth, 5½ × 8½ in., viii and 222 pp., 8 figs., tables, subject index, $3.50.

REVIEWED BY L. R. JACKSON[4]

THIS work contains ten chapters: (1) Introductory Chapter, 5 pages; (2) General Relations Between Low Temperatures and Mechanical Properties, 9 pages; (3) Aluminum Alloys, 33 pages; (4) Ferrous Alloys, 40 pages; (5) Notched-Bar Tests and Welds, 28 pages; (6) Alloy Steels, 29 pages; (7) Magnesium Alloys, 17 pages; (8) Copper and Copper Alloys, 26 pages; (9) Nickel, Zinc, Tin, and Lead, and Their Alloys, 16 pages; and (10) Conclusion, 3 pages.

The book is mainly concerned with the presentation of tables of experimental data describing mechanical properties of metallic materials at low temperatures. There are 45 major numbered tables and numerous minor unnumbered tables in the text. In general, the author has avoided the temptation to discuss possible relations between low-temperature properties and structure of alloys. For example, there is very little discussion of the effect of metallographic structure on the notched-bar performance of alloy steels. "Slack quenching" is not discussed and low-temperature toughness is related primarily to composition.

The book should be useful in providing a design engineer with selected examples of the low-temperature behavior of a wide variety of metals and alloys.

A detailed and well-organized index makes the contents of the book easily accessible.

Process Heat Transfer

PROCESS HEAT TRANSFER. By Donald Q. Kern. McGraw-Hill Book Company, Inc., New York, N. Y., 1950. Cloth, 6 × 9 in., xii and 871 pp., tables, illus., author and subject indexes, $8.

REVIEWED BY NEWMAN A. HALL[5]

IN THE consideration of the engineering field of heat transfer, any author is confronted with the competitive demands of a comprehensive treatment of fundamental analytical methods and the great diversity of specific applications. It appears to be well established by the content of technical literature that even an extensive statement of fundamentals in this case is not sufficient to serve as a guide for many applied problems.

This situation causes continual dissatisfaction with many treatments of heat transfer, and with constant shifting of applied emphasis and refinement of treatments of special problems even the best sources tend to become obsolete. While the basic principles of convection, conduction, and radiation are well established and may be simply stated, there has been extensive development in their application in recent years. Among the more rapidly expanding engineering fields, that of process operation has depended as much as any upon an adequate understanding of heat transfer.

The present work is concerned primarily with the needs of this field of process engineering. Accordingly, the major emphasis is on specific problems in a number of general types of heat-transfer systems. The approach to each problem is well developed from

[4] Research Supervisor, Battelle Memorial Institute, Columbus, Ohio

[5] Professor of Mechanical Engineering, University of Minnesota, Minneapolis, Minn. Mem. ASME.

fundamentals and illustrates in detail the analysis of the system under consideration.

The first five chapters outline the basic concepts of heat transfer, the principles of conduction, convection, and radiation, and the general position of temperature and its measurement. It is not intended by the author that this outline be theoretically comprehensive, but merely sufficient to introduce the applications to follow.

The following nine chapters are concerned with the major heat-transfer systems and processes. The analysis of the more important heat-exchanger configurations together with condensation and evaporation phenomena is illustrated with a number of examples worked out in full detail.

The remaining seven chapters are concerned with several heat-transfer devices and certain general related items. In particular, the treatment of cooling towers is unusually comprehensive. The analysis of batch and nonsteady process operation is considered. The final chapter discusses the control of operating states in process heat transfer.

The text is unfortunately long. But in developing the subject of heat transfer in such detail, length is unavoidable. The design engineer will find on adequate study that this will be one of his best references.

The Rolling of Metals

THE ROLLING OF METALS—Theory and Experiment. With a foreword by Sir Andrew McCance. By L. R. Underwood. Volume 1. John Wiley and Sons Inc., New York, N. Y., 1950. Cloth, 5½ × 8½ in., xv and 344 pp., 142 figs., 19 tables, bibliography, index to vol. 1, $6.50.

REVIEWED BY PETER E. KYLE[6]

THE technical literature on the theory of the rolling of metals has appeared over the years in widely scattered sources. Much has been written in German and for that reason has not been as widely read by English-speaking students and engineers as it should have been. Under the auspices of the British Iron and Steel Federation, Dr. Underwood made an exhaustive survey of all of the available literature on the subject. The results of his survey were very carefully correlated and published first as a special report of the British Iron and Steel Institute. As a result of this work, the federation arranged to have the author make a more extensive study to include additional details and to summarize the work in the form of an account of the basic principles of rolling and their relation to practical rolling problems. The results of this latter effort are being published in two volumes of which this is volume one.

Volume one covers the fundamental principles of rolling between plain cylindrical rolls and omits rolling between grooved rolls. It does not include any detailed reference to the metallurgical aspects of the subject. Volume two will deal with the application of these fundamental principles to practice.

In order to follow the theory developed in this volume it is necessary that the reader have a knowledge of mechanics and stress analysis and for this reason it should not be considered an elementary book on rolling theory.

Following an introductory chapter explaining the sequence of subject matter of the book there is a chapter on the forces acting in the region of contact and a discussion of the no-slip angle. Chapter three discusses the forward slip as a measure of external friction and the effects of many factors such as temperature, metal or alloy composition, roll diameter, speed, width, tension, roll flattening, and roll roughness.

Chapters four and five include the experimental results of flow tests, especially those where surface grids were used, and a related discussion of the forces required to cause yielding. The effects of strain rates and temperature are discussed.

External friction between rolls and material is the subject of chapter six where such factors as speed, material, roll roughness, and temperature are treated. A considerable portion of this chapter is devoted to the methods of measuring friction both by rolling and nonrolling tests.

Chapters seven, eight, and nine cover the subjects of rolling loads, specific roll pressures, theories of rolling, and the effects of strip tension and work-hardening with specific application to strip and sheet. The effects of the many variables on the roll pressures developed is discussed in considerable detail. Included also is a critical discussion of the theoretical work by von Kármán, Trinks, Nadai, Tselikov, Smith, Orowan, Cook, and Larke.

The final chapter is devoted to the effects of roll flattening on the calculated values of specific roll pressure. Following the last chapter is a bibliography classified according to subject matter, containing references from the English, French, German, and Russian literature.

Dr. Underwood's book is a valuable contribution to the literature in the field of metal forming because it is not only a complete correlated review of the literature but it is written in such a way as to arouse the interest of the reader in the various phases of the work on which more high-caliber research is needed.

[6] Assistant Director, School of Chemical and Metallurgical Engineering, Cornell University, Ithaca, N. Y.

Modern Operational Calculus

MODERN OPERATIONAL CALCULUS. With Applications in Technical Mathematics. By N. W. McLachlan. The Macmillan Company, New York, N. Y., 1949. Cloth, 5½ × 8½ in., figs., bibliography, xiv and 218 pp., $5.

REVIEWED BY WILLIAM R. AHRENDT[7]

ALTHOUGH comparatively recently published in London, this book on applied mathematics was actually completed in 1941 but was withheld from publication because of the war and postwar conditions. The author has made numerous earlier contributions on the subject, perhaps the most notable of which is "Complex Variable and Operational Calculus,"[8] since it also deals with operational calculus and a closely related subject. The engineer will find the present book much more difficult reading and lacking in the easy style which characterized the earlier book. Dr. McLachlan states that no mathematical text is intended to be read like a novel, and assures it to be the case by making almost half of this book in the form of mathematical expressions. This is not to say that the book is not a valuable contribution to the applied mathematician—it is a much more significant and advanced work than the earlier book. Most readers, however, would find the earlier book extremely valuable background for the study of the present volume.

The book consists of seven chapters, followed by extensive appendixes. The first chapter deals with the Laplace transform (the p multiplied form), its definition, and theorems regarding its properties. In the second chapter are presented many theorems used in conjunction with the transform. Each is proved, and in many cases, examples of the application given. The solution of ordinary linear differential equations with constant coefficients is discussed in the next chapter, followed by a treatment of partial differential equations. Field problems, including some detailed examples of physical systems, are studied. Chapter 5 deals with an application of the Laplace transform quite uncommon to

[7] President, The Ahrendt Instrument Company, Inc., College Park, Md. Jun. ASME.

[8] The Macmillan Company, New York, N. Y., 1942.

engineering books on the subject, namely, the evaluation of finite and infinite integrals and the application of Laplace transform theorems to other mathematical problems. The next chapter is concerned with deriving Laplace transforms not by the integral commonly used, but by other means. The last chapter presents largely a study of the Laplace transform of bounded continuous functions. The appendixes deal with such related subjects as convergence of series and integrals. There follows a wealth, of technical problems to challenge the student, and which, incidentally, present other Laplace transform formulas and theorems not set forth in the text.

The book is intended to present, with rigor, theorems regarding the Laplace transform, and in this endeavor it is eminently successful.

Elements of Aerodynamics of Supersonic Flows

ELEMENTS OF AERODYNAMICS OF SUPERSONIC FLOWS. By Antonio Ferri. The Macmillan Company, New York, N. Y., 1949. Cloth, 6 × 9 in., 434 pp., illustrated, 5 tables, bibliography, $10.

REVIEWED BY ASCHER H. SHAPIRO[9]

THE literature of supersonic flows is now voluminous, and this treatise, bringing together as it does many parts of the subject, will occupy an important place on the bookshelves of those interested in the dynamics of compressible fluids.

To be able to navigate within this book, the reader should bring to it a comprehension of the general principles of fluid dynamics and of the methods used in incompressible aerodynamics, as well as the mathematical background usually covered in courses titled "Advanced Calculus." The book will have its main appeal, therefore, to professional engineers having this background and will serve as a useful reference text for graduate courses in the subject. It is not especially suitable as an introductory graduate text because of the brief treatment of elementary principles and also because it does not contain problems.

The first third of the book is given over to two-dimensional flows of a frictionless gas. There are detailed descriptions of the method of characteristics and of normal and oblique shock waves, including the simplifications which are applicable in the case of small perturbations. Various interactions between shock waves, continuous waves, solid boundaries, and free boundaries are discussed. A brief outline of the method of characteristics for two-dimensional rotational flow is set out. Then follow three chapters covering in great detail and depth, and with many useful illustrations and curves, the practical fields of (1) supersonic profiles, (2) two-dimensional effusers (supersonic nozzles), and (3) supersonic diffusers.

A special chapter is inserted covering the methods of making measurements of speed, pressure, and mach number, temperature, and density in supersonic flows. Here are given discussions of the special probes required, together with the optical methods of measurement.

The latter half of the book covers three-dimensional flows. First come several chapters relating especially to axisymmetric flow or nearly axisymmetric flow, including the method of small perturbations, the method of conical fields, and the method of characteristics for both irrotational and rotational flow. These methods are outlined for internal flows, and for external flows about bodies of revolution without and with yaw.

Finally come two chapters outlining the latest methods for calculating the pressure distribution over finite supersonic wings. These chapters will be especially useful to the student, since the mathematical details are given in full.

Five sets of tables and two large-scale charts are appended for facilitating the numerical computation of supersonic flows.

Those subjects covered in the text are treated with great fullness and detail. One might have wished for a somewhat broader coverage for example, (*a*) the boundary layer in supersonic flow, and (*b*) slightly supersonic flows with a more succinct treatment of the mathematical steps, but this is perhaps a matter of taste. The clarity of treatment is, by and large, adequate, except in a few cases where so much attention is given to detail that it is difficult to see the forest for the trees.

Finally, this reviewer cannot help but remark that the composition of a text such as this is a labor of love, and that all those interested in this field owe a debt to Dr. Ferri for having brought forth this work.

[9] Associate Professor of Mechanical Engineering, Massachusetts Institute of Technology, Cambridge, Mass. Mem. ASME.

Foundations of Aerodynamics

FOUNDATIONS OF AERODYNAMICS. By A. M. Kuethe and J. D. Schetzer. John Wiley and Sons, Inc., New York, N. Y., Chapman and Hall, Ltd., London, England, 1950. Cloth, 5¾ × 9 in., figs., tables, problems, author and subject indexes, ix and 374 pp., $5.75.

REVIEWED BY HUGH L. DRYDEN[10]

THIS book undertakes to present in a textbook of one volume a perspective view of the entire field of aerodynamics, especially of those theoretical approximations to the flow of actual fluids which permit the wider generalization and exploitation of experimental data. Each of these approximations has become a major field of specialization in theoretical fluid mechanics, i.e., classical hydrodynamics or the flow of "perfect" fluids, subsonic flow of compressible fluids, supersonic flow of compressible fluids, transonic flow, flow of viscous incompressible fluids, flow of viscous compressible fluids. The specialization is so great that there is danger that the student of aerodynamics will forget that these separate fields are but approximations to the flow of the same actual fluid, which should, at least from the point of view of engineers, be the principal object of study. "Foundations of Aerodynamics" is the prototype of an integrated presentation of the whole field.

The content is indicated by the chapter headings, which are as follows: The Fluid Medium; Kinematics of a Fluid Field; Dynamics of a Fluid Field; The Flow About a Body; The Thin Airfoil; Finite Wing; Introduction to Compressible Fluids; The Energy Relations; Some Fundamental Aspects of Isentropic Flow; Waves; Airfoils in Compressible Flow; Introduction to the Dynamics of Viscous Fluids; Laminar Flow in Tubes and Boundary Layers; Turbulence; Turbulent Flow in Tubes and Boundary Layers; Transition from Laminar to Turbulent Flow; Some Aspects of Viscous Compressible Flow; Aerodynamic Characteristics of Wings. There are included tables of properties of the standard atmosphere, flow parameters versus Mach number for isentropic, subsonic and supersonic flow, and for flows with shock waves. About 100 problems are included for the use of students.

The reviewer, who has had little teaching experience, finds some lack of integration of the theoretical and experimental material. The authors state that they have assumed no previous knowledge of aerodynamics and that the book is intended for a senior undergraduate or first-year graduate course. However, such technical words as boundary layer, wake, airfoil, stalling, turbulence are used without explanation long before these concepts are discussed in detail. In one instance, there is a reversal in order of what

[10] Director, National Advisory Committee for Aeronautics, Washington, D. C. Fellow ASME.

would seem to be the natural order of presentation of new ideas. Thus, except for occasional use of the words, turbulent flow is incidentally discussed on page 211 with a reference to turbulent transfer processes. The treatment of turbulence begins with chapter 14, page 240, dealing principally with isotropic turbulence. Chapter 15 follows on turbulent flow in tubes and boundary layers. Only then comes transition in chapter 16, and at the end of this chapter a description of the ways in which the transition to turbulent flow is experimentally detected. It would appear more logical to discuss transition first, and to begin with the descriptive observations of the process. Experimental data on wings are segregated in the final chapter. An early introductory chapter on the experimental aspects of actual fluid flows to illustrate such concepts as boundary layer, wake, transition, and separation and to indicate those phenomena which could be described with theories which neglect viscosity or compressibility, or both, would have been useful to the beginner.

The authors mention that the mathematician will note compromises with rigor. Some readers will take exception to the use of the word "inelastic" in the sense of "incompressible" (page 10) and to the statement (page 13) that "if the formulation of a problem introduces these anomalies (discontinuity and infinite value), the regions in which they exist must be outside the boundaries of the physical field."

The book is based on notes of courses given by the authors at the University of Michigan, and is a worthy candidate for use as a first course at the graduate level.

Principles of a New Energy Mechanics

PRINCIPLES OF A NEW ENERGY MECHANICS. By Jakob Mandelker. Philosophical Library, New York, N. Y., 1949. Leatherette, 6 × 9¼ in., viii and 73 pp., 17 figs., $3.75.

REVIEWED BY J. ORMONDROYD[11]

THE author proposes an "energy mechanics" which is to replace the classical mechanics of Newton and the special relativity theory of Einstein. The basic concepts and procedures are similar to those of the special relativity theory. Einstein placed at the basis of his special relativity theory the following postulates: (1) The velocity of light in vacuo is the same in all co-ordinate systems moving uniformly, relative to each other—no matter which one of these systems may contain the source of the light; (2) All laws of nature, mechanical and electromagnetic, must be invariant (have identical functional form) in all co-ordinate systems moving uniformly relative to each other.

Mandelker rejects the first postulate and accepts the second. He also accepts, as experimentally proved facts, that the inherent energy in a mass m is $E = mc^2$ and that mass is a function of velocity, $m = \frac{m_0}{\sqrt{1 - v^2/c^2}}$. He understands c to be the velocity of light in the laboratory of the investigator and v to be the velocity of a particle relative to the laboratory, the particle at rest in the laboratory having mass m_0. Mandelker's time is absolute in the Newtonian sense. His speed of light is relative. Starting with the invariance of the laws of light propagation in several two-dimensional co-ordinate systems which have constant relative velocities in the x direction, given as

$$(x_0^2 - c_0^2 t^2) = (x_1^2 - c_1^2 t^2) = (0 - c_n^2 t^2)$$

He gets, by division throughout by the absolute t^2,

$$c_0\sqrt{1 - v_0^2/c_0^2} = c_1\sqrt{1 - v_1^2/c_1^2} = c_n$$

He states this to mean that a ray of light with velocity c_0 in k_0 appears with velocity c_1 in k_1 and velocity c_n in k_n. In several places later Mandelker states that this justifies him in saying that any velocity W_n in co-ordinate system k_n would appear as $W_0 = W_n\sqrt{1 - v^2/c^2}$ in co-ordinate system k_0 moving relative to k_n with constant velocity $-v$. Here the author seems to endow the velocity of light c with some special kinematic magic, having rejected Einstein's brand of magic. Why should the velocity W_n replace c outside the square-root sign if the velocity c inside the square-root sign remains unchanged? Well, for one thing, by doing this the author gets a very painless derivation of the Lorentz transformation formula—with which he agrees. For another, he gets Fizeau's experimental value of the velocity of light in moving water by a very simple calculation.

Another achievement claimed for "energy mechanics" is an explanation for the appearance of the half-quantum value of the "zero-point" energy in the kinetic energy of a linear oscillator which violates the fundamental postulate of quantum mechanics. The energy mechanics shows this to be an approximation to an expression in which only whole quantum values appear.

According to the author the most significant result of the new mechanics is an evaluation of the kinetic energy of an accelerated particle. In contradiction to Newton and Einstein the author contends that the mere existence of relative velocity does not create energy. For the author, only transformations of energy occur between kinetic and potential aspects in a special way. For Einstein the total energy of a moving particle consists in its potential rest energy plus the kinetic energy created by its motion.

This little book is disarmingly simple. It displays simple formal mathematical manipulations. Almost any undergraduate would think he understood the book if he read it. The special theory of relativity has stood the critical scrutiny of forty-five years. Many men, for a great variety of reasons only one of which was pure intellectual curiosity, have tried to show that this theory was invalid. Professor Mandelker is a bold David come to challenge this hitherto undefeated Goliath.

This book should be of interest to atomic physicists. For readers of the JOURNAL OF APPLIED MECHANICS it probably would arouse little interest. After all, the highest velocities we can dream of are in the order of $^1/_{10,000}$ of the velocity of light. Both Mandelker and Einstein agree that Newton is still good enough for us.

The Inelastic Behavior of Engineering Materials and Structures

THE INELASTIC BEHAVIOR OF ENGINEERING MATERIALS AND STRUCTURES. By Alfred M. Freudenthal. John Wiley & Sons, Inc., New York, N. Y., 1950. Cloth, 5½ × 8¼ in., xvi and 587 pp., illus., tables, references, author and subject indexes, $7.50.

REVIEWED BY JOHN C. FISHER[12]

ESSENTIALLY, this book is a survey of a large number of topics related to the mechanical behavior of materials. The subject matter ranges from atomic theory and quantum mechanics to impact and fatigue testing of materials. The first few chapters, dealing with the structure of matter, contain a number of errors, some of which may result from the author's desire to simplify his treatment. In the later chapters much emphasis is placed upon phenomenological equations relating the variables, stress, strain, strain rate, and temperature. A back-

[11] Professor of Engineering Mechanics, University of Michigan, Ann Arbor, Mich. Mem. ASME.

[12] Research Laboratory, General Electric Company, The Knolls, Schenectady, N. Y. Jun. ASME.

ground of experimental evidence in support of these equations would have added to their value.
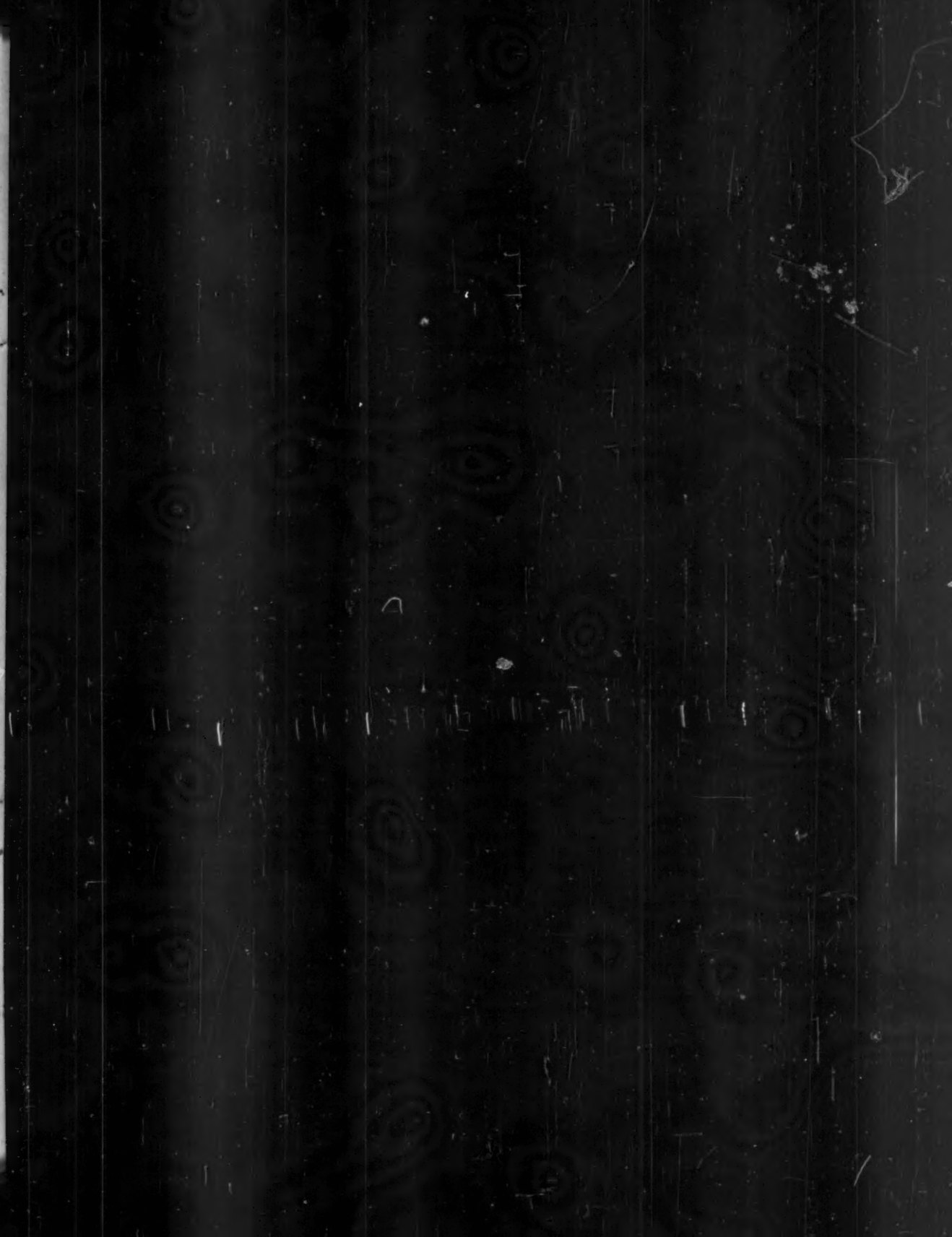
The book is valuable as a source that touches upon practically every aspect of mechanical behavior in a wide range of engineering materials. An excellent set of references is included for those who wish to follow a given subject in more detail.